NANCY 1
FACULTE DES SCIENCES & TECHNIQUES

U.F.R. : STMP
Ecole Doctorale : EMMA
Département de Formation Doctorale : Physique et Chimie de la Matière et des Matériaux

Thèse

présentée pour l'obtention du titre de

Docteur de l'Université Henri Poincaré Nancy-I

en Physique et Chimie de la Matière et des Matériaux

par **Afidah BINTI ABDUl RAHIM**

Caractérisations physico-chimiques des tannins de Mangrove comme inhibiteurs de corrosion

Thèse soutenue le 22 décembre 2005

Membres du jury :

Président :	M. Mustapha Kamal AHMAD SHUKRI	Professeur
Rapporteurs :	M. Xavier DEGLISE	Professeur,
	M. Noordin MOHD KASSIML JAIN	Professeur
Examinateurs :	M. Pierre STEINMETZ	Professeur,
	M. Jean STEINMETZ	Professeur
	M. Mohamad KAMAL HARIN MADIA	Professeur
Invités :	M. Mustapha KAMAL AIMAD SHUKRI	Professeur

Laboratoire de Chimie du Solide Minéral – UMR 7555
Faculté des Sciences & Techniques - 54506 Vandœuvre-lès-Nancy

ACKNOLEDGEMENTS

I would like to express my sincere appreciation and gratitude to my supervisors Prof. Jean Steinmetz, Assoc. Prof. Mohd Jain Noordin Md. Kassim, Assoc. Prof. Md. Sani Ibrahim and Dr. Emmanuel Rocca for the guidance, inspiration, support and patience throughout this study. I would like to acknowledge Dr. Rohana Adnan for her assistance in the molecular modelling studies.

I would like to thank the technical staff of the School of Chemical Sciences, Universiti Sains Malaysia and the Laboratoire de Chimie du Solide Mineral, Universite Henri Poincare, in particular Mr. Sobri Aziz Hassan, Mr. Ali Zaini, Mr. Aw Yeong Cheok Hoe, Mr. Alan and Mr. Jean-Paul for their help throughout the course of this study.

I would like to acknowledge the Universiti Sains Malaysia and the French Embassy for granting me the scholarship which covers my tuition fees and supports my living expenses during the term of this study.

My sincere thanks to all my friends and colleagues who never fail to help and encouraged me during my study.

Last but not least, my sincere appreciations to my husband, Abdul Rahman who constantly supports me, my children Mua'dz, Aufa and Najwa from whom I had been away and my parents for always being there for me.

TABLE OF CONTENTS

LISTS OF TABLES

LIST OF FIGURES

LIST OF ABBREVIATIONS

FTIR	Fourier transform infrared spectroscopy
TGA	Thermogravimetic analysis
DTG	Differential thermogravimetric
NMR	Nuclear magnetic resonance
XRD	X-ray diffraction
SEM	Scanning electron microscopy
EDS	Electron dispersive X-ray spectroscopy
HOMO	Highest occupied molecular orbitals
LUMO	Lowest unoccupied molecular orbitals
SHE	Standard hydrogen electrode
I_{corr}	Corrosion current
E_{corr}	Corrosion potential
R_p	Polarisation resistance
wt	weight
v	volume
w/v	weight per volume
min	minutes
hr	hour
ha	hectar
g L^{-1}	gram per liter
mg mL^{-1}	milligram per millilitre
mL min^{-1}	milliliter per minute
mV	millivolts
mV s^{-1}	millivolt per second
µA	microampere
br	broad

s	strong
m	medium
w	weak

PHYSICO-CHEMICAL CHARACTERISATION OF MANGROVE TANNINS AS CORROSION INHIBITORS

ABSTRACT

Tannins from mangrove barks have been successfully extracted using 70 % aqueous acetone and purification by LH-20 column chromatography afforded condensed tannins of high purity. The reversed-phase HPLC analysis of condensed tannins following depolymerisation in phloroglucinol and acidic ethanol revealed mainly four terminal units namely catechin, epicatechin, epigallocatechin and epicatechin gallate. Substantial anti-oxidant capabilities have been shown by mangrove tannins which were comparable to the synthetic standards used.

The electrochemical experiments have shown that the inhibitive efficiency of mangrove tannins on steel which was largely contributed by the condensed tannins, increased with increasing concentrations at very low pH. The inhibitive performance of mangrove tannins was comparable with that of commercial mimosa, quebracho and chestnut tannins at pH 0, 0.5 and 2.0. All tannins that were investigated are cathodic inhibitors in acidic media and the inhibition efficiency of all tannins was found to decrease with increasing pH. At pH 0 and 0.5 the adsorption mechanism was attributed to chemisorption of tannin molecules onto the iron surface while at higher pH, the formation of ferric-tannates resulted in a low protective effect. The electrochemical studies have shown that the flavanoid monomers that constitute mangrove tannins are potential inhibitors for steel in acidic medium. All monomers act mainly as cathodic inhibitors of the steel corrosion and its inhibitive performance dependent on concentration in acidic conditions. To explain the adsorptive

behaviour of the molecules on the steel surface, a semi-empirical approach involving quantum chemical calculations using HyperChem 6.0 was undertaken. The correlation between the electronic density of the molecule and the inhibiting properties was established. The most probable adsorption centers were found in the vicinity of the phenolic groups.

Inhibition efficiency of pre-rusted steel in 3.5 % NaCl solution containing 3.0 g L^{-1} tannins was found to be dependent on the concentration of phosphoric acid added and pH of solution. The correlation between ferric-tannate formation and the low inhibition efficiency observed at high pH from the electrochemical studies was established from phase transformation studies, evaluated via FTIR, XRD, SEM, EDS, humidity chamber and salt spray tests. All methods of evaluation inferred a temporary and low corrosion protection by mangrove tannins.

PENCIRIAN FISIKOKIMIA TANIN BAKAU SEBAGAI PERENCAT KAKISAN

ABSTRAK

Tanin daripada kulit kayu bakau telah diekstrak menggunakan 70 % aseton akueus dan penulenan tanin menggunakan kromatografi turus LH-20 menghasilkan tanin terkondensasi yang bertulenan tinggi. Analisis HPLC fasa berbalik selepas proses pendepolimeran dalam floroglusinol beralkohol menghasilkan empat unit penghujung iaitu katecin, epikatecin, epigallokatecin dan epikatecin gallat. Tanin bakau turut menunjukkan keupayaan anti-oksidan yang setanding dengan bahan piawai sintetik yang digunakan.

Kajian elektrokimia menunjukkan bahawa keupayaan perencatan terhadap keluli yang sebahagian besarnya disumbang oleh tanin terkondensasi, bertambah dengan peningkatan kepekatannya pada pH rendah. Keupayaan perencatan tanin bakau adalah setanding tanin mimosa, quebracho dan chestnut pada pH 0, 0.5 dan 2.0. Kesemua tanin yang diselidik adalah perencat katodik dalam media berasid yang mana keupayaan perencatannya berkurang dengan peningkatan pH. Pada pH 0 dan 0.5, mekanisme perencatan adalah oleh proses pengkimierapan molekul tanin ke atas permukaan besi manakala pada pH yang lebih tinggi, pembentukan ferik-tanat memberikan perlindungan kakisan yang rendah. Kajian elektrokimia juga telah menunjukkan monomer flavanoid yang terkandung dalam tanin bakau berpotensi bertindak sebagai agen perencat kakisan terhadap keluli pada media berasid. Kesemua monomer flavanoid yang dikaji adalah perencat katodik dan keupayaan perencatan kakisan adalah bergantung pada kepekatan dalam media berasid. Untuk menerangkan sifat penjerapan molekul ke atas keluli, pendekatan pengiraan

kuantum kimia menggunakan Hyperchem 6.0 dijalankan. Korelasi antara ketumpatan elektron dan sifat perencatan kakisan dikenalpasti. Kajian menunjukkan penjerapan tertumpu pada kumpulan fenol. Keupayaan perencatan terhadap kakisan keluli dalam 3.5 % larutan NaCl yang mengandungi 3.0 g L^{-1} tanin bergantung pada kepekatan asid fosforik dan pH larutan. Korelasi antara pembentukan ferik-tanat dan keupayaan perencatan rendah yang ditunjukkan oleh kajian elektrokimia dikenalpasti melalui kajian perubahan fasa yang dinilai melalui kaedah FTIR, XRD, SEM, EDS, ujian kelembapan dan semburan garam. Kesemua kaedah penilaian menunjukkan tanin bakau memberikan perlindungan yang rendah dan bersifat sementara terhadap kakisan.

CARACTÉRISATION ÉLECTROCHIMIQUE DES TANNINS DE LA MANGROVE EN TANT QU'INHIBITEURS DE CORROSION

RÉSUMÉ

Des tannins ont pu être extraits avec succès des écorces de mangrove grâce à une solution aqueuse d'acétone à 70 % et leur purification par chromatographie sur colonne LH-20 a permis d'obtenir des tannins condensés très purs. L'analyse des tannins condensés par HPLC à polarité de phase inversée, après dépolymérisation dans le phloroglucinol et l'éthanol acide, a révélé l'existence de quatre unités terminales principales, à savoir la catéchine, l'épicatéchine, l'épigallocatéchine et l'épicatéchine gallate. Ces tannins de mangrove ont montré des capacités anti-oxydantes importantes, comparables aux standards synthétiques utilisés.

Les expériences électrochimiques ont démontré que l'efficacité inhibitrice de corrosion des tannins de mangrove sur l'acier, due en grande partie à la présence des tannins condensés, croît avec leur concentration à très bas pH. Leur capacité inhibitrice s'est avérée comparable à celle des tannins commerciaux de mimosa, de québracho et de châtaignier à pH 0, 0,5 et 2,0. Tous les tannins étudiés sont des inhibiteurs cathodiques en milieu acide et, pour tous, l'efficacité d'inhibition diminue lorsque le pH augmente. A pH 0 et 0,5, le mécanisme d'adsorption a été attribué à la chimisorption des molécules de tannin sur la surface du fer, alors qu'à pH plus élevé, la formation de tannates ferriques a conduit à un faible effet protecteur. Les études électrochimiques menées ont également démontré que les monomères flavanoïdes qui constituent les tannins de la mangrove sont en eux-même des

inhibiteurs potentiels pour l'acier en milieu acide. Tout comme les tannins de mangrove, les monomères agissent principalement comme des inhibiteurs cathodiques de la corrosion de l'acier et leurs performances inhibitrices dépendent de leur concentration en milieu acide.

Afin d'expliquer le comportement d'adsorption des molécules sur la surface de l'acier, une approche semi-empirique, impliquant des calculs de chimie quantique et utilisant HyperChem 6.0, a été adoptée. Ainsi, nous avons pu établir une corrélation entre la densité électronique de la molécule et les propriétés inhibitrices. Les centres d'adsorption les plus probables se situent dans le voisinage des groupes phénoliques.

D'autre part, l'efficacité d'inhibition de la corrosion sur des échantillons d'acier pré-rouillés, observée dans une solution de NaCl à 3,5 % contenant 3 g L^{-1} de tannins, est apparue dépendante de la concentration d'acide phosphorique ajouté et du pH de la solution. La corrélation entre la formation de tannates ferriques et la faible efficacité d'inhibition observée à pH élevé lors des études électrochimiques a été confirmée par (l'observation de transformations de phases réalisée par à enlever) des analyses IRTF, DRX, MEB, EDS et des tests en enceinte humidotherme et en brouillard salin. Toutes les méthodes d'évaluation ont permis de conclure à une protection contre la corrosion par les tannins de mangrove faible et temporaire.

CHAPTER ONE

INTRODUCTION

1.1 Mangrove forests in Malaysia

Mangrove forests in Malaysia develop well in sheltered estuaries where waters are brackish, and wave and tidal conditions are conducive to mud accumulation. In total, there are about 641,000 ha of mangrove forests in Malaysia of which 57 % are found in Sabah, 26 % in Sarawak and the remaining 17 % in peninsular Malaysia. Of the total, about 446,000 ha or 70 % have been gazetted as forest reserves. Currently, there are a total of 112 mangrove forest reserves in the country. These reserves form part of the country's Permanent Forest Estate which is managed for sustainable forestry production.

In peninsular Malaysia, the total extent of mangrove forests is about 107,700 ha. About 92,300 ha (85.7 %) are forest reserves while the remaining 15,400 ha (14.3 %) are stateland mangroves. Amongst the 11 states in Peninsular Malaysia, Perak has the greatest number of mangrove reserves of which 19 reserves form the Matang mangroves (Clough, 1993).

Traditionally, mangroves are harvested for fuel (as firewood or first converted to charcoal) and for poles (now mainly used as piling). Species of the family Rhizophoraceae, mainly *Rhizhphora apiculata, R. mucronata and Bruguiera parviflora* are particularly favoured for making charcoal because of their hard, dense timber, claimed by some to produce the best charcoal in the world. In the

Matang mangroves in the State of Perak, we see what is considered to be the best managed mangrove forest in the world (Gan, 1995). The Matang mangroves are a large expanse of mangrove forest (about 51km of coastline and 13km wide) stretching from Kuala Gula in the north to Bagan Panchor in the south. It represents the largest intact tract of mangrove forest with several semi-permanent lakes in Peninsular Malaysia and one of the last mangrove areas with all major habitats and forest types.

The main vegetation types of Matang (Silvius *et al.*, 1986) are :

- "Bakau type" (*Rhizophora* spp.). More than 80 % of the mangroves are mainly *R. apiculata* due to refforestation;
- "Api api-Perapat" type (*Avicennia-Sonneratia*). This type occurs mainly in the accreting mangrove zone. In some areas, *Avicennia* covers large areas of forest;
- "Berus type" (*Bruguiera cylindrica*), which occurs close to the coast mostly behind the *Avicennia-Sonneratia* type;
- "Lenggadai type" (*B. parviflora*); and
- "Tumu type" (*B. gymnorhiza*), which is the climax mangrove forest type, preceeding the inland forest.

With a total of about 41,000 ha of managed forest, 1,000-1,300 ha of the Matang mangroves are now cut annually on a 30 year rotation. Two thinning are carried out, the first at 15 years and the second at 20 years. Poles cut during thinning are used for construction, and in some cases for firewood. Gross revenue from charcoal and other products has been estimated at about US$6

million. Extraction and processing of timber from the Matang mangrove forest has been estimated to provide employment for a direct workforce of about 1,400 people and an indirect workforce of a further 1,000 (Clough,1993).

However, due to forest harvesting, the major part of the forest is not higher than 10-20 m. The soil is basically mixed with a high percentage of clay, varies from compact blue clay, containing little or no organic matter, in the more recent deposits on the sea face, to the brown "mangrove loam", with a high proportion of partly decomposed organic matter and a varying amount of sand, in the centre of the islands and along the mainland boundary (Gan,1995).

1.1.1 *Rhizophora* in general (Family-Rhizophoraceae)

All *Rhizophora* species have arching stilt roots that emerge from the trunk, hence their scientific name *Rhizophora* which means "root bearer" in Greek. These roots not only hold up the tree in soft mud, but are also permeable to gases, while remaining impermeable to salts. The entire upper root system including the trunk and prop roots that emerge from the branches have this feature. Thus the roots also help the tree to breathe. *Rhizophora* use ultrafiltration at the root level to exclude salt. It is believed that they store any salt that gets through in old leaves which they later shed. *Rhizophora* grow best in wet, muddy and silty sediments.

The tiny flowers are wind-pollinated, producing lots of powdery pollen and no fragrance or nectar. They are also self-pollinating. The fruit does not fall away when it ripens. Instead, the single seed within the fruit starts to germinate while

it is still on the mother tree, and the mother tree channels nutrients to the growing seedling (vivipary). The seedling forms a stem (called a hypocotyl). When the seedling finally falls, at first it floats horizontally, and drifts with the tide. It can survive for long periods at sea. After some weeks, the tip gradually absorbs water and the seedling floats vertically and starts to sprout its first leaf from the top, and roots from the bottom. When it hits land, it grows more roots to anchor itself upright, and then more leaves. *Rhizophora* seedlings grow rapidly to avoid being submerged at high tide. They can grow by 60cm in the first year. Because *Rhizophora* are fast growing and flower within their first year, they are often used to replant mangroves either for conservation or as part of a managed forest to produce timber for construction or charcoal (Tan, 2001).

1.1.2 *Rhizophora apiculata* (bakau minyak)

The commonly found mangrove species within the *Rhizophora* genus are *Rhizophora mucronata, Rhizophora stylosa, Rhizophora mangle* and *Rhizophora apiculata.* The *Rhizophora apiculata* tree can reach up to 20 m tall. It has elliptic leaf blades with tiny black spots below the leaf blades, with red stipules and the leaf stalks are often tinged red. The paired stalkless flowers are cream-coloured sitted on a short, stout dark grey stalk. Its fruits are pear-shaped and brown in colour (Fig. 1.1). Although *Rhizophora apiculata* have been used mainly for charcoal making, leaving the barks (Fig. 1.2) as waste products, Mohd. Ali *et al.*, (1981) reported that the 10% tannin content extracted from the barks of *Rhizophora apiculata* was sufficient for commercial exploitation.

(a) (b)

Fig. 1.1 (a) Branch tip of *Rhizophora apiculata* with red stipule and (b) young to old fruits showing the seedling (Ng and Sivasothi, 2001).

Fig. 1.2 Mangrove barks as waste products of the Larut Matang charcoal industry.

1.2 What are tannins?

The name 'tannin' is derived from the French 'tanin' (tanning substance) and is used for a range of natural polyphenols. Since ancient times it is known that certain organic substances have tanning properties and are able to tan animal skins to form leather. In nature the tannins are found worldwide in many different families of the higher plants such as in chestnut, pine and oak wood, depending on their origin, their chemistry varies widely, having a molar mass of up to 20,000D. High tannin concentrations are found in nearly every part of the plant, such as in the bark, wood, leaves, fruit, roots and seed.

The nomenclature of the tannins is full of misunderstanding, erroneous interpretations, and changes caused by advances in this field. Definitions include the plant tannins as water soluble phenolic compounds with a molar mass between 300 and 3,000, showing the usual phenol reactions (e.g. blue colour with iron (III) chloride and precipitating alkaloids, gelatine and other proteins (Bates-Smith and Swain,1962) tannins with a molecular weight that can reach 5000, contain sufficient phenolic hydroxyl groups to permit the formation of stable cross-links with proteins, and as a result cross-linking enzymes may be inhibited (Ximenes,1998) and tannins have also been described as oligomeric compounds with multiple structure units with free phenolic groups, having molecular weight ranging from 500 to >20,000 and soluble in water with the exception of some high molecular weight structures (Tannins : Chemical Structure, 2001). Tannins were initially classified into two broad groups: the hydrolysable and condensed tannins (Okuda *et al.*,1989). Gallic acid [Fig.1.3(a)] and hexahydroxydephinic acid with HHDP group [Fig.1.3(b)] represent the

polyphenolic part in the molecules of hydrolysable tannins as a result of their hydrolysis and condensation in the presence of acid and enzyme. Those having the HHDP group have been named ellagitannins as they produce ellagic acid upon hydrolysis and those having only the galloyl groups are called gallotannin.

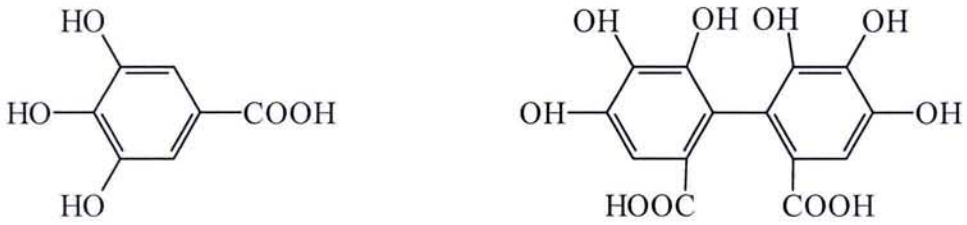

(a) (b)

Fig. 1.3 (a) Gallic acid and (b) hexahydroxydiphenic acid.

However, based on the molecular structures of the currently known tannins, their origin and role in plant life, tannins are recently divided into four major groups : *Gallotannins, ellagitannins, complex tannins and condensed tannins* (Fig. 1.4).

(1) Gallotannins are all those tannins in which galloyl units or their *meta*-depsidic derivatives are bound to diverse polyol-, catechin-, or triterpenoid units.

(2) Ellagitannins are those tannins in which at least two galloyl units are C-C coupled to each other, and do not contain a glycosidically linked catechin unit.

(3) Complex tannins are tannins in which a catechin unit is bound glycosidically to a gallotannin or an ellagitannin unit.

(4) Condensed tannins are all oligomeric and polymeric proanthocyanidins formed by linkage of C-4 of one catechin with C-8 or C-6 of the next monomeric catechin (Khanbabaee and Van Ree, 2001).

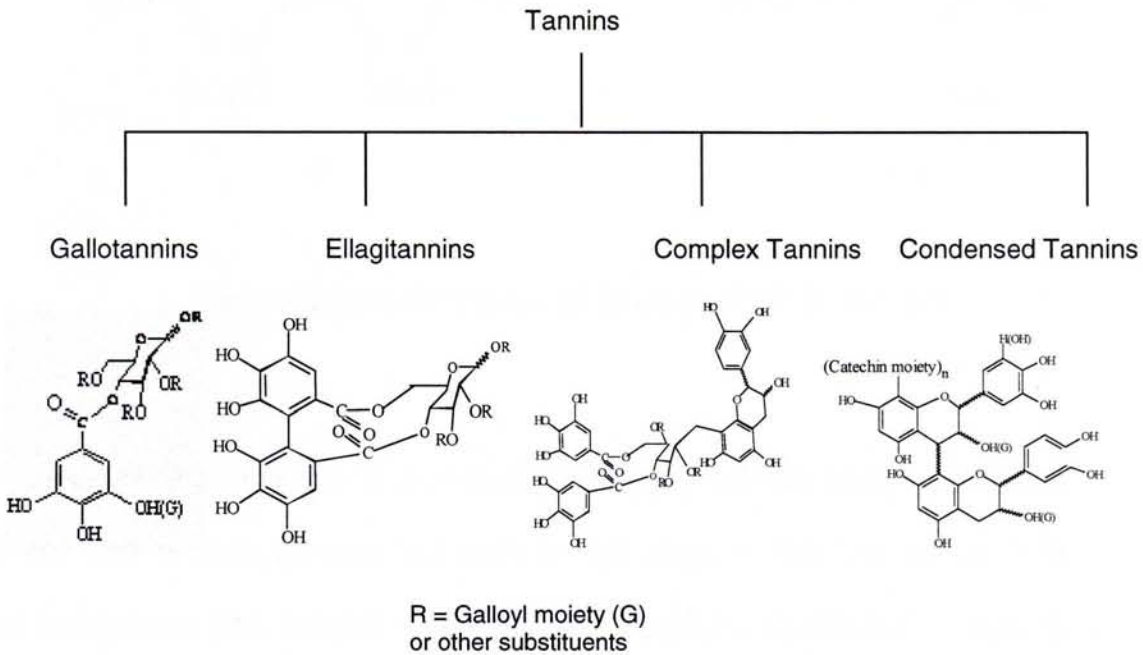

Fig. 1.4 Classifications of tannins (Khanbabae and Van Ree, 2001).

1.2.1 Condensed tannins (or proanthocyanidins)

Proanthocyanidins (condensed tannins) are a group of phenolic polymers which are widely distributed in the plant kingdom particularly with woody growth habit. These compounds consist of flavan-3-ol units linked together through C4-C6 or C4-C8 bonds (Fig.1.5). Structural variation of proanthocyanidins ranges from dimers and trimers to more complex oligomers and polymers depending on the nature of the interflavanoid lingkage, hydroxylation and stereochemistry at the three chiral centres (carbon 2, 3 and 4) of the C-ring. They are the most widespread polyphenols in plants after lignins and can be found in leaves, fruit woods, barks or roots and are known to play various nutritional and ecological roles (Hernes *et al.*, 2001).

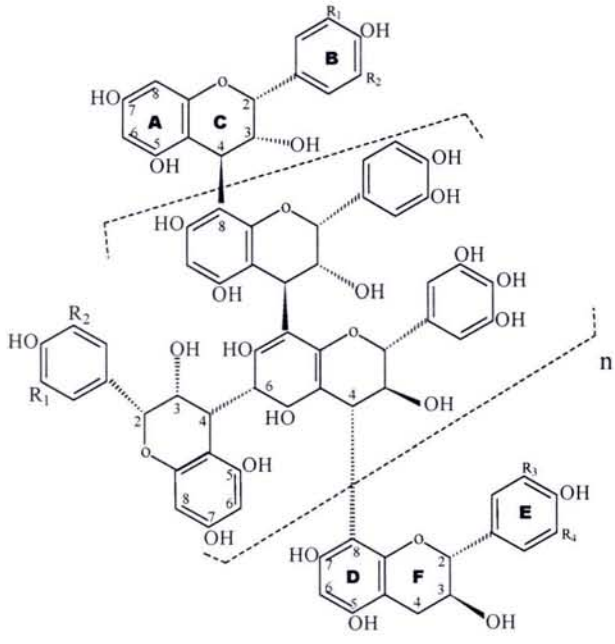

Fig. 1.5 Structure of a condensed tannin (Hernes *et al.*, 2001).

These flavan-3-ol oligomers produce anthocyanidins by cleavage of a C-C bond under strongly acidic conditions. The most important features of the flavan-3-ols pertaining to the chemistry of oligomeric proanthocyanidins are the nucleophilicity of the A-rings, the aptitude of their heterocyclic rings to cleavage and subsequent rearrangement, the susceptibility of analogues with pyrocatechol- or pyrogallol-type B-rings to phenol oxidative coupling, and the conformational mobility of their pyran rings (Farreira *et al.*, 1999). With the growing realization of the importance of these compounds as antioxidants in the human diet, this has let to a sharp increase in research effort. Extensive studies were carried out on the isolation and characterization of condensed tannins from various plant sources mainly by using NMR techniques (Karchesy and Hemingway, 1980; Porter *et al.*, 1982; Marimoto *et al.*, 1986; Kashiwada *et al.*, 1986; Ishimatsu *et al.*, 1989; Cai *et al.*, 1991; Toki *et al.*, 1991; Danne *et al.*, 1993; Nam-In *et al.*, 1994) and HPLC analysis (Da Silva, 1991; Rigaud *et al.*, 1993; Prieur *et al.*, 1994; Jean-Marc *et al.*, 1996; Guyot *et al.*, 1997; Hammerstone *et al.*, 1999) as well as TLC techniques (Porter et al., 1985; Foo and Karchesy, 1991; Kolodziej *et al.*, 1991; Young-Soo *et al.*, 1994). The review that follows demonstrates that, although considerable progress has been made in definition of proanthocynidin structure, understanding of the properties of these complex compounds is still rather limited.

1.2.1.1 Analysis of condensed tannins

Analysis of condensed tannins is complicated by the diversity of structures found within this group of compound. Many analytical methods have been used to quantify condensed tannins in plant materials. Commonly used methods include the vanillin assay (Price *et al.* 1978; Makkar and Becker, 1994; Naczk *et al.*, 1994) and oxidative depolymerization reactions such as the acid-butanol assay (Hagerman and Butler 1988; Makkar *et al.*, 1999). Other methods involve protein precipitation reactions (Makkar, 1989), Stiasny reaction (Yazaki, 1985), acid cleavage reactions, enzyme and microbial inhibition and gravimetric procedures (Schofield *et al.*, 2001). A more recent addition to the list of analysis is the use of flow injection spectrophotometry (Ferreira and Nogueira, 2000). An excellent review with regard to the most appropriate procedures to choose for a sample is given by Schofield *et al.* (2001).

Depolymerisation reactions in the presence of nucleophiles are frequently employed for the structural analysis of proanthocyandins. The nucleophile forms adducts with the extender units in the polymer, which are purified or analysed by chromatography. Their structure, once established, can be used to determine the nature of the monomer units within the polymer. Numerous nucleophiles have been used including benzylthiol (Foo and Karchesy,1991), benzyl mercaptan (Guyot *et al.*,1997; Matthews *et al.*,1997) or phrologlucinol (Brandon *et al.*,1982; Koupai-Abyazani *et al.*,1992; Prieur *et al.*,1994; Achmadi *et al.*,1994). Depolymerisation in the presence of a nucleophile offers several advantages. Associated with the quantitative analysis of the products by

chromatography, it may simultaneously offer information on the nature of the proanthocyanidins. In contrast to colorimetric methods, interferences with other plant constituents are avoided due to the nonambiguous identification identification of the proanthocyanidin-derived products. In comparison to the butanol/HCl depolymerisation, the reaction preserves the stereochemistry at the C2-C3 positions of the polymer units. The use of a nucleophile limits the occurrence of side reactions that could affect recovery yields of the products (Matthew *et al.*, 1997).

1.2.2 Uses of tannins

The tannins are applied widely, with uses ranging from tanning, known over millennia (since *ca.* 1500 BC), through medical uses to uses in the food industry. The biological significance (e.g. protection of plant from insects, diseases and herbivores) and current uses (e.g. leather manufacture) and promising new uses (e.g. as pharmaceuticals and wood preservatives) of tannin rest on their complexation with other biopolymers (e.g. proteins and carbohydrates, or metal ions) (Farreira *et al.*,1999).

Leather tanning industry is one of the most ancient industries known. Although the technology of leather has evolved over the years, the basic principles for the production of leather have remained the same. Hide proteins, mainly collagen, are rendered insoluble and dimensionally more stable by treatment with chemical products such as natural vegetable tannins so as to produce leather which is more resistant to mechanical ware and less susceptible to biological

and other types of attack. In view of the continuing interests in producing quality leathers, a new formulation of sulfonated melamin-urea-formaldehyde resin containing different vegetable tannins which is able to produce leather with the same good characteristics of leather prepared with chrome salts has been developed (Simon and Pizzi, 2003). In addition Pizzi *et al.* (2004) have established the correlation between the antioxidant capability of tannins and the problem of colour variation of leather.

Tannins as adhesives perhaps are the second most important bulk use other than for leather. Their use as wood adhesives is based mainly on the reaction, gelling and hardening of these tannins and formaldehyde (Garnier *et al.*, 2002). Recent studies on tannin-based adhesives have included rheological studies of various tannin extracts (Garnier *et al.*, 2001; Garnier *et al.*a,b, 2002), the building of time-temperature-transformation curing diagrams for the understanding of the behaviour of thermosetting resins under isothermal cure conditions and continuous heating transformation (Garnier and Pizzi, 2001), condensed tannin of Douglas-fir and polyethylenimine as formaldehyde-free wood adhesives (Li *et al.*, 2004) and bonding quality of Eucalyptus globules plywood using tannin-phenol-formaldehyde adhesives (Vazquez *et al.*, 2003).

Following the realisation that a wide range of herbal medicines and foodstuffs may be credited for preventive effects on chronic diseases due to their radical scavenging activities or antioxidant properties, increasing attention has been directed to the development of safe and effective functional foods and extraction of novel antioxidants from medicinal plants (Latte and Kolodziej, 2004). Indeed

the radical scavenging activities or antioxidant capabilities of tannins have been confirmed by several authors evaluated by colorimetry (Minussi *et al.*, 2003; Gulcin *et al.*, 2003; Goh *et al.*, 2003; Mi-Yea *et al.*, 2003; Cakir *et al.*, 2003; Nessa *et al.*, 2004), electron spin resonance (ESR) techniques (Noferi *et al.*, 1997; Fedeli *et al.*, 2004), chemiluminescence (CL) techniques (Ohtani *et al.*, 2000; Latte and Kolodziej, 2004) and Rancimat and Oxidograph tests (Lampart-Szczapa *et al.*, 2003). An overview on the biological activities of proanthocyanidins as regards to its antimicrobial and antiviral properties, enzyme-inhibiting properties, mutagenicity, antimutagenicity and antitumoral activity and antioxidative properties have also been summarised (De Bruyne *et al.*, 1999).

Recent development of the industrial uses of tannins as corrosion inhibitors in the formulations of pigments in paint coatings (Foster *et al.,* 1991; Matamala *et al.*, 1994; Batis *et al.*,1997; Clough, 1997; Pardini *et al.*,2001), flocculants (Kelly *et al.*,1988; Meyer and Woods,1993; Lamb and Decusati, 2002;) depressants (Bulatovic and Salter,1989), viscosity modifier agent, chemical cleaning agents for removing iron-based deposits (AL-Mayauf, 1997) and oxygen scavengers for boiler water treatment system (Sato et al., 1990; Yoshiaki and Toshinobu, 1994) reflects their importance as industrial raw materials relative to the synthetic phenols.

1.3 Corrosion inhibitors

In many industries, the need to use constructional materials safely, but cost-effectively, is a primary consideration. Frequently, physical requirements can be satisfied easily, but corrosion effects seriously complicate the selection of suitable materials. Generally, increased corrosion-resistance can only be obtained at increased cost. However, the actual material-related costs incurred in a project will depend on the corrosivity of the environment concerned, the required design life, the physical requirements of the material, and the readily available stocks. In some cases, appearance may also dictate the use of a more expensive material. The costs and problems associated with corrosion-resistant materials means that, in many cases, the use of corrosion inhibitors is a practical and economic alternative. Industrial use of corrosion inhibitors is, therefore, now broad based and extensive.

1.3.1 Classification of corrosion inhibitors

At the simplest level, a corrosion inhibitor is a substance which when added in small concentration to an environment effectively reduces the corrosion rate of a metal exposed to that environment. Scientifically, exacting definition is really not possible in general sense where mechanistic and/or chemical considerations serve to sub-divide corrosion inhibitors into specific types or classes.

Classification of corrosion inhibitors is somewhat a subjective exercise being very much dependent on the method employed. For example, one could choose

to classify in terms of mechanism and environment to which they are added. Inhibitor such as 2,5-bis(3-pyridyl)-1,3,4-thiadiazole (El Azhar *et al.*, 2002) is catogerised as an anodic inhibitor, 2-napthalene sulfonic acid (Vracar and Drazic, 2002) and salicyclic acid hydrazide (Quraishi *et al.,* 2001) as cathodic inhibitors while mercapto-triazole derivatives (Wang *et al.*, 2004), 2-mercaptobenzoimidazole (Morales-Gil *et al.*, 2004), benzoic acid hydrazide (Quraishi *et al.*, 2001), diazoles (Popova *et al.*, 2003), L-ascorbic acid (Ferreira *et al.*, 2004) and triphenyl phosphonium chloride (Khaled, 2004) are mixed type inhibitors. These categorisations however are dependent on the metals, type and concentrations of the corrosion medium under study. For example 3,5-bis(4-methylthiophenyl)-4H-1,2,4-triazole on mild steel is a mixed type inhibitor in 1 M HCl and a cathodic inhibitor in 0.5 M H_2SO_4 (Lagrenee *et al.,* 2002).

1.3.2 Effects of corrosion inhibitors on corrosion processes

Studies have shown that the efficiency of inhibition can be qualitatively related to the amount of adsorbed inhibitor on the metal surface. The adsorption of inhibitors is governed by the residual charge on the surface of the metal and by the nature and chemical structure of the inhibitor. The two main types of adsorption of an inhibitor on a metal surface are physical or electrostatic and chemisorption. Adsorption isotherms are often used to demonstrate the performance of adsorbent-type inhibitors. The adsorption of several inhibitors have been described by Langmuir (El Azhar *et al.*, 2002; Morales-Gil *et al.,* 2004; Hui-Long *et al.*, 2004), Temkin (Quraishi *et al.*, 2001; Hosseini *et al.*,

2003; Lgamri *et al.,* 2003; Khaled, 2004) and Frumkin (Vracar and Drazic, 2002; Popova *et al.*, 2003) adsorption isotherms.

Physical adsorption is due to the electrostatic attraction between the inhibiting ions or dipoles and the electrically charged surface of the metal. The forces in the electrostatic adsorption are generally weak. The inhibiting species adsorbed on the metal due to electrostatic forces can also be desorbed easily. A main feature of electrostatic adsorption is that the ions are not in direct physical contact with the metal. A layer of water molecules separates the metal from the ions. The physical adsorption process has a low activation energy and is relatively independent of temperature (Mansfield, 1987a).

Chemisorption is probably the most important type of interaction between the metal surfaces and an inhibitor molecule. The adsorbed species is in contact with the metal surface. A coordinate type of bond involving electron transfer from inhibitor to the metal is assumed to take place in the process. An opposing view, that there is necessarily no chemical bond between the metal and the adsorbed species. The chemisorption process is slower than electrostatic sorption and has higher activation energy. The temperature dependency shows higher inhibition efficiencies at higher temperatures. Unlike electrostatic adsorption, it is specific for certain metals and is not completely reversible. Adsorption results from polar or changed nature of the organic molecule/ionic species first establishing a physisorbed surface film (through Van der Waals forces) which may further stabilize through chemisorption to form a donor type bond. Electron transfer from the adsorbed species is favoured by the presence of relatively loosely bound electrons such as in anions and neutral

organic molecules containing lone pair electrons or π-electron systems associated with multiple bonds, especially triple, bonds or aromatic rings. In general, the organic inhibitors used have functional groups which are sites for the chemisorption process. Lone pair electrons for coordinate bonding occur in functional groups containing elements of group V and VI of the Periodic table. The tendency to stronger co-ordinate bond formation (and hence stronger adsorption) by these elements increases with decreasing electronegativity is in the order O < N < S < Se and depends on the nature of the functional groups containing these elements (Mansfield, 1987a).

The above sequence has also been explained on the basis of electron density and polarizability of the elements. On this basis, a surface bond of the Lewis acid-base type, normally with the inhibitor as electron donor and the metal as electron acceptor has been postulated. The hard and soft acid base theory has been applied to the corrosion inhibition phenomena with inhibitors being arbitrarily termed as 'hard' and 'soft' inhibitors. Softness and hardness are associated with high and low polarizability respectively. According to the hard and soft acid base (HSAB) principle, hard acids react with hard bases more readily than with soft bases. Neutral metal atoms are soft acids which tend to react with soft bases such sulphur-bearing inhibitors. Nitrogen-containing or oxygen-containing inhibitors are considered to be hard bases and may establish weaker bonds with metal surfaces (Mansfield, 1987a; Sastri, 1998c).

1.3.3 Mechanism of adsorption of inhibitors

The corrosion of metals in aqueous acidic solutions can be inhibited by a very wide range of substances including CrO_4^{2-}, MoO_4^{2-} (Abd Rehim *et al.*, 2004; Wang *et al.*, 2004; Refaey, 2005), phosphates (Refaey, 2005), bismuth(III) compounds (Hayashi *et al.*, 1996) and organic compounds that contain nitrogen, sulphur, oxygen and multiple bonds in the molecules. These organic compounds have therefore continued to provoke research interests (Lagrenee *et al.*, 2002; Branzoi *et al.*, 2002; Hosseini *et al.,* 2003; Lgamri *et al.,* 2003; Osman *et al.*, 2003; Maayta and Al-Rawashdeh, 2004; Ozcan *et al.,* 2004; Ravichandran *et al.*, 2004; Hui-Long *et al.*, 2004; Morales-Gil *et al.*, 2004; Ferreira *et al.*, 2004). It is often not possible to assign a single general mechanism of action to an inhibitor, because the mechanism may change with experimental conditions. Thus, the predominant mechanism of action of an inhibitor in acidic solutions may vary with factors such as concentration, the pH of the acid, the nature of the anion of the acid, the presence of other species in the solution, the extent of reaction to form secondary inhibitors and the nature of the metal (Shreir, 1978).

The anodic and cathodic reactions involved in the corrosion of metal in acidic solutions are:

$M \rightarrow M^{n+} + ne$ anodic (1.1)

$H^+ + e \rightarrow H$ cathodic (1.2)

$H + H \rightarrow H_2$ (1.3)

The adsorbed inhibitor blocks either the anodic or cathodic reaction or both. Adsorption is the primary step in achieving inhibition in acid solutions. This is a consequence of the fact that the corroding metal surface to be inhibited is usually oxide-free allowing the inhibitor ready access to retard the cathodic and/or the anodic electrochemical processes of corrosion. Once the inhibitor has adsorbed on the metal surface it can then affect the corrosion reactions in a number of ways: by offering a physical barrier to the difussion of ions or molecules to or from the metal surface; direct blocking of anodic and/or cathodic reaction sites; interaction with corrosion reaction intermediates; change the make-up of the electrical double layer which develops at the metal/solution interface and so affect the rate of electrochemical reactions (Harrop, 1991).

The adsorbed inhibitor may not cover the entire metal surface, but occupies sites which are electrochemically active and thereby reduces the extent of anodic or cathodic reaction or both. The corrosion rate will be decreased in proportion to the extent to which the electrochemically active sites are blocked by the adsorbed inhibitor. Comparison of the electrochemical polarization curves obtained both in the presence and absence of an inhibitor shows a shift of the polarization curves in an inhibitor containing solutions to lower current density values without any change in Tafel slopes. This shows that there is no change in the reaction mechanism. Anodic dissolution of metals is assumed to be a stepwise reaction with adsorbed intermediates on the surface of the metal. In the anodic dissolution of iron, adsorbed intermediate FeOH is assumed and on addition of an organic inhibitor, a complex of the type [FeOH.I] adsorbed on the surface of iron is assumed. This surface complex changes the reaction

mechanism with an increase in the anodic Tafel slope (Shreir, 1978b; Mansfield, 1987a).

Inhibition of the corrosion of metals and alloys in near-neutral aqueous solutions has been achieved in many cases by using inorganic compounds (Refaey and Abd El Rehim, 1996; El Sherbini and Abd El Rehim, 2000; Abdel Rehim *et al.*, 2004; Amin, 2005) as well as organic compounds (Rocca *et al.*, 2001; Rocca and Steinmetz, 2001; Rocca *et al.*, 2004; Peultier *et al.*, 2003). The corrosion processes result in the formation of sparingly soluble surface products such as oxides, hydroxides, or salts. The cathodic partial reaction is oxygen reduction. In these cases, the inhibitor action will be exerted on the oxide-covered surface by increasing or maintaining the protective characteristics of the oxide or of the surface layers in the aggressive solutions. The displacement of preadsorbed water molecules by adsorbing inhibitor molecules may be usually considered the fundamental step of inhibition. Chemical or electrochemical reactions of the inhibitor at the surface may also be assumed in order to explain the inhibitor efficiency. Because of these reactions, additional inhibitor uptake may take place.

As a result of the adsorption of the inhibitor at the oxide-covered metal surface, there may be different inhibition mechanisms. Thick surface layers having poor electronic-conductive properties are found in the presence of inhibitors that restrict diffusion of oxygen; these additives interfere with the oxygen reduction reaction and are referred to as cathodic inhibitors. Additives giving rise to thin passivating films usually inhibit the anodic metal dissolution reaction; as a

consequence, these types of inhibitors are considered anodic inhibitors (Mansfield, 1987a).

Mansfield (1987a) further remarked that the mechanism of action of both inorganic and organic inhibitive anions on the corrosion of various metals such as Fe, Al, and Zn in near-neutral solutions involves the following:

- Stabilization of the passivating oxide film by reducing its dissolution rate
- Repassivation of the surface due to repair of the oxide film by promoting re-formation of the oxide
- Repair of the oxide film by formation of insoluble surface compounds and consequent plugging of pores
- Prevention of the adsorption of aggressive anions because of the competitive adsorption of inhibitive anions.

1.4 Methods of evaluations of corrosion inhibition

Good reproducibility of the levels of inhibition in test procedures is rendered difficult due to the complexity of the factors controlling corrosion and its inhibition. These factors include the surface condition of the metal, temperature and the composition of the environment. Similar difficulties exist in the assessment of corrosion and its inhibition. Since corrosion inhibitors are used in a wide range of applications, no universal test method is possible. Even within one type of application there will be a range of requirements and a diversity of opinions on the definition of effective inhibition.

Measurement of mass loss is probably the widely used method of inhibition assessment. However care is required in both the technique and the interpretation of results. In the solution analysis method, determinations are made of the changes with time in the content of metal ions measured and inhibition will be reflected in the analytical data. There are also published tests methods, often referred to as standard test methods. These test methods are identified by numbered documents such as the salt spray (fog) corrosion test which is given in ASTM B117. The electrochemical methods which are applied to liquid phase systems include the measurement of electrode potential, polarization of electrode reactions, galvanic currents, electrical resistance, capacitance, ac impedance techniques and noise measurements (Mercer, 1985). However, mass loss measurements (Lagrenee *et al.*, 2002; El Azhar *et al.*, 2002; Abd. El-Maksoud, 2002 ; Hui-Long *et al.*, 2004; Maayta *et al.*, 2004; Ravichandran *et al.*, 2004; Ferreira *et al.*,2004) polarization measurements

(Tommesani *et al.*, 1997 ; Vracar and Drazic, 2002 ; El Azhar *et al.*, 2002; Abd. El-Maksoud, 2002; Hoesseini *et al.*, 2003; Popova *et al.*, 2003; Quraishi and Jamal, 2003 ; Osman *et al.*, 2003 ; Hui-Long *et al.*, 2004; Maayta *et al.*, 2004; Ozcan *et al.*, 2004; Ravichandran *et al.*, 2004;) and ac impedance techniques (Tommesani *et al.*, 1997; El Azhar *et al.*, 2002; Abd. El-Maksoud, 2002; Yadaf *et al*, 2004; Lgamri *et al.*, 2003; Hoesseini *et al.*, 2003; Popova *et al.*, 2003; Ravichandran *et al.*, 2004; Ozcan *et al.*, 2004) remained as the commonly used methods of evaluation.

1.4.1 Stern-Geary theory

Most modern corrosion techniques are based on the theoretical analyses of the shape of polarisation curves by Stern and Geary which was first introduced in 1957 (Stern and Geary, 1957) and since then has been expended and developed (Sastri, 1998a). In a simple non-corroding system containing M and M^+ at equilibrium:

$$M^+ + e \Leftrightarrow M^o \tag{1.4}$$

$$i_{R,M} = i_{O,M} = i_{ex} \tag{1.5}$$

where $i_{R,M}$ is the current for reduction of M^+

$i_{O,M}$ is the current for oxidation of M

i_{ex} is the exchange current (similar to i_{corr} in a corrosion process)

If a potential is applied on the metal from an external source and the reaction rate is controlled by a slow chemical step that requires an activation energy:

$$i_{R,M} = i_{ex} e^{-\eta/\beta} \tag{1.6}$$

$$i_{O,M} = i_{ex} e^{\eta/\beta''} \tag{1.7}$$

Where η is the overvoltage, the difference between the potential applied on the metal and the corrosion potential ($\eta = E_{app} - E_{corr}$) and β' and β'' are constants. Taking the logarithm of equations (1.6) and (1.7) and solving for η gives

$$\eta = -\beta_c \log \frac{i_{R,M}}{i_{ex}} \tag{1.8}$$

$$\eta = \beta_A \log \frac{i_{O,M}}{i_{ex}} \tag{1.9}$$

Where β_c =2.3β' and $\beta_A = 2.3\beta''$

Equations (1.8) and (1.9) are known as Tafel equation after J. Tafel who proposed equations of a similar form to express hydrogen overvoltage as a function of current density.

The equilibrium state of the reaction is perturbed by the application of an external potential. Experimentally, the total current is measured which is the difference between the rate of oxidation and rate of reduction.

$$i_{meas} = i_{R,M} - i_{O,M} \tag{1.10}$$

As the difference between E_{app} and E_{corr} becomes more negative, i_{meas} approaches $i_{R,M}$. Substituting equation (1.11) into equation (1.12) gives equation (1.13)

$$10^{-\eta/\beta_c} = \frac{i_{R,M}}{i_{corr}} \tag{1.11}$$

$$\log \frac{i_{R,M}}{i_{corr}} = -\eta / \beta_c \tag{1.12}$$

$$\eta = \beta_c \log \frac{i_{meas} + i_{O,M}}{i_{ex}} \tag{1.13}$$

Deviation from Linear Tafel behaviour occurs at low current levels. When the oxidation current becomes insignificant with respect to reduction current, a true Tafel behaviour can be expected.

The relationships given so far depend only on activation overvoltage. The measurement maybe affected by concentration polarisation and a drop in resistance. Concentration polarisation occurs when the reaction rate is so high that the electroactive species cannot reach or be removed from the electrode surface at a sufficiently rapid rate. The reaction rate becomes diffusion controlled. As η increases, the current becomes diffusion limited and the linear current range becomes smaller. Stirring the solution minimizes the effect of concentration polarisation.

The drop in resistance across the solution can also cause non-linear Tafel behaviour at high currents:

$$E_{IR} = i_{meas} R_{soln} \tag{1.14}$$

R_{soln} is the uncompensated resistance of the solution or the resistance between the working electrode and the reference electrode bridge tube and this depends on the geometry of the electrodes. As i_{meas} increases, E_{IR} also increases, causing an error in the true potential at the working electrode. The effects of

concentration polarisation and resistance drop are serious when i_{ex} or i_{corr} is large and high currents are required to verify Tafel behaviour. As a general rule, linearity over two decades of current is desirable. This may then necessitate current measurements in the region of $1000 i_{corr}$.

In a corroding system, the situation is more complicated. In addition to the reaction discussed so far,

$$M^+ + e \Leftrightarrow M^o \tag{1.4}$$

where M^o/M^+ is the redox system related to the solvent, the corroding metal must also be considered

$$C^+ + e \Leftrightarrow C^o \tag{1.15}$$

and each of these systems has its own equilibrium potential, exchange current and Tafel slope. At the corrosion potential,

$$i_{R,M} + i_{R,C} = i_{O,M} + i_{O,C} \tag{1.16}$$

The corrosion rate by definition is $i_{O,C} - i_{R,C}$. By rearranging equation (1.16) it may also be defined as $i_{R,M}$-$i_{O,M}$. When the corrosion potential of the mixed electrode system is sufficiently different from the equilibrium potentials of the individual reactions, then $i_{R,C}$ and $i_{O,M}$ become insignificant in comparison to $i_{O,C}$ and $i_{R,M}$ respectively. The corrosion rate i_{corr} then becomes equal to $i_{O,C}$ or $i_{R,M}$. The corrosion potential is closely approximated by the potential at which

$$i_{R,M} = i_{O,C}. \tag{1.17}$$

A high corrosion current in conjunction with a low diffusion-limited current and a high solution resistance may reduce the linear portion of the Tafel region to

such an extent that an extrapolation to i_{corr} becomes difficult. In most instances, non-linear Tafel behaviour can be minimized by stirring the solution and compensating instrumentally for resistance drop (*IR*) effects.

1.4.2 Use of Tafel plots

A Tafel plot can be performed on a sample by polarising the sample about 300mV anodically (positive potential direction) and cathodically (negative potential direction) from the corrosion potential, E_{corr}. The potential does not have to be scanned but can be stepped in a staircase waveform. The potential scan rate can be 0.1 – 1.0 mV s^{-1}. The resulting current is plotted on a logarithmic scale as shown in Fig. 1.6. The corrosion current, i_{corr} is obtained from a Tafel plot by extrapolation of the linear portion of the curve to E_{corr}.

According to the Tafel equation:

$$\eta = \beta \log \frac{i}{i_{corr}} \tag{1.18}$$

where η is the overvoltage, which is the difference between the potential of the sample and its corrosion potential, β is the Tafel constant, i is the current in μA corresponding to the overvoltage and i_{corr} is the corrosion current, in μA.

$$\eta = \beta(\log i - \log i_{corr}) \tag{1.19}$$

When η is plotted against log i, this equation should give a straight line with a slope of β. When η=0 (at E_{corr}), $\log \frac{i}{i_{corr}}$=0 or $\frac{i}{i_{corr}} = 1$ or $i = i_{corr}$. (1.20)

Tafel constants, β_A and β_C can be calculated for both the anodic and cathodic parts of the Tafel plot and are expressed in mV decade^{-1}.

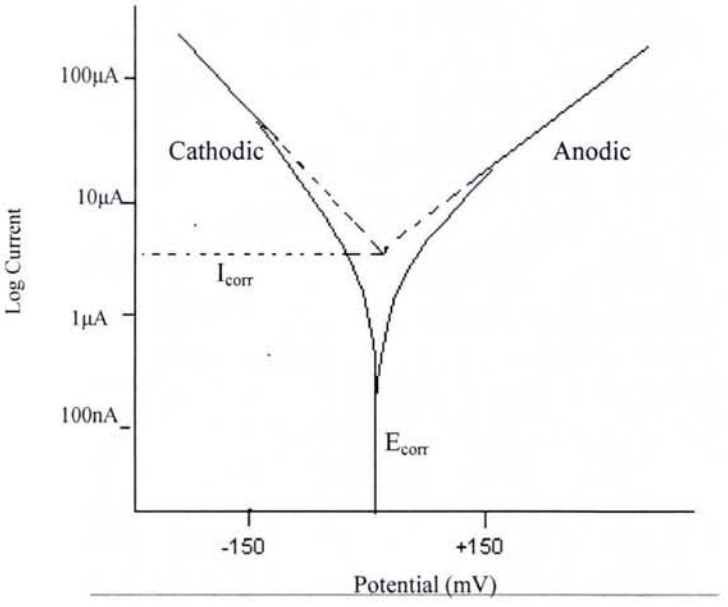

Fig. 1.6 An example of a Tafel plot.

1.4.3 Polarisation resistance

This technique is used to measure absolute corrosion rates, usually expressed in milli-inches per year (mpy). This technique, also known as linear polarisation, is rapid (in less than ten minutes) and the corrosion rate data obtained by this technique correlate well with data from the weight-loss method. Polarisation resistance measurement may be performed by scanning through a potential range of about 25 mV above and below the corrosion potential. The resulting current is plotted against the potential as shown in Fig. 1.7. The corrosion current, i_{corr}, is related to the slope of the line

$$\frac{\Delta E}{\Delta i} = \frac{\beta_A + \beta_C}{2.3(i_{corr})(\beta_A + \beta_C)} \qquad (1.21)$$

Where $\Delta E/\Delta i$ is the slope which is the polarisation resistance, β_A and β_C are anodic and cathodic Tafel constants and i_{corr} is the corrosion current in μA.

Rearranging the above equation, we have

$$i_{corr} = \frac{\beta_A \beta_C}{2.3(\beta_A + \beta_C)}\left(\frac{\Delta i}{\Delta E}\right) \tag{1.22}$$

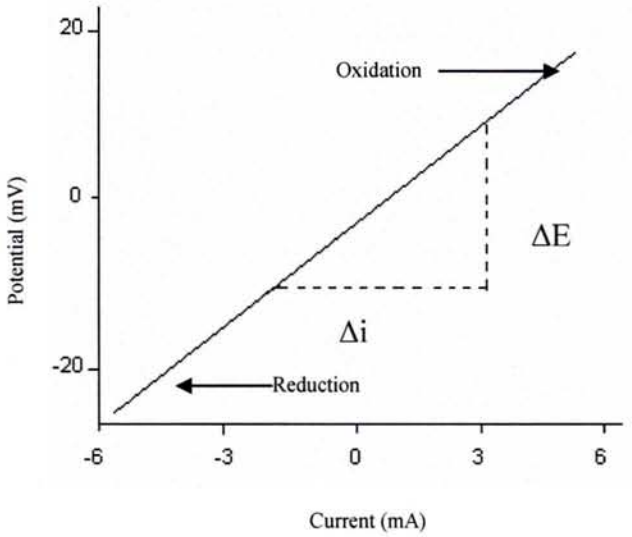

Fig. 1.7 An example of a polarisation resistance curve.

The theoretical basis for polarisation resistance measurements provided by Stern and Geary can be summarised as follows. In a corroding system, two co-existing chemical reactions are present.

$$C^+ + e \Leftrightarrow C^o \tag{1.15}$$
$$Z^+ + e \Leftrightarrow Z^o \tag{1.23}$$

Where C is the corroding metal and Z is another species in solution. The equilibrium potentials of the couple are $E_{eq,C}$ and $E_{eq,Z}$. When the corrosion potentials are sufficiently removed from the equilibrium potentials ($E_{eq,C}$, $E_{eq,Z}$)

the rate of reduction of C^+ becomes insignificant compared to the rate of oxidation of C, and the rate of oxidation of Z becomes insignificant with respect to the reduction of Z^+. The corrosion potential is the potential at which the rate of oxidation of $C(i_{O,C})$ is equal to the rate of reduction of $Z^+(i_{R,Z})$. The net current is the difference between the oxidation and reduction currents

$$i_{meas} = i_{O,C} - i_{R,Z} = 0 \text{ at } E_{corr} \text{ and } i_{corr} = i_{O,C} = i_{R,Z} \quad (1.24)$$

When a potential is applied on the sample from an external source such as a potentiostat, the measured current

$$i_{meas} = i_{O,C} - i_{R,Z} \quad (1.25)$$

The anodic and cathodic currents obey the Tafel equations

$$\eta = \beta_A \log \frac{i_{O,C}}{i_{corr}} \quad (1.26)$$

$$\eta = \beta_C \log \frac{i_{R,Z}}{i_{corr}} \quad (1.27)$$

Where $\eta = E_{app} - E_{corr}$. Rearrangement of the above equation gives

$$\log \frac{i_{O,C}}{i_{corr}} = \eta / \beta_A \quad (1.28)$$

$$\log \frac{i_{R,Z}}{i_{corr}} = -\eta / \beta_C \quad (1.29)$$

The above equations may be rewritten as

$$\log 10^{\eta/\beta_A} = \frac{i_{O,C}}{i_{corr}} \quad (1.30)$$

$$\log 10^{-\eta/\beta_C} = \frac{i_{R,Z}}{i_{corr}} \quad (1.31)$$

Then the equation for measured current will be

$$i_{meas} = i_{corr}\left(10^{\eta/\beta_A} - 10^{-\eta/\beta_C}\right) \tag{1.32}$$

Considering the power series

$$10^x = 1 + 2.3x + \frac{(2.3x)^2}{2!} + \ldots + \frac{(2.3x)^n}{n!} \tag{1.33}$$

When x has a small value, the third and higher terms become negligible

$$10^{\eta/\beta_A} = 1 + 2.3\,\eta/\beta_A \tag{1.34}$$

$$10^{\eta/\beta_C} = 1 - 2.3\,\eta/\beta_C \tag{1.35}$$

Substituting these values into the i_{meas} equation and simplifying

$$i_{meas} = 2.3 i_{corr}\eta\left(\frac{\beta_A + \beta_C}{\beta_A \beta_C}\right) \tag{1.36}$$

The above equation in the case of polarisation resistance becomes

$$\eta/i_{meas} = \frac{\beta_A \beta_C}{2.3 i_{corr}(\beta_A + \beta_C)} \tag{1.37}$$

This equation is valid when η/β is small, with typical value of β=100 mVdecade^{-1} with an overvoltage less than 10 mV.

The polarisation resistance method is an extremely rapid technique for the determination of corrosion rates. Rapidity of the technique makes it as a useful method for the qualitative evaluation of inhibitors. Since the applied potential is not far removed from the corrosion potential, the surface of the sample is not very much affected and hence the sample can be used repeatedly.

1.5 Tannins - an alternative choice in corrosion protection

The atmospheric corrosion of steel structures often results in the formation of iron oxyhydroxides such as geothite (α-FeOOH), lepidocrocite (γ-FeOOH), and akagonite (β-FeOOH) as well as iron oxides such as magnetite (Fe_3O_4) and maghemite (γ-Fe_2O_3) (Naszarani, 1997). The specific composition of a given rust formed depends on pH, temperature and the presence or absence of atmospheric pollutants. The atmospheric corrosion or rusting of iron and steel is electrochemical in nature. The anodic partial reaction is given by the metal dissolution :

$$Fe \rightarrow Fe^{2+} + 2e \qquad (1.38)$$

And the cathodic partial reaction involves oxygen reduction as the dominant reaction :

$$\tfrac{1}{2}O_2 + H^+ + 2e \rightarrow OH^- \qquad (1.39)$$

Hydrogen reduction may also occur :

$$2H^+ + 2e \rightarrow H_2 \qquad (1.40)$$

The hydrogen reduction should dominate over the oxygen reduction at pH values below 4, but it has been shown experimentally that the electrolyte on top of iron based metals is well buffered (pH 5.8-7) and therefore the rate of hydrogen reduction is negligible as compared to the rate of oxygen reduction (Stratmann,1990).

A third cathodic reaction is the reduction of Fe^{3+} ions within the rust scale :

$$8FeOOH + Fe^{2+} + 2e \rightarrow 3Fe_3O_4 + 4H_2O \qquad (1.41)$$

According to Pourbaix (1973), the corrosion of iron gives rise to the dissolution of metal mainly with the formation of green ferrous ions :

$$Fe + 2H^+ \rightarrow Fe^{2+} + H_2 \quad (1.42)$$

or the green dihypoferrite ions depending on whether the pH is greater or less than 10.6:

$$Fe + 2H_2O \rightarrow FeOOH^- + H^+ + H_2 \quad (1.43)$$

At pH below about 6 – 7, Fe^{2+} ions may change to black magnetite :

$$3\ Fe^{2+} + 4H_2O \rightarrow Fe_3O_4 + 6\ H^+ + H_2 \quad (1.44)$$

or into white ferrous hydroxide :

$$Fe^{2+} + 2H_2O \rightarrow Fe(OH)_2 + 2H^+ \quad (1.45)$$

Due to their thermodynamically unstable state, ferrous hydroxide and magnetite may be oxidised to ferric hydroxide and ferric oxide respectively :

$$4Fe(OH)_2 + O_2 + 2H_2O \rightarrow 4Fe(OH)_3 \quad (1.46)$$

and

$$4\ Fe_3O_4 + O_2 \rightarrow 6Fe_2O_3 \quad (1.47)$$

1.5.3 Tannins as corrosion inhibitors and rust converters

Tannins as corrosion inhibitors are applied both in solvent and waterborne pretreatment formulations. These formulations could be applied on partially rusted substrates, reducing the effort needed for cleaning the surface by sandblasting or other methods which proved to be expensive and are not applicable in many situations. They have been called rust converters since their presence converts active rust into compounds that are more stable and corrosion resistant.

Various concrete structures are exposed to physical and chemical conditions which directly or indirectly affect the concrete structures. In order to solve problems due to moisture, waterproof treatments are commonly performed on most concrete facilities. According to Do-Chul and Won-Hwa (2004), tannins when added in waterproof admixture composition for concrete acted as antioxidant by reacting with calcium salts of calcium silicate hydrate, which is formed by hydration of cement. Hence the carbonation between calcium silicate hydrate and carbon dioxide in air which causes corrosion of reinforced concrete, is hindered.

Known corrosion inhibitors for medium and low pressure boiler systems for protecting metals contacted with water are hydrazines, sulfites or sugars. However, hydrazines have been found to be harmful to human bodies, sulfites are corrosion accelerators and sugars have been found to be insufficient in corrosion inhibiting capabilities. Thus a formulation comprising tannic acid and /or salt thereof; a sugar; and at least one member selected from aldonic acids or hexoses or salts thereof and aldonic acids of heptoses of salts thereof was carried out and was found to exhibit excellent corrosion inhibiting capabilities and not harmful to the human bodies (Sato *et al.,* 1990).

In another study on tannins as corrosion inhibitors, the use of tannic acid chelant agents in cleaning chemicals to remove iron-based deposits was found to show better inhibitive efficiency in neutral and weak acidic Na_2SO_4 solutions with the addition of thiosemicarbazide depending on the concentration of thiosemicarbazide, pH and immersion time (Mayouf, 1997). This study was

undertaken to overcome the problem of iron oxide deposits interfering with water flow in piping systems, tube overheating and the speeding of corrosion under deposits. Therefore removal of deposits will maximise thermal efficiency and help prevent serious problems.

Proper surface preparation is the key to obtaining good performance by a surface coating. The major problem in preparing a steel surface is the removal of all mill scale, rust and associated contaminants from the substrate. Common steels are protected from corrosion principally by painting schemes in such applications as manufacturing, structure protection, and automobile fabrication. Paint life depends on various factors such as the metallic substrate, the selected painting scheme and the paint-substrate inter-phase. In automobile and manufacturing industries, where plain steel generally is painted, a wash primer coat is typically used to increase the adherence and to improve the anticorrosive quality of painting films. These primers, known as reaction primers are formulated basically with phosphoric acid (H_3PO_4) and zinc chromate ($ZnCrO_4$) in alcohol medium, where polyvinyl butyral participates as a ligand of the reaction product (Mansfield,1987b).

Chromate based pigments have been used for many years as anticorrosive pigments in wash primers and other alkyd and epoxy primers. In recent years, chromium, and especially chromates (hexavelant chromium), have have been found to cause irritation of the respiratory tract, produce ulcerations and perforations of the nasal septum, and produce lung cancer in workers employed in chromium manufacturing plants in West Germany and the United States

(Foster *et al.*,1991). Due to its toxicity, chromates constitute a hazard and need to be replaced by more environmentally acceptable corrosion inhibitors. In this sense a system containing tannins, a class of natural, non-toxic, biodegradable organic compounds has been proposed. Hydrolysable tannin, mainly from a chestnut tree, condensed tannin such as the mimosa tannin from the wattle tree and tannins comprising of hydrolysable and condensed tannin such as the oak tannin have since been the subject of inhibition studies (Ross and Francis, 1978; Gust,1991; Gust and Bobrowicz,1993; Gust and Sulwalski,1994; Pardini *et al.*, 2001; Martinez and Stern, 2001; Martinez and Stern, 2002; Martinez, 2002). Matamala *et al.* (1994, 2000) have also reported on the anticorrosive protection of tannins extracted from acacia and pine barks.

One of the reaction mechanisms of tannins with rust is suggested by Deslauriers (1987) which involves three general steps: (i) adsorption of the tannin to the rusty surface, (ii) complexation of ferrous/ferric ions or complexation of surface iron hydroxides/oxides followed by dissolution, and (iii) partial or complete readsorption of the iron-tannate complexes to the substrate. The following corrosion inhibiting mechanism was proposed when a reaction primer formulated with pine tannins at pH 3.2 was used :

$$Fe + 3H^+ + \tfrac{3}{4}\ O_2 = Fe^{3+} + 3/2\ H_2O \qquad (1.48)$$

$$Fe + 2H^+ + \tfrac{1}{2}\ O_2 = Fe^{2+} + H_2O \qquad (1.49)$$

$$Fe^{2+} + \tfrac{1}{4}\ O_2 + H^+ = Fe^{3+} + \tfrac{1}{2}\ H_2O \qquad (1.50)$$

$$\text{Tannin-OH} + Fe^{3+} = (\text{Tannin-O-}\ Fe^{3+})^{2+} + H^+ \qquad (1.51)$$

$$\text{Tannin-2OH} + Fe^{3+} = (\text{Tannin-2O-}\ Fe^{3+})^{+} + 2H^+ \qquad (1.52)$$

$$\text{Tannin-2OH} + (\text{Tannin-2O-}\ Fe^{3+})^{+} = (\text{2Tannin-4O-}\ Fe^{3+})^{-} + 2H^{+} \quad (1.53)$$

In the presence of oxides on the steel surface, the tannin reacted with ferrous or ferric ions according to the following reactions:

$$FeOOH + 3H^{+} = Fe^{3+} + 2H_2O \quad (1.54)$$

$$Fe_3O_4 + 8H^{+} = 2Fe^{3+} + Fe^{2+} + 4H_2O \quad (1.55)$$

$$Fe^{2+} + \tfrac{1}{4}O_2 + H^{+} = Fe^{3+} + \tfrac{1}{2}H_2O \quad (1.50)$$

The ferric ions formed in reactions (1.54) and (1.55) in turn reacted with tannins according to reactions (1.51) and (1.52). The iron-tannates formed contained corrosion inhibitor characteristics. Tannate formation acidified the reaction environment, making its reaction with clean or oxidized metallic substrate selfcatalysed (Matamala *et al.*, 1994).

A rapid reaction was found to occur between rusty iron and natural tannins. The transformation of rusty iron into the blue-black coating layer has been attributed to the complexation of the polyphenolics moiety of the tannin to the iron oxides and oxyhydroxides. Although other complexation products undoubtedly formed, the ferric tannate complex has been cited as the major product (Pardini *et al.*, 2001). Gust and Suwalski (1994) have reported that via Mossbauer spectroscopy, a mixture of mono and bis complexes (Fig.1.8) were formed as a result of a reaction between rust-phase components and oak tannins in aqueous solution while a reaction on a rusted surface covered with oak tannin gave mainly mono-type complexes. Similar mixture of mono and bis-type complexes was also observed by Jaen *et al.* (1999) when reacting several plant

extracts of Panama with ferrous and ferric salts. The view that ferric-tannate of dark blue colour are highly insoluble and acts as a barrier layer on the metal surface are shared by several authors (Seavell,1978; Gust and Bobrowicx,1993; Pardini *et al.*, 2001).

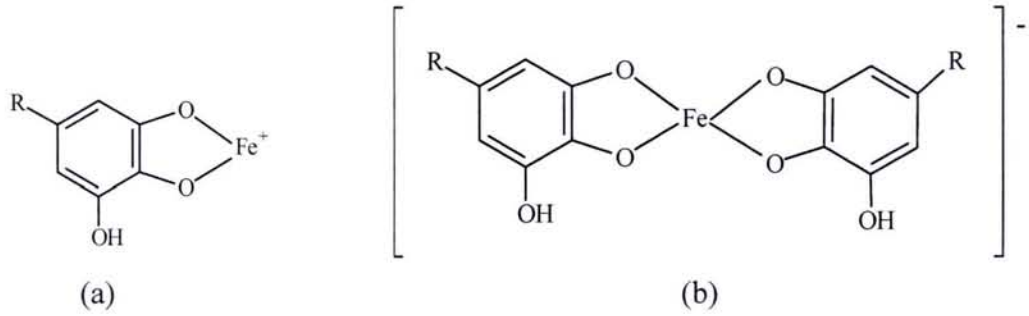

Fig. 1.8 Iron-tannate with (a) mono-complex and (b) bis-complexes.

The iron-tannate complexes formed from rust have been characterized as amorphous structures (Ross and Francis, 1978). However the protective efficiency of ferric-tannate against further corrosion generated contradictory opinions. According to Gust and Bobrowicz (1993) and Matamala *et al.* (1994), tannins are more effective when used in conjunction with phosphoric acid. On the other hand, Barrero *et al.* (2001) and Pardini *et al.* (2001) found the efficiency of this type of pretreatment to be inadequate. There is no universal agreement in the scientific literature on the changes undergone by rust layers on the application of tannins, but some (Ross and Francis, 1978; Lahodny-Sarc and Kapor, 2002) believe that the rust is transformed to magnetite. According to Ross and Francis (1978), mimosa solution was able to reduce ferric ions to ferrous ions forming ferrous- tannate, leading to the formation of magnetite by the following reaction, where R denotes the tannin molecule :

$$Fe(OR)_2 + 2FeOOH \rightarrow Fe_3O_4 + R2OH \qquad (1.56)$$

This reaction was assumed to have taken place after the solution had dried and the ferrous-tannate would probably exist within the rust and away from the atmosphere or the tannin may have directly reduce the lepidocrocite :

$$3FeOOH + ROH \rightarrow Fe_3O_4 + 2H_2O + R - O^{\cdot} \quad (1.57)$$

The tannin forms a radical and is then converted to unknown oxidation products. On the other hand, infrared spectroscopy studies (Nasrazadani, 1997) have shown that transformation to magnetite by tannic acid was not evident. Rather, tannic acid dissolves γ-FeOOH and precipitates ferric-tannate. This view is shared by Favre and Landolt (1993), proposing that lepidocrocite initially undergoes reduction with the formation of ferrous complex, where $R(OH)_n$ designates a tannin molecule :

$$\gamma\text{-}FeOOH + 2\{R(OH)_{n-1}O^-\} + 3H^+ + e \rightarrow Fe\{R(OH)_{n-1}O\}_2 + 2H_2O \quad (1.58)$$

But with time and in presence of air, the ferrous complex is oxidized, precipitating the insoluble ferric complex :

$$2\ Fe\{R(OH)_{n-1}O\}_2 + 2\{R(OH)_{n-1}O^-\} + 1/2O_2 + 2H^+ = 2\ Fe\{R(OH)_{n-1}O\}_3 + 2\ H_2O \quad (1.59)$$

Similarly, Jaen *et al.* (1999) observed the formation of solely insoluble chelating iron compounds, inferring the inhibition of the formation of oxides and oxyhydroxides of corrosion when reacting several plant extracts of Panama with ferrous and ferric salts.

1.6 Objectives

Due to the diversity of the material used in different studies, different explanations on the inhibitory mechanisms have been suggested. Despite the long and extensive studies of various tannin extracts in metallic corrosion inhibition and protection, little is known about the corrosive efficiency of mangrove tannins. It is therefore the aim of this research to :

i. Extract and identify the tannins of the barks of mangrove (*Rhizophora apiculata*), which are waste products of the charcoal industry.

ii. Determine the anticorrosive performance of mangrove tannins on steel through chemical and electrochemical evaluations in order to develop value-added mangrove-based products for industrial uses.

iii. Determine the inhibitory performance of the individual constituent of mangrove tannin on steel via electrochemical methods.

iv. Study the phase transformations induced by mangrove tannins on pre-rusted steels.

CHAPTER TWO

EXPERIMENTAL

2.1 Tannin extraction and condensed tannin isolation

Mangrove (*Rhizophora apiculata*) bark samples were obtained from the Larut Matang, Taiping, Malaysia charcoal industry. The barks were dried and grinded to ~ 250 mesh followed by further drying until a constant weight was obtained. The extraction of tannin from mangrove barks was carried out by total immersion of the finely ground barks in 70 % aqueous acetone for 72 hours (24 hours x 3 days) at 30 °C, according to the procedure by Ohara and Ohmura (1998) with a slight modification. The acetone (Merck) was removed under pressure and the resulting aqueous fraction was freeze-dried. The residual aqueous phase (1.5 g) was defatted with hexane, followed by the extraction with ethyl acetate (Merck) and the aqueous phase was freeze-dried. A fraction of the aqueous phase (1.0 g) was dissolved in methanol/water 1:1 and loaded onto a Sephadex LH-20 (Fluka) column. The column was washed with methanol (R&M chemicals)/water 1:1 to eliminate sugars and sugar-containing components and was eluted with acetone/water 1:1 to produce condensed tannin. A schematic diagram of the condensed tannin isolation process is as given in Figure 2.1.

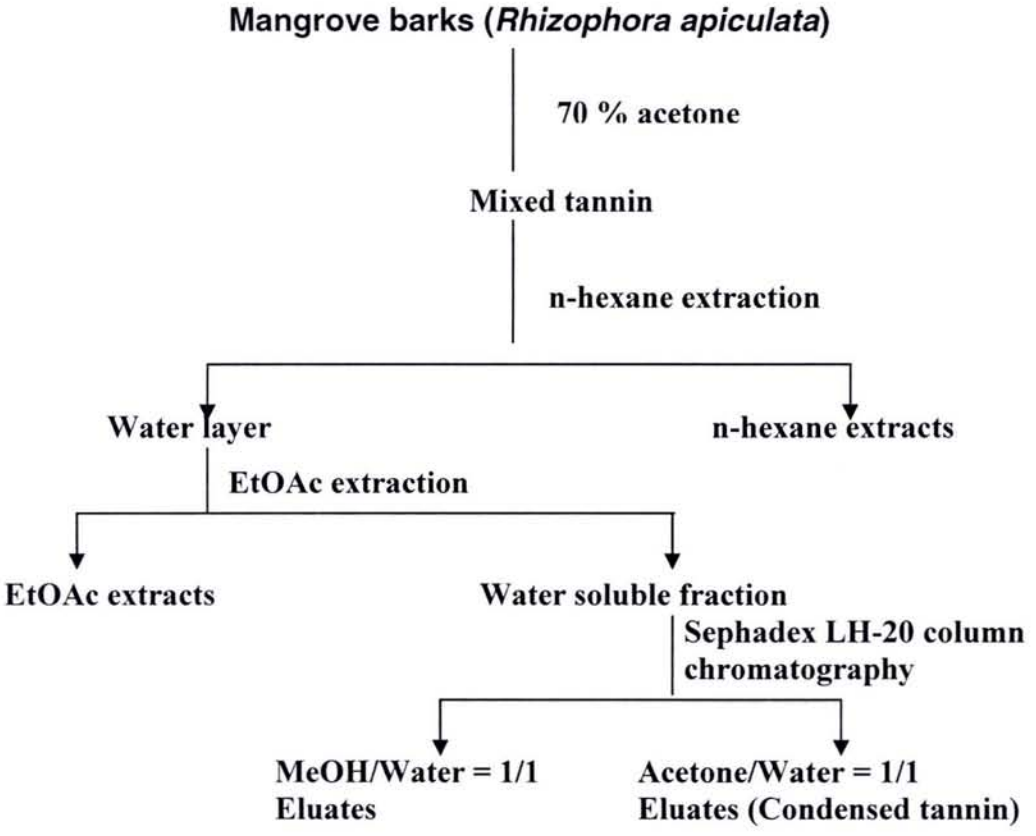

Fig 2.1 A schematic diagram of the extraction of condensed tannins.

FTIR spectrums of the extracted tannin and the mimosa, quebracho and chestnut tannins obtained from SILVACHIMICA, Italy were taken using a Perkin Elmer System 2000 Spectrometer. TGA/DTG analysis of the extracted tannins was conducted on Perkin Elmer Thermogravimetric analyser TGA 7. Experiments were done in oxygenated air at a heating rate of 20 °C min^{-1} and sample masses were about 5-10 mg.

2.1.1 Prussian blue assay for total phenols

The total phenols present in tannin samples was determined by the method proposed by Price and Butler (1977). In this method, $1.0x10^{-2}$ g sample was dissolved in 10 mL methanol (R&M chemicals). A volume of 0.10 mL sample was dispensed. This was followed by the addition of 50.00 mL distilled water and after one minute, 3.00 mL 0.1 M ferric ammonium sulfate, $FeNH_4(SO4)_212H_2O$ (Fluka)(prepared in 0.1 M HCl) was added and the resultant mixture swirled. After 20 minutes, 3.00 mL $8.0x10^{-3}$ M potassium ferriccyanide, $K_3Fe(CN)_6$ (Fluka) was added. The mixture was again swirled. After an interval of 20 minutes, the absorbance was read at 720 nm. The procedure was repeated for the blank and the standard solutions. A range of $5.0x10^{-4}$ M to $1.0x10^{-2}$ M gallic acid monohydrate (Fluka) standard solutions dissolved in methanol were prepared. The absorbance of each sample was taken in triplicates.

2.1.2 Vanillin assay for the determination of condensed tannins

The method by Price *et al.* (1978) was adopted for this assay. An amount of 1.0 % (w/v) of vanillin (Fluka) in methanol (R&M chemicals) was prepared and stored in a dark bottle and kept at 40 °C. The (+)-catechin hydrate (Fluka) standard solutions dissolved in methanol (R&M chemicals) ranging from $5.0x10^{-2}$ mg mL^{-1} to 0.3 mg mL^{-1} were prepared and stored in a dark bottle and kept at 4 °C. The vanillin reagent prepared daily was diluted with the same volume of 8.0 % HCl (J&T Baker) solution (prepared in methanol). The vanillin

reagent and 4.0 % HCl solutions were incubated at 30 °C before the start of the analysis.

An amount of 1.0 mL samples ($3.0x10^{-4}$ - $5.0x10^{-4}$ g mL^{-1}) were added into a test tube and incubated in the water bath. Two sets of each sample were prepared. Vanillin reagent (5 mL) was added at one minute interval to one set of samples and to the other set of samples 4.0 % HCl solution was added for the same time interval. After exactly 20 minutes of the vanillin reagent addition, the absorbance reading was taken at 280 nm. The procedure was repeated for the (+)-catechin hydrate standards. The absorbance of each sample was taken in triplicates.

2.1.3 Identification of condensed tannins

2.1.3.1 Phloroglucinol degradation

Two samplings of mangrove barks were collected a year apart and the condensed tannins was extracted according to the procedure in section 2.1.

Method 1. In the method proposed by Matthews *et al.* (1997), condensed tannins (25.0 mg), phloroglucinol (Fluka) (8.0 mg) and dioxane/aqueous HCL 0.2 M, 1:1 (0.5 mL) were added in a tube which was sealed and heated at 80 °C for 20 minutes. An aliquot was then diluted exactly with HPLC grade methanol (Fisher chemicals)/water 1:1.

Method 2. In this modified method by Foo and Karchesy (1991), condensed tannin ($1.0x10^{-2}$ g) was dissolved in 1.5 mL of the phloroglucinol (Fluka) solution [5 mg mL^{-1} phloroglucinol in acidic ethanol (Merck)] and allowed to react at room temperature overnight. The solvent was then evaporated under nitrogen, and the residue dissolved in 0.5 mL distilled water. This solution was extracted three times with ethyl acetate (Merck) (1.5 mL per extraction). The three ethyl acetate fractions were combined and evaporated under nitrogen. The residue was dissolved in 1.0 mL of 70 % aqueous HPLC grade methanol (Fisher chemicals). The procedure was repeated using (+)-catechin hydrate, (-)-epicatechin (Fluka), (-)-catechin, (-)-gallocatechin, (-)-epigallocatechin, (-)-catechin gallate, (-)-epicatechin gallate, (-)-gallocatechin gallate, (-)-epigallocatechin gallate (Sigma) and methanol-water fraction samples.

Method 3. The third method which was proposed by Achmadi *et al.* (1994) consisted of reacting condensed tannin (0.5 g) with phloroglucinol (Fluka) (0.5 g) in ethanol (Systerm) (5.0 mL) in the presence of acetic acid (1.0 mL) catalyst at 105 °C for 12 hours in a sealed ampule. After cooling, the product was diluted to 10 mL with water and extracted five times with ethyl acetate (20 mL per extraction). The ethyl acetate fractions (1.0 mL) were dissolved in 1.0 mL of 70 % aqueous methanol.

2.1.3.2 HPLC analysis

Degradation products were analysed on a Shimadzu AD-VP, utilizing a Crestpak C18S column (4.6 mm I.D.x 150 mm L), at a flow-rate of 1.0 mL min^{-1} and detected at 280 nm using a UV detecter. All solvents were filtered with

0.45 µm Millipore filter paper and degassed ultrasonically for 15-20 minutes. Of each sample 20 µL was injected. The elution conditions for method 1 (Matthews *et al.*, 1997) were as follows: Solvent A, water/phosphoric acid 999 : 1; solvent B, Methanol (Fisher chemicals); linear gradient 0-90 % B in 30 minutes.

Two elution conditions were used for method 2 : (i) Solvent A, 1.0 % aqueous acetic acid; solvent B, methanol; 0-30 minutes, 0-15 % B in A (linear gradient); 30-45 minutes 15-60 % B in A (linear gradient); 45-50 minutes, 60 % B in A (isocratic) (Koupai-Abyazani *et al.*, 1992). (ii) Solvent A, 1.0 % aqueous acetic acid; solvent B Methanol : Solvent A, 60 : 40 (v/v); t=0, 100 % solvent A; t=60 minutes, 40 % solvent A, 60 % solvent B; t= 65 min, 100 % solvent B (modified from Koupai-Abyazani *et al.*, 1992).

Elution of all flavanoid standards (1.0 mg mL^{-1}) were conducted at a flow rate of 0.5 mL min^{-1} and 1.0 mL min^{-1} using elution condition (i). The phloroglucinol (Fluka) and flavanoid standards (1 mg mL^{-1}) prepared in 70 % aqueous HPLC grade methanol (Fisher chemicals) were used to identify the peaks. Quantification of monomers was carried out on six degraded samples of condensed tannin by injecting duplicate samples. Calibration curves for (+)-catechin, (-)-epicatechin, (-)-epigallocatechin and (-)-epicatechin gallate were done using standard solutions of various concentrations.

2.2 Anti-oxidant activities

2.2.1 Reducing power

The reducing power of samples was determined by the method proposed by Gulcin *et al.* (2003) after a slight modification. Standard L(+)-ascorbic acid (Merck) solution of concentrations $2.0x10^{-2}$ mg mL^{-1} – 0.1 mg mL^{-1} were prepared. To 1.0 mL of the standard solution, 2.5 mL of 0.2 M phosphate buffer at pH 6.6 (prepared from the addition of 0.2 M Na_2HPO_4 and 0.2 M NaH_2PO_4 (AJAX chemicals) and 2.5 mL of 1% (w/v) potassium ferricynide,$K_3Fe(CN)_6$ (Fluka) solution were added. The mixture was incubated at 50 °C for 20 minutes after which 2.5 mL 10 % (w/v) trichloroacetic acid (ACROS) was added. The resultant mixture was centrifuged for 20 minutes at 2500 rpm. The upper layer (2.5 mL) was dispensed and 2.5 mL distilled water and 0.5 mL of 0.1 % (w/v) ferric chloride hexahydrate, $FeCl_36H_2O$ (Fluka) solution were added. The absorbance was measured at 700 nm. The procedure was repeated for (+)-catechin hydrate (Fluka) standard solutions, mangrove tannins, mimosa tannins, quebracho tannins and chestnut tannins (SILVACHIMICA, Italy).

2.2.2 DPPH free radical scavenging activity

The free radical scavenging activity of samples was measured according to the procedure by Glucin *et al.* (2003) with a slight modification. 1,1-diphenyl-2-picryl-hydrazil, DPPH (Aldrich) radical solution was prepared by dissolving appropriate amount of DPPH in methanol (Fisher chemicals) to obtain a concentration of 1.0 mM. To 4.0 ml standard solutions of L(+) ascorbic acid

(Merck) ranging between $5.0x10^{-3}$ mg mL^{-1} – 0.1 mg mL^{-1}, 0.5 mL of DPPH solution was added. The absorbance of the mixture was measured after thirty minutes at 517 nm. The procedure was repeated with standard solutions of butylated hydroxytoluene, BHT and (+)-catechin hydrate (Fluka), followed by mangrove tannins, mimosa tannins, quebracho tannins and chestnut tannins (SILVACHIMICA, Italy). A blank sample (without anti-oxidants), containing the same amount of methanol and DPPH radical was prepared and measured daily. DPPH radical standard solution was freshly prepared daily, covered with aluminium foil and stored at 4 °C between the measurements. The scavenging ability of antioxidants was calculated according to the following equation :

DPPH scavenging activity (%) = $[(A_0 – A/ A_0)] \times 100$

where A_0 is the absorbance of the control reaction and A is the absorbance in the presence of samples.

2.2.3 ABTS free radical scavenging activity

The scavenging activity measurement by Goh *et al.* (2003) with a slight modification was adopted. 2,2'-azino-bis-(3-ethlybenthiazoline-6-sulfonic acid), ABTS as the free radical provider was prepared by reacting 3.75 mM ABTS diammonium salt (Fluka) and 1.225 mM potassium persulphate (BDH chemicals) overnight. The mixture was diluted 10 times with 99.5 % ethanol (Systerm) before use. To 1.0 mL (L)-ascorbic acid (Merck) standards ($5.0x10^{-3}$ mg mL^{-1} – 0.1 mg mL^{-1}), 3.0 mL of the diluted ABTS radical was added. The absorbance of the resultant mixture was measured after 60 minutes at 414 nm. The procedure was repeated with (+)-catechin hydrate (Fluka)

standard solution, followed by mangrove tannins, mimosa tannins, quebracho tannins and chestnut tannins (SILVACHIMICA, Italy). A blank sample (without anti-oxidants), containing the same amount of ethanol and ABTS radical was prepared and measured daily. The scavenging ability of antioxidants was calculated according to the following equation :

ABTS scavenging activity (%) = $[(A_0 - A/ A_0)] \times 100$

where A_0 is the absorbance of the control reaction and A is the absorbance in the presence of samples.

2.3 Electrochemical tests

The following experiment sequence was used for all the electrochemical studies :

(i) Measurement of the corrosion potential (E_{corr}) and the polarisation resistance (R_p), performed every 1 hour 30 minutes for a duration of 18 hours, with a scan rate of 0.166 mV s^{-1} for a range ($E_{corr} \pm 20$ mV).

(ii) Recording the potentiodynamic curve, $i = f(E)$, from -300 to 300 mV versus E_{corr} with a sweep rate of 1 mV s^{-1}.

2.3.1 Inhibition studies on mangrove tannins

Electrochemical tests were carried out in a three-electrode electrochemical cell (Fig. 2.2) connected to an EGG Princeton 263A or 273A potentiostats. A circular and horizontal working electrode (2.8 cm^2) was placed at the bottom of the cell under a Pt-disk electrode. Acquisition of data and calculation of electrochemical parameters were done by a 352 Soft Corr software. The reference electrode was a KCL-saturated calomel electrode (E = 0.241 V/SHE), and all working electrode potentials are measured versus this reference electrode. The electrochemical corrosion tests were carried out using a galvanized steel which was dipped in the stripping chemical solution consisting of HCL and allylthiourea to remove the zinc layer.

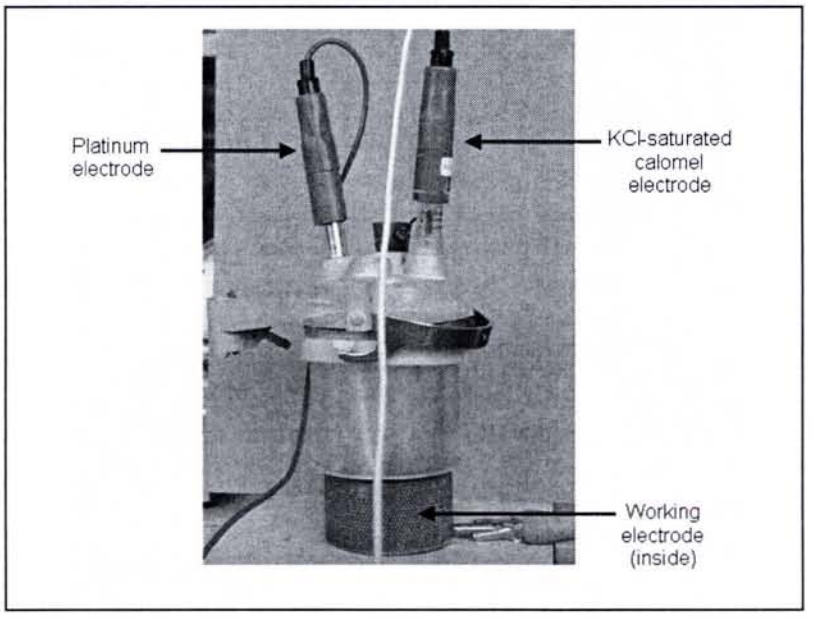

Fig. 2.2 Three electrode electrochemical cell consisting of platinum counter electrode, KCl saturated calomel electrode and steel working electrode.

Prior to each experiment, the electrodes were polished mechanically on a Struers Rotopol-2 polishing machine using SiC paper of 120, 400 and up to a final 1200 grit. After rinsing with distilled water, the test electrodes were cleaned with alcohol and dried in air, then immediately immersed in the aerated test solution.

The test solutions containing tannin ranging from 0.1 g L^{-1} to 6.0 g L^{-1} were prepared by diluting the tannin sample in a 0.5 M HCl solution. The pH of the solutions was increased by the addition of 3.0 M NaOH solutions. The electrochemical tests were carried out at pH 0, 0.5, 2.0, 4.0, and 8.0. The X-ray diffraction pattern of the surface of the working electrode after the electrochemical process was analysed using a Goniometre C diffractometer, incorporating a cobalt radiation (λ = 1.78892 Å). Data analysis and identification of peaks were carried out using EVA software.

2.3.2 Comparison of the inhibitory action with several tannins

Similar electrochemical tests as previously described were carried out with mangrove condensed tannin, quebracho tannin, mimosa tannin and chestnut tannins. A concentration of 3.0 g L^{-1} tannin at pH 0, 0.5, 2.0 and 4.0 were used as test solutions.

2.3.3 Synthesis of iron-tannates

The iron-tannates were prepared by the addition of 40 mL 5.0 g L^{-1} tannin solution (prepared in 0.5 M HCl) and 10 mL 0.1 M ferric ammonium sulfate, $FeNH_4(SO_4)_2 12H_2O$ (Fluka) solution at pH 0.5, 1.5, 2.0, 3.0, 4.0, 6.0 and 8.0. All solutions were adjusted to the appropriate pH by the addition of 3 M NaOH solution. The mixture was mechanically stirred and left to react at room temperature for 24 hours. The mixture was then centrifuged on Kubota 5920 for 20 minutes. The iron-tannates were collected and dried in an oven at 40 °C. A Perkin Elmer System 2000 spectrometer was used to obtain the FTIR spectrums of the tannates while a Goniometre C diffractometer, incorporating a cobalt radiation (λ=1.78892 Å) was used to obtain the X-ray diffraction pattern of the tannates. Data analysis and identification of peaks were carried out using EVA software. The UV-visible spectrums of the supernatant solution after centrifugation at all pH were also carried out on Hitachi U-200 spectrophotometer. The TGA/DTG analysis of the tannates synthesized at pH 3.0 and 8.0 was conducted on Perkin Elmer Thermogravimetric analyser TGA 7. Experiments were done in oxygenated air at a heating rate of 20 °C min^{-1} and sample masses were about 5-10 mg.

2.3.4 Inhibitory performance of catechin, epicatechin, epigallocaechin and epicatechin gallate

Electrochemical tests were carried out in a three-electrode electrochemical micro cell connected to an EGG Princeton 273A potentiostat. A circular and horizontal working electrode (0.58 cm^2) was placed at the bottom of the cell.

The test solutions containing the (+)-catechin hydrate, (-)-epicatechin, (Fluka), (-)-epigallocatechin and (-)-epicatechin gallate monomers (Sigma) ranging from $1.0x10^{-3}$ M to $5.0x10^{-2}$ M were prepared in 25 % (v) ethanolic HCl due to the low solubility of the monomers at higher concentrations. The pH of the solution was adjusted to pH 0.5. Ethanolic HCl solution [25 % (v)] was used as the standard solution. The inhibitory performance was compared with various concentrations of 2-naphthalene sulfonic acid.

2.3.4.1 Molecular modelling

Quantum chemical calculations were performed using Hyperchem 6.0 package. The geometry optimisation of the flavanoids was obtained with PM3 semi-empirical parameterisation. The potential energy minimum was determined using a steepest descent algorithm and the iteration terminated when the RMS energy gradient reached $1.0x10^{-2}$ kcal $Å^{-1}mol^{-1}$. Single point calculation was used to determine the molecular properties of the flavanoids with the minimum energy conformation.

2.3.5 Determination of the redox potentials of flavanoid monomers and tannins

In cyclic voltammetry, the potential of a small, stationary working electrode is changed linearly with time starting from a potential where no electrode reaction occurs and moving to potentials where reduction or oxidation of a solute occurs. After traversing the potential region in which one or more electrode reactions take place, the direction of the sweep is reversed and the electrode reactions of

intermediates and products formed during the forward scan is often detected. It is a powerful tool for the determination of formal redox potentials, detection of chemical reactions that precede or follow the electrochemical reaction and evaluation of electron transfer kinetics (Evans *et al.*, 1983).

A three-electrode cell consisting of a platinum rotating disk (0.39 cm^2), platinum counter electrode and saturated calomel reference electrode, immersed in a double-walled glass electrochemical cell was employed.

The following experiment sequence was used :

(i) Measurement of the open circuit potential, performed for one hour

(ii) Recording the cyclic polarisation curves at -0.7 V, 1.2 V and -0.7 V of initial, final and vertex potentials respectively versus the open circuit potential and at various sweep-rates ranging from 10 – 1000 mV s^{-1}.

Standard $5.0x10^{-4}$ M and $1.0x10^{-3}$ M catechin solutions were used as test solutions. Prior to each experiment, the test solution was deaerated by passing through nitrogen for 3 hours and the bubbling was continued throughout the experiment. Five cycles of the above experimental sequence were carried out to ensure repeatability of results. The above procedure was repeated with $1.0x10^{-3}$ M epicatechin, 3.0 g L^{-1} mangrove tannins, 3.0 g L^{-1} mimosa tannins, 3.0 g L^{-1} quebracho tannins and 3.0 g L^{-1} chestnut tannins.

2.4.1 Preparation of pre-rusted steel plates

The zinc layer was stripped from the steel plates prior to each preparation. Three types of preparations were employed :

i. Immersion in 3.5 % (w/v) NaCl solution for 35 days at room temperature (20 °C)

ii. Alternated Immersion Tests (8 hours immersion and 16 hours drying in an oven at 40 °C) for two weeks

iii. Salt Spray tests (6 hours exposure in 5 % (w/v) NaCl at 98 % humidity, 1.0 mL hr^{-1} spray rate, 1.0 kg cm^{-3} of pressure and followed by drying in the oven at 40 °C).

2.4.1.1 Inhibitory performance of mangrove tannins, mimosa tannins and phosphoric acid on pre-rusted steel

Electrochemical tests were carried out in a three-electrode electrochemical microcell connected to an EGG Princeton 273A potentiostat. A circular and horizontal working electrode (2.8 cm^2) consisting of pre-rusted sample prepared by salt spray exposure was placed at the bottom of the cell.

The standard solution consisted of 3.5 % (w/v) NaCl and the test solution contained 3.0 g L^{-1} tannin, 3.0 g L^{-1} mimosa tannin, the addition of 15 % (w/v), 30 % (w/v) and 50 % (w/v) phosphoric acid to the 3 g L^{-1} tannin solutions and 15 % (w/v), 30 % (w/v) and 50 % (w/v) phosphoric acid. All solutions were prepared in 3.5 % (w/v) NaCl solution. The pH of the solution was adjusted to pH 0.5, 2.0 and 5.5.

2.5 Phase transformation studies

2.5.1 Phase transformation of rust induced by tannins

X-ray diffractions and SEM analysis were carried out on all pre-rusted specimens prepared. The SEM analysis was carried using SEM S-2500 Hitachi Thermo NORAN equipped with an energy-dispersive X-ray spectrometer and prior to SEM-EDS studies the surface was carbon/gold-coated using a vacuum evaporator Edwards Auto 306. The pre-rusted plates (2.5 cm x 4.0 cm) were immersed in 0.5 % (w/v) mangrove tannin solutions at pH 2.0, 4.0 and 8.0. The changes in the rust structures and morphologies were observed via X-ray diffraction, SEM, EDS and FTIR analyses.

2.5.2 Phase transformation of rust in the presence of tannins and phosphoric acid

Pre-rusted samples (2.5 cm x 4.0 cm) prepared according to procedure (i) and (ii) of section 2.4.1 were immersed in solutions containing 15 % (w/v) and 30 % (w/v) phosphoric acid, 0.5 % (w/v) mangrove tannin and 15 % (w/v) phosphoric acid and 0.5 % (w/v) mangrove tannin and 30 % (w/v) phosphoric acid. The pH of the solution was adjusted to pH 4.0. The phase transformation was evaluated via X-ray diffraction, FTIR, SEM and EDS analyses.

2.5.3 Phase transformation of individual rust components in the presence of mangrove tannins and phosphoric acid

Standard powders (10 mg) of goethite (α-FeOOH), lepidocrocite (γ-FeOOH), magnetite (Fe_3O_4) and maghemite (γ-Fe_2O_3) (Alfa Aeser) were mixed with 10 mL of test solutions consisting of :

i) 0.5 % (w/v) mangrove tannins

ii) 15 % (w/v) phosphoric acid

iii) 0.5 % (w/v) mangrove tannin and 15 % (w/v) phosphoric acid

and 2 mL of 2.0 % (w/v) mangrove tannin (initially dissolved in methanol and let to dry before diluting to 2 mL with distilled water).

The resultant solution was adjusted to pH 4.0. Samples were collected at intervals of 1 day, 1 week, 2 weeks and 1 month. Collected samples were filtered using filter paper, dried at 40 °C for 2-3 hours before being analysed. The FTIR spectrums of the collected samples were then taken using Perkin Elmer System 2000 Spectrometer while a Goniometre C diffractometer, incorporating a cobalt radiation (λ=1.78892 Å) was used to obtain the X-ray diffraction pattern of the samples.

2.6 Corrosion protection via humidity chamber tests and salt spray tests

The pre-rusted plates (2.5 x 7.0 cm for humidity chamber and 4.0 cm x 4.0 cm for salt spray) prepared according to procedure (iii) of section 2.4.1 were immersed in 0.5 % (w/v) mangrove tannin and mimosa tannin solutions, 0.5 % (w/v) mangrove tannin + 15 % (w/v) phosphoric acid and 0.5 % (w/v) mimosa

tannin + 15 % (w/v) phosphoric acid. The pH of the solution was adjusted to pH 4.0. The plates were then subjected to the humidity chamber (Liebisch KBEA 300) tests [8 hours at 100 % humidity and 40 °C and 16 hours of drying at ambient conditions (standard method DIN 50017)] for 45 days. The salt spray tests of the plates were carried out according to the ASTM B 117 standard procedure for 6 hours.

CHAPTER THREE

RESULTS

3.1 Tannin extraction

The 70 % aqueous acetone extract of the mangrove bark yielded 27-29 % (wt) dark brown tannin powder. The FTIR spectrum of the mangrove tannin shows (Fig. 3.1, Table 3.1) a broad absorption band between 3700 and 2700 cm^{-1} which is due to the presence of hydroxyl groups. Three peaks occurring at 1611, 1522 and 1447 cm^{-1} are characteristic of aromatic compounds. Various peaks between 1000 and 1300 cm^{-1} correspond to substituted benzene rings.

Table 3.1 IR spectral data of mixed mangrove tannins.

Functional group	Wavenumber (cm^{-1})
O-H (stretch)	3382 (s, br)
C-H (stretch)	2933 (m)
C=C (stretch)	1611 (s), 1522 (s), 1447 (s)
O-H (in-plane bend)	1360 (m)
C-O (C-O-C stretch)	1284 (m), 1051 (m)
C-H (out-of-plane bend)	817 (w), 780 (w)

The aqueous ethyl acetate extract was loaded onto sephadex LH-20 column and eluted with acetone/water 1:1 to afford 45 % (wt) fluffy light brown condensed tannin powders while the methanol-water fraction yielded 25 % (wt) sticky dark brown powder. The FTIR spectrums of acetone-water extract and the methanol-water extract are presented in Fig. 3.2. It could be observed that the spectrum of the acetone-water fraction is similar to the mixed tannin. All the major peaks shown are typical peaks of condensed tannins as observed by Gust (1991). Likewise the spectrum corresponding to the second

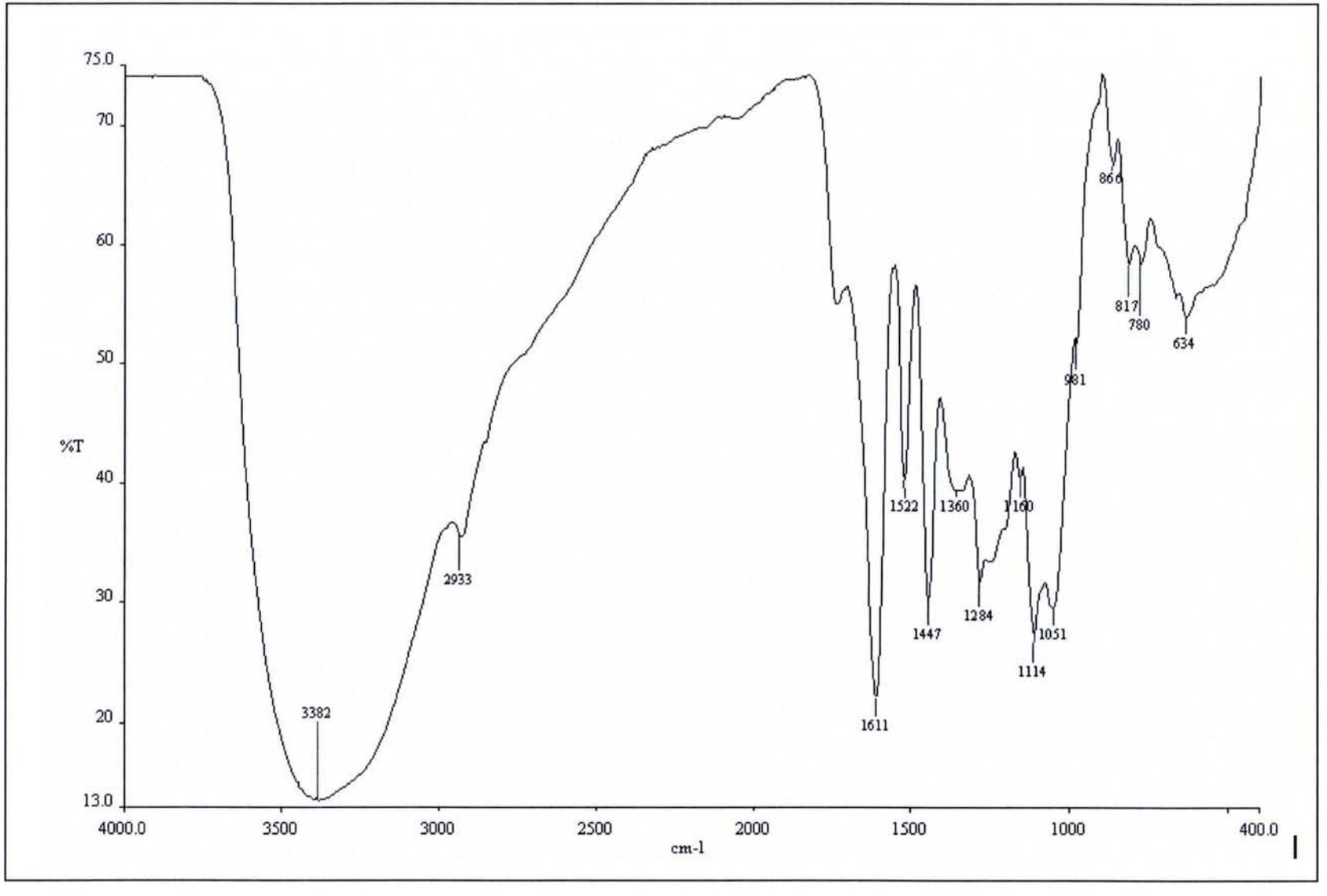

Fig. 3.1 FTIR spectrum of 70 % aqueous acetone extract (mixed tannins).

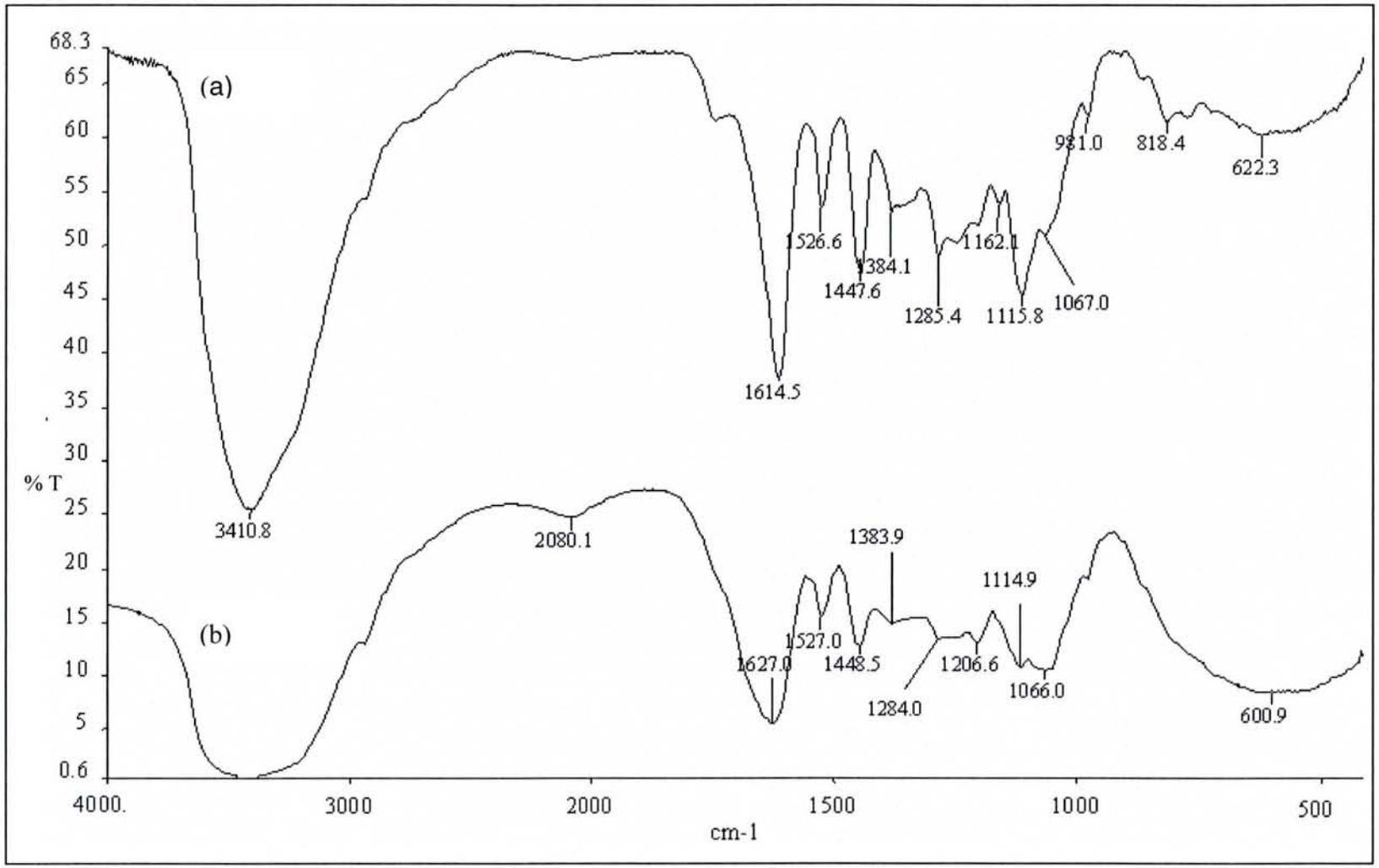

Fig. 3.2 FTIR spectrum of (a) acetone-water extract and (b) methanol-water extracts following sephadex LH-20 column chromatography.

acetone-water extraction gave rise to similar major peaks. The spectrum of the methanol-water extract showed similar major peaks but were of lower intensities. A broad adsorption peak at 1066 cm^{-1} was observed. In addition, the bands at 1115 cm^{-1} and 1066 cm^{-1} are essentially of the same intensities. The spectrum also presented a broad band between 700 to 900 cm^{-1}.

From Fig. 3.3, the IR spectrum of the mixed mangrove tannin showed a close resemblance to the IR spectrum of the quebracho and mimosa tannins, well known condensed tannins (Pizzi and Stephanau, 1993). In contrast, the chestnut tannin a hydrolysable tannin, (Martinez and Staglar, 2003) showed a strong absorption at 1735 cm^{-1}, corresponding to the existence of C-O stretch of the ester group.

3.1.1 Thermogravimetric analysis

Thermogravimetric analysis (TGA) and differential thermogravimetric analysis (DTG) of the different extracts were carried out and is shown in Fig. 3.4. Thermal decomposition of the 70 % acetone extract (mixed tannin) showed 43.6 % weight loss at 327.6 °C. A further 32 % weight loss occurred at 455.8 °C The methanol-water extract showed 43.6 % weight loss at 313.0 °C and 74.6 % weight loss at 455.4 °C. A complete degradation of condensed tannins was observed. The condensed tannin produced a small weight loss of 15.2 % at 270.0 °C and a large weight loss of 91.3 % occurred at 401.3 °C. As a comparison, thermogravimetric analysis and differential thermogravimetric analysis of mimosa, quebracho and chestnut tannins were conducted. Mimosa

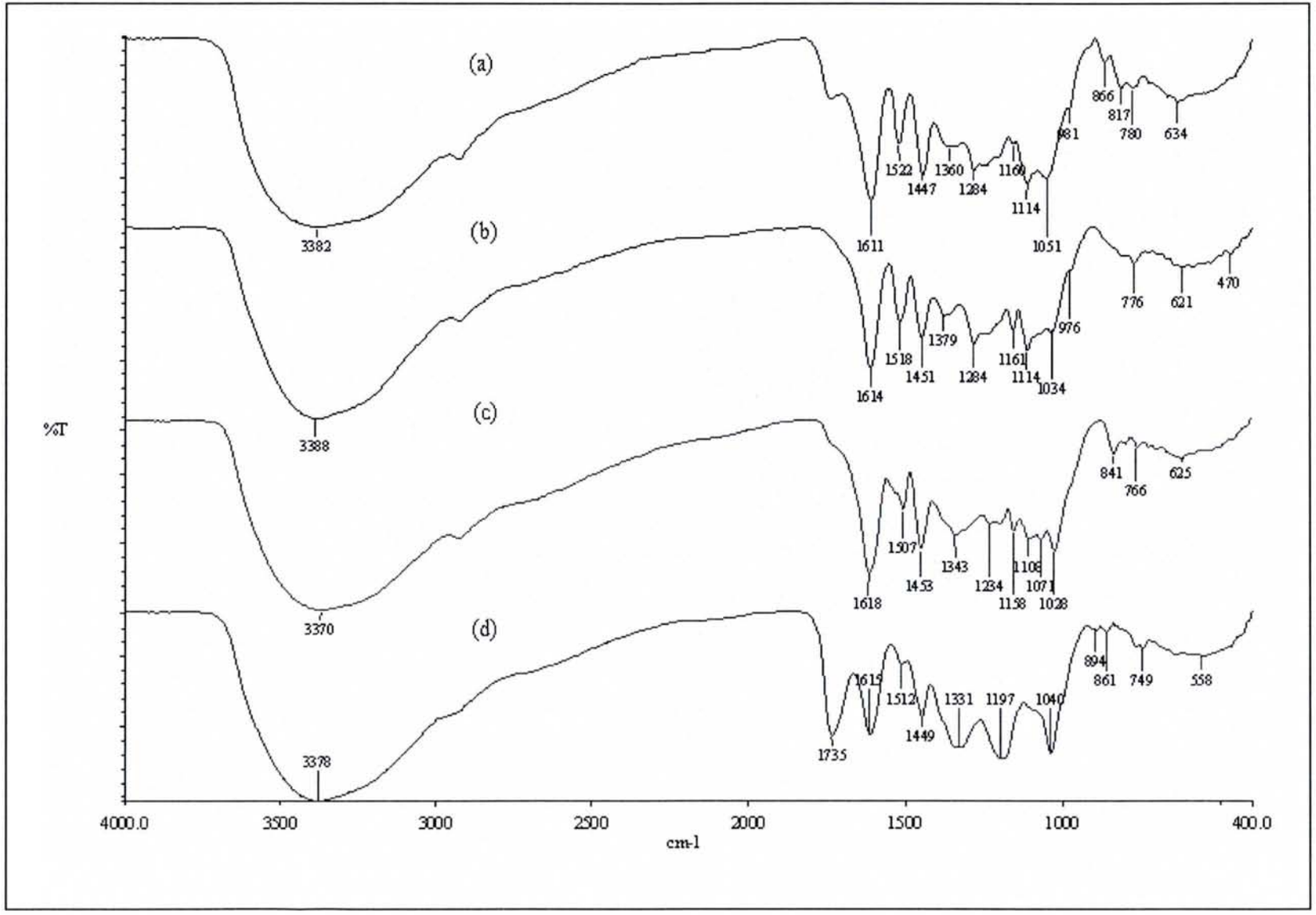

Fig. 3.3 FTIR spectrum of (a) mangrove tannins (b) quebracho tannins (c) mimosa tannins and (d) chestnut tannins.

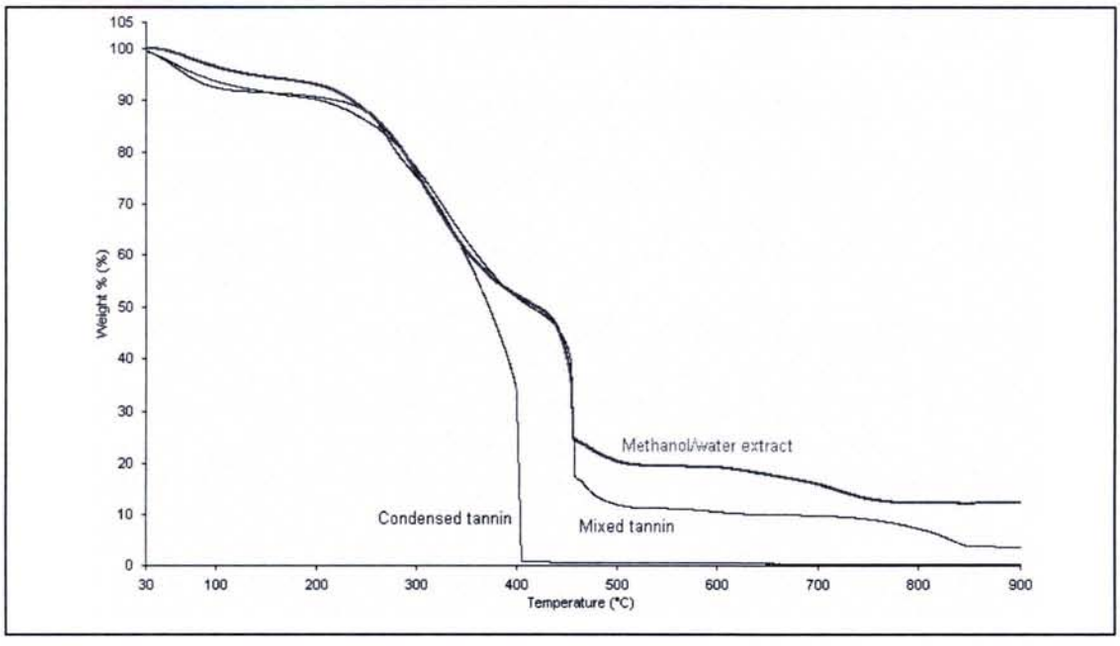

Fig. 3.4 Thermogravimetry analysis (TGA) of mixed tannins, condensed tannins and methanol-water extract.

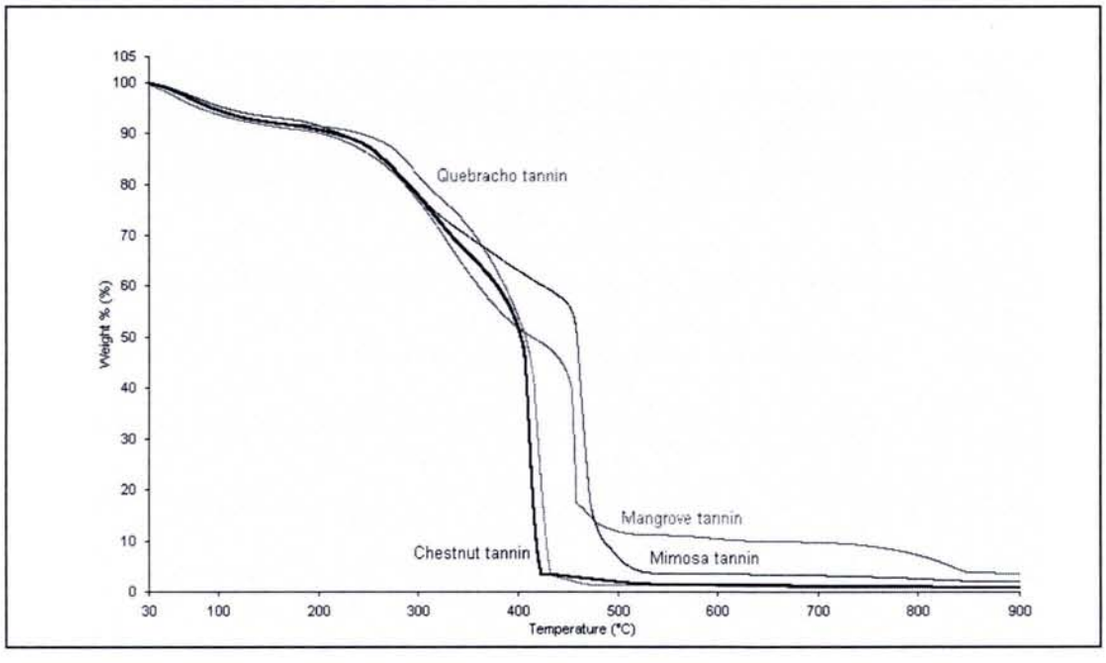

Fig. 3.5 Comparison of the thermogravimetry analysis (TGA) of mangrove tannins with the commercial mimosa, quebracho and chestnut tannins.

and quebracho tannins both show two distinct thermal decomposition peaks (not shown) similar to mangrove tannins. For mimosa tannin, the first peak at 277.2 °C corresponds to 33.2 % weight loss while the second peak at 460 °C recorded a weight loss of 90.9 %. A 15.1 % weight loss at 292.9 °C and 91.1 % weight loss at 416.9 °C were observed for quebracho tannin. The thermal decomposition of chestnut tannin gave rise to two weak and one strong decomposition peaks (not shown). The peaks at 278.0 °C, 317.6 °C and 409.6 °C correspond to 11.0 %, 25.5 % and 91.1 % weight losses respectively.

3.1.2 Prussian blue assay for total phenols in mangrove tannins

This method of quantifying total phenols involves an oxidation-reduction reaction as shown below (Schofield *et al.*, 2001) :

Polyphenol + $2Fe(CN)_6^{3-}$ (ferricyanide ion) → oxidised polyphenol + $2Fe(CN)_6^{4-}$ (ferrocyanide ion)

$3Fe(CN)_6^{4-}$ (ferrocyanide ion) + $3Fe^{3+}$ → $Fe_4[Fe(CN)_6]_3$ (Prussian blue).

The results of the total phenolic content of every $1.0x10^{-2}$ g sample of starting material are presented in Table 3.2. From the gallic acid standard curve in appendix 1, the phenolic content of condensed tannins and the methanol-water extract was found to be 31.9 % and 37.6 % gallic acid equivalent respectively. A total of 80 % gallic acid equivalent was obtained for mixed tannin.

Table 3.2 Total phenol content by Prussian blue assay of isolated tannin extracts.

Sample	Absorbance	Total Phenol Content (% equivalent gallic acid per g sample)
70% acetone extract (mixed tannin)	0.705	80.9 ± 1.6
Acetone/water extract (condensed tannin)	0.273	31.9 ± 1.2
Methanol/water extract	0.334	37.6 ± 1.4

3.2 Identification of condensed tannins via HPLC analysis

Fig. 3.6 shows the chemical structure of the monomer standards used in this study and chromatograms containing a mixture of all standards eluted at a flow rate of 1.0 mL min^{-1} and 0.5 mL min^{-1} of elution condition (i) are shown in Fig. 3.7. Seven peaks were obtained at a flow rate of 1.0 mL min^{-1} in comparison to eight peaks at 0.5 mL min^{-1}. Although the elution at a rate of 0.5 mL min^{-1} was able to separate peaks 4 and 5, the retention times were very close. Hence, identification of peaks by spiking the condensed tannin sample with the appropriate standards was resorted.

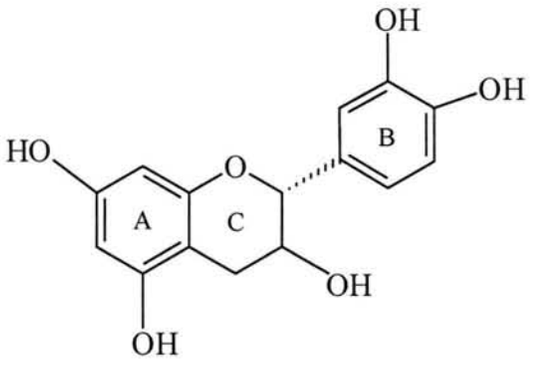

(+)-catechin

([2R, 3S]-2-[3, 4-Dihydroxyphenyl]-3, 4-dihydro-1[2H]-benzopyran-3, 5, 7-triol)

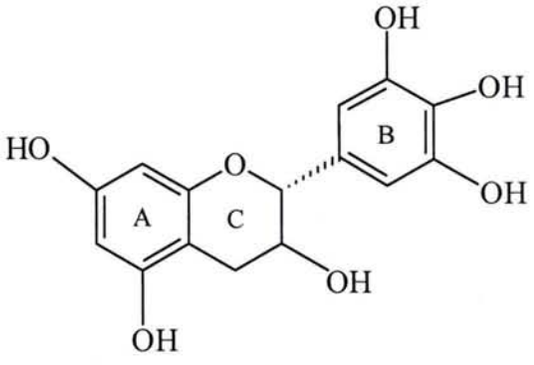

(-)-gallocatechin

([2R, 3S]-2-[3, 4, 5-Trihydroxyphenyl]-3, 4-dihydro-1[2H]-benzopyran-3, 5, 7-triol)

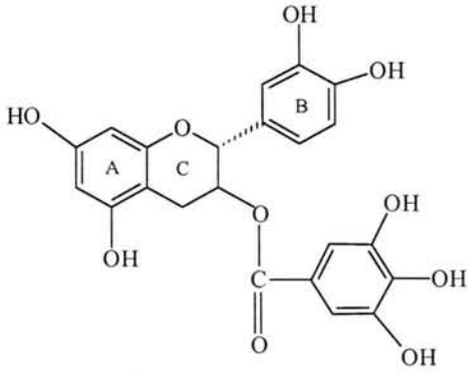

(-)-catechin gallate

([2R, 3S]-2-[3, 4-Dihydroxyphenyl]-3, 4-dihydro-1[2H]-benzopyran-3, 5, 7-triol 3-[3, 4-dihydroxybenzoate])

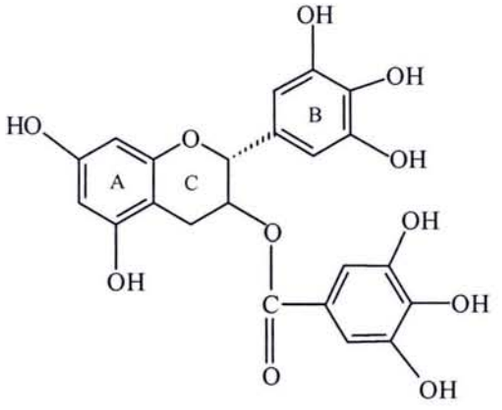

(-)-gallocatechin gallate

([2R, 3S]-2-[3, 4, 5-Trihydroxyphenyl]-3, 4-dihydro-1[2H]-benzopyran-3, 5, 7-triol 3-[3, 4, 5-trihydroxybenzoate])

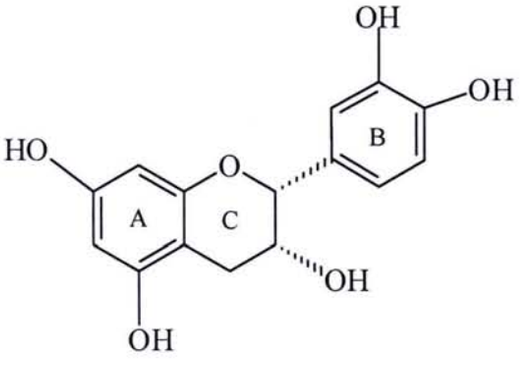

(-)-epicatechin

([2R, 3R]-2-[3, 4-Dihydroxyphenyl]-3, 4-dihydro-1[2H]-benzopyran-3, 5, 7-triol)

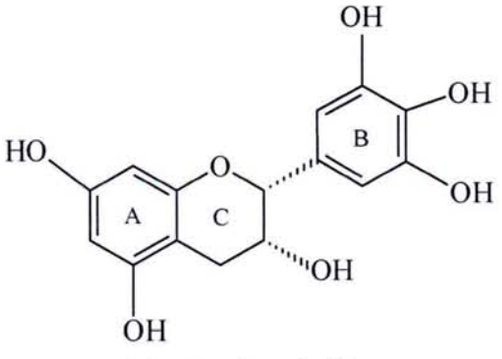

(-)-epigallocatechin

([2R, 3R]-2-[3, 4, 5-Trihydroxyphenyl]-3, 4-dihydro-1[2H]-benzopyran-3, 5, 7-triol)

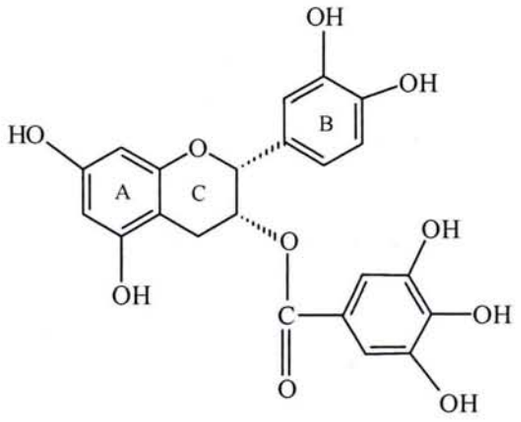

(-)-epicatechin gallate

([2R, 3R]-2-[3, 4-Dihydroxyphenyl]-3, 4-dihydro-1[2H]-benzopyran-3, 5, 7-triol 3-[3, 4-dihydroxybenzoate])

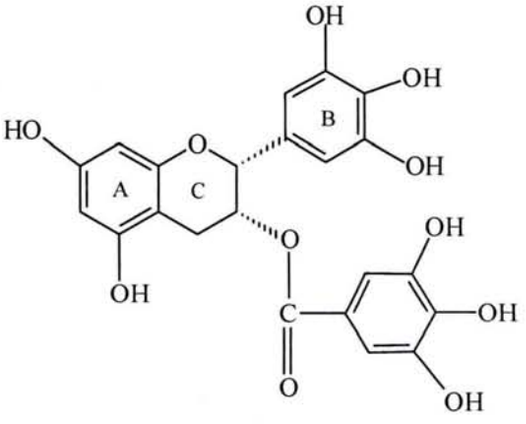

(-)-epigallocatechin gallate

([2R, 3R]-2-[3, 4, 5-Trihydroxyphenyl]-3, 4-dihydro-1[2H]-benzopyran-3, 5, 7-triol 3-[3, 4, 5-trihydroxybenzoate])

Fig. 3.6 Chemical structure of flavan-3-ol monomer standards.

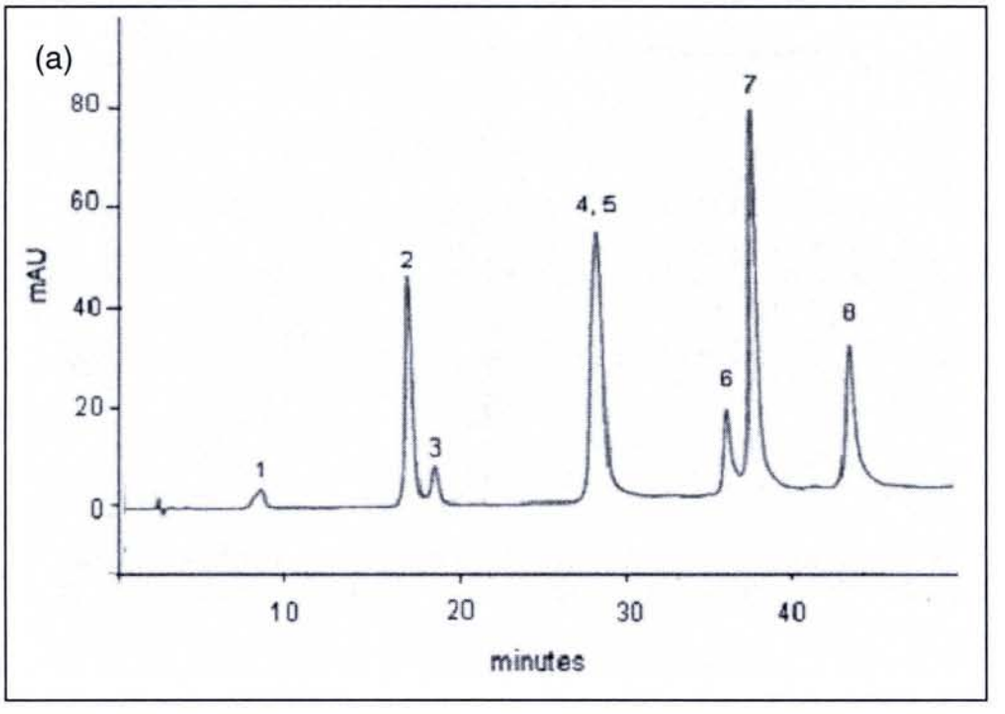

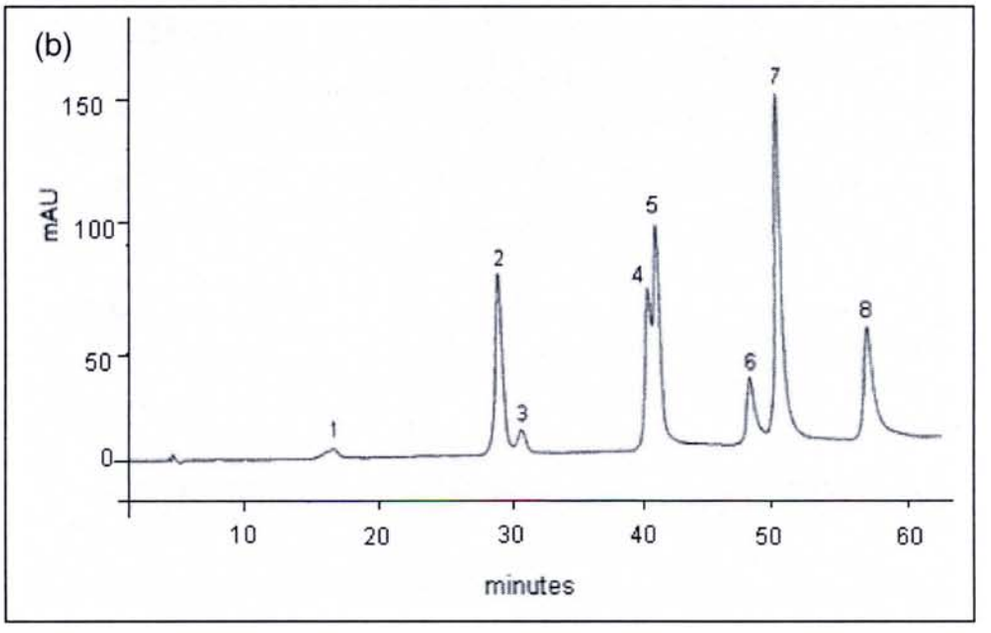

Fig. 3.7 HPLC chromatogram of flavan-3-ol standards eluted at a flow rate of (a) 1 mL min^{-1} and (b) 0.5 mL min^{-1} of elution condition (i). Peaks : 1 = (-)-gallocatechin, 2 = (+)-catechin/(-)-catechin, 3 = (-)-epigallocatechin, 4 = (-)-epigallocatechin gallate, 5= (-)-epicatechin, 6= (-)-gallocatechin gallate, 7= (-)- epicatechin gallate, 8= (-)-catechin gallate.

In the acid depolymerisation in the presence of phloroglucinol, the interflavan bonds are protonated and broken, leaving the terminal unit intact and the extender unit as a carbocation. The carbocation is then captured either alpha or beta to the C-ring producing a monomer phloroglucinol adduct. The depolymerisation products were then separated on reversed-phase HPLC. The depolymerisation reaction (Hernes *et al.,* 2001) is schematically shown in Fig. 3.8.

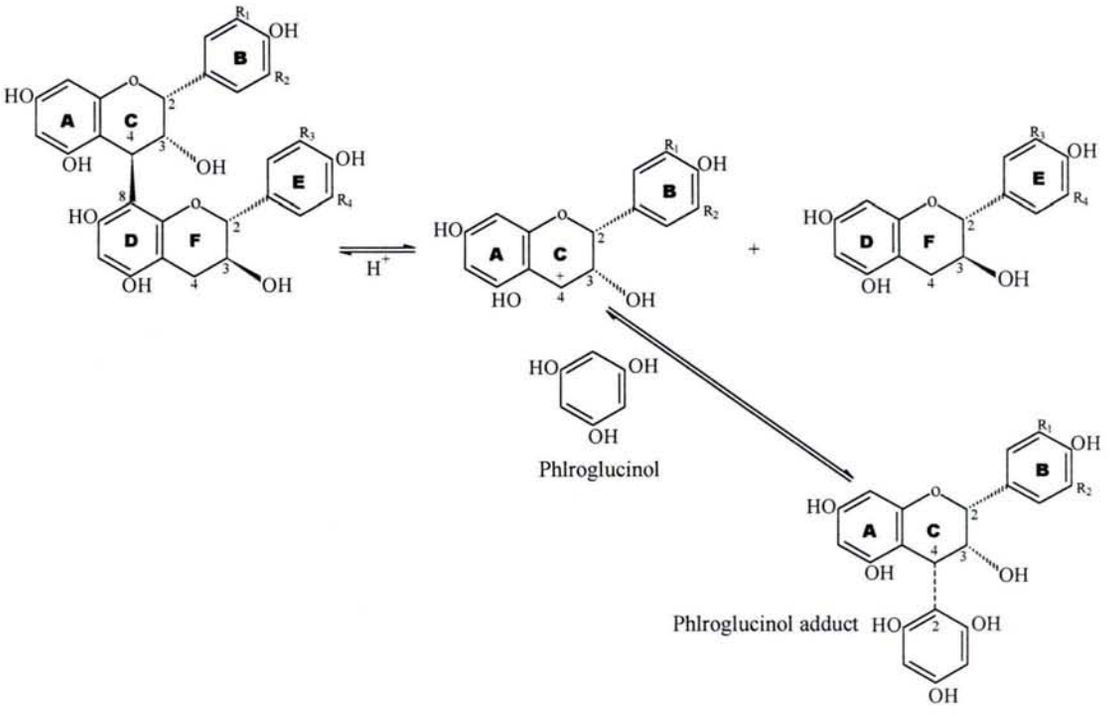

Fig. 3.8 Acid depolymerisation of condensed tannins in the presence of phloroglucinol. "ACB" and "DFE" represents extender and terminal units respectively. R_1, R_3=OH and R_2, R_4=H for pyrocathecol; R_1, R_3=OH and R_2, R_4=OH for pyrogallol .

When the condensed tannin (first sampling) was subjected to acid degradation in the presence of phloroglucinol and dioxane according to the procedure as described in section 2.1.3, two main narrow peaks and an intensed broad peak were observed on the HPLC chromatogram (Fig. 3.9). The two narrow peaks were identified as being phloroglucinol and phloroglucinol adduct. When the condensed tannin was submitted to acid degradation in the presence of phloroglucinol and ethanol (method 2) of elution condition (i), five peaks (terminal units) followed by a hump were observed (Fig. 3.10).

However when elution condition (ii) was adapted, the HPLC chromatogram as shown in Fig. 3.11 was obtained, showing well resolved peaks with no hump. Thus this elution condition was used for subsequent determinations. Spiking the samples with the flavanoid standards confirmed the presence of catechin, epigallocatechin, epicatechin and epicatechin gallate as terminal units. An example of a chromatogram of the sample spiked with catechin standard is shown in Fig. 3.12.

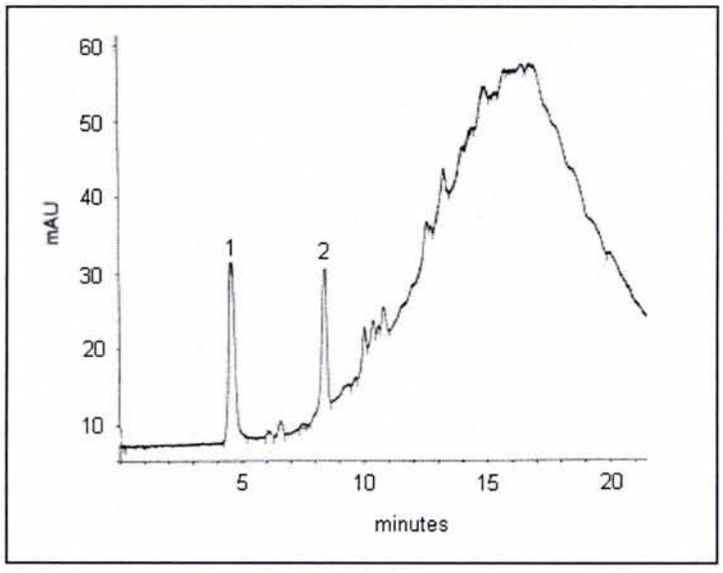

FIG. 3.9 HPLC chromatogram of condensed tannins degraded in the presence of acidic dioxane and phloroglucinol.

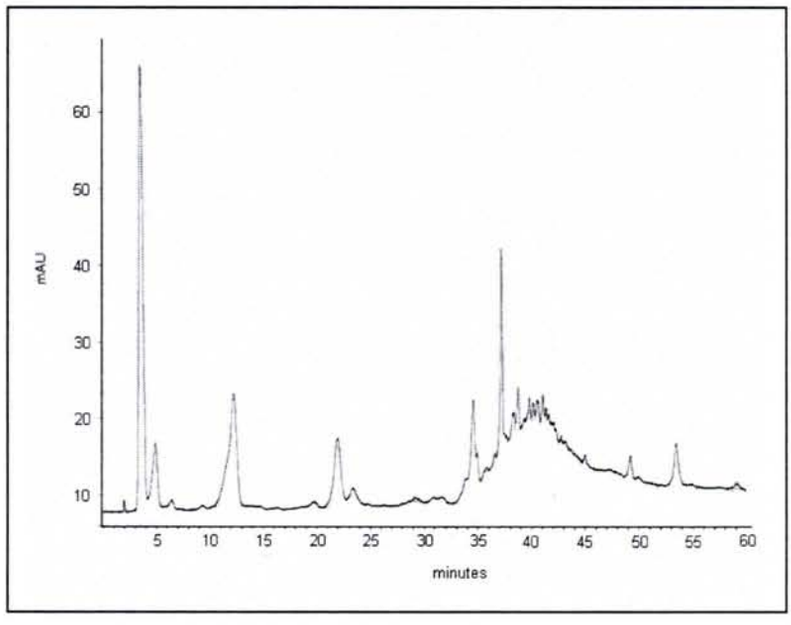

Fig. 3.10 HPLC chromatogram of condensed tannins degraded in the presence of acidic ethanol and phloroglucinol using elution condition (i).

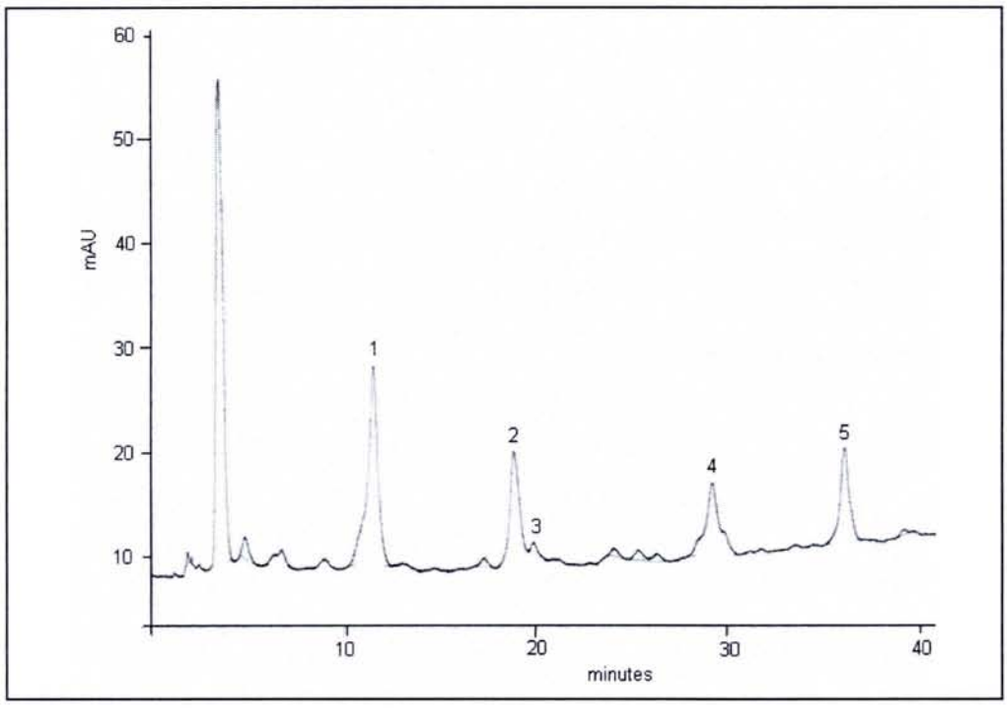

Fig. 3.11 HPLC chromatogram of condensed tannins (first sampling) degraded in the presence of acidic ethanol and phloroglucinol using elution condition (ii). Peaks : 1= phloroglucinol adduct, 2= catechin, 3= epigallocatechin, 4= epicatechin, 5= epicatechin gallate.

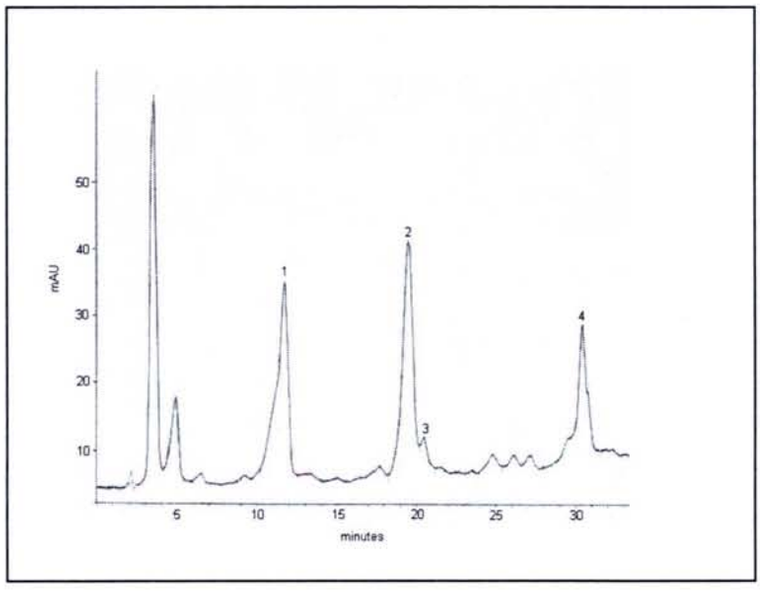

Fig. 3.12 HPLC chromatogram of condensed tannins degraded in the presence of acidic ethanol and phloroglucinol spiked with catechin standard. Peaks : 1= phloroglucinol adduct, 2= spiked catechin standard, 3 = epigallocatechin, 4= epicatechin.

The condensed tannin which was extracted from a second sampling of mangrove barks gave rise to the chromatogram in Fig. 3.13. The same number of peaks corresponding to the same flavanoid monomers were obtained. In contrast to the first sampling, a higher intensity of epigallocatehin was obtained as compared to catechin (Fig. 3.14).

Due to the unavailability of phloroglucinol adducts commercially, the adducts were synthesised in the laboratory. When the sample was spiked with the synthesised catechin adduct and epicatechin adducts, a pair of adduct peaks appeared (Fig. 3.15), indicating the absence of catechin and epicatechin monomers as the extender unit. Similarly for all the other adducts synthesised, additional peaks were again evident.

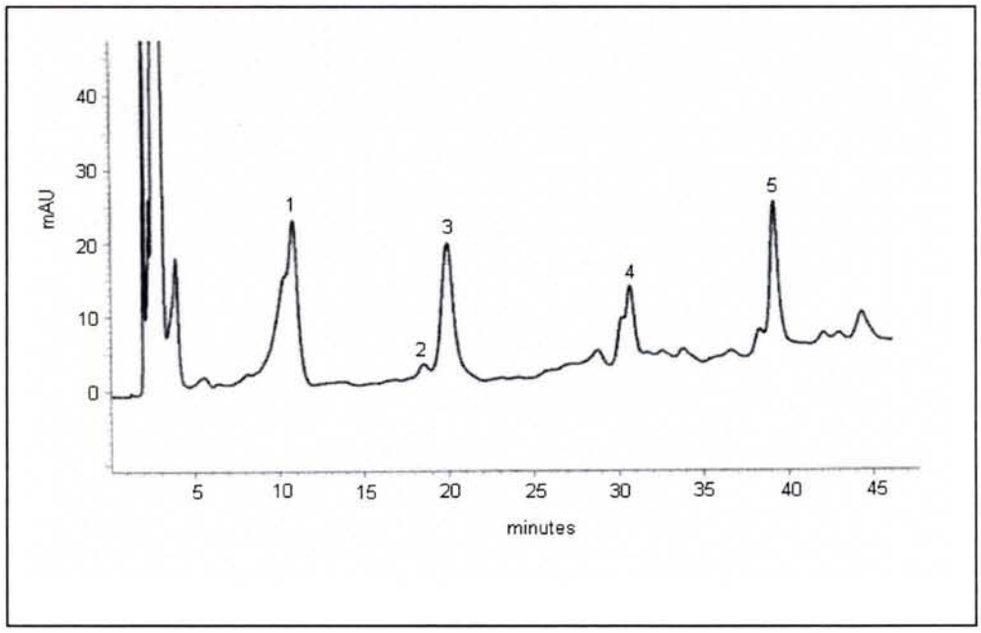

Fig. 3.13 HPLC chromatogram of condensed tannins (second sampling) degraded in the presence of acidic ethanol and phloroglucinol using elution condition (ii). Peaks : 1= phloroglucinol adduct, 2= catechin, 3= epigallocatechin, 4= epicatechin, 5= epicatechin gallate.

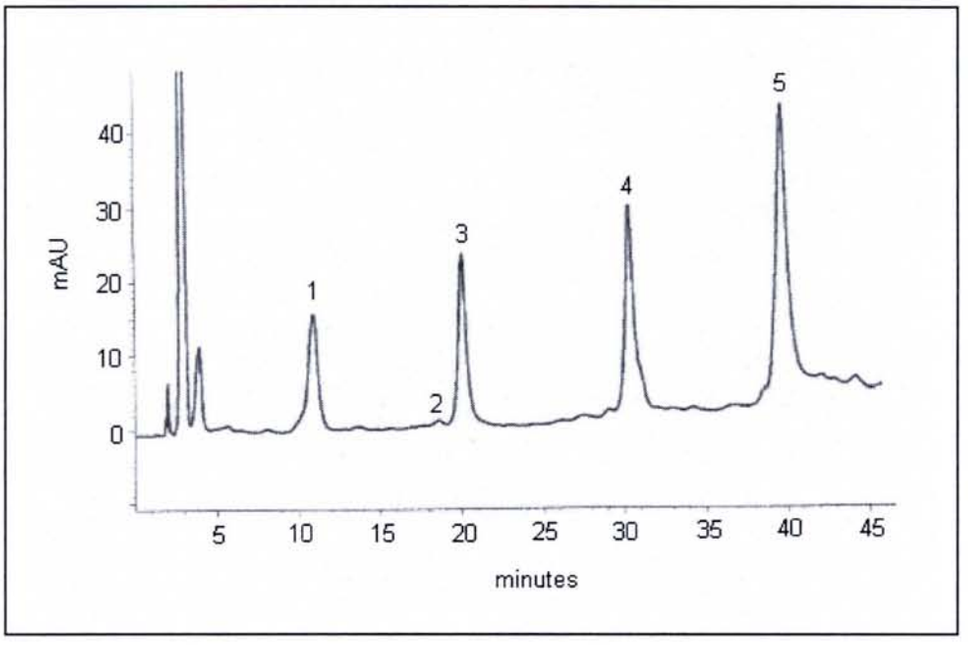

Fig. 3.14 HPLC chromatogram of condensed tannins (second sampling) degraded in the presence of acidic ethanol and phloroglucinol using elution condition (ii). Peaks : 1= phloroglucinol adduct, 2= catechin, 3= spiked epigallocatechin standard, 4= spiked epicatechin standard, 5= spiked epicatechin gallate standard.

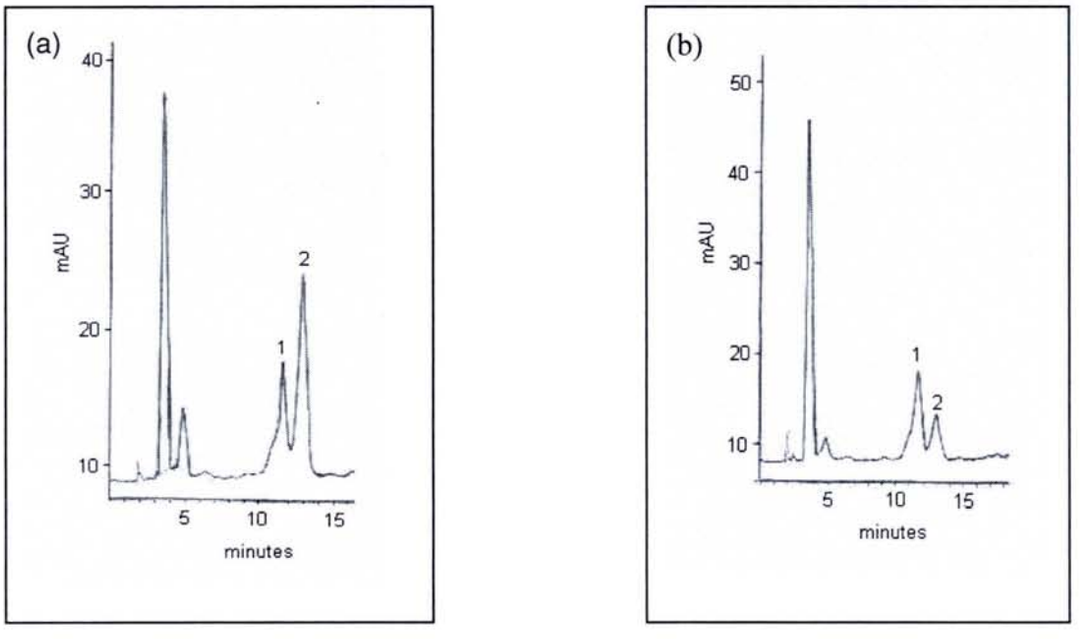

Fig. 3.15 HPLC chromatogram of condensed tannins when spiked with the synthesised adducts of (a) (+)-catechin and (b) (-)-epicatechin. Peaks : 1= phloroglucinol adduct of condensed sample, 2 = corresponding synthesised catechin/ epicatechin adducts.

The depolymerisation reaction was also conducted on the methanol-water extract and HPLC chromatogram of the reaction products is as shown in Fig. 3.16 below. The emergence of several peaks of low intensities signifies the presence of condensed tannins.

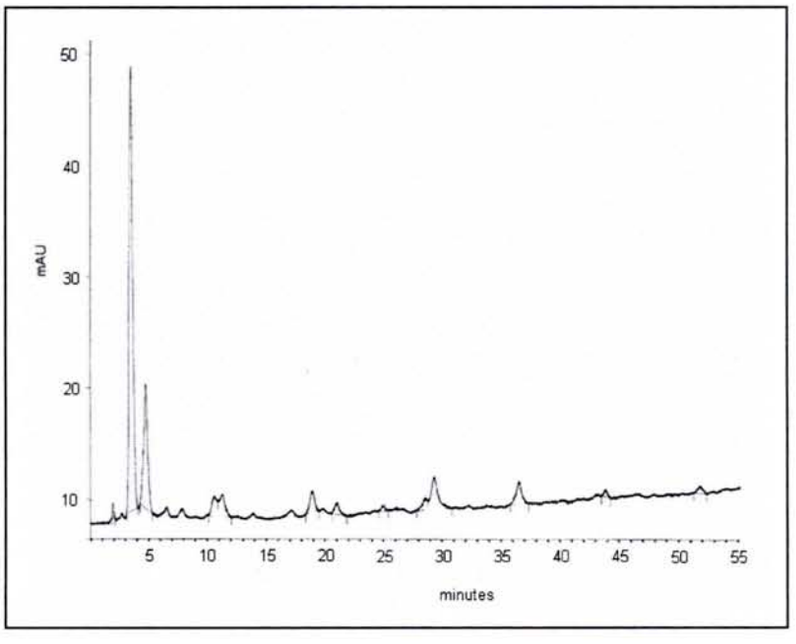

Fig. 3.16 HPLC chromatogram of the methanol-water extract following degradation reaction in the presence of acidic ethanol and phloroglucinol.

3.2.1 Quantification of condensed tannins

3.2.1.1 Vanillin assay

The vanillin method depends on the reaction of vanillin with condensed tannins forming a red coloured complex. The underlying vanillin assay reaction is shown in Fig. 3.17.

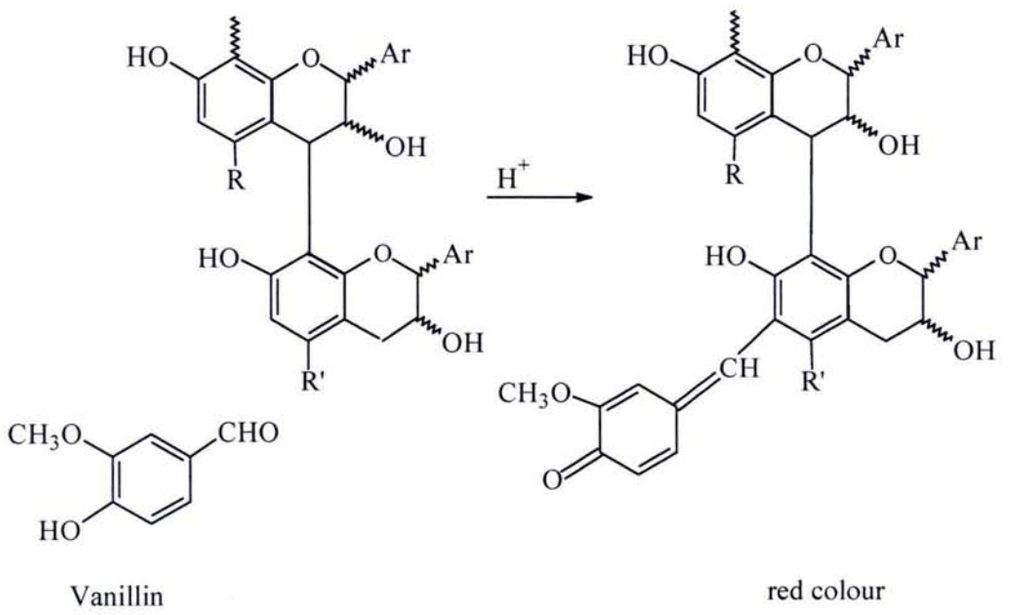

Fig. 3.17 Chemistry of the vanillin assay for condensed tannins (Schofield *et al.* 2001).

The results of the assay are depicted in Table 3.3. Based on the (+)-catechin standard curve in appendix 2, the spectrometric quantification of condensed tannin from mangrove barks yielded an average total content of 36 % in (+)-catechin equivalent. According to this assay, no difference was noted in the catechin content between the first and second extracted samples of the condensed tannin. The (+)-catechin equivalent in the methanol/water extract was found to be 6 %.

Table 3.3 Content of condensed tannins as determined by vanillin assay.

Sample	Weight of sample (g)	Absorbance	Content of condensed tannins [% (wt) (+)-catechin equivalent per g sample]
Acetone/water extract			
Sample 1	3.4×10^{-4}	0.058	35.6 ± 1.2
Sample 2	3.5×10^{-4}	0.055	
Sample 3	3.5×10^{-4}	0.057	
Methanol/water extract			
Sample 1	4.1×10^{-4}	0.026	6.4 ± 0.8
Sample 2	4.0×10^{-4}	0.029	
Sample 3	4.1×10^{-4}	0.023	

3.2.1.2 Quantification of flavanoid monomers via HPLC analysis

Since the HPLC analysis shows that none of the flavanoid monomers are present as extender units, it was possible to quantitatively determine the flavanoid content in the condensed tannin sample without undergoing depolymerisation reactions.

The flavanoid monomer content in mangrove tannins were calculated from the monomer standard curves in appendix 3-6 and the results are tabulated in Table 3.4. From the tabulated results, it could be observed that the concentrations of epicatechin and epicatechin gallate were essentially the same for both samplings. For the first sampling, the content of catechin was higher than epigallocatechin, whereas for the second sampling the epigallocatechin and catechin contents were found to be reversed.

Table 3.4 Quantification of flavanoid monomers as determined by HPLC.

Sampling 1	Content (mg)	Content [% (wt) per g sample]
(+)-catechin	$4.6 \times 10^{-2} - 6.8 \times 10^{-2}$	0.55 ± 0.09
(-)-epigallocatechin	$5.0 \times 10^{-3} - 1.0 \times 10^{-2}$	$(7.5 \pm 1.7) \times 10^{-2}$
(-)-epicatechin	$4.0 \times 10^{-2} - 4.2 \times 10^{-2}$	0.41 ± 0.01
(-)-epicatechin gallate	$2.0 \times 10^{-2} - 2.4 \times 10^{-2}$	0.22 ± 0.02
Sampling 2		
(+)-catechin	$4.0 \times 10^{-3} - 6.0 \times 10^{-3}$	$(5.0 \pm 0.7) \times 10^{-2}$
(-)-epigallocatechin	0.19 - 0.26	2.2 ± 0.3
(-)-epicatechin	$3.0 \times 10^{-2} - 4.2 \times 10^{-2}$	0.37 ± 0.04
(-)-epicatechin gallate	$1.6 \times 10^{-2} - 2.0 \times 10^{-2}$	0.19 ± 0.02

3.3 Anti-oxidant properties of mangrove tannins

Tannins are antioxidant species often characterised by a reducing power (Mi-Yea *et al.*, 2003 and Gulcin *et al.*, 2003) and scavenging activities (Peng and Jay-Allemand, 1991; Alonso *et al.,* 2003; Cakir *et al.*, 2003; Minussi *et al.*, 2003). The reducing power of mangrove tannin and the scavenging activities of mangrove tannin using ABTS and DPPH assays were undertaken and compared with several commercial tannins.

Mechanistic studies of catechins as antioxidants against radical oxidation by Kondo *et al.* (1999) have proven that catechins are powerful antioxidants against lipid peroxidation. Meanwhile Minussi *et al.* (2003) demonstrated a positive correlation between the total antioxidant potential of wine and gallic acid, (-)-epicatechin, (+)-catechin and total phenol content. Based on these reports and the HPLC analysis which indicated that catechin monomer was present in mangrove tannin, (+)-catechin has been chosen as an antioxidant

standard along with known synthetic L-ascorbic acid and BHT standards (Alonso *et al.*, 2003).

3.3.1 Reducing power of tannins

The reducing power of mangrove tannins was determined from the method proposed by Gulcin *et al.* (2003) after a slight modification. In this procedure, $Fe(CN)_6^{3-}$ ions will be reduced to $Fe(CN)_6^{4-}$ ions when an anti-oxidant is added. The ferric chloride solution will then react with these ions to form $Fe_4[Fe(CN)_6]_3$ complex. The Fe^{2+} present in the complex will detected at 700 nm. Thus, increased absorbance indicates increased reducing power. The results obtained are shown in Fig. 3.18.

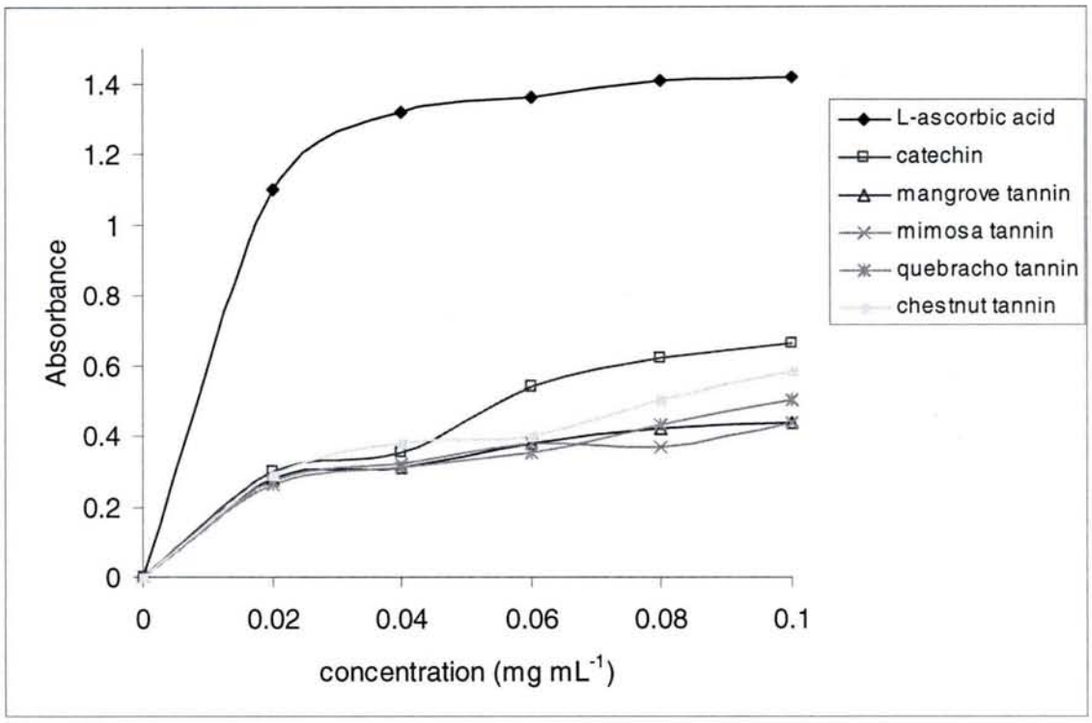

Fig. 3.18 The reducing power of tannins as compared to the L-ascorbic and catechin standards.

The reducing power of mangrove tannin increased slightly as the concentration increased to $6.0x10^{-2}$ mg mL^{-1}, after which it reached a plateau. While mimosa tannin exhibited the same behaviour as mangrove tannin, the reducing power of quebracho tannin and chestnut tannin continued to increase slightly as the concentrations were increased. Although the reducing power of mangrove tannin falls far below that of ascorbic acid standard and slightly below the catechin standard, the reducing power is comparable with that of catechin at the lower concentrations ($2.0x10^{-2}$ mg mL^{-1} and $4.0x10^{-2}$ mg mL^{-1}) and other commercial tannins investigated regardless of concentrations.

3.3.2 DPPH and ABTS free radical scavenging activity

In the DPPH assay, DPPH radical will receive a hydrogen atom to form a reduced stable diamagnetic diphenyl-picrylhydrazine molecule with the addition of an anti-oxidant (Mi-Yea *et al.*, 2003 and Nessa *et al.*, 2004). The absorbance decreases as a result of colour changes from purple to yellow as the radical is scavenged by antioxidants. The more rapidly the absorbance decreases, the more potent is the antioxidant activity of the compound in terms of hydrogen donating ability (Yen and Duh, 1994).

According to this study, mangrove tannins as well as other tannins investigated tannins presented a substantial scavenging activity (Fig. 3.19). An increase of scavenging activity was observed as the concentrations of tannins increased and a maximum scavenging activity was reached at $3.0x10^{-2}$ mg mL^{-1}. A drastic

increase of scavenging activity of almost 50 % was observed for chestnut tannins when the concentration increased from $5.0x10^{-3}$ mg mL^{-1} to $1.0x10^{-2}$ mg mL^{-1}. The scavenging ability of all tannins was comparable to that of (+)-catechin and L-ascorbic acid antioxidant standards and even exceeded the DPPH radical scavenging ability of the synthetic antioxidant BHT from $5.0x10^{-3}$ mg mL^{-1} to $5.0x10^{-2}$ mg mL^{-1}.

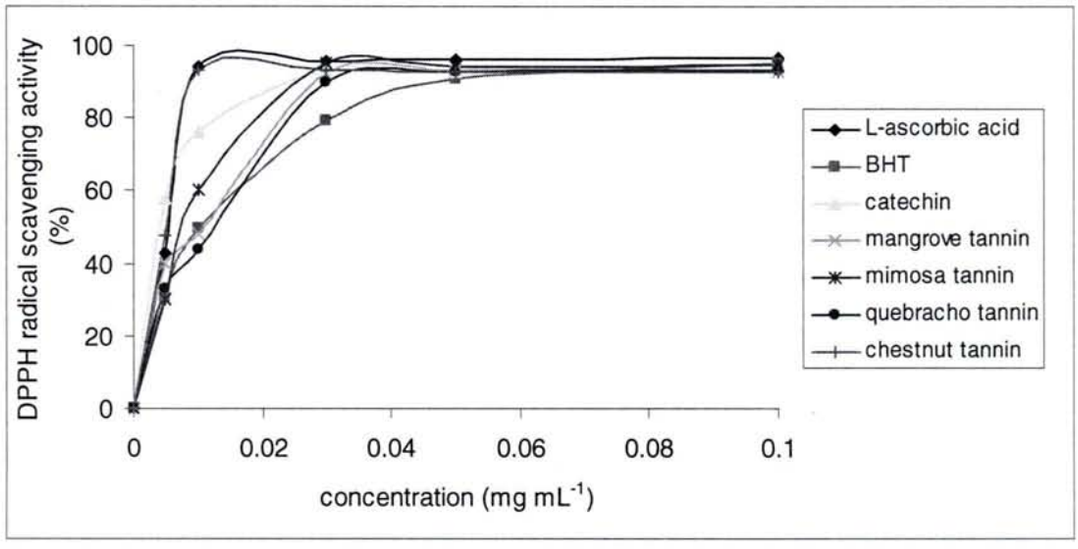

Fig. 3.19 Free radical scavenging activities of tannins measured using DPPH assay. L-ascorbic acid, BHT and catechin were used as reference compounds.

Similarly, in the ABTS assay, azide radicals will attack phenolic compounds rather indiscriminately owing to their strong electrophilicity (Rice-Evans *et al.*,1996). The absorbance at 414 nm decreases as a result of the bleaching of the blue-green solution as the radical is scavenged by anti-oxidants through donation of hydrogen from the phenolic group to form the stable ABTS-H (Goh *et al.*, 2003).

Similar scavenging activity pattern was observed for the ABTS assay (Fig. 3.20). An increase of scavenging activity was observed as the concentrations of tannins increased to reach a plateau at $5.0x10^{-2}$ mg mL^{-1}. All tannins exhibited essentially the same percentage scavenging activity as the catechin and L-ascorbic acid antioxidant standards from then on, signifying that all tannins, particularly mangrove tannin are potent antioxidants.

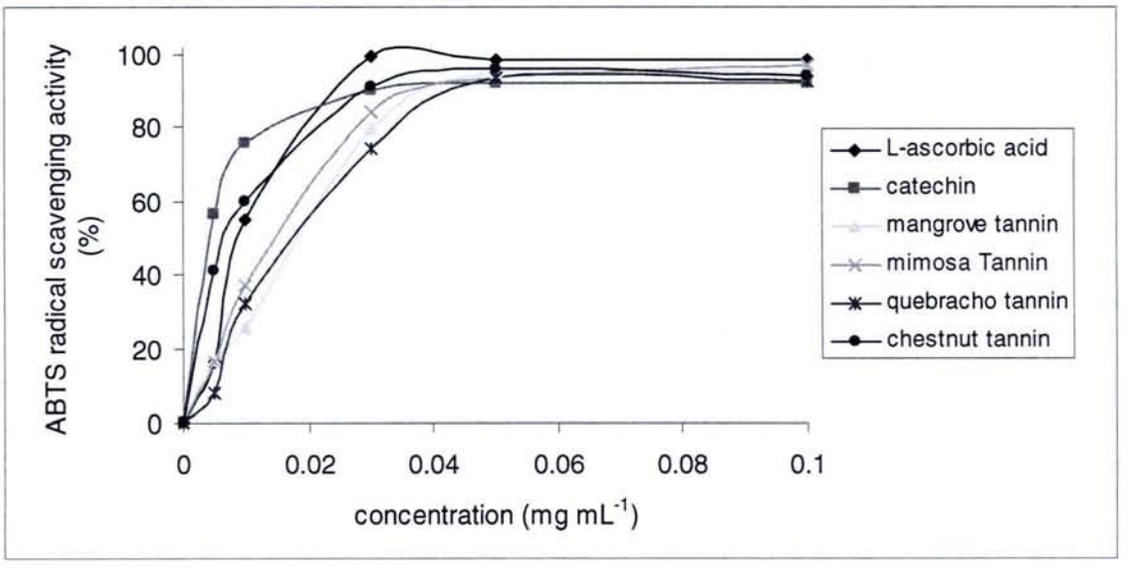

Fig. 3.20 Free radical scavenging activities of tannins measured using ABTS assay. L-ascorbic acid and catechin were used as reference compounds.

3.4 Electrochemical tests

3.4.1 Inhibition studies of mangrove tannins

Initially the influences of the different concentrations of mangrove tannins on mild steel corrosion were conducted at pH 0.5 and pH 8.0. Fig. 3.21 shows the effect of concentration on the inhibitory performance of mangrove tannins at pH 0.5. Although no inhibition effect was observed after the addition of 0.1 g L^{-1} tannin, a gradual decrease of the same gradient in the cathodic curves were observed as the tannin concentration increased from 1.0 g L^{-1} to 6.0 g L^{-1}.

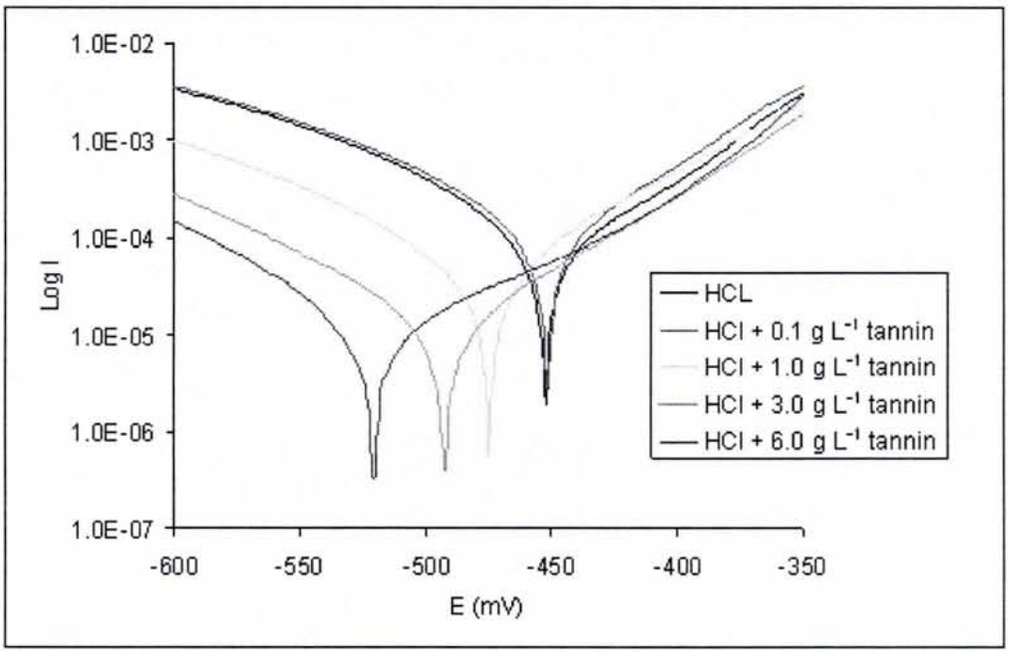

Fig. 3.21 The effect of concentration of mangrove tannins on the potentiodynamic curves of steel at pH 0.5.

This observation suggests that the mechanism of the hydrogen evolution reaction was the same as these concentrations were increased. It has also been proposed that no change in Tafel slopes prove the blocking effect as a reason of the decrease in the cathodic current (Vracar and Drazic, 2002).

Table 3.5 summarises the inhibition efficiency, *IE* (%) of mild steel in 0.5 M HCl containing the various concentrations of mangrove tannins based on $Icorr$ from the Tafel curves which was calculated according to the following equation :

$$IE(\%) = \frac{Icorr_O - Icorr}{Icorr_O} x100 \qquad (3.1)$$

Where $Icorr_o$ and $Icorr$ are the uninhibited and inhibited corrosion current densities respectively while the inhibition efficiency, *IE* (%) calculated by the polarisation resistance according to the following equation :

$$IE(\%) = \frac{Rp - Rp_O}{Rp} x100 \qquad (3.2)$$

Where Rp_O and Rp are the uninhibited and inhibited polarisation values respectively, assuming that β_A and β_c are unmodified by inhibition.

Table 3.5 Comparison of the inhibition efficiency, *IE (%)* of steel at pH 0.5 containing the various concentrations of mangrove tannins.

Concentration of mangrove tannins ($g\ L^{-1}$)	*IE (%)* (from Tafel curve)	*IE (%)* (from *Rp*)
0.1	0	0
1.0	66.9	66.7
3.0	88.2	87.9
6.0	92.1	89.9

The inhibition efficiency calculated using both methods was found to be similar. A gradual increase in efficiency as the concentrations of mangrove tannin were increased was observed. More than 80 % inhibition was achieved with 3.0 $g\ L^{-1}$ and 6.0 $g\ L^{-1}$ of mangrove tannins.

Conversely, no inhibition was observed at pH 8.0 (Fig. 3.22). The curves remained cluttered with no significant change in the E_{corr} and I_{corr} values. Thus, from the results obtained, the possibility of corrosion inhibition at a much lower pH than 0.5 was investigated and Fig. 3.23 shows the results of the inhibition of tannin at pH 0. It produced similar curves to that of pH 0.5. However the inhibition at this pH was limited to 3.0 g L^{-1} tannin due to the lower solubility of the tannin at this pH. Our studies have also shown that corrosion rate was reduced in HCl solution at pH 2.0 and pH 4.0 in the presence of 3.0 g L^{-1} mangrove tannin.

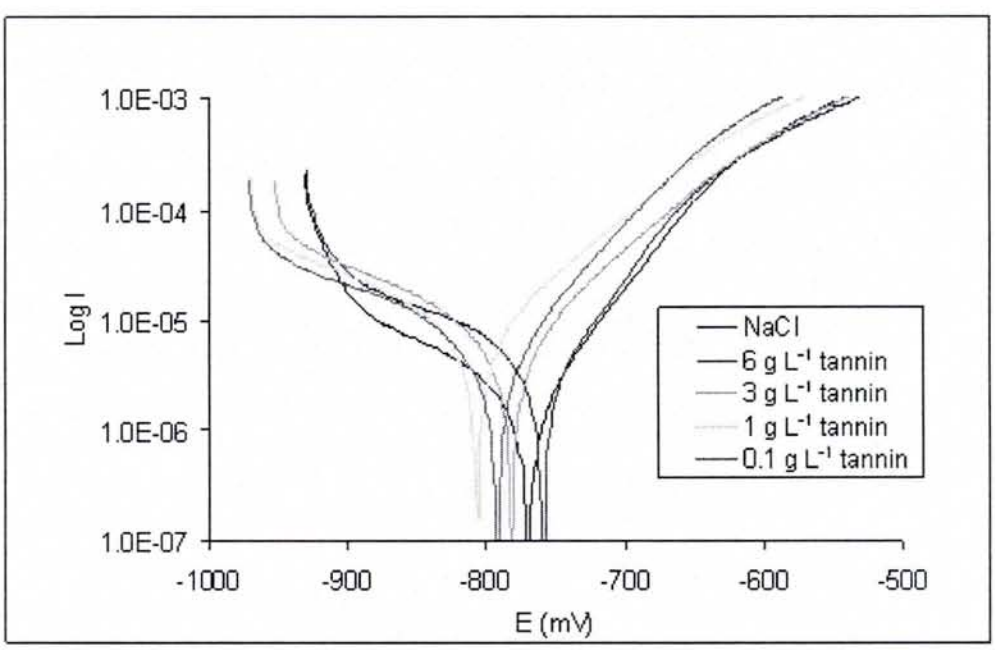

Fig. 3.22 The effect of concentration of mangrove tannins on the potentiodynamic curves of steel at pH 8.0.

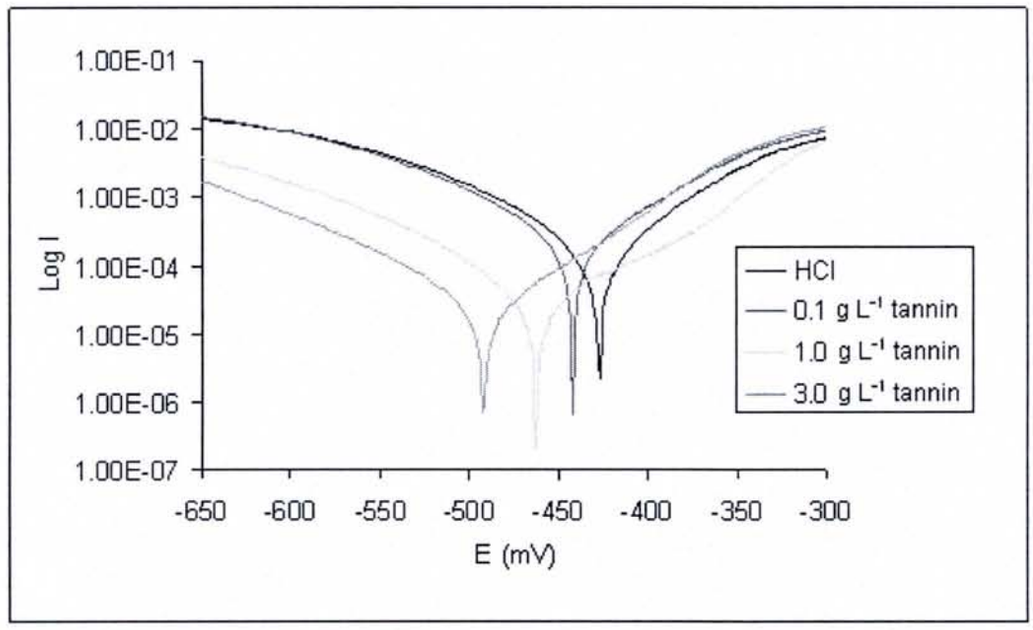

Fig. 3.23 The effect of concentration of mangrove tannins on the potentiodynamic curves of steel at pH 0.

As shown from the FTIR spectrums, HPLC and TGA analyses in sections 3.1 and 3.2, the mangrove tannin consisted predominantly of condensed tannins. Thus studies were undertaken to compare the inhibition behaviour between the entire mangrove tannins (mixed tannins) and condensed tannins. The condensed tannins showed similar potentiodynamic curves as the mixed tannins with particularly almost the same E_{corr} values as shown in Table 3.6. The E_{corr} values decrease according to the 0.06 pH variation of the H^+/H_2 system equilibrium potential.

Table 3.6 Corrosion potentials of mixed tannins and condensed tannins at different pH values.

pH	E_{corr} (mV/SCE)	E_{corr} (mV/SCE)
	Mixed tannins	Condensed tannins
0.02	-492	-451
0.5	-492	-441
2.0	-609	-630
4.0	-759	-763

Table 3.7 represents the percentage inhibition based on the I_{corr} and R_p respectively. The condensed tannin showed a decrease in the percentage inhibition with increasing pH, similar to the mixed tannin. The small percentage difference between the entire mangrove tannin and condensed tannin indicated that the inhibition is predominantly provided by the condensed tannin substituent of mangrove tannin.

Table 3.7 Comparison of the inhibition efficiency, *IE (%)* of steel in HCl at pH 0, 0.5, 2.0 and 4.0 containing 3.0 g L^{-1} of the various tannins investigated.

Types of tannins and pH values	*IE (%)* (from Tafel curve)	*IE (%)* (from *Rp*)
pH=0		
Mangrove tannin	87.9	84.5
Mimosa tannin	97.6	94.1
Quebracho tannin	95.5	94.0
Chestnut tannin	97.2	96.3
Condensed tannin of mangrove	82.4	79.6
pH=0.5		
Mangrove tannin	88.2	87.4
Mimosa tannin	96.2	95.4
Quebracho tannin	80.2	86.3
Chestnut tannin	87.9	84.2
Condensed tannin of mangrove	82.0	68.2
pH=2.0		
Mangrove tannin	71.6	68.2
Mimosa tannin	82.3	80.5
Quebracho tannin	54.8	57.6
Chestnut tannin	28.2	17.6
Condensed tannin of mangrove	62.1	46.6
pH=4.0		
Mangrove tannin	44.2	21.9
Mimosa tannin	0	0
Quebracho tannin	0	0
Chestnut tannin	0	0
Condensed tannin of mangrove	41.2	0

3.4.1.1 Comparison of the inhibitory action with several commercial tannins

Since 3.0 g L^{-1} and 6.0 g L^{-1} mangrove tannins displayed almost the same inhibition efficiencies, 3.0 g L^{-1} of tannins were used for subsequent studies. The similarity in tannin behaviour shown from the antioxidant properties (section 3.3) is again reflected in the electrochemical studies. From this study it was found that the potentiodynamic curves of mimosa, quebracho and chestnut tannins exhibited shifts in the cathodic curves to lower density currents similar to mangrove tannins at pH 0, 0.5 and 2.0, signifying that all tannins act as cathodic inhibitors. An example of these observations is given in Fig. 3.24.

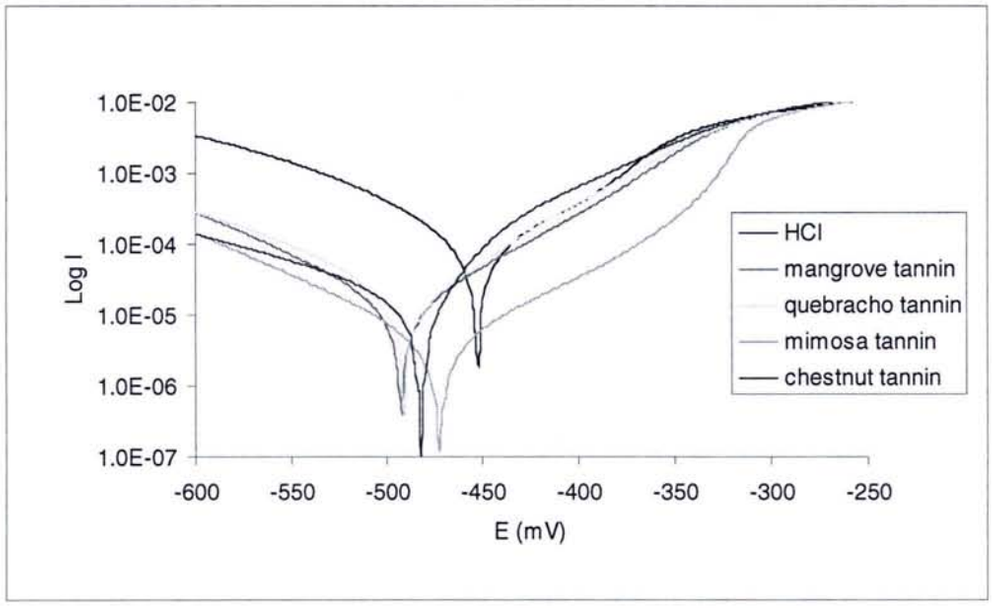

Fig. 3.24 The potentiodynamic curves of mild steel containing various tannins at pH 0.5.

Table 3.7 also represents the inhibition efficiency, *IE* (%) based on I_{corr} and R_p measurements for mild steel in HCl containing the various tannins at pH 0, 0.5, 2.0 and 4.0. Regardless of whether the inhibition efficiency was calculated from

I_{corr} from the potentiodynamic curves or *Rp* measurements, all tannins show a similar pattern of a decrease in efficiency with the increase in pH. More than 80 % inhibition efficiency was achieved at pH 0 and 0.5 for all tannins. A drastic reduction in efficiency was observed for chestnut tannin as the pH increased from pH 0.5 to 2.0.

The advantage of mangrove tannins as an inhibitor is shown from the variation of R_p with time of immersion at pH 4.0 in Fig. 3.25. Right from the beginning, mangrove tannin produced R_p values of almost twofold higher than the rest of the tannins. It began to produce higher R_p values than that of HCl solution after 8 hr of immersion. The R_p for chestnut and mimosa tannins remained almost constant throughout. Although there was a steady increase of R_p with time for quebracho tannin, it did not surpass the R_p of HCl.

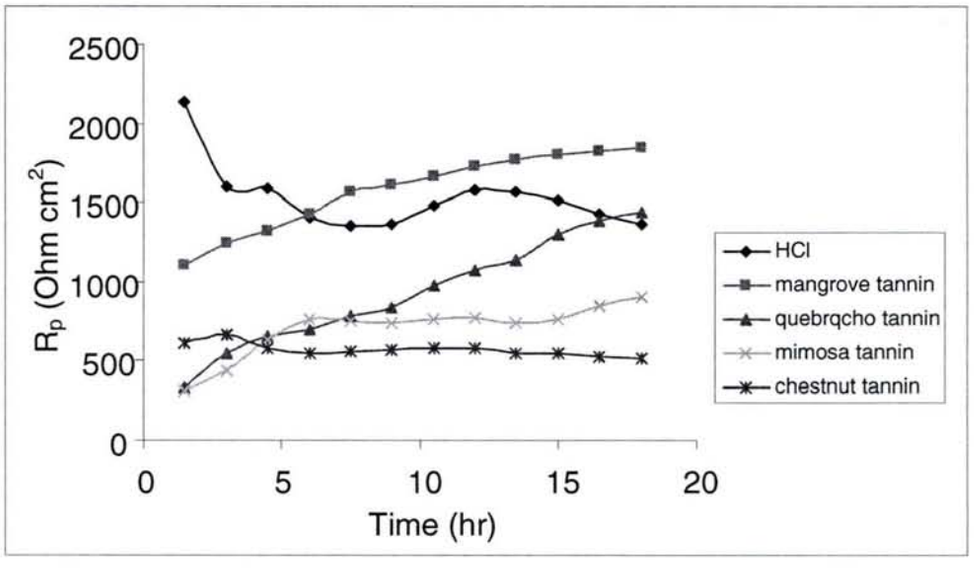

Fig. 3.25 Variation of polarisarion resistance, R_p with time of immersion containing 3.0 g L^{-1} tannins in HCl solution at pH 4.0.

3.4.1.2 Synthesis of ferric-tannates

Observation of the surface of the working electrode after the electrochemical process revealed the existence of blue-black precipitate typical to that of ferric-tannates (Seavell, 1992) for pH 2.0, 4.0 and 8.0. The formation of ferric-tannates which induces an increase in the protective efficiency of the surface has been claimed by several authors (Ross and Francis, 1978; Deslauriers, 1987; Gust, 1991; Matamala *et al.*, 1994; Pardini *et al.*, 2001). Hence ferric-tannates were synthesised between ferric salts and mangrove tannins at several pH and its role in corrosion protection is correlated. Precipitates of increasing mass were obtained as the pH of solution increased. The colour of the supernatant and precipitate formed after centrifugation are shown in Table 3.8.

Table 3.8 Colour of supernatant and precipitate following centrifugation.

pH	supernatant	Precipitate
0.5	orange	Brownish
1.5	orange	Brownish
2.0	bluish-green	blue-black
3.0	almost clear	blue-black
4.0	almost clear	blue-black
6.0	almost clear	blue-black
8.0	almost clear	blue-black

The XRD pattern of ferric-tannates confirmed that it is amorphous (Fig. 3.26). The UV-visible spectrum of the supernatant after the centrifugation process was taken and the following spectrums in Fig. 3.27 were obtained.

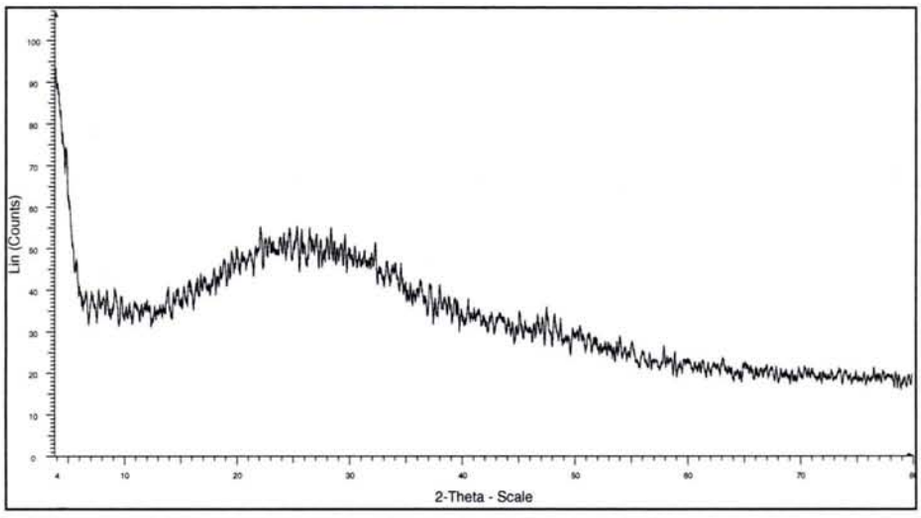

Fig. 3.26 XRD pattern of ferric-tannates synthesised at pH 3.0.

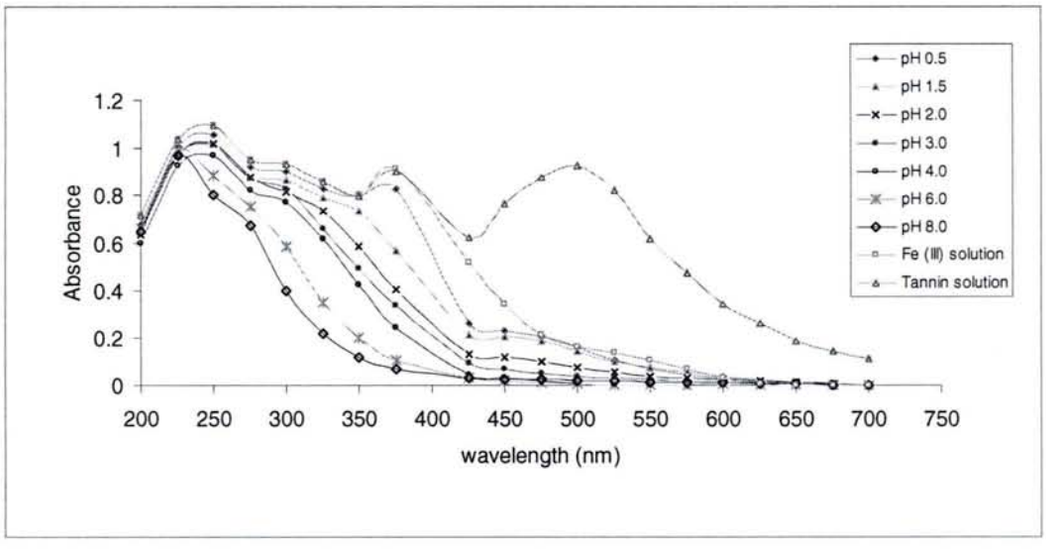

Fig. 3.27 UV-visible spectrum of ferric-tannate solution synthesised at several pH following the centrifugation process.

The Fe (III) solution and mangrove tannin solution produced the same λ_{max} at 240 nm, 300 nm and 375 nm. The tannin solution however produced an additional λ_{max} at 500 nm. With increasing pH from 0.5 to 4.0, the absorbance of

the ferric-tannates was found to decrease and the λ_{max} reduced to two from pH 2.0 onwards. The ferric-tannate formation at pH 6.0 and 8.0 resulted in further reduction in absorbance and the λ_{max} not only reduced to one but also shifted to lower wavelength at 225 nm.

Comparison between the tannin FTIR spectrum and the ferric-tannate spectrums in Fig. 3.28 revealed that several of the peaks not only shifted slightly, but reduced in intensity. The reduced intensity of a broad peak at around 3300 cm^{-1} (not shown) designates the reduction of free OH groups (Gust, 1991) since it is the proximity of hydroxyl groups on the aromatic rings which enable the tannins to chelate iron ions. The spectrum of the complex formed at pH 0.5 resembled more of the tannin than the ferric-tannates at pH 3.0 and 4.0. The 1516 cm^{-1} peak became less intensed at pH 4.0 and totally disappeared at pH 6.0 and 8.0. In addition the ferric-tannates at pH 6.0 and pH 8.0 presented new peaks at 471 cm^{-1} and 1020 cm^{-1} respectively. The peaks at 471 cm^{-1} and 1020 cm^{-1} are characteristic peaks of lepidocrocite, γ-FeOOH (Naszarani, 1997).

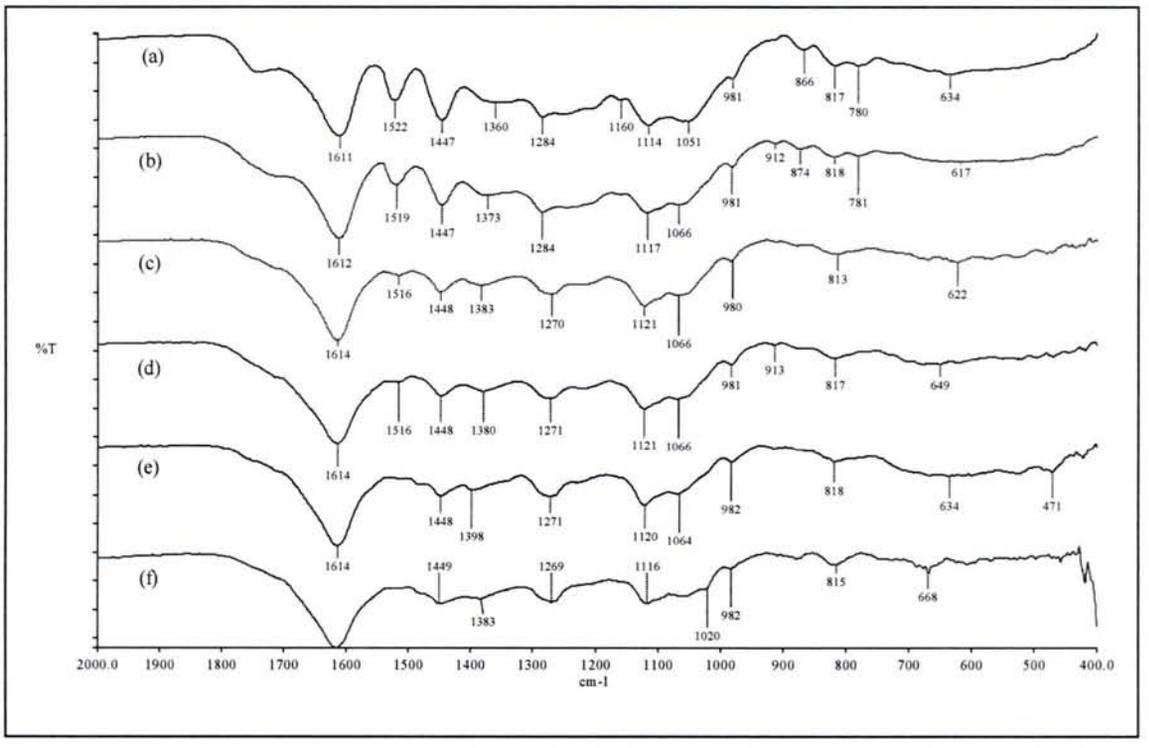

Fig. 3.28 FTIR spectrum of (a) mangrove tannins and ferric-tannates synthesised at pH (b) 0.5 (c) 3.0 (d) 4.0 (e) 6.0 and (f) 8.0 after immersion in mangrove tannin solution for 24 hours.

In view of these results, the effect of time of immersion on ferric-tannate formation at pH 3.0 was explored and the results of the FTIR analysis are shown in Fig. 3.29. The formation of ferric-tannates was instantaneous as witnessed from the similarity in major peaks shown by ferric-tannates

Although the above results have shown that ferric-tannate formation was instantaneous, the UV spectrums of the supernatant after centrifugation showed otherwise (Fig. 3.30). Similar absorbance profiles were obtained only after 1 hour of immersion.

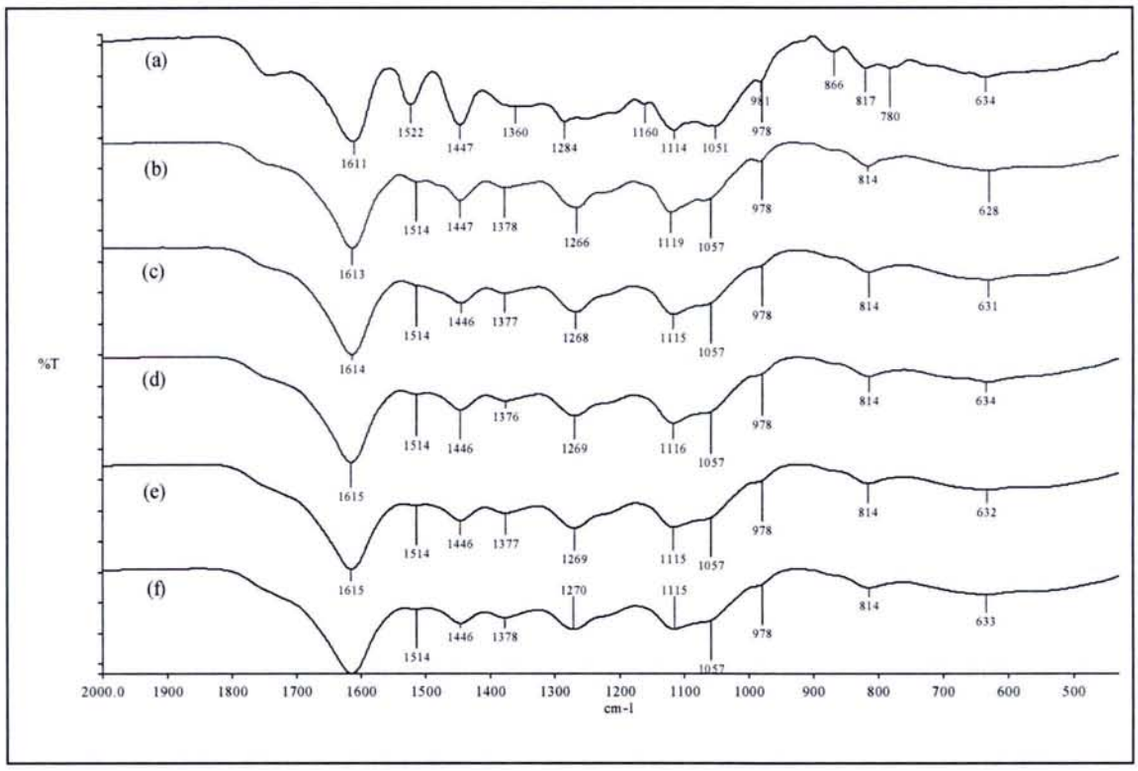

Fig. 3.29 FTIR spectrum of (a) mangrove tannins and ferric-tannates after (b) 0.25 hr (c) 1 hour, (d) 7 hours, (e) 24 hours and (f) 48 hours immersion in mangrove tannin solution at pH 3.0.

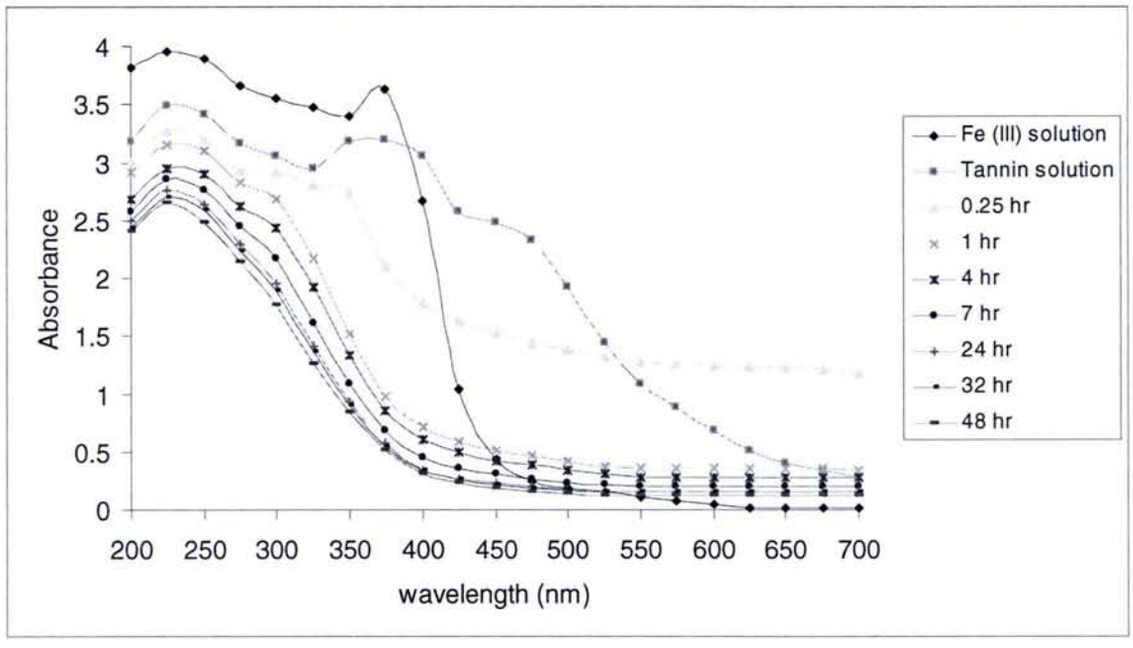

Fig. 3.30 UV spectrums of ferric-tannate solution synthesised at pH 3.0 with respect to time of immersion in mangrove tannin solution.

The formation of ferric-tannates is further confirmed from the TGA/DTG analysis of tannates at pH 3.0 and pH 8.0 (Fig. 3.31). The decomposition profile of the tannates was definitely different from the decomposition profile of mangrove tannin. The ferric-tannates formed at pH 3.0 recorded 53.0 % weight loss at 260.2 °C and a further 19.7 % weight loss at 314.4 °C while the ferric-tannates formed at pH 8.0 showed 43.2 % weight loss at 223.3 °C and 58.2 % weight loss at 310.3 °C. The XRD analysis of the decomposition products revealed the conversion of mangrove tannates to hydrohematite, $Fe_2O_3.xH_2O$ at pH 3.0. From the mass of the oxide formed, it was found that a bis-complex of ferric-tannate was formed for the reaction between tannins and Fe^{3+} (Appendix 7). On the other hand a different XRD pattern of the decomposition of ferric-tannates at pH 8.0 was obtained, which suggested that hydro iron oxide, $Fe_2O_3.0.27H_2O$ was formed.

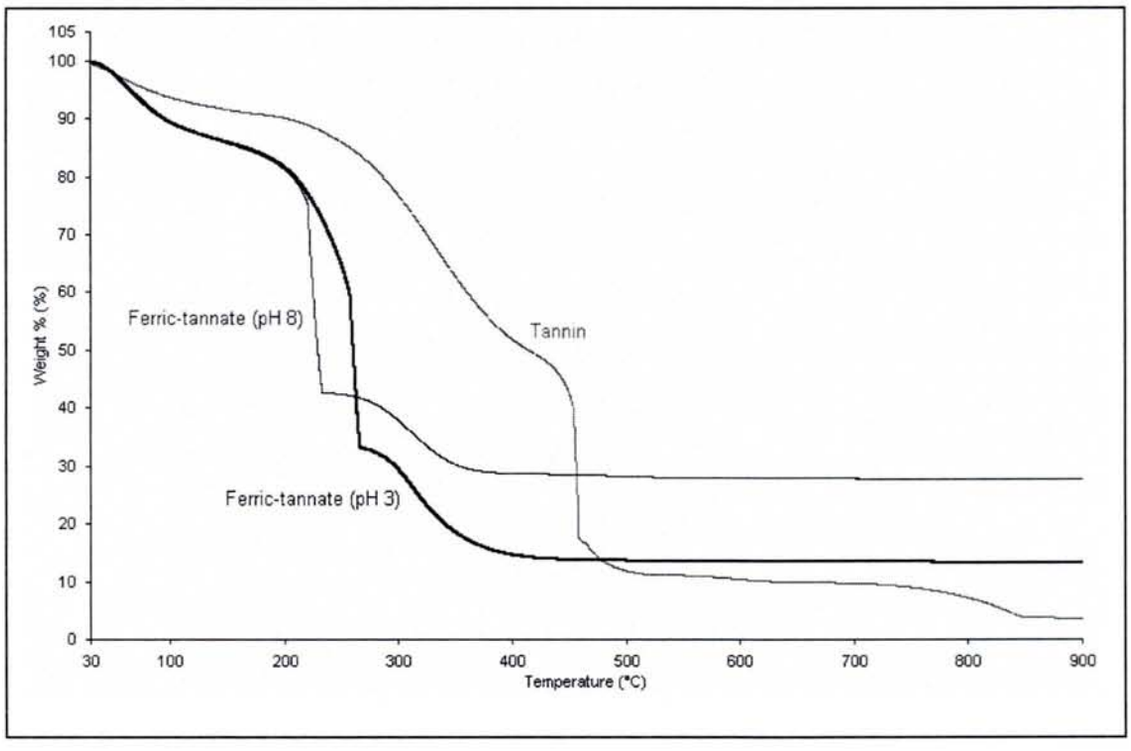

Fig. 3.31 Thermal decomposition profiles of ferric-tannates synthesised at pH 3.0 and pH 8.0.

3.4.2 Inhibitory performance of catechin, epicatechin, epigallocatechin and epicatechin gallate

In our previous study (section 3.2), the characterisation of mangrove tannin was carried out by depolymerising condensed tannin in the presence of phloroglucinol nucleophiles in acidic ethanol. This was followed by the separation of flavan-3-ols and their phloroglucinol adducts using reversed phase high performance liquid chromatography. As a result of the analysis, four major components constituting mangrove tannin were identified. These monomers are catechin, epicatechin, epicatechin gallate and epigallocatechin. The inhibitory performance of these monomers was evaluated in HCl solution at pH 0.5 so as to have a better rationalization of mangrove tannin inhibitory action.

From the results of the inhibitory performance of the monomers via electrochemical tests, it was found that all monomers caused some degree of inhibition for concentrations as low as $2.5x10^{-3}$ M. The potentiodynamic curves of steel in HCl at pH 0.5 containing catechin, epicatechin, epigallocatechin and epicatechin gallate are shown in Fig. 3.32. The inhibitory performance was found to be dependent on concentration as witnessed from the different responses of the individual monomers with respect to concentration. Interestingly, one could observe that all monomers exhibited shifts in the cathodic curves to lower density currents at all concentrations. The cathodic Tafel slope of ~110 mV $decade^{-1}$ and the anodic slope of ~100 mV $decade^{-1}$ corresponding to the reduction of H^+ to H_2 and oxidation of Fe to Fe^{2+},

respectively, remained unchanged after the addition of the various concentrations of monomers.

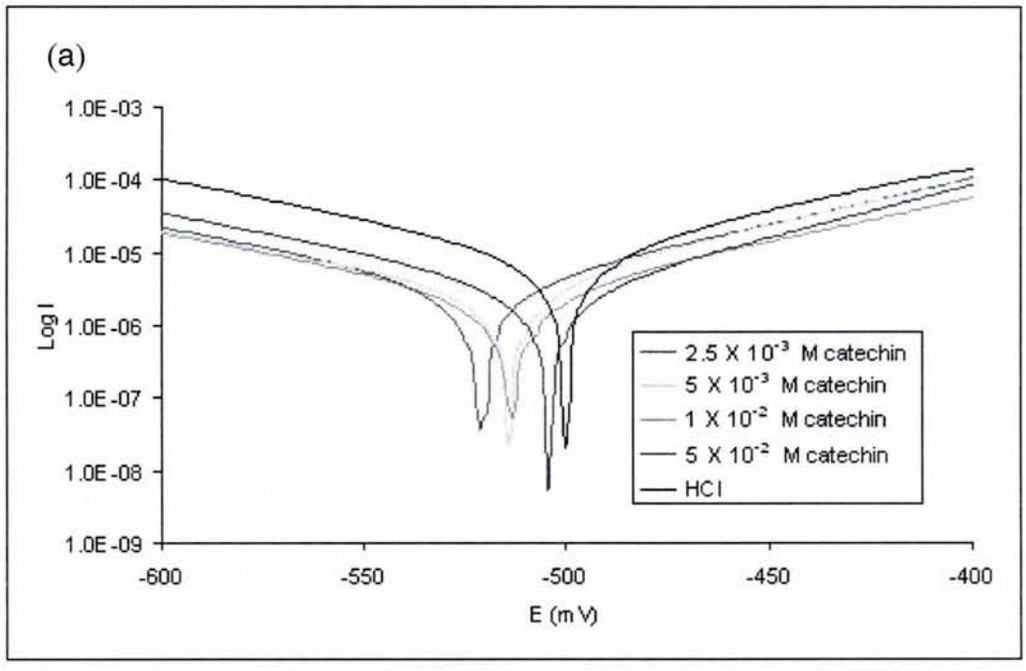

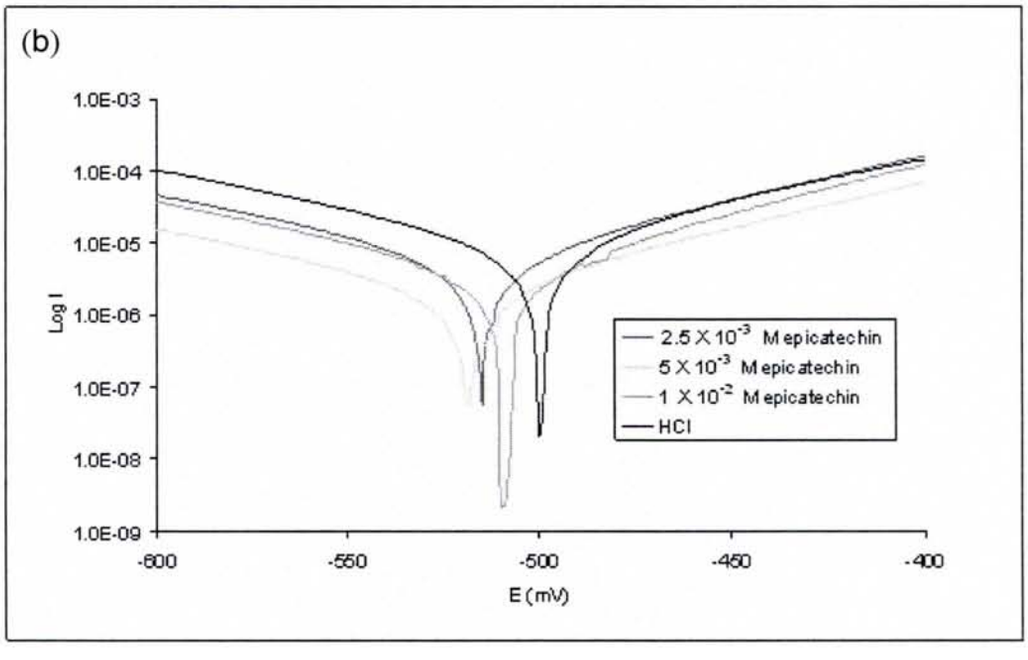

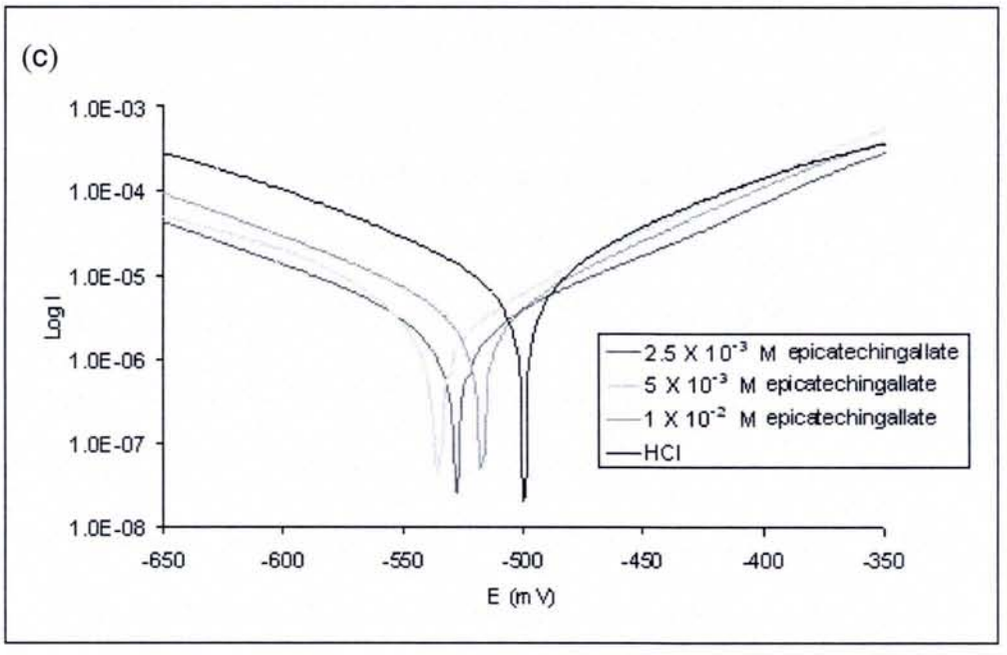

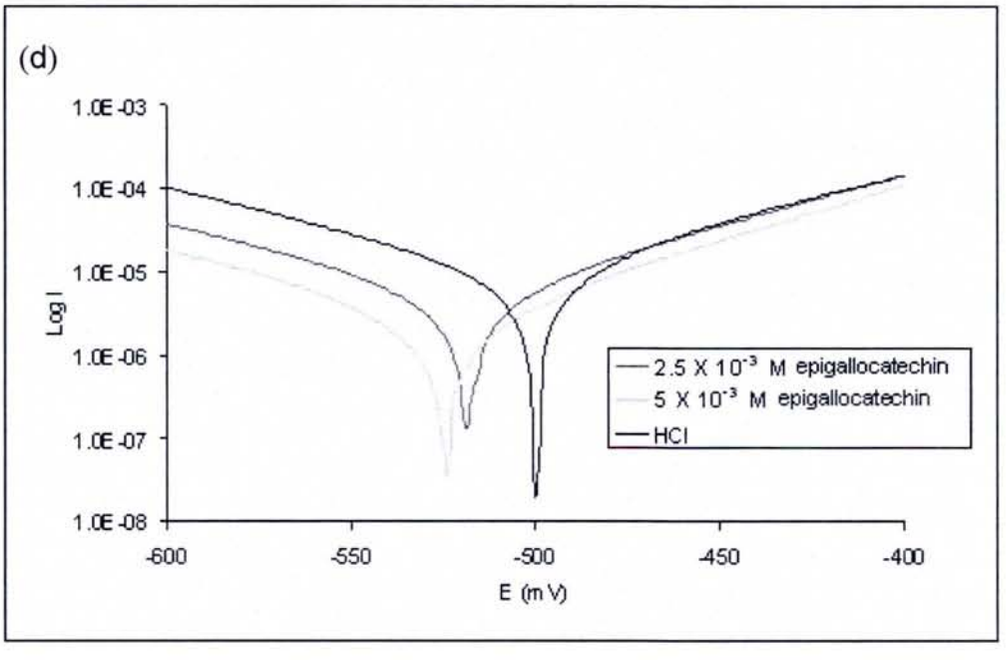

Fig. 3.32 Potentiodynamic curves of steel in HCl at pH 0.5 containing various concentrations of (a) catechin, (b) epicatechin, (c) epicatechin gallate and (d) epigallocatechin.

Fig. 3.33 shows the R_p evolution with immersion time. At a concentration of $2.5x10^{-3}$ M, *Rp* values decreased slightly with time of immersion for all monomers. With the exception of epigallocatechin, the R_p values at a concentration of $5.0x10^{-3}$ M initially decreased to a certain point, and after 10 hours of immersion, the R_p slowly increased. At the higher concentration of $1.0x\ 10^{-2}$ M, the R_p for catechin reduced to reach a minimum after 9 hours of immersion, after which the R_p then increased, reaching a plateau after 13.5 hours. The R_p for all the other monomers initially reduced and finally remained constant after 7.5 hours. Epicatechingallate, epicatechin and catechin gave the highest R_p at $2.5x10^{-3}$ M, $5.0x10^{-3}$ M and $1.0x10^{-2}$ M respectively throughout 18 hours of immersion. Nevetheless, the R_p values have the same order of magnitude for all monomers, indicating the same inhibition efficiency.

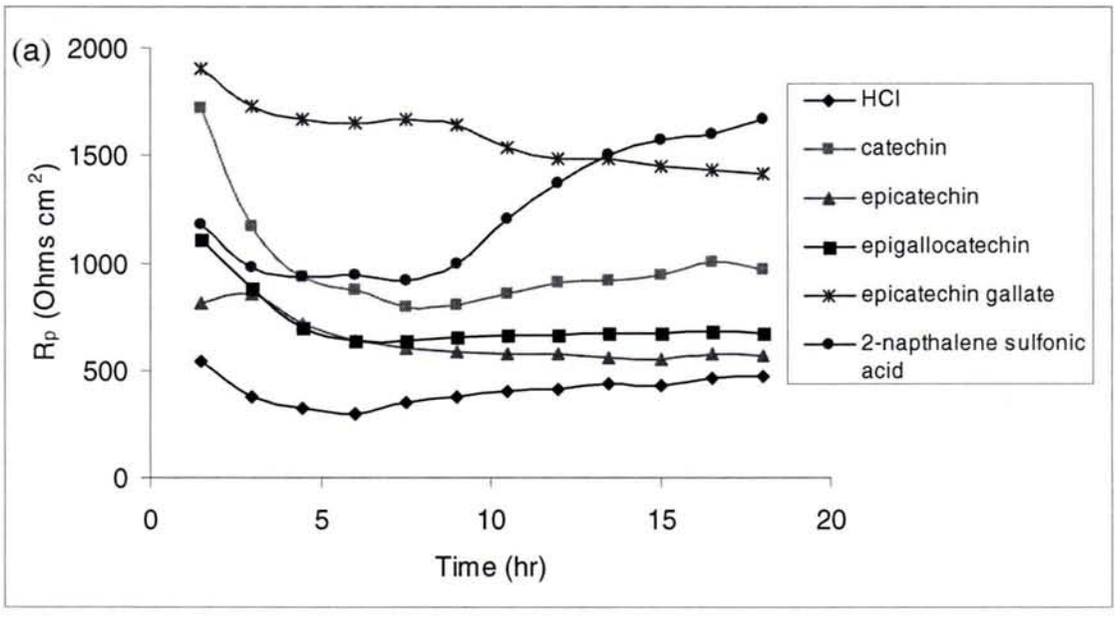

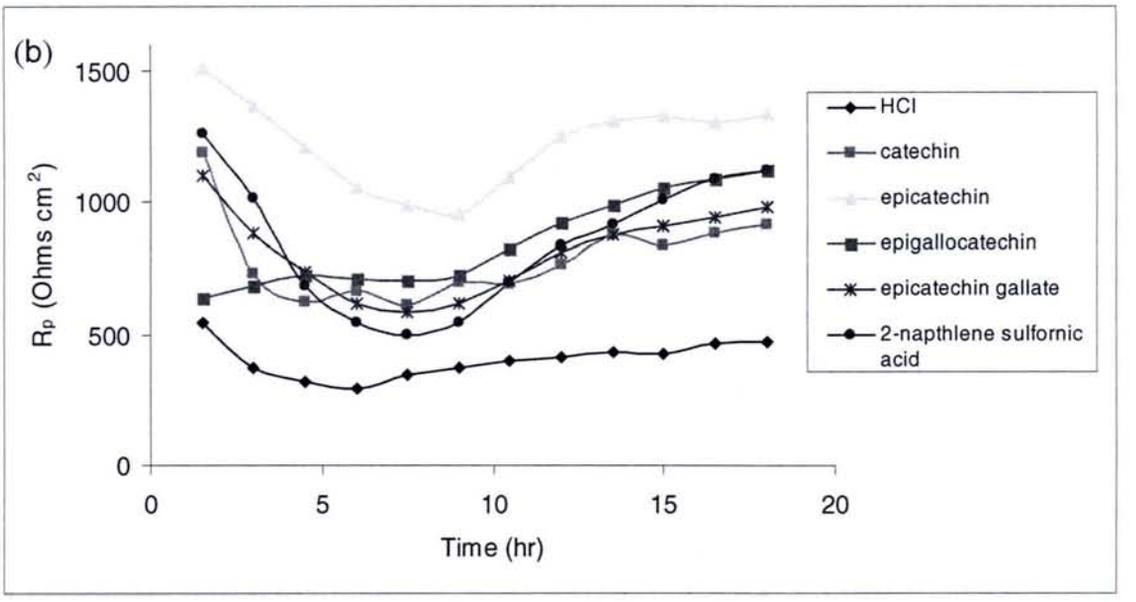

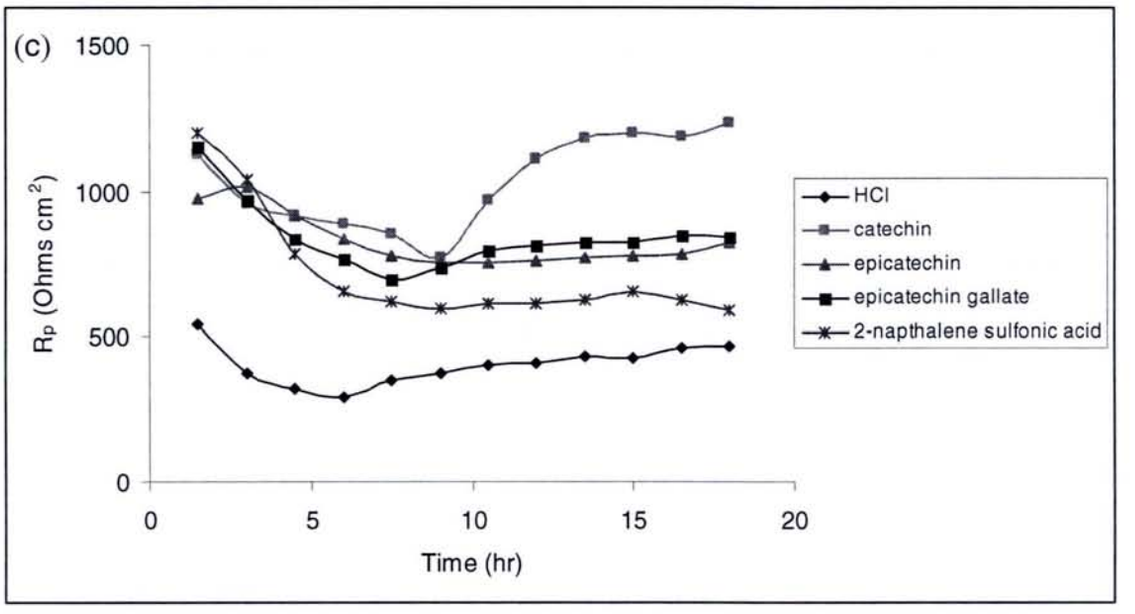

Fig. 3.33 Variation of polarisarion resistance, R_p with time of immersion containing (a) 2.5×10^{-3} M, (b) 5.0×10^{-3} M and (c) 1.0×10^{-2} M flavanoids and 2-napthalene sulfonic acid in HCl at pH 0.5.

As a comparison, the inhibitory performances of the monomers were compared with that of 2-napthalene sulfonic acid, a cathodic inhibitor as claimed by Vracar and Drazic (2002). It was indeed quite difficult to compare the performance of 2-napthalene sulfonic acid to the monomers from the potentiodynamic curves. This difficulty however was overcome by comparing the inhibitory performance from the R_p measurements (Fig. 3.33). At a concentration of $2.5x10^{-3}$ M, the R_p values for 2-napthalene sulfonic acid were initially below that of catechin and epicatechin gallate and were almost constant for the first nine hours of immersion after which the R_p values increased to exceed all flavanoids after 18 hours of immersion. At a concentration of $5.0x10^{-3}$ M, the evolution of R_p was similar to the flavanoids while at $1.0x10^{-2}$ M, it initially gave the highest R_p values but as the time of immersion increased the R_p values dropped to produce the lowest R_p values as compared to the flavanoids.

Table 3.9 lists the inhibition efficiency, *IE* (%) calculated by the polarisation resistance measurements. For almost all the monomers investigated, a maximum inhibition of more than 70 % was achieved. Catechin produced inhibition of between 56 %-69 % and a maximum was reached at $1.0x10^{-2}$ M. A wider variation of inhibition efficiency of 33 % - 72 % was observed for epicatechin with the highest value at $5.0x10^{-3}$ M. On the other hand, for epicatechin gallate a decrease in efficiency as the concentrations increased was observed, attaining 74 % inhibition at the lowest concentration of $2.5x10^{-3}$ M. Due to the scarcity of epigallocatechin, inhibition efficiency investigated was limited to concentrations up to $5.0x10^{-3}$ M, with a maximum inhibition of 65 % at this concentration. On the whole, the monomers produced

more than 50 % inhibition for concentrations of $1.0x10^{-2}$ M and below. The inhibition efficiency of 2-napthalene sulfonic acid decreased as the concentration was increased to $1.0x10^{-2}$ M and exceeded 80 % only when concentrations were increased to $5.0x10^{-2}$ M and $1.0x10^{-1}$ M.

Table 3.9 Inhibition efficiency of steel corrosion at different concentrations of flavanoids based on polarisation resistance, R_p measurements at pH 0.5.

Flavanoid monomers	Concentration (M)	*IE (%)* (from *Rp*)
Catechin	2.5×10^{-3}	61
	5.0×10^{-3}	61.5
	1.0×10^{-2}	69.4
	5.0×10^{-2}	56.3
Epicatechin	2.5×10^{-3}	33.5
	5.0×10^{-3}	71.9
	1.0×10^{-2}	54.4
	5.0×10^{-2}	44.1
Epicatechin gallate	2.5×10^{-3}	73.6
	5.0×10^{-3}	61.8
	1.0×10^{-2}	55.4
Epigallocatechin	1.0×10^{-3}	0
	2.5×10^{-3}	44.1
	5.0×10^{-3}	55.4
2-napthalene sulfonic acid	2.5×10^{-3}	77.5
	5.0×10^{-3}	66.3
	1.0×10^{-2}	36.2
	5.0×10^{-2}	88.5
	$1.0x10^{-1}$	92.6

3.4.2.1 Molecular modelling of flavanoid monomers

Electrochemical techniques coupled with surface analytical techniques can provide basic information on the mechanism of corrosion inhibition. A need exist for a systematic approach for characterisation of the interaction between the organic inhibitor molecule and the metal or alloy. Theoretical approaches provide means of analysing these interactions.

The effectiveness of a corrosion inhibitor can be related to its molecular spatial structure and molecular electronic structure in addition to its hydrophobicity, solubility and dispersibility (Sastri and Perumarredi, 1994, 1997). An example of an optimised molecular structure of a catechin monomer with its HOMO density is as shown in Fig. 3.34 (a). The highest values of the electron density of the frontier orbital were found within the vicinity of the A aromatic ring. Conversely, for epicatechin [Fig. 3.34 (b)] and epigallocatechin [Fig. 3.34 (c)] highest values of the electron density of the frontier orbital were found within the vicinity of the B aromatic ring.

(a)

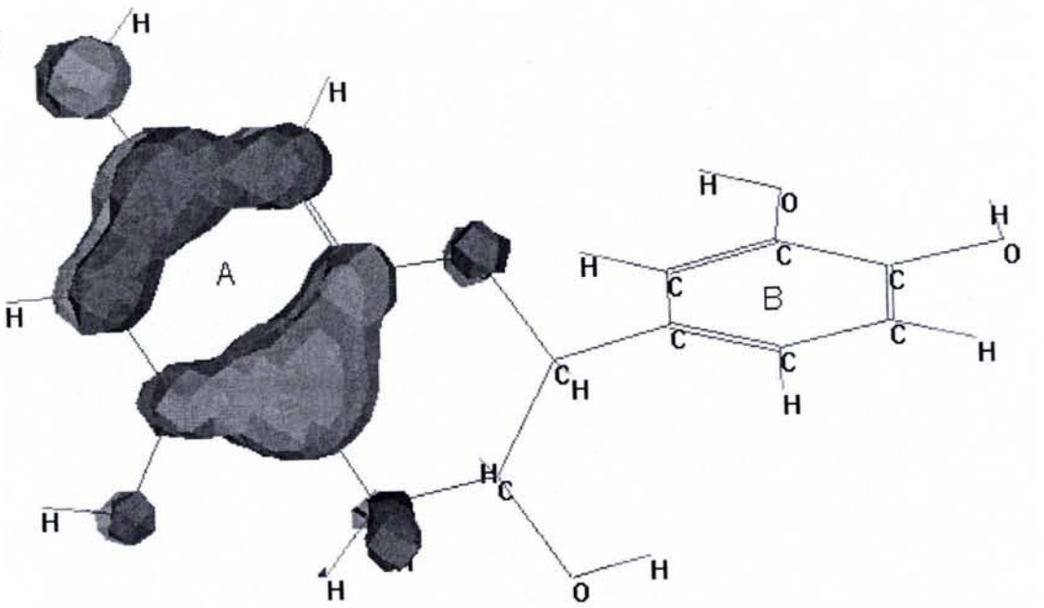

(b)

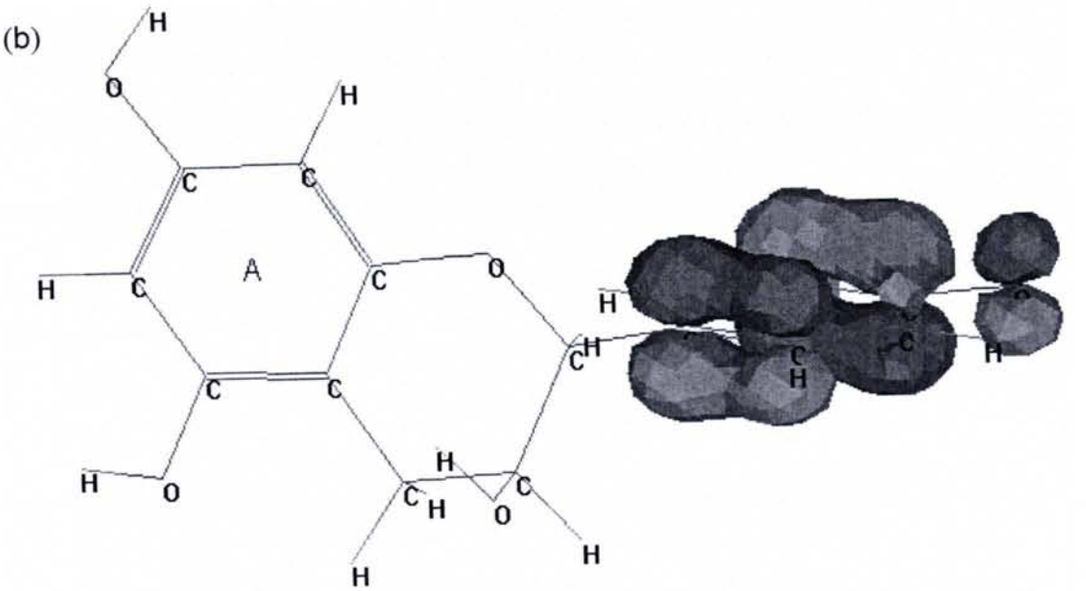

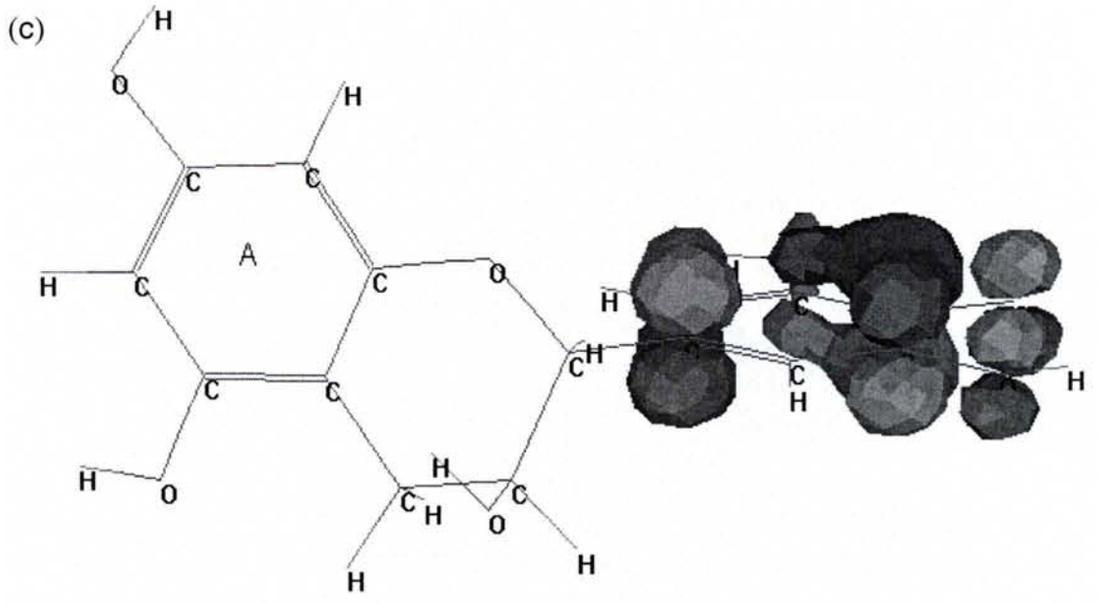

Fig. 3.34 HOMO density as an isosurface for (a) catechin, (b) epicatechin and (c) epigallocatechin monomers in optimised conformations.

The HOMO density of flavanoid monomers having the structures shown in Fig. 3.35 in optimised conformations are summarised in Table 3.10. For structure 3.35 (a), introduction of the -OH groups to the B ring did not change the HOMO density as the electron density remained to be found within the vicinity of the A aromatic ring. With structure 3.35 (b), the HOMO density was initially concentrated at the A aromatic ring

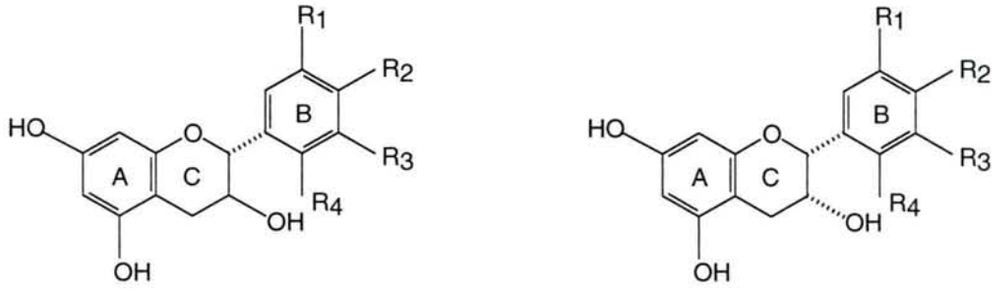

Fig. 3.35 Two structural formulas of flavanoids investigated in the molecular modelling experiment.

Table 3.10 Distribution of HOMO electron density of flavanoid molecules.

Structure (a)	Electron Density
(i) R_1=H, R_2=OH, R_3=H, R_4=H (afzelechin)	Ring A
(ii) R_1=OH, R_2=OH, R_3=H, R_4=H (catechin)	Ring A
(iii) R_1=OH, R_2=OH, R_3=OH, R_4=H (gallocatechin)	Ring A
(iv) R_1=OH, R_2=OH,R_3=OH,R_4=OH	Ring A
Structure (b)	
(i) R_1=H, R_2=OH, R_3=H, R_4=H (epiafzelechin)	Ring A
(ii) R_1=OH, R_2=OH, R_3=OH, R_4=H (epicatechin)	Ring B
(iii) R_1=OH, R_2=OH, R_3=OH, R_4=H (epigallocatechin)	Ring B
(iv) R_1=OH, R_2=OH,R_3=OH,R_4=OH	Ring B

of epiafzelechin. Further addition of the –OH groups to the B ring, witnessed the transfer of the electron density to B ring.

The total energy, binding energy, heat of formation, total dipole moment, HOMO energies, LUMO energies, HOMO-LUMO energy gap and the fraction of electrons transferred from the flavanoid molecule to the iron atom, ΔN for α electrons are shown in Table 3.11. The fraction of electrons transferred from the flavanoid molecule to the iron atom, ΔN is given by (Martinez, 2002) :

$$\Delta N = \frac{X_{\mathrm{Fe}} - X_{\mathrm{inh}}}{2(\eta_{\mathrm{Fe}} - \eta_{\mathrm{inh}})} \qquad (3.3)$$

Where a theoretical value of X_{Fe} ~ 7 eV is taken for iron and η_{Fe} = 0 is taken assuming that the ionization potential, $I = A$, the electron affinity for bulk metals. The absolute electronegativity, X and the absolute hardness, η of iron and the flavanoid molecule is given by :

$$X = \frac{1}{2}(I + A) \qquad (3.4)$$

$$\eta = \frac{1}{2}(I - A) \tag{3.5}$$

Where A = - E_{LUMO} and I = - E_{HOMO}.

For structure 3.35 (a), the increase in the –OH groups on the B ring increased the total dipole moment of the molecule. No specific trend was observed for structure 3.35 (b). The HOMO-LUMO energy gap of 8.79-9.19 eV and 0.27-0.30 fraction of electrons transferred were obtained for both structures.

Table 3.11 Total energy, binding energy, heat of formation, total dipole moment, HOMO energies, LUMO energies, HOMO-LUMO energy gap and the fraction of electrons transferred from the flavanoid molecule to the iron atom, ΔN for α electrons calculated from the molecular modelling.

Structure (a)	Total Energy (kcal mol^{-1})	Binding Energy (kcal mol^{-1})	Heat of Formation (kcal mol^{-1})	Total Sum Dipole (Debyes)	E_{HOMO} (eV)	E_{LUMO} (eV)	$E_{LUMO-HOMO}$ (eV)	ΔN
(i) R1=H, R2=OH, R3=H, R4=H	-79816.92	-3757.55	-166.97	2.13	-8.94	-0.02	8.92	0.2825
(ii) R1=OH, R2=OH, R3=H, R4=H	-86592.26	-3860.37	-210.23	2.17	-8.99	-0.06	8.94	0.2771
(iii) R1=OH, R2=OH, R3=OH, R4=H	-93367.89	-3963.49	-253.80	3.03	-8.99	-0.13	8.99	0.2756
(iv) R1=OH, R2=OH, R3=OH, R4=OH	-100140.87	-4063.95	-294.70	3.28	-8.91	-0.19	8.72	0.2805
Structure (b)								
(i) R1=H, R2=OH, R3=H, R4=H	-79817.44	-3758.06	-167.49	1.48	-9.06	0.13	9.19	0.2762
(ii) R1=OH, R2=OH, R3=H, R4=H	-86592.84	-3860.94	-210.81	2.41	-8.89	0.02	8.91	0.2876
(iii) R1=OH, R2=OH, R3=OH, R4=H	-93368.54	-3964.13	-254.44	2.22	-8.96	0.07	9.03	0.2828
(iv) R1=OH, R2=OH, R3=OH, R4=OH	-100141.95	-4065.03	-295.78	1.54	-8.74	0.04	8.79	0.3032

3.4.3 Cyclic voltammetry

The pH of the individual solution measured in its natural aqueous state is shown in Table 3.12.

Table 3.12 The pH of flavanoids and tannin solution investigated.

Type of solution	pH
Catechin	5.80
Epicatechin	5.85
Mangrove tannin	3.60
Mimosa tannin	4.50
Quebracho tannin	3.90
Chestnut tannin	4.80

3.4.3.1 Redox potential patterns of $1x10^{-3}$ M and $5x10^{-4}$ M catechin

At a scan rate as low as 10 mV s^{-1}, three anodic peaks at 420, 800 and 1225 mV and two cathodic peaks at 250 and 1050 mV were observed [Fig. 3.36 (a)]. As the scan rates were increased to 20 and 50 mV s^{-1}, an additional anodic peak was noticed while the two cathodic peaks remained. The reduction of the magnitude of anodic signals with subsequent cycles indicated the irreversibility of the oxidised species. The redox potential curves at different scan rates are shown in Fig. 3.36 (b) and 3.36 (c). At 100, 200 and 300 mV s^{-1}, the cathodic peak reduced to one, producing reduction potentials at 100, 120 and 140 mV respectively and the anodic peaks reduced to two peaks. The anodic signals reduced and the cathodic signals increased with subsequent cycles at 100 mV s^{-1} while at 200 and 300 mV s^{-1}, the cathodic signals remained constant and the anodic signals increased. Further increments in scan rates to finally at 1.0 V s^{-1}, three anodic peaks at 550 mV, 1000 mV and 1250 mV and one cathodic peak at 160 mV were observed. All redox signals remained constant throughout subsequent cycles at these higher scan rates.

(a)

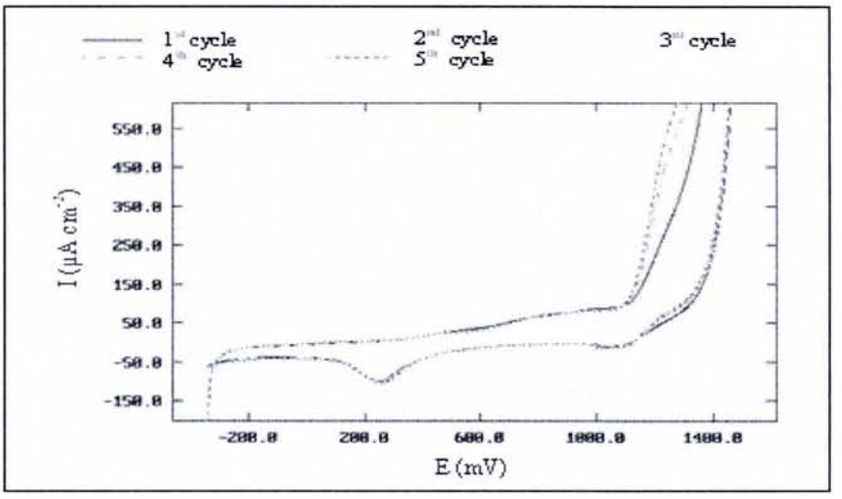

(b)

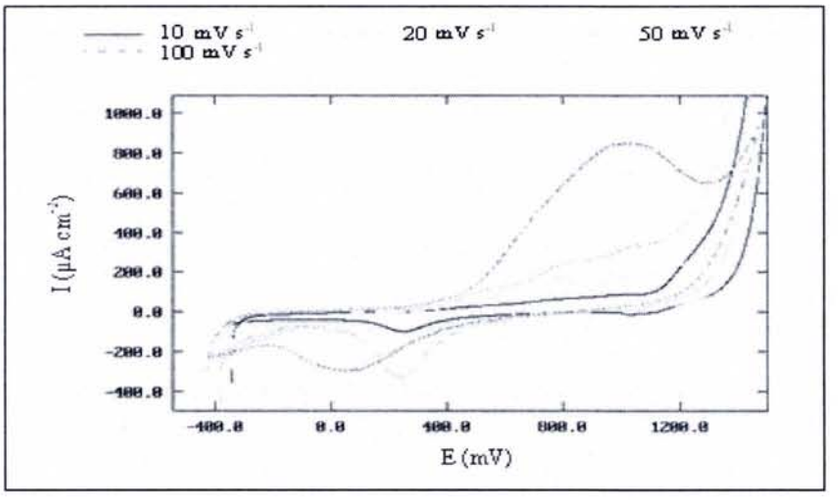

(c)

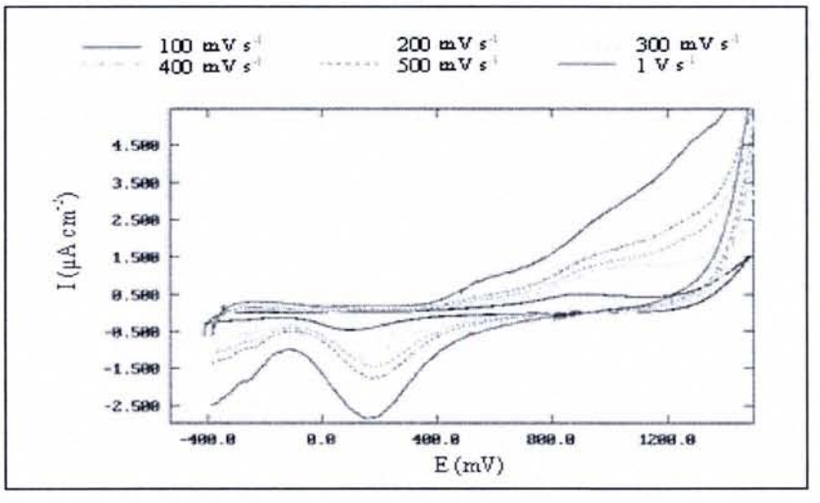

Fig. 3.36 Cyclic voltammograms of $1x10^{-3}$ M catechin at (a) different cycles with a scan rate of 10 mV s^{-1}, (b) scan rates of 10 – 100 mV s^{-1} and (c) scan rates of 100 – 1000 mV s^{-1}.

When $5.0x10^{-4}$ M catechin was used, two anodic peaks and one cathodic peak were observed regardless of scan rates (Fig. 3.37). Shifts in anodic peaks with respect to scan rates could be observed [Fig. 3.37 (a)]. Similarly, the current peaks were found to increase with increasing scan rates.

3.4.3.2 Redox potential patterns for $1x10^{-3}$ M epicatechin

Since better redox signals were given by $1x10^{-3}$ M catechin, epicatechin of the same concentration was used. From Fig. 3.38 (a), it was observed that as the scan rate increased, the anodic peak increased from a single peak (750 mV) at 10 mV s^{-1} to three peaks (300 mV, 550 mV and 850 mV) at 100 mV s^{-1} while the cathodic peak remained as one peak. The anodic peak was found to shift slightly to more positive potential and the cathodic peak moved to more negative potentials (100 mV to -140 mV) with increasing scan rates. It was also observed that the magnitude of anodic signals reduced with subsequent cycles. Unlike the anodic peaks, the cathodic peaks remained almost constant. As the scan rates were further increased to 1.0 V s^{-1}, the oxidation peaks at 550 mV, 1000 mV and 1250 mV were recorded. The reduction peak remained as one peak at 75 mV [Fig. 3.38 (b)] and the magnitude of the redox signals remained constant throughout the five cycles.

(a)

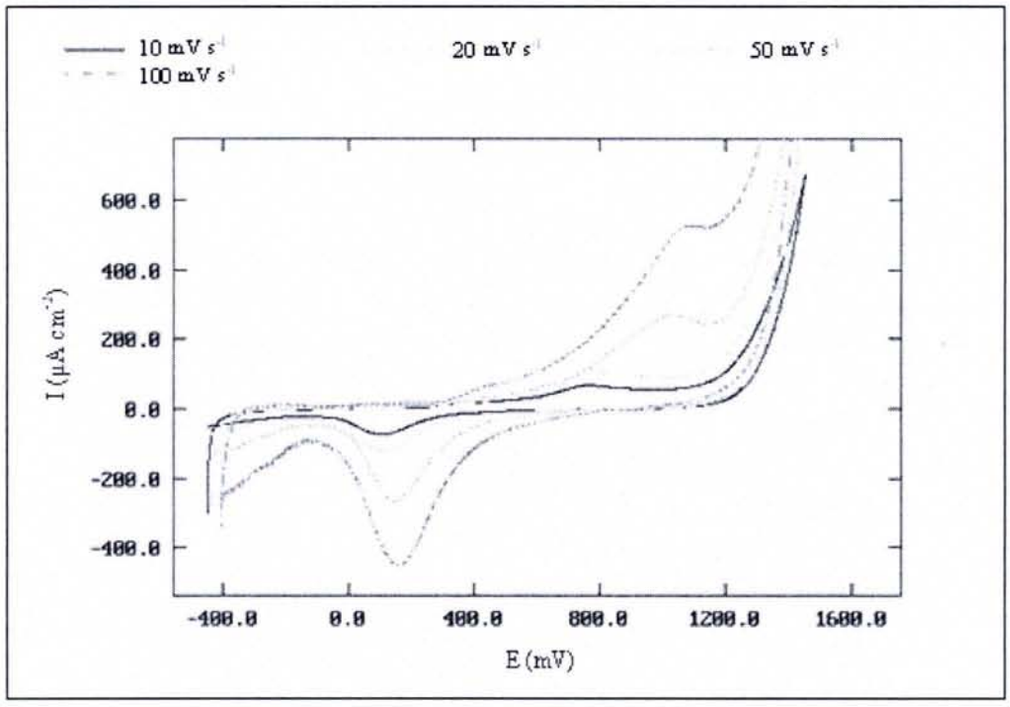

(b)

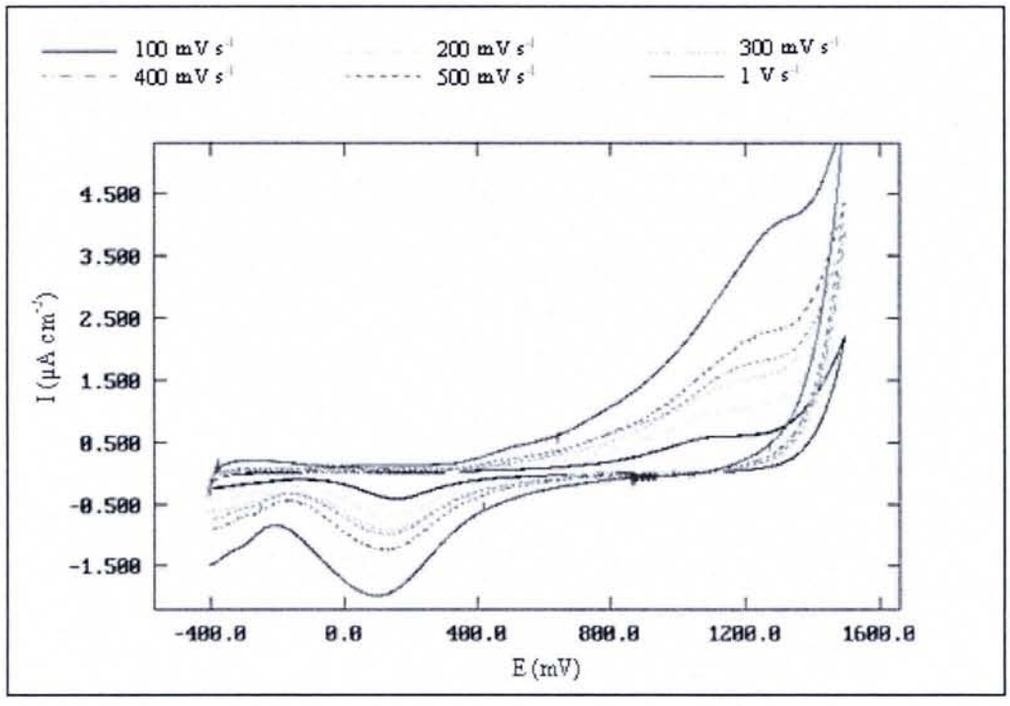

Fig. 3.37 Cyclic voltammograms of 5 X 10^{-4} M catechin at (a) scan rates of 10 – 100 mV s^{-1} and (b) scan rates of 100 – 1000 mV s^{-1}.

(a)

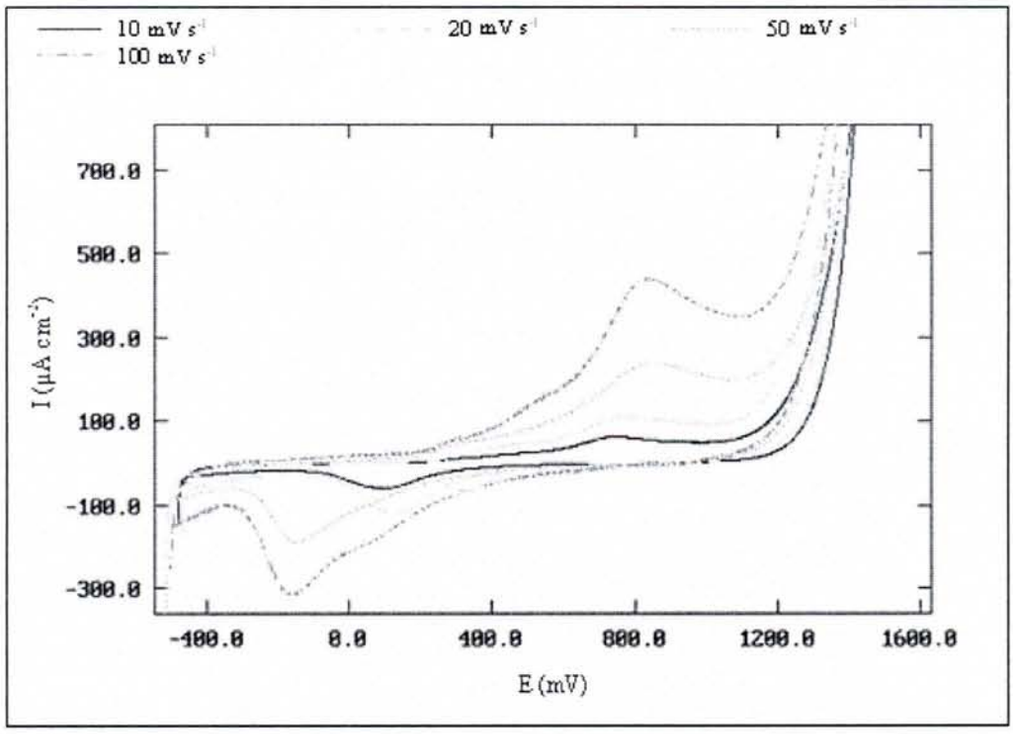

(b)

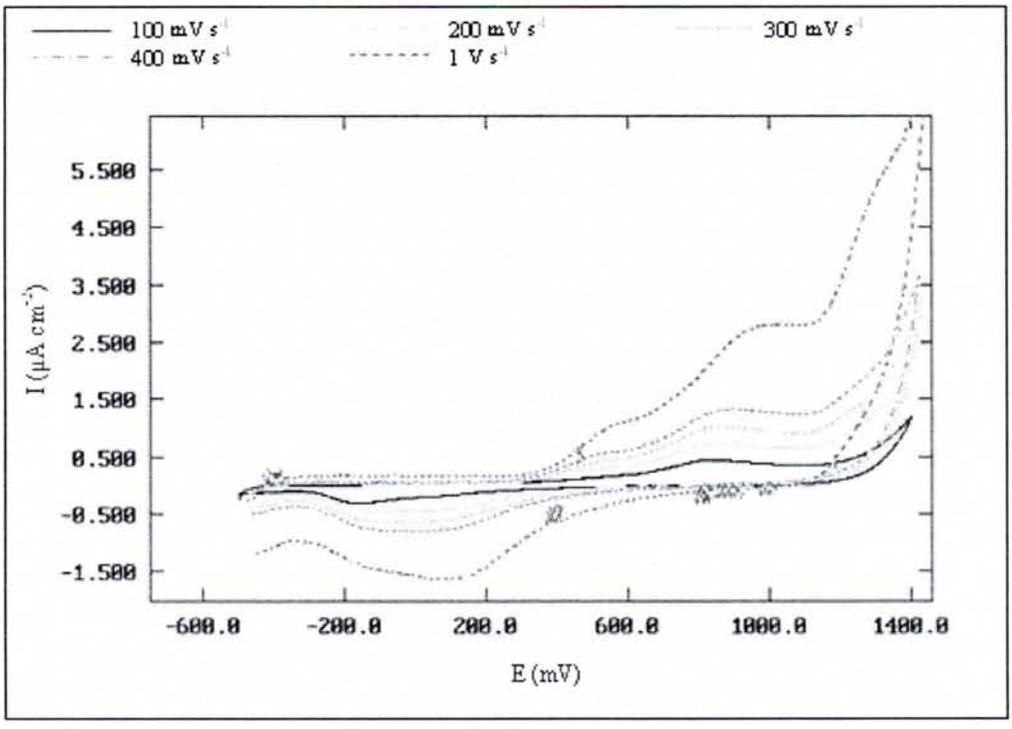

Fig. 3.38 Cyclic voltammograms of $1x10^{-3}$ M epicatechin at (a) scan rates of 10 – 100 mV s^{-1} and (b) scan rates of 100 – 1000 mV s^{-1}.

3.4.3.3 Redox potential patterns of tannins

The redox potential curves for mangrove tannin recorded two anodic peaks and two cathodic peaks at all scan rates investigated. The anodic peaks slowly shifted from 400 mV and 1100 mV at 10 mV s^{-1} to 600 mV and 1300 mV, respectively at 1.0 V s^{-1} (Fig. 3.39). The magnitude of redox signals remained almost constant throughout the five cycles at all scan rates.

Due to the weak signals shown by mimosa tannin at the lower scan rates (below 100 mV s^{-1}), identification of peaks was difficult. Initially only one weak anodic at ~ 1000 mV and one cathodic peak at 110 mV were observed [Fig. 3.40 (a)]. However as the scan rates were increased to 1V s^{-1}, additional anodic peaks at 500 mV and 1300 mV became noticeable [Fig. 3.40 (b)].

From Fig. 3.41 (a), it could be seen that at lower scan rates, quebracho tannin depicted potential curves similar to that of 5.0 x 10^{-4} M catechin. Of the individual scan rates below 100 mV s^{-1}, the magnitude of the peaks especially the anodic peaks reduced with subsequent cycles. At 100 mV s^{-1} and above, the magnitude of the peaks remained constant throughout the five cycles. The two anodic peaks at 300 mV and 100 mV were more noticable at the lower scan rates as compared to the higher scan rates. One cathodic peak at 100 mV remained for all scan rates and an anodic peak at ~ 350 mV was witnessed at 100 mV s^{-1} and above [Fig. 3.41 (b)].

Chestnut tannin initially gave rise to one anodic peak and two cathodic peaks at 10 mV s^{-1} which then exhibited two anodic peaks at 400 mV and 1000 mV and one cathodic peak at 200 mV as the scan rates increased to 100 mV s^{-1} [Fig. 3.42 (a)]. These peaks continued to be observed at above 100 mV s^{-1} in addition to an anodic peak at - 400 mV [Fig. 3.42 (b)].

(a)

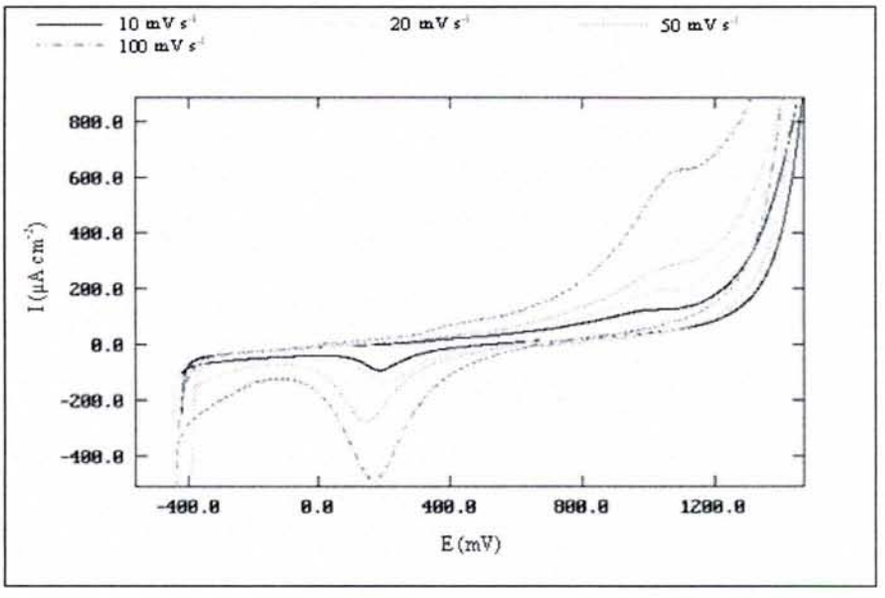

(b)

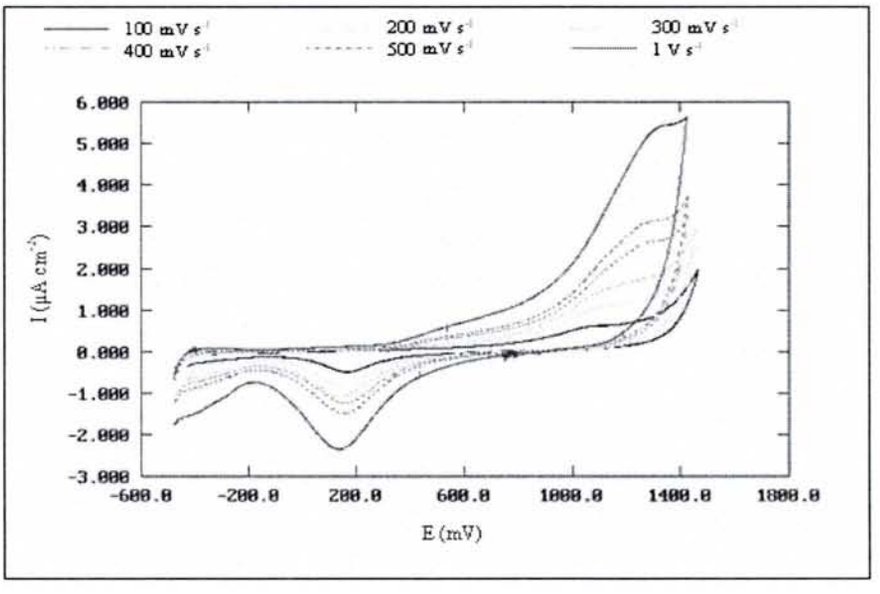

Fig. 3.39 Cyclic voltammograms of 3.0 g L^{-1} mangrove tannins at (a) scan rates of 10 – 100 mV s^{-1} and (b) scan rates of 100 – 1000 mV s^{-1}.

(a)

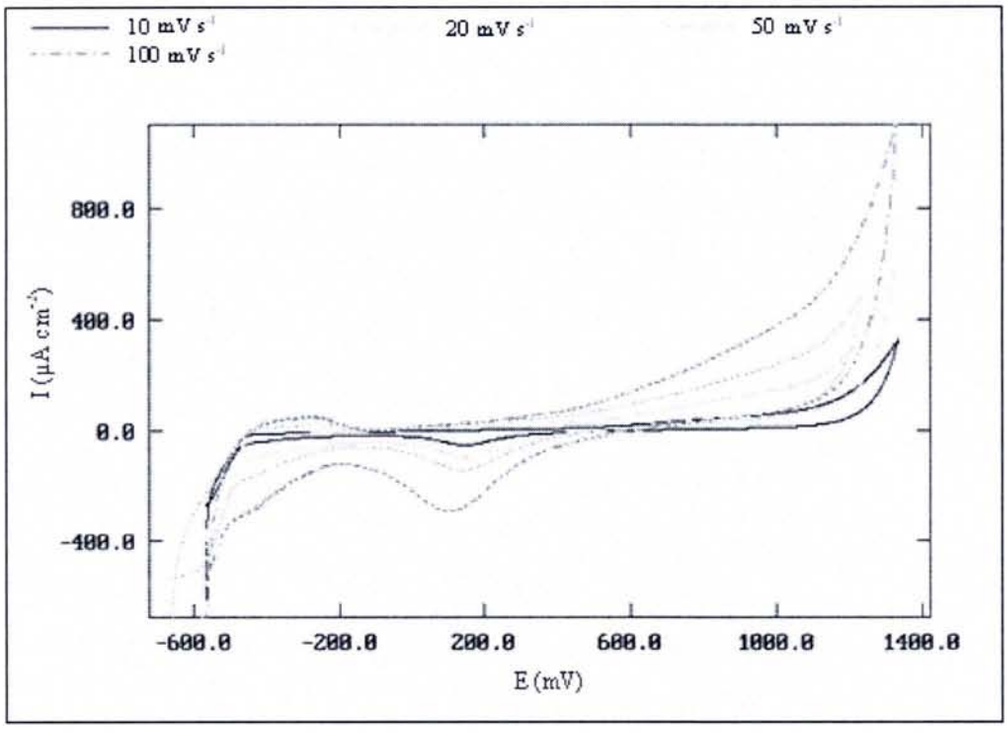

(b)

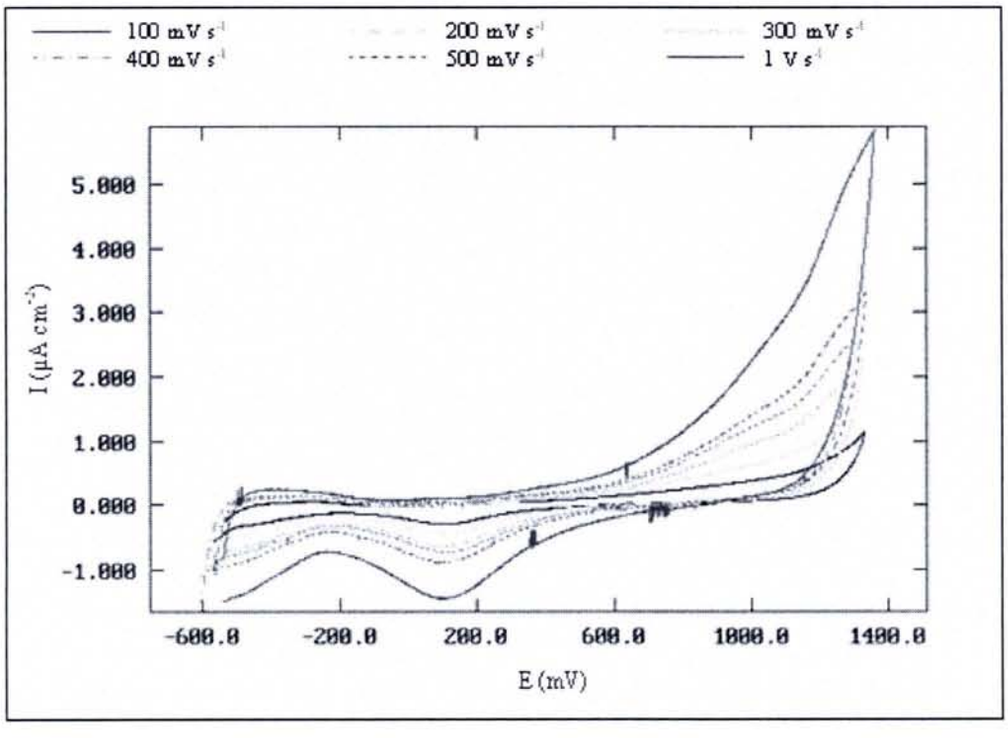

Fig. 3.40 Cyclic voltammograms of 3.0 g L^{-1} mimosa tannins at (a) scan rates of 10 – 100 mV s^{-1} and (b) scan rates of 100 – 1000 mV s^{-1}.

(a)

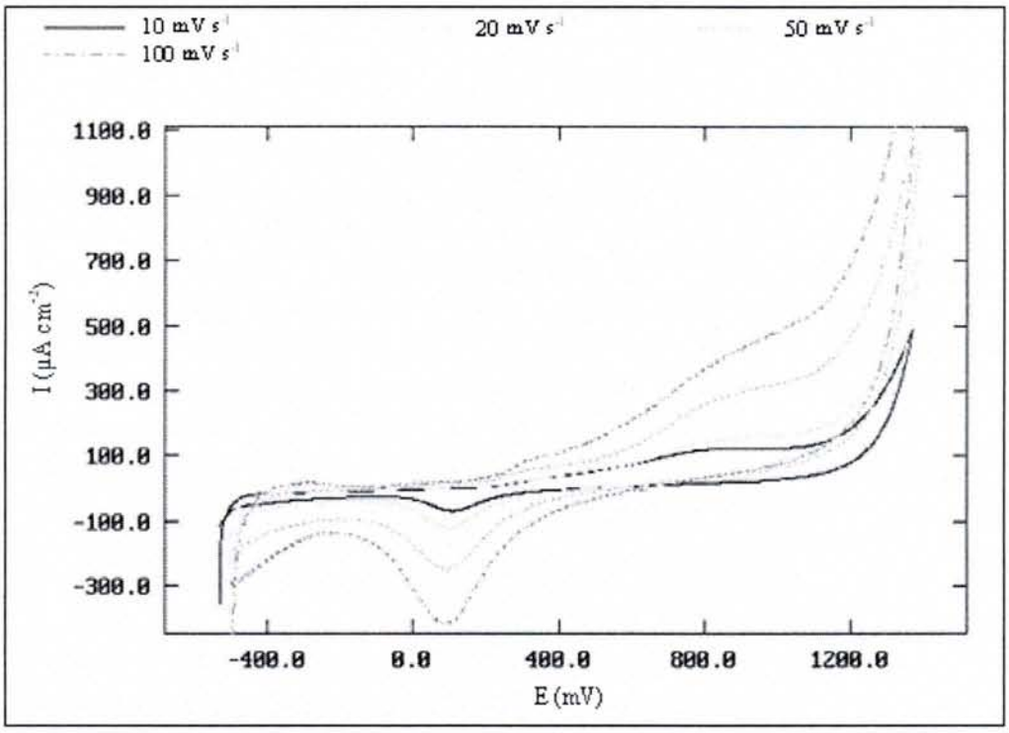

(b)

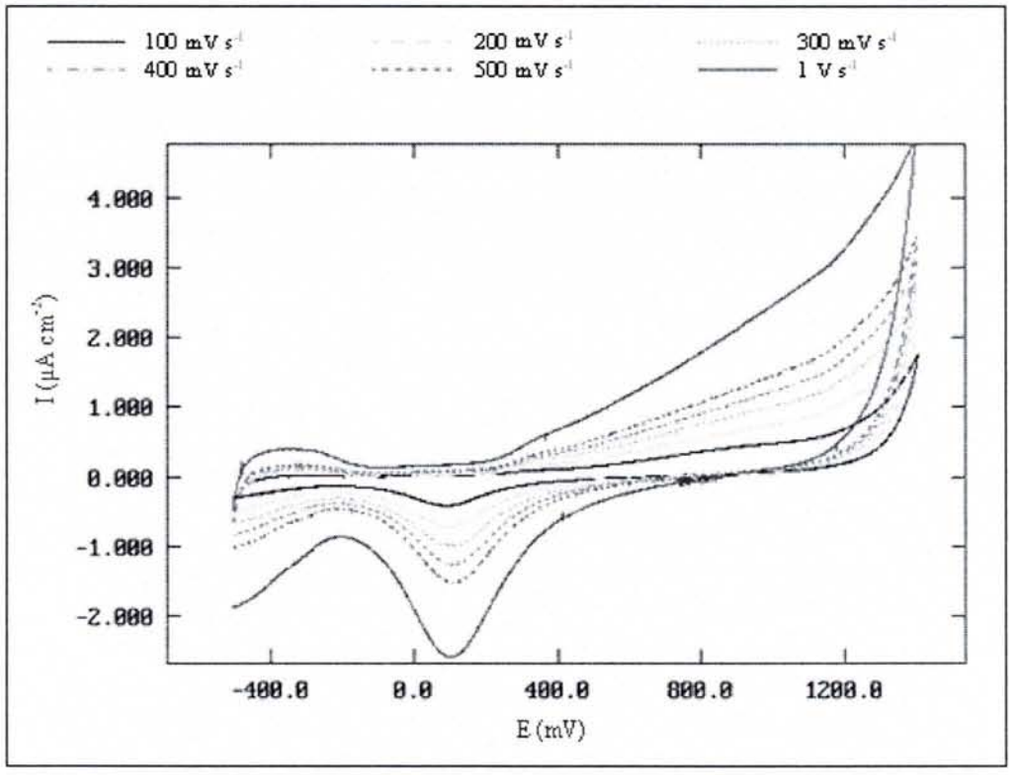

Fig. 3.41 Cyclic voltammograms of 3.0 g L^{-1} quebracho tannins at (a) scan rates of 10 – 100 mV s^{-1} and (b) scan rates of 100 – 1000 mV s^{-1}.

(a)

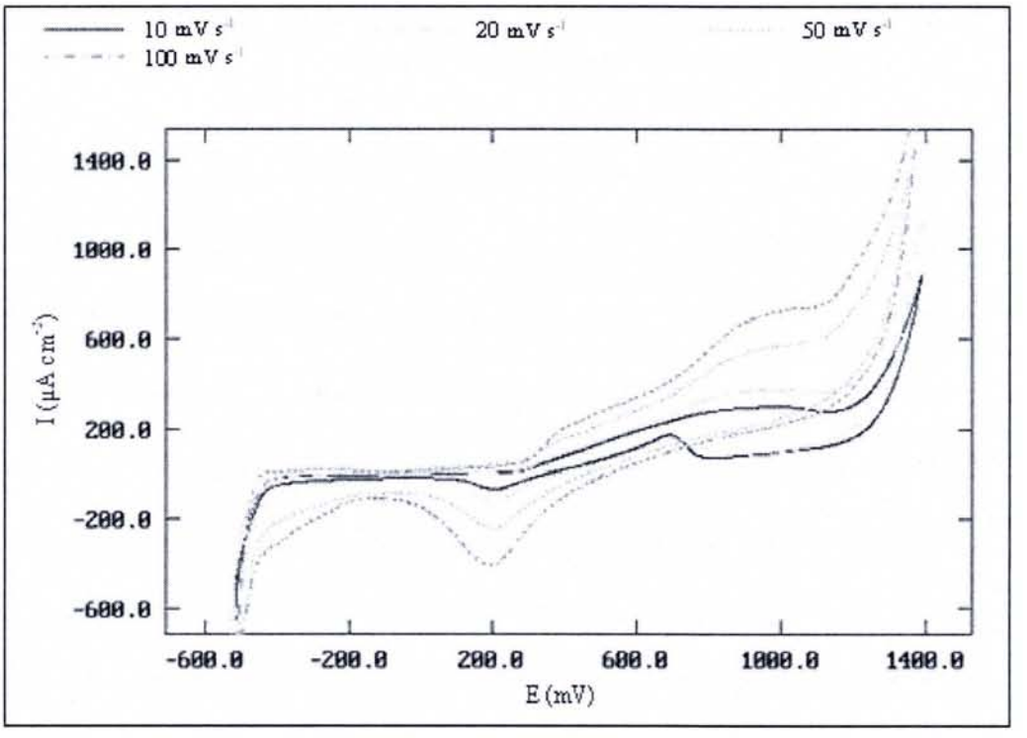

(b)

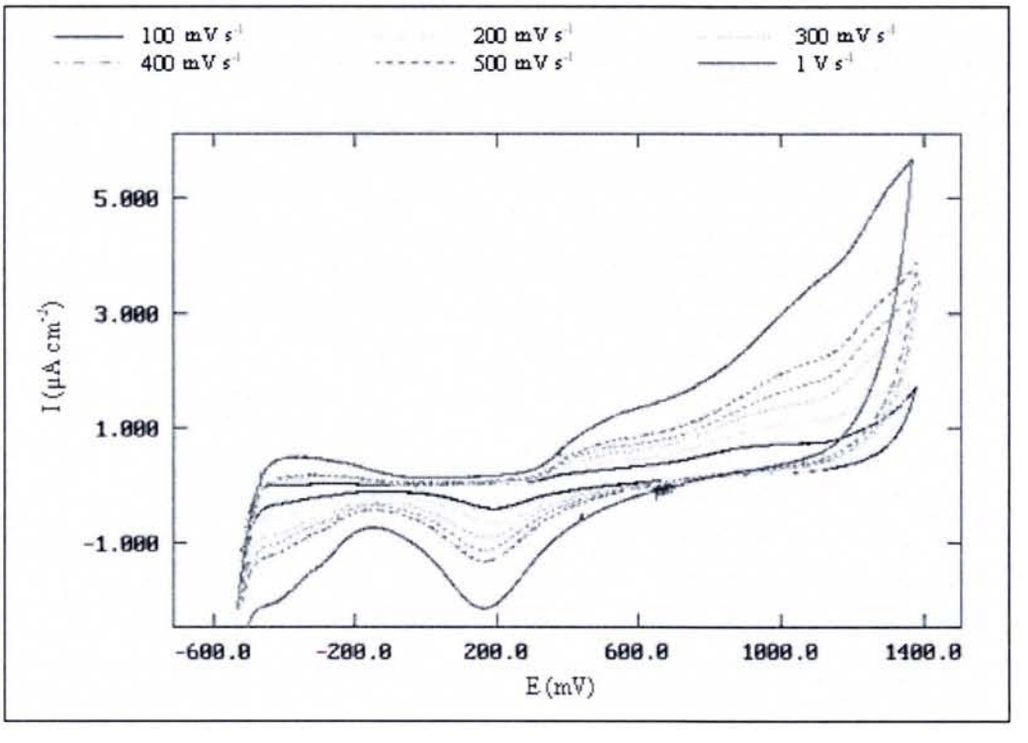

Fig. 3.42 Cyclic voltammograms of 3.0 g L^{-1} chestnut tannins at (a) scan rates of 10 – 100 mV s^{-1} and (b) scan rates of 100 – 1000 mV s^{-1}.

3.4.4 Inhibitory performance of mangrove tannins, mimosa tannins and phosphoric acid on pre-rusted steel

In view of the various results reported on the influence of the phosphoric acid addition as discussed in section 1.5.1, electrochemical studies of steel in the presence of mangrove tannin and phosphoric acid was explored and compared to presence of phosphoric acid in mimosa tannin. A concentration of 15 % phosphoric acid was used based on the report by Almeida *et al.* (1997). Table 3.13 summarises the percentage inhibition calculated from the polarisation resistance measurements performed at pH 0.5, 2.0 and 5.5 on pre-rusted steels in 3.5 % NaCl solution. The inhibition efficiency of mangrove tannin and mimosa tannin on pre-rusted steels was found to decrease with increments in pH similar to the trend observed for the inhibition performance of tannins on clean steels as discussed in section 3.4.1.1. Conversely, the efficiency increased with increasing pH when phosphoric acid was used alone.

Table 3.13 Percentage inhibition of 3.0 $g.L^{-1}$ mangrove tannins and mimosa tannins with the addition of 15 %, 30 % and 50 % phosphoric acid in 3.5 % NaCl solution.

Solution composition	Percentage inhibition (%)		
	pH 0.5	pH 2.0	pH 5.5
Mangrove	77.30	57.56	38.67
Mangrove + 15 % H_3PO_4	79.04	30.74	33.10
Mangrove + 30 % H_3PO_4	56.40	24.58	73.10
Mangrove + 50 % H_3PO_4	59.23	26.85	54.40
Mimosa	77.4	24.06	0
Mimosa + 15 % H_3PO_4	64.3	12.74	10.40
Mimosa + 30 % H_3PO_4	50.50	0	60.26
Mimosa + 50 % H_3PO_4	58.50	0	20.36
15 % H_3PO_4	0	18.16	66.90
30 % H_3PO_4	0	0	90.10
50 % H_3PO_4	0	0	52.60

At pH 0.5, inhibition of almost 80 % was achieved when mangrove tannins and mimosa tannins were used. The corrosion protection provided by both tannins however was not improved with the addition of 15 % phosphoric acid. The inhibition efficiency was further reduced with increasing phosphoric acid concentrations. The potentiodynamic curves of pre-rusted steels revealed modifications of the anodic and cathodic curves with the addition of mangrove tannins alone as well as the addition of mangrove tannins and phosphoric acid. The anodic curves presented a passive domain and the E_{corr} also shifted to more positive values (Fig. 3.43).

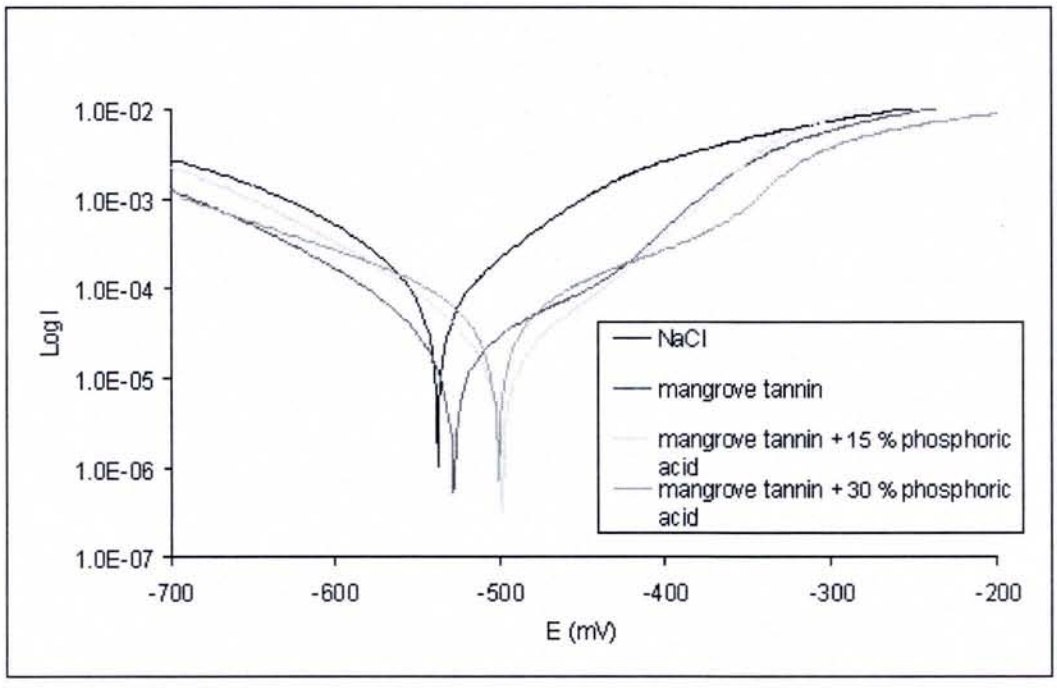

Fig. 3.43 Potentiodynamic curves of pre-rusted steel containing mangrove tannins and phosphoric acid in 3.5 % NaCl solution at pH 0.5.

At pH 2.0, mangrove tannins indicated a better protection as shown by the 57 % inhibition achieved as compared to the 24 % inhibition produced by mimosa tannins. The addition of 15 %, 30 % and 50 % phosphoric acid to the mangrove tannin reduced the inhibition efficiency by almost 50 %. The addition of 15 %

phosphoric acid to mimosa tannin also resulted in further suppression of inhibition efficiency. In addition, the increase in phosphoric acid concentrations to 30 % and 50 % resulted in totally no inhibition. This is not surprising since from the variation of R_p measurements with time of immersion in Fig. 3.44, the R_p values were found to decrease with the increase in concentration of phosphoric acid and even indicated an acceleration of corrosion when 30 % and 50 % phosphoric acid were used.

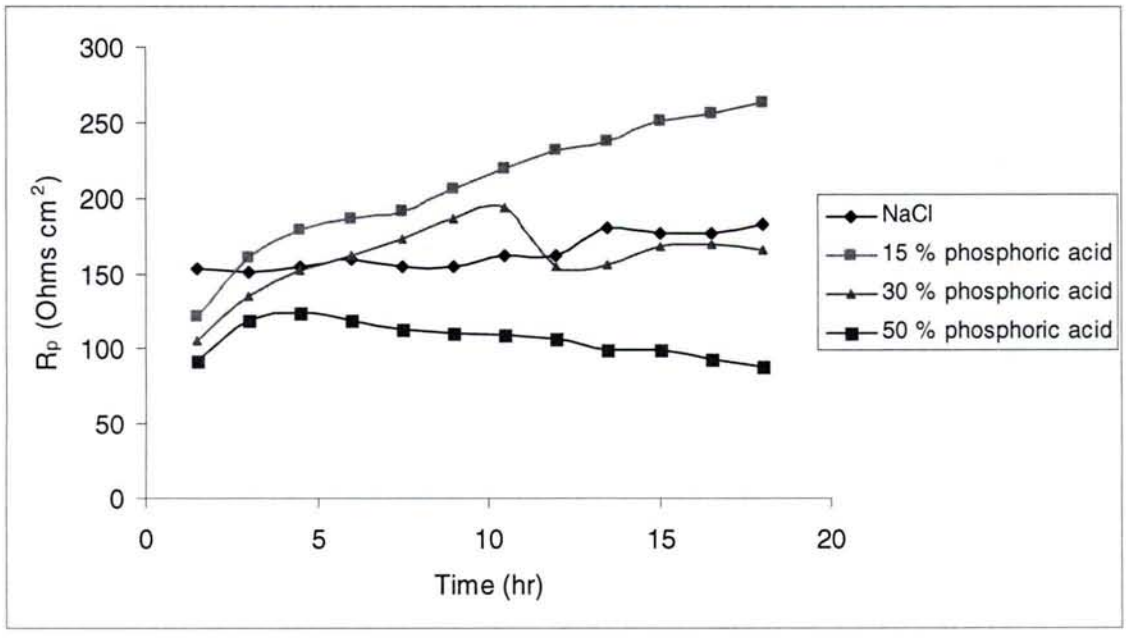

Fig. 3.44 Variation of polarisation resistance, R_p with time of immersion containing 15 %, 30 % and 50 % phosphoric acid in 3.5 % NaCl solution at pH 2.0.

When the inhibition studies was carried out at pH 5.5, which is the natural pH of 3.5 % NaCl solution, the inhibition was improved and the E_{corr} shifted to more positive values with the addition of 30 % and 50 % phosphoric acid to the mangrove tannin (Fig. 3.45). The addition of mangrove tannins and phosphoric acid produced a synergistic effect of lowering both the cathodic and anodic curves. From the shifts of the anodic curves, it is also interesting to note that the

addition of 30 % phosphoric acid affected the anodic reaction to a greater extend than the addition of 50 % phosphoric acid. This observation is consistent with the results obtained from the potentiodynamic curves of steels containing phosphoric acid alone as shown in Fig. 3.46. One could observe that anodic shifts were evident for all phosphoric acid concentrations, with the addition of 30 % phosphoric acid giving the greatest anodic shift to lower density current and consequently the greatest inhibition. Using phosphoric acid alone is certainly favoured at pH 5.5 especially with the use of 30 % phosphoric acid when 90 % inhibition was achieved. Similarly, from Table 3.13 the addition of 30 % phosphoric acid to mimosa tannin improved the inhibitive performance as compared to the use of mimosa alone. No inhibition was observed for mimosa tannin at pH 5.5 as compared to mangrove tannin indicating the advantage of the usage of mangrove tannin at this pH.

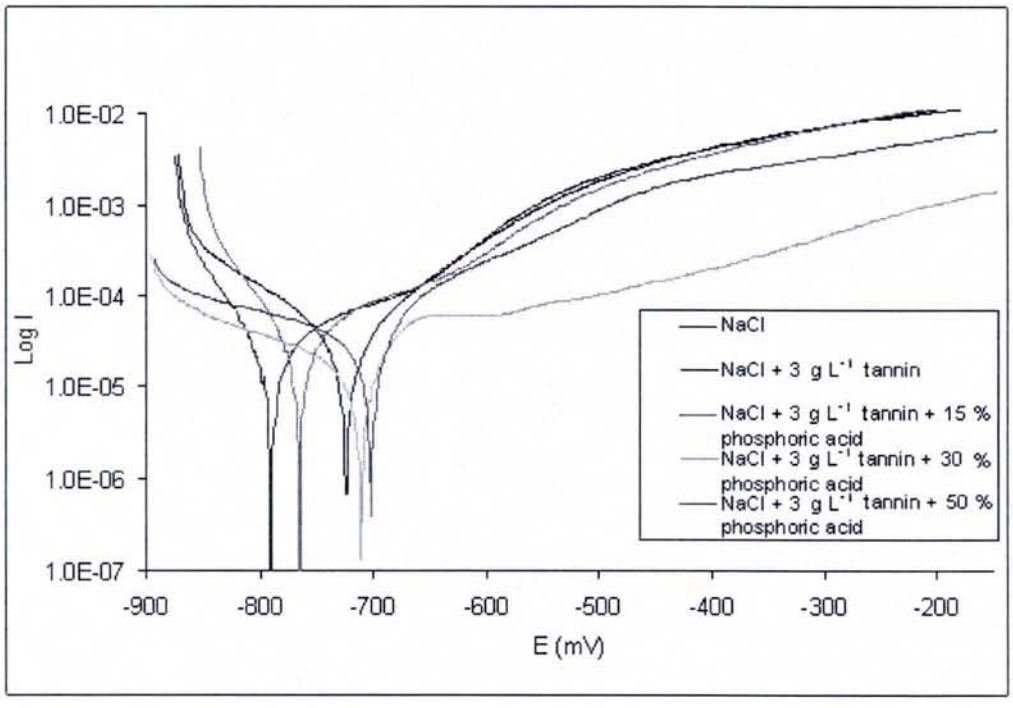

Fig. 3.45 Potentiodynamic curves of pre-rusted steel containing 3.0 g L^{-1} mangrove tannins and phosphoric acid in 3.5 % NaCl at pH 5.5.

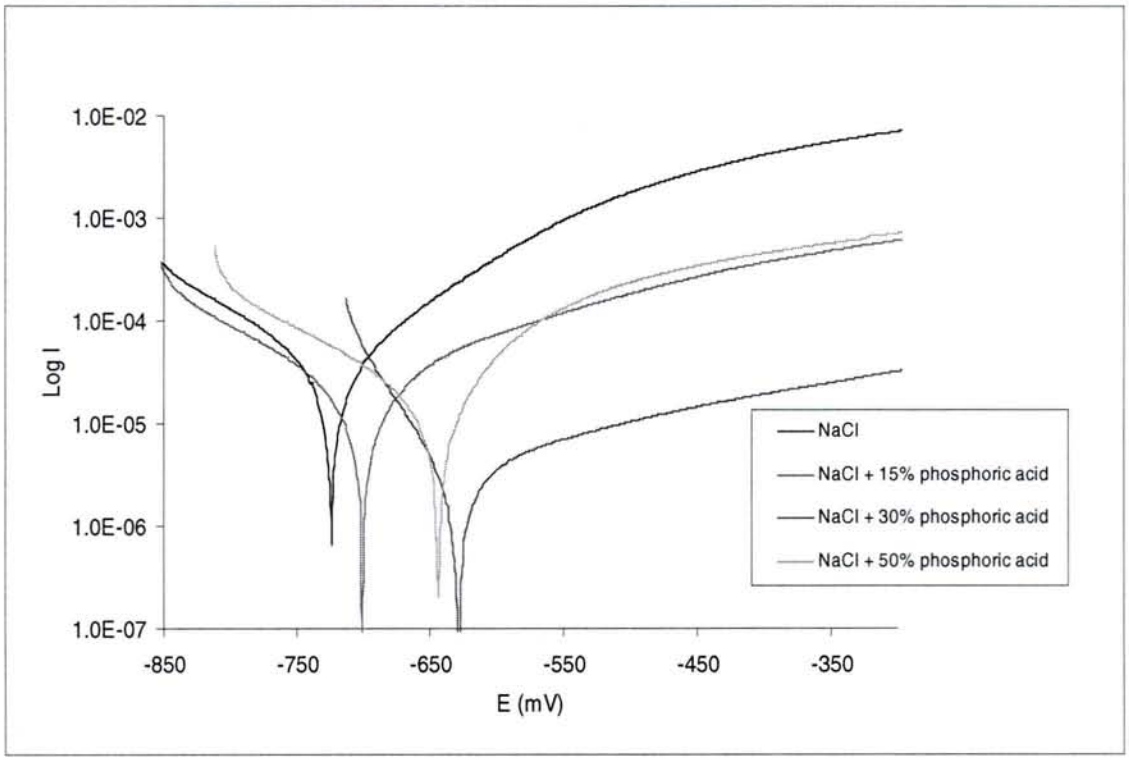

Fig. 3.46 Potentiodynamic curves of pre-rusted steel containing 15 %, 30 %, and 50 % phosphoric acid in 3.5 % NaCl solution at pH 5.5.

3.5 Phase transformation studies

Three types of pre-rusted sample preparations were employed for the transformation studies. Samples prepared via NaCl immersion, alternative NaCl immersion test and salt spray will herein be designated as sample A, B and C respectively. The pre-rusted samples prepared are as shown below :

Sample A Sample B Sample C

The evenly covered rust samples indicated that sample preparation period was adequate. As one can notice from the above pictures, sample A produces the smallest grains of rust, resulting in a powdery surface as compared to samples B and C. The respective rust weight is as shown in Table 3.14. Although sample B has the highest rust weight, loose rust is easily removed as the rust formed is flaky in nature.

Table 3.14 Average rust weight of prepared pre-rusted samples.

Method of preparation	Average rust weight (mg cm^{-2})
Immersion in NaCl solution (sample A)	2.58
Alternative NaCl immersion (sample B)	4.87
Salt spray (sample C)	4.00

When the pre-rusted samples were immersed in 5.0 g L^{-1} mangrove tannin solution at pH 2.0, pH 4.0 and pH 8.0, the best deposition was achieved at pH 4.0 for all samples. Thus, the plates immersed at pH 4.0 were used for subsequent analyses.

From Fig. 3.47 of the X-ray diffraction pattern, it was observed that after two days of immersion in NaCl solution, the iron surface of sample A was mainly covered with lepidocrocite, γ-FeOOH. It was difficult to distinguish the XRD patterns of magnetite and maghemite due to the similarity in peak values. Scraping the outermost rust layer revealed a black adherent layer, characteristic of magnetite, Fe_3O_4 (Barrerro et al., 2001).

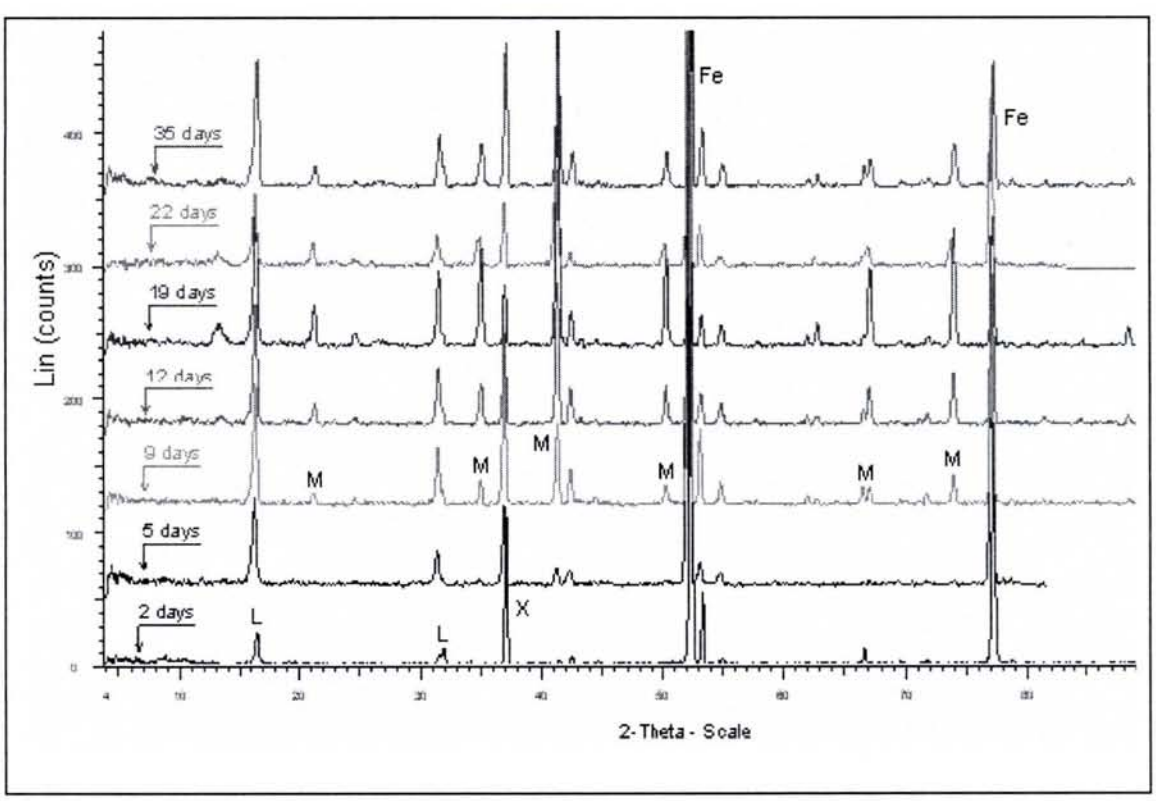

Fig. 3.47 XRD patterns of rusted surface of sample A with respect to time of immersion : L- lepidocrocite, M- magnetite, X- NaCl.

Hence after nine days of immersion the magnetite peaks were seen to become stronger. These two forms of rust remained, only changing in intensities for the next 20 days after which the immersion process was finally terminated. A chloride peak which was formed after two days of immersion remained on the surface throughout the one month immersion.

Lepidocrocite, magnetite and goethite, α-FeOOH were the main rust components for sample B after 14 days of immersion (Fig. 3.48). The chloride peak was also found to disappear after 14 days of immersion. Similarly, sample C gave rise to lepidocrocite, magnetite and goethite, differing only in the number of peaks and intensities.

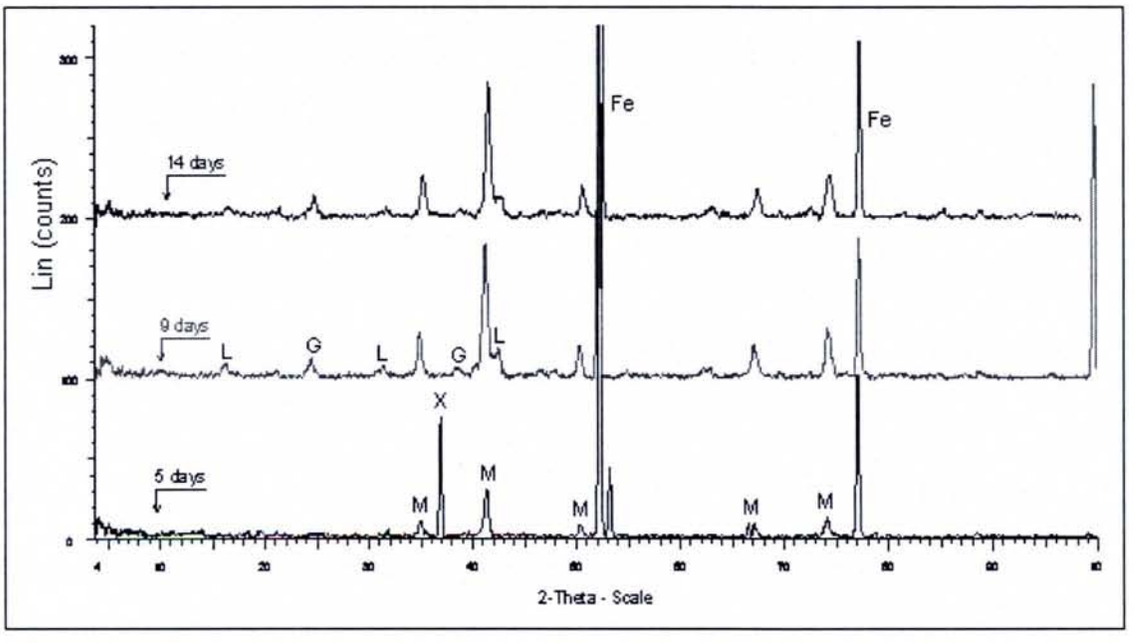

Fig. 3.48 XRD patterns of rusted surface of sample B with respect to time of immersion : L- lepidocrocite, M- magnetite, G-geothite, X- NaCl.

3.5.1 Phase transformation of rust by tannins

In order to establish the correlation between ferric-tannate formation and low inhibition efficiency observed at high pH from the electrochemical studies, phase transformations of pre-rusted steels in the presence of tannins were evaluated. Fig. 3.49 shows the SEM micrographs of the rust surfaces before and after immersion in the mangrove tannin solution at pH 4.0. Sample A shows basically flower-like flakes with finger-like structures protruding in a random manner. This structure disappeared with the tannin treated samples and was replaced by a coarse layer with cracks of irregular shapes, more rounded than angular. The edges seem to lift from the surface indicating the lack of adhesion.

Samples B and C both illustrated coral-like structures in addition to the same structures showed by sample A. They also produced the same morphology with the tannin treated samples. The outer coarse layer is much thicker and the irregular-shaped cracks are much wider than that was witnessed in sample A. A closer inspection of the surface of each crack revealed tiny flowered-like structures stacked on top of one another. For all converted samples, unconverted rust structures were observed underneath the transformed tannins.

The X-ray diffraction pattern of sample A (Figure 3.50) shows the disappearance of lepidocrocite peaks after the addition of mangrove tannin, inferring the possibility of the transformation of rust into ferric-tannates. A slight increment in the intensity of magnetite peaks was observed.

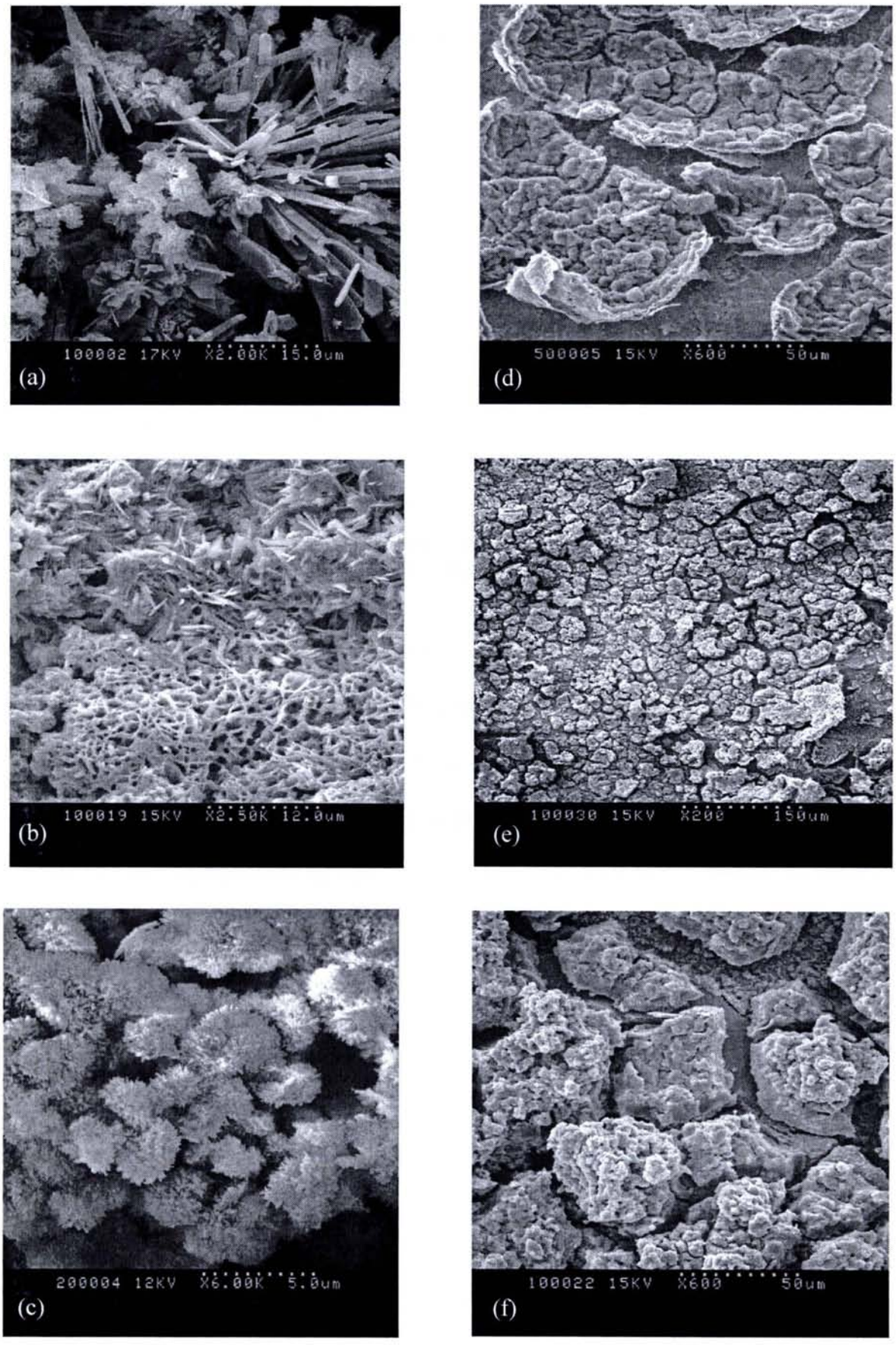

Fig. 3.49 SEM micrographs of pre-rusted steel surface before tannin immersion for samples (a) A, (b) B and (c) C and after tannin immersion for samples (d) A, (e) B and (f) C.

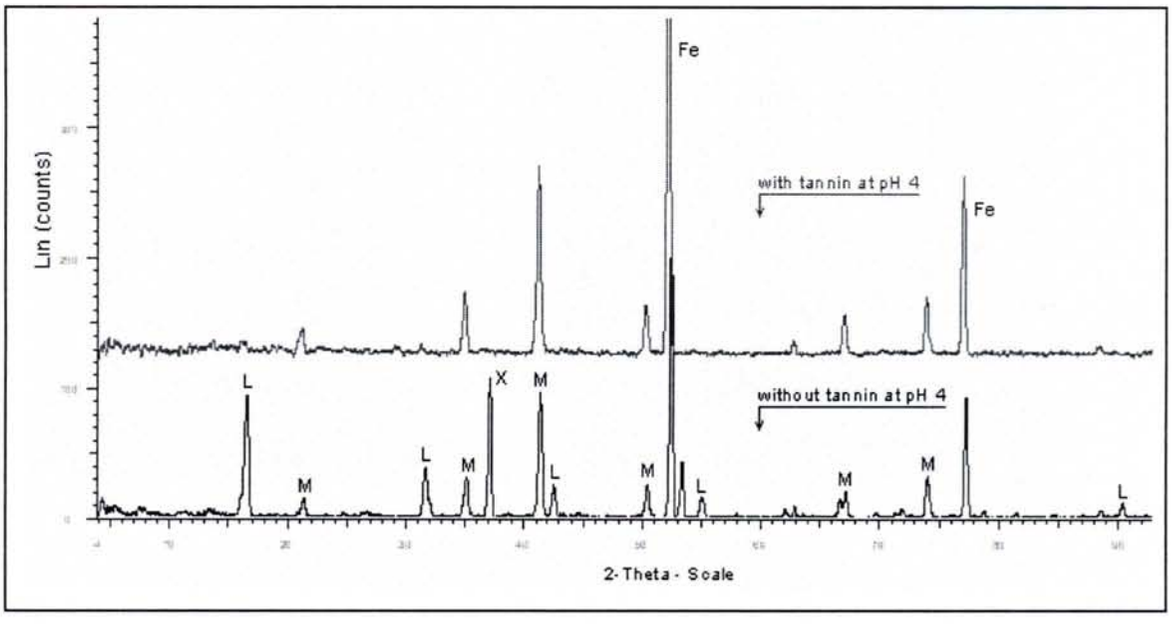

Fig. 3.50 XRD patterns of rust surface when treated with 0.5 % mangrove tannin for sample A : L- lepidocrocite, M- magnetite, X- NaCl.

It is also noteworthy that the X-ray diffraction pattern of mangrove tannin covered rust showed the absence of chloride compound peak as compared to the rust alone. This observation is also indicated in the EDS analysis (Fig. 3.51). While reductions of lepidocrocite and goethite peaks were observed for sample B, sample C portrayed a reduction of mainly lepidocrocite in favour of ferric-tannate formation (Fig. 3.52).

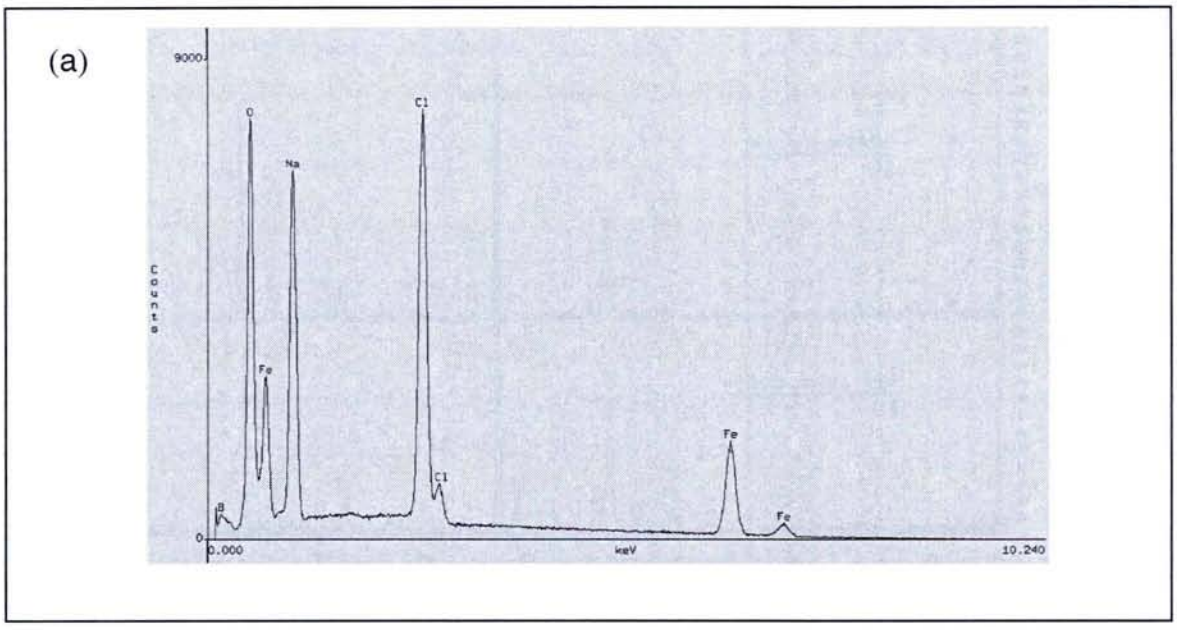

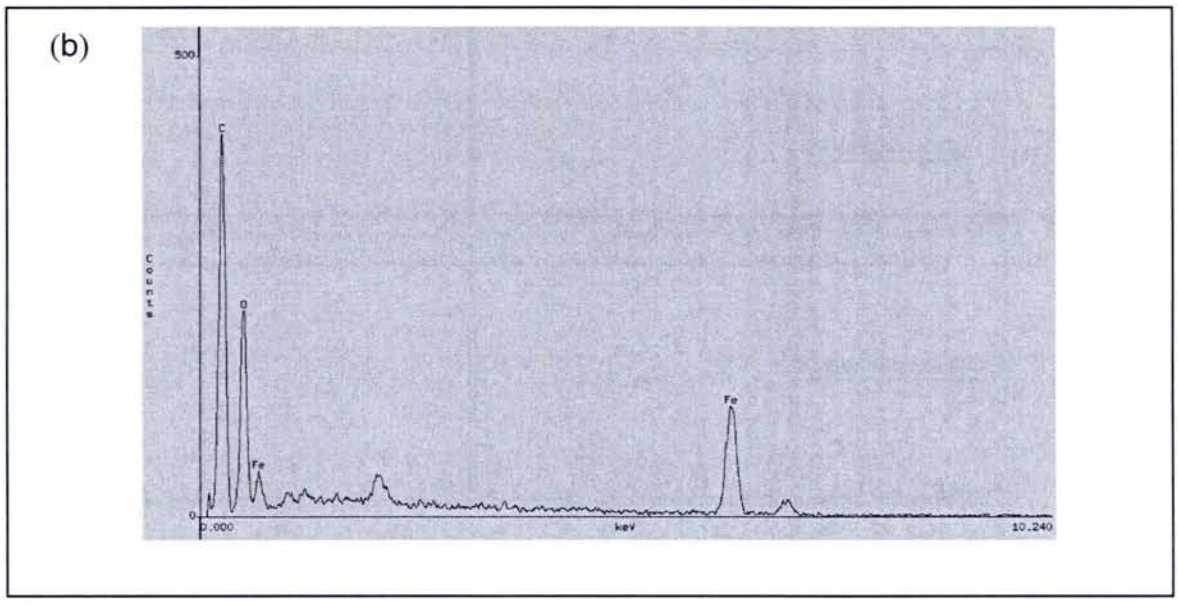

Fig. 3.51 EDS spectra of (a) rust and (b) tannin treated rust surface for sample A.

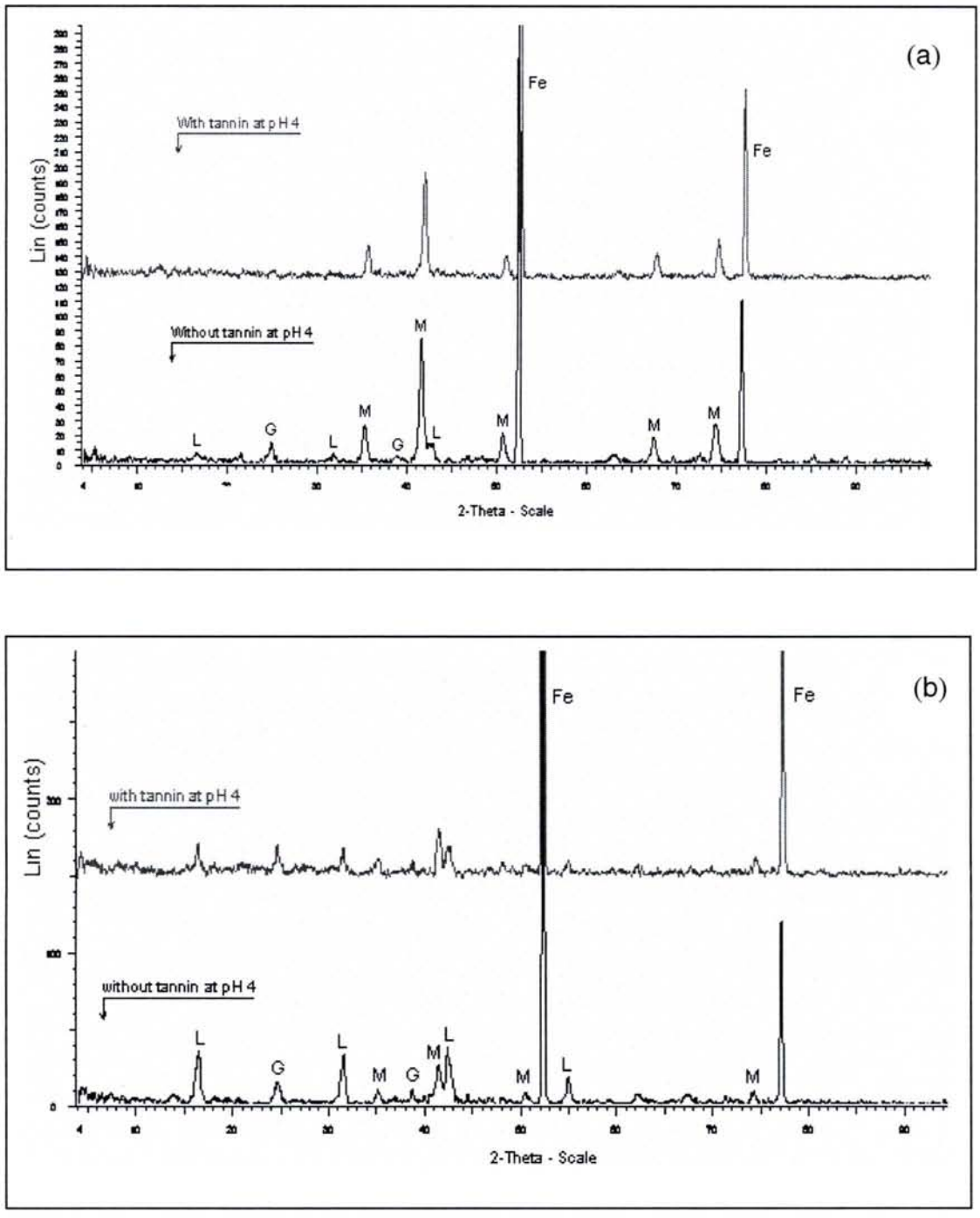

Fig. 3.52 Phase transformation of bare rust surface when treated with 0.5 % mangrove tannin for (a) sample B and (b) sample C : G-geothite, L- lepidocrocite, M- magnetite.

The principal FTIR peaks of the various standard iron oxides are shown in Table 3.15. From this table, the peaks at 1021 and 579 cm^{-1} for sample A [Fig. 3.53 a (i)] designated the presence of lepidocrocite and magnetite respectively. The formation of tannates was also supported by the FTIR spectrums whereby tannate peaks at 1262, 1106 and 1054 cm^{-1} were evident for sample A [Fig. 3.53 b (i)]. From Table 3.15 one could observe that the lepidocrocite phase still remains. It is difficult to determine the existence of magnetite as the principal peak of magnetite at 571 cm^{-1} is being superimposed by the broad band between 700 and 400 cm^{-1} attributed to the tannate. The FTIR spectrum of sample B [Fig. 3.53 a (ii)] showed the presence of lepidocrocite (1021 cm^{-1}) and goethite (798 cm^{-1}). The principal magnetite peak at 571 cm^{-1} may have been superimposed by the broad and strong 583 cm^{-1} peak. Similarly sample C exhibited the presence of lepidocrocite (1022, 891 and 474 cm-1), goethite (800 cm^{-1}) and magnetite (571 cm^{-1}) [Fig. 3.53 a (iii)]. Both samples B and C showed the presence of tannate peaks when treated with mangrove tannins [Fig. 3.53 b (ii & iii)]. A reduction in the intensity of the lepidocrocite peak was also observed for both samples.

Table 3.15 Principal absorption peaks of the various standard iron oxides

Species	Wave number [cm^{-1}]
Lepidocrocite, γ – FeOOH	1021, 892, 752, 475
Geothite, α - FeOOH	904, 798, 667, 616, 492
Maghemite, γ – Fe_2O_3	692, 639, 592
Magnetite, Fe_3O_4	571

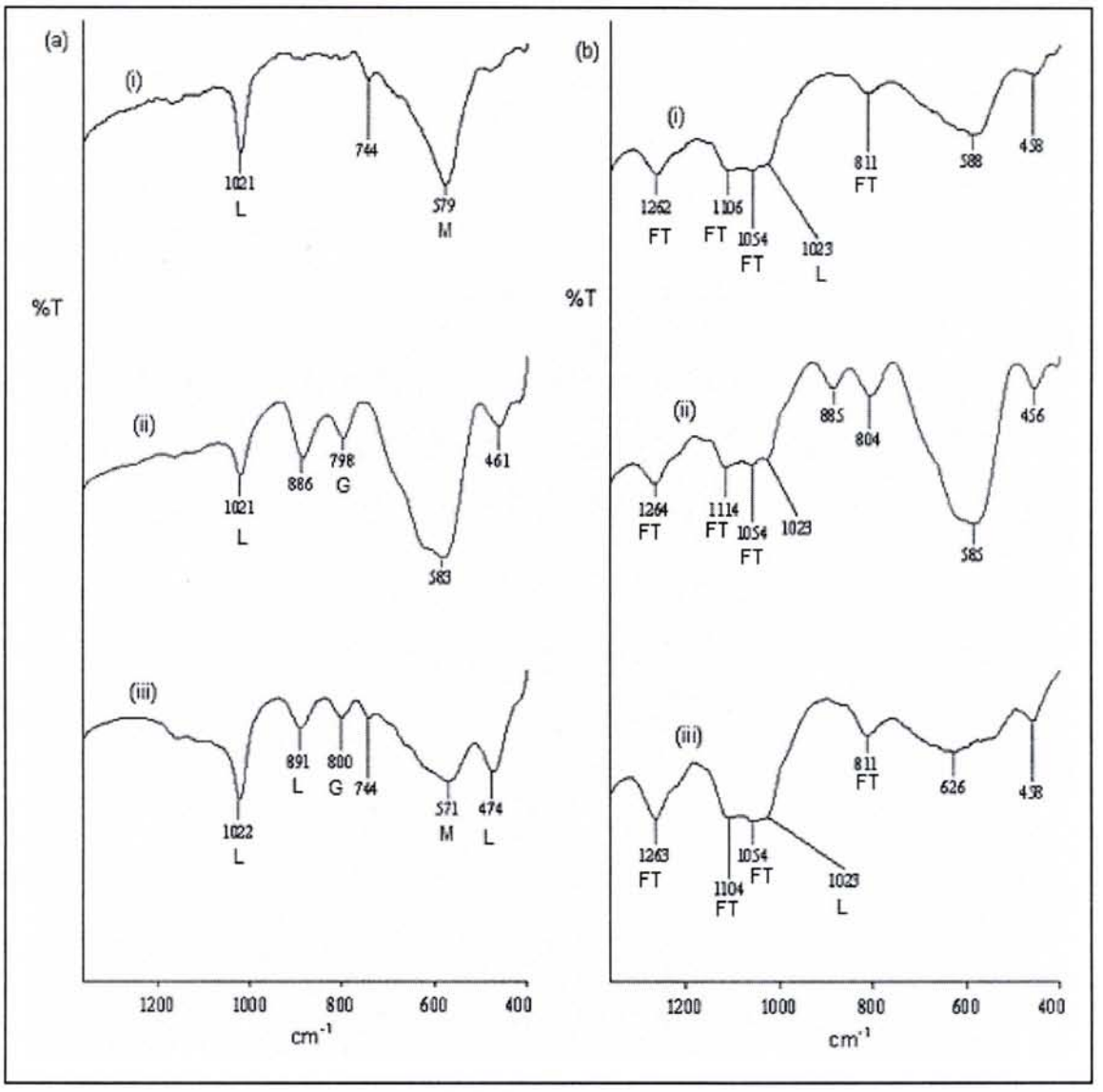

Fig. 3.53 FTIR spectrums of (a) bare rust and (b) converted rust for samples (i) A, (ii) B and (iii) C : FT-ferric-tannate, G-geothite, L-lepidocrocite, M-magnetite.

3.5.2. Phase transformation of rust in the presence of mangrove tannins and phosphoric acid

The rust transformation was best observed from the X-ray diffraction pattern of sample A (Fig. 3.54). It could be clearly seen that with the addition of 15 % and 30 % phosphoric acid, the lepidocrocite and magnetite components were reduced and the chloride compound peak vanished in favour of phosphate formation. The white-bluish colour of the deposit, characteristic of iron phosphate was identified by XRD as vivianite, $Fe_3(PO_4)_2.8H_2O$. In the presence of tannins and 15 % phosphoric acid, the rust components also reduced in favour of tannate and vivianite formation (Fig. 3.54 b). With the addition of tannins and 30 % phosphoric acid, the transformation of rust into ferric-tannate and vivianite were also evident although the vivianite intensities were much reduced. Similarly for sample C, the rust was transformed into phosphates and tannates along with reduced lepidocrocite and magnetite peaks with the addition of 15 % and 30 % phosphoric acid and mangrove tannins.

The formation of phosphates was also confirmed from the FTIR spectrums which exhibited a broad characteristic peak of phosphate at 1042-1051 cm^{-1}, superimposing the tannate and lepidocrocite peaks for samples A and C (Fig. 5.55).

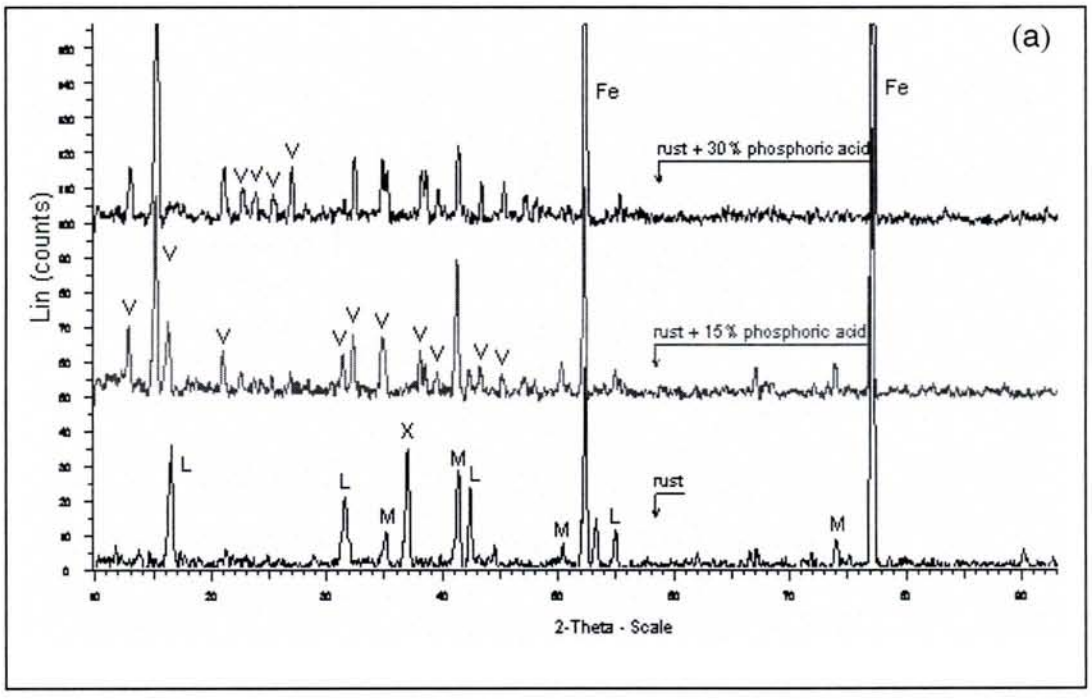

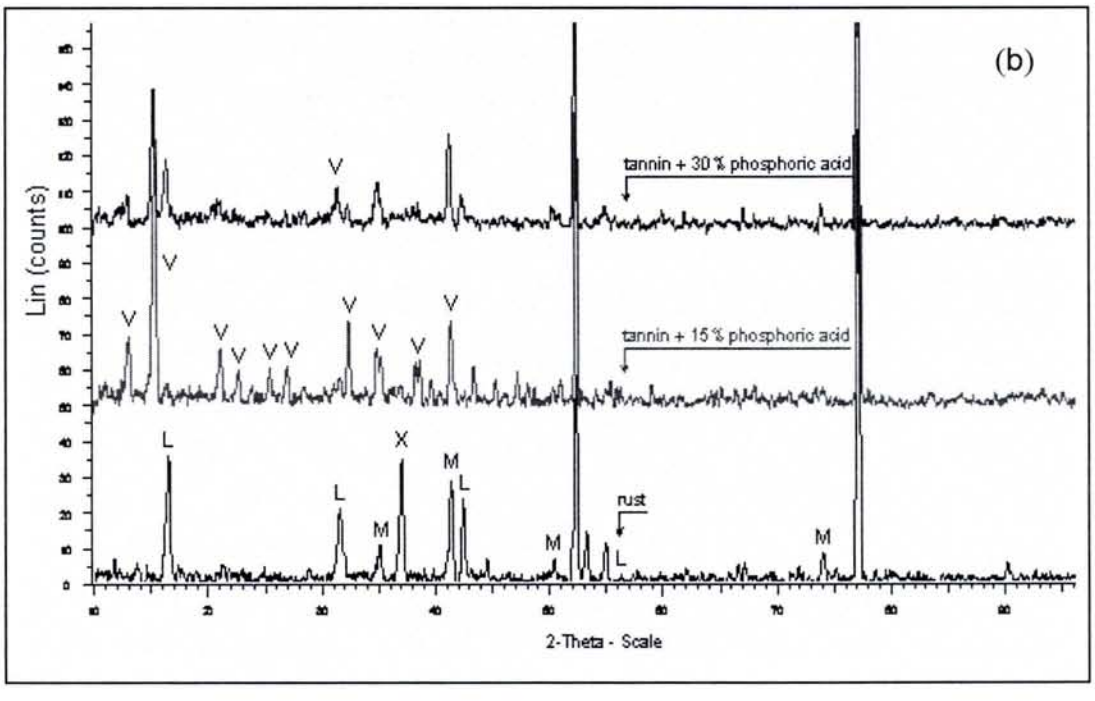

Fig. 3.54 Phase transformation of bare rust surface for sample A immersed in (a) phosphoric acid and (b) 0.5 % mangrove tannin and phosphoric acid solutions : G-geothite, L- lepidocrocite, M- magnetite, V- vivianite, X- NaCl.

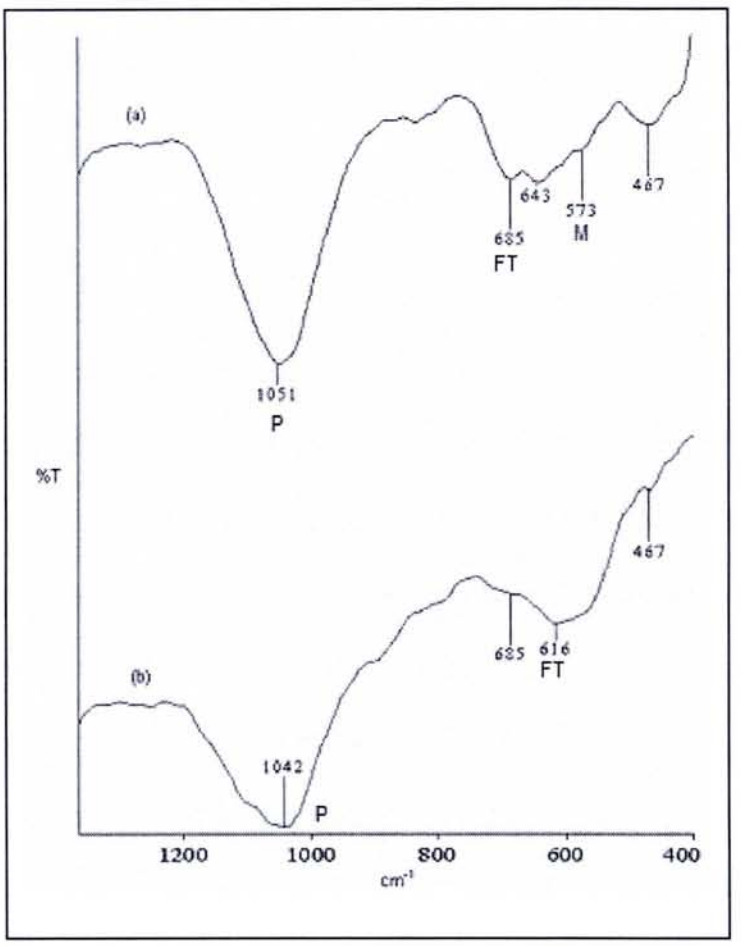

Fig. 3.55 FTIR spectrum of phosphate and tannate of treated rust for samples (a) A and (b) C : FT-ferric-tannate, P-phosphates.

Surface analysis of pre-rusted samples with the addition mangrove tannins and phosphoric acid were compared with that of mimosa tannins. The SEM micrographs in Fig. 3.56 of tannins and phosphoric acid treated samples showed some interesting features. Samples A and C portrayed mainly tiny flakes of phosphates with irregular shaped cracks. When phosphoric acid was added to mangrove tannins, the flakes were replaced by a blend of tannate and phosphate structures with cracks still visible for both samples. With the addition of mimosa tannins and phosphoric acid, the morphology was transformed into

spectacular structures of sea-shells scattered amidst the cracked structures of tannates.

Table 3.16 shows the EDS analysis for mangrove treated samples. The emergence of carbon, C_x and phosphorous, P content clearly shows the formation of tannates and phosphates respectively on the surface of the rust. A drop in the iron content as one added tannin and phosphoric acid indicated the increase of phosphate and tannate formation onto the rust surface. A better rust transformation was also achieved with the addition of mangrove tannin as compared to phosphoric acid alone. The transformation was further enhanced with the addition of both tannin and phosphoric acid. Consistent with the XRD patterns, the chloride content was also absent with the addition of tannin and phosphoric acid in the EDS analysis.

As a comparison, the mimosa tannin treated samples showed some differences between samples A and C (Table 3.17). While better deposition was achieved with mimosa treated sample A, sample C showed a reduction of deposition as compared to the addition of phosphoric acid alone. With the addition of phosphoric acid to mimosa tannin, deposition for sample A remained almost the same while the deposition was enhanced for sample C. What is clearly noticable is the fact that some traces of chloride, Cl were detected for mimosa treated samples as compared to mangrove-covered samples.

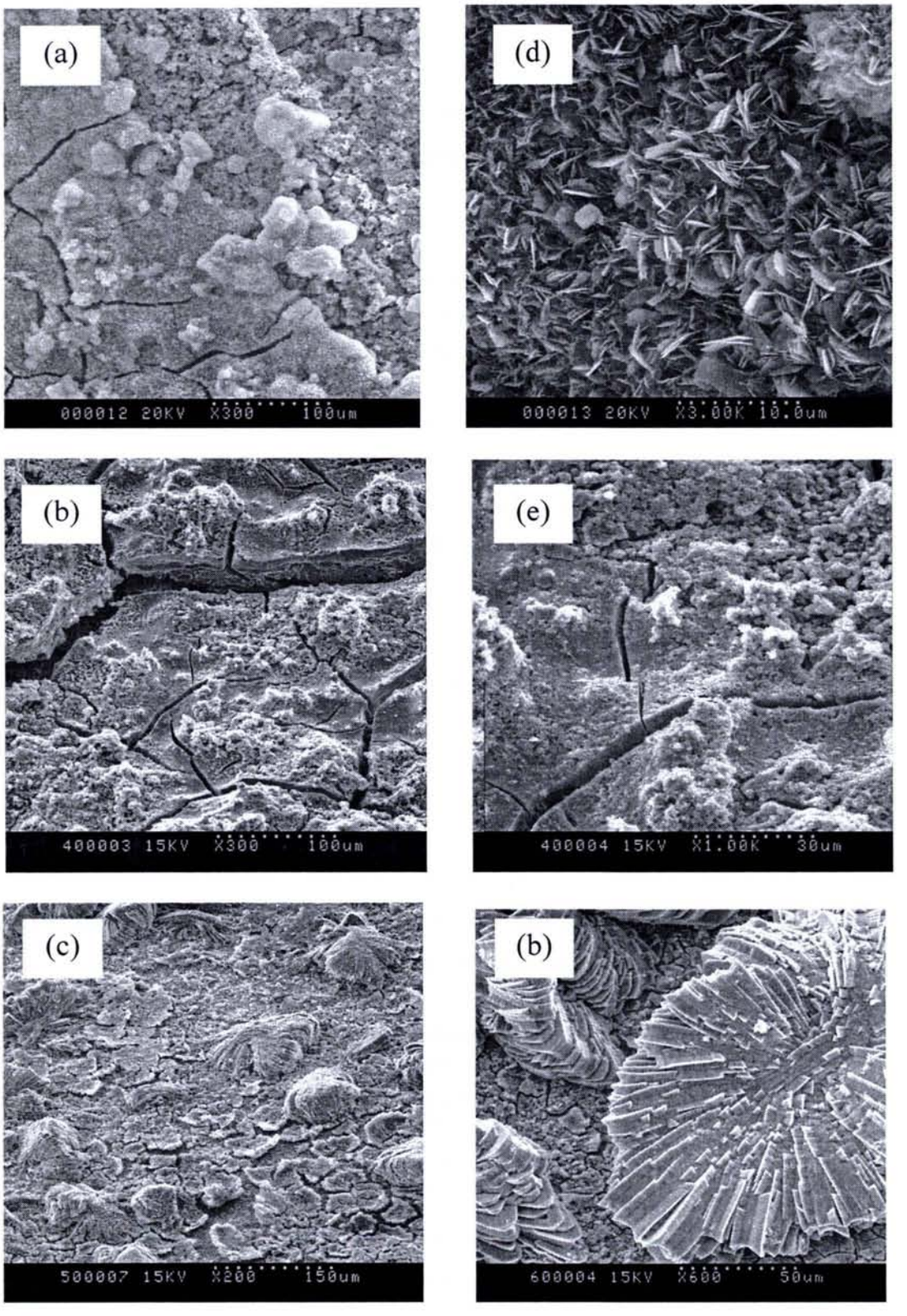

Fig. 3.56 SEM micrographs of pre-rusted plates for sample A containing (a) 15 % H_3PO_4, (b) 15 % H_3PO_4 and 0.5 % mangrove tannins and (c) 15 % H_3PO_4 and 0.5 % mimosa tannins and for sample C containing (d)15 % H_3PO_4, (e) 15 % H_3PO_4 and 0.5 % mangrove tannins and (f) 15 % H_3PO_4 and 0.5 % mimosa tannins.

Table 3.16 EDS analysis of pre-rusted samples before and after treatments with 0.5 % mangrove tannins and 15 % phosphoric acid.

	Atom %									
	Sample A					Sample C				
	C_x	O	P	Cl	Fe	C_x	O	P	Cl	Fe
Rust alone	-	34.13	-	15.19	33.69	-	62.31	-	7.8	29.87
Rust + mangrove tannin	54.82	36.77	-	-	8.42	53.36	40.02	-	-	6.24
Rust + 15 % H_3PO_4	-	64.90	13.40	-	20.55	-	64.90	14.01	-	19.32
Rust + mangrove tannin + 15 % H_3PO_4	32.76	47.60	8.29	-	1.52	52.79	34.53	5.75	-	1.82

Table 3.17 EDS analysis of pre-rusted samples before and after treatments with 0.5 % mimosa tannins and 15 % phosphoric acid.

	Atom %									
	Sample A					Sample C				
	C_x	O	P	Cl	Fe	C_x	O	P	Cl	Fe
Rust alone	-	34.13	-	15.19	33.69	-	62.31	-	7.8	29.87
Rust + 15 % H_3PO_4	-	64.90	13.40	-	20.55	-	64.90	14.01	-	19.32
Rust + mimosa tannin	54.33	40.56	-	-	5.11	40.16	31.61	-	1.27	26.97
Rust + mimosa tannin + 15 % H_3PO_4	48.06	37.17	2.90	0.22	9.02	42.01	40.66	5.6	0.03	8.72

3.5.3. Phase transformation of the individual rust component in the presence of mangrove tannins

The XRD analysis and FTIR spectroscopy have shown that the rust composition of the pre-rusted plates prepared was mainly lepidocrocite, magnetite and goethite. However Ocampo *et al.* (2004) have reported that traces of maghemite were present as one of the rust components when pre-rusted samples were prepared by alternated immersion tests. Thus apart from studying the relation between the partial transformation of pre-rusted steel samples by tannins and the degree of transformation of the individual rust components, the study was extended to the transformation of maghemite by tannins.

3.5.3.1 Interactions of mangrove tannins with lepidocrocite, magnetite, goethite and maghemite via infrared spectroscopy

Untreated lepidocrocite has FTIR bands at 1021, 892, 752 and 475 cm^{-1} (Fig. 3.57). Among these bands, 1021 cm^{-1} is the strongest and could be considered as lepidocrocite's major band. The 0.5 % mangrove tannin appeared to initially dissolve the lepidocrocite, followed by the formation of a new phase. The lepidocrocite peak seems to initially reduce after one day immersion but lepidocrocite peaks remained unchanged after one week onwards although several tannate peaks were evident.

However, when the tannin concentration was increased to 2.0 %, the dissolution of lepidocrocite was more rapid and the reduction of the 1021 cm^{-1} band with time was noticeable as early as a day of immersion and after 28 days this peak

almost diminished. All other peaks belonging to lepidocrocite also reduced with time (Fig. 3.58).

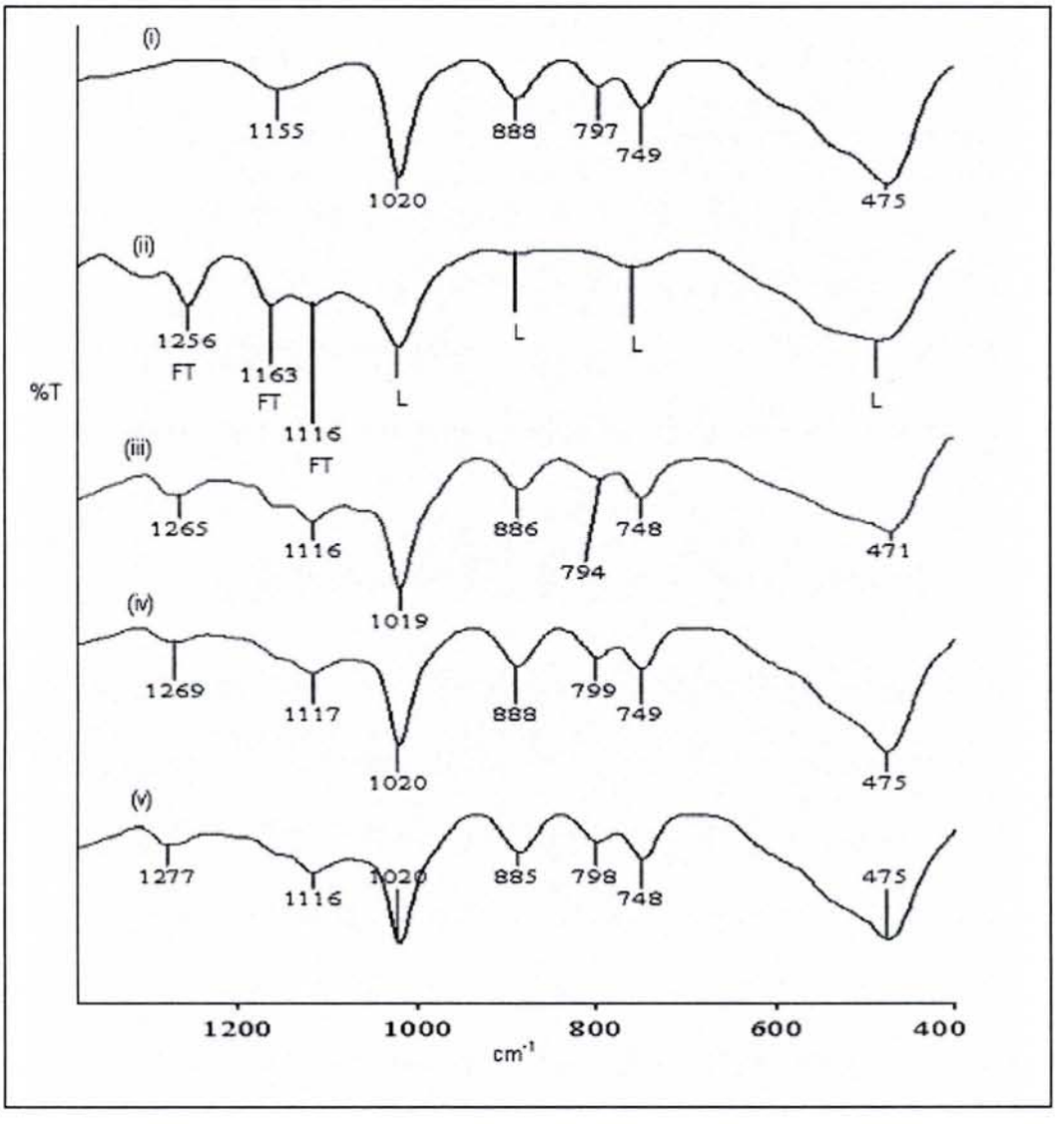

Fig. 3.57 FTIR spectrum of (i) untreated lepidocrocite and treated with 0.5 % mangrove tannins after (ii) 1 day, (iii) 1 week, (iv) 2 weeks and (v) 1 month immersion : FT-ferric-tannate, L-lepidocrocite.

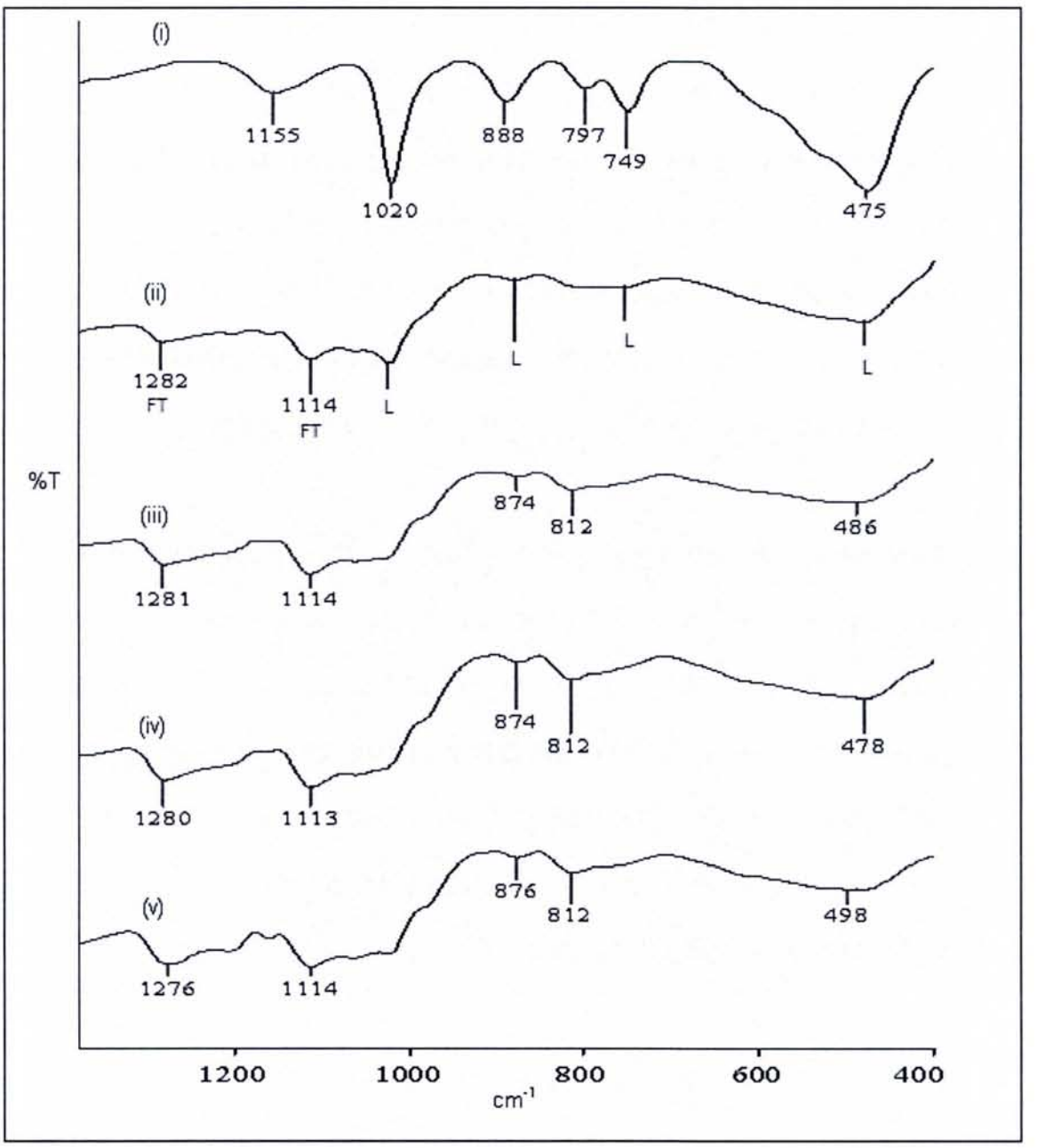

Fig. 3.58 FTIR spectrum of (i) untreated lepidocrocite and treated with 2.0 % mangrove tannins after (ii) 1 day, (iii) 1 week, (iv) 2 weeks and (v) 1 month immersion : FT-ferric-tannate, L-lepidocrocite.

The observed infrared spectrum in Fig. 3.59 of untreated magnetite contained one characteristic peak at 571 cm^{-1}. The IR spectrum treated with 0.5 % tannin showed ferric-tannate peaks along with the unreacted magnetite peak throughout the one month immersion. The magnetite peak reduced slightly after two weeks immersion. With the increment of tannin concentration to 2.0 %, the reduction of the magnetite peak at 571 cm^{-1} increased with time and the conversion to ferric-tannate was increased indicated by the high ratio of tannate to magnetite band intensities beginning from a week of immersion (Fig. 3.60).

Geothite has the following wave numbers in its untreated state: 903, 797, 667, 616 and 494 cm^{-1} (Fig. 3.61). After 28 days, both of the prominent goethite peaks (904 and 797 cm^{-1}) were present along with ferric-tannate peaks. Patterns of goethite treated with 2.0 % tannin showed all of the goethite and ferric-tannate peaks. The two prominent goethite peaks seemed to reduce significantly only after 28 days of immersion, signifying a slow conversion to ferric-tannate complex (Fig. 3.62).

Untreated maghemite has adsorption bands at 692, 639 and 592 cm^{-1} (Fig. 3.63). With the addition of 0.5 % tannins, all maghemite peaks remained unchanged after 28 days immersion. When treated with 2.0 % tannins, the 592 cm^{-1} shifted to lower wavenumbers, the 639 cm^{-1} band reduced and 692 cm^{-1} band diminished with time of immersion in favour of tannate formation (Fig. 3.64).

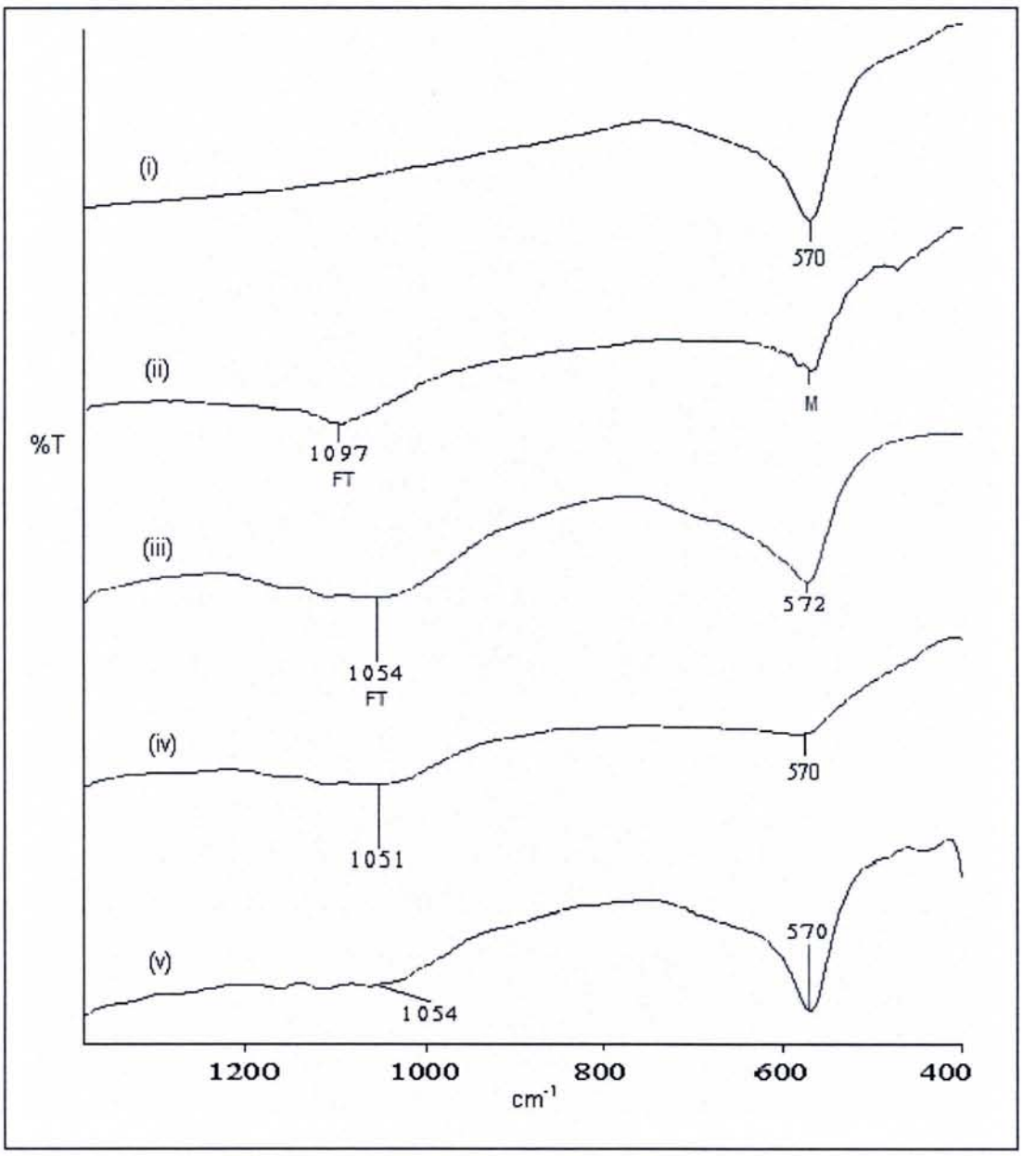

Fig. 3.59 FTIR spectrum of (i) untreated magnetite and magnetite treated with 0.5 % mangrove tannins after (ii) 1 day, (iii) 1 week, (iv) 2 weeks and (v) 1 month immersion : FT-ferric-tannate, M-magnetite.

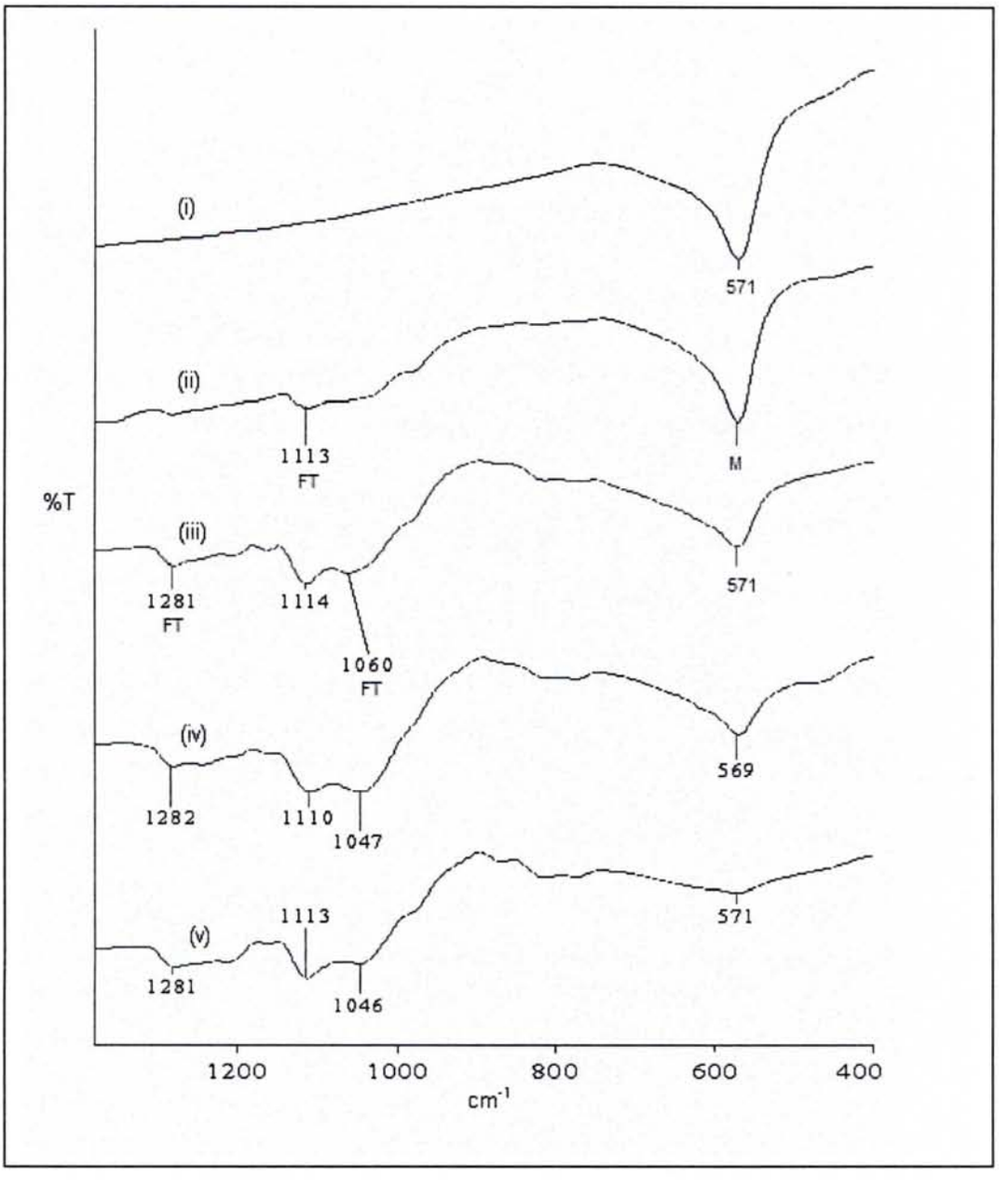

Fig. 3.60 FTIR spectrum of (i) untreated magnetite and magnetite treated with 2.0 % mangrove tannins after (ii) 1 day, (iii) 1 week, (iv) 2 weeks and (v) 1 month immersion : FT-ferric-tannate, M-magnetite.

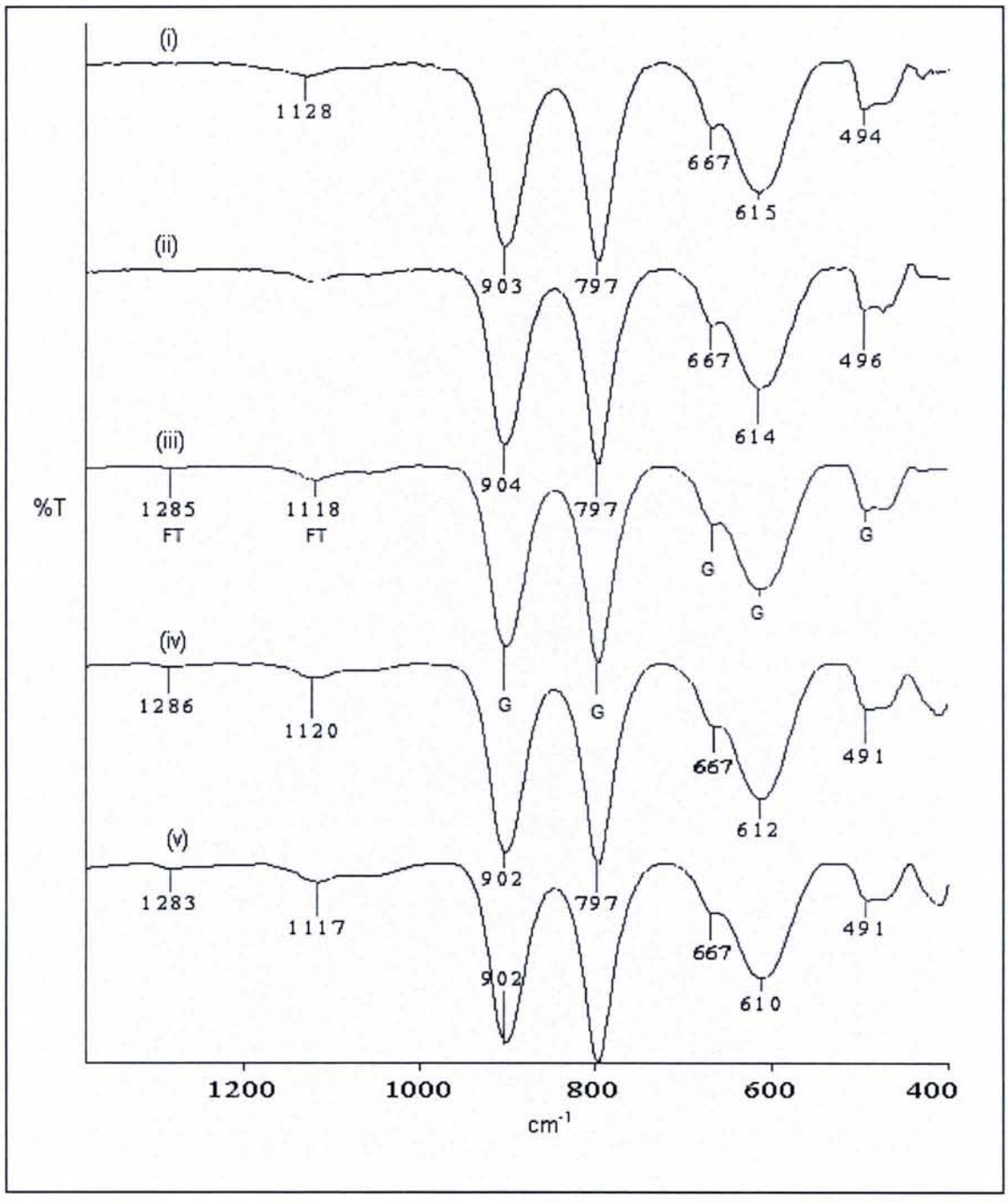

Fig. 3.61 FTIR spectrum of (i) untreated geothite and goethite treated with 0.5 % mangrove tannins after (ii) 1 day, (iii) 1 week, (iv) 2 weeks and (v) 1 month immersion : FT-ferric-tannate, G-geothite.

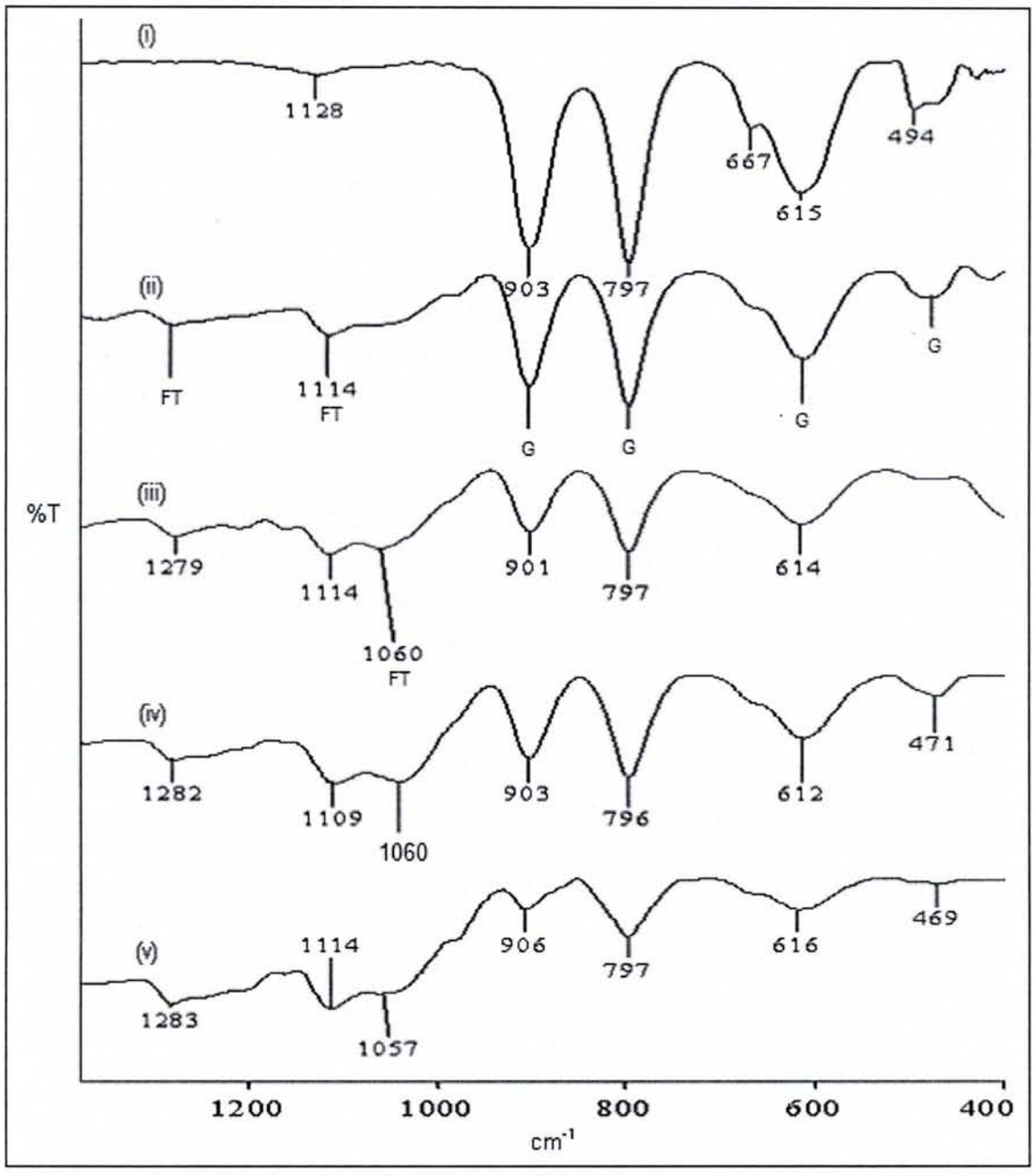

Fig. 3.62 FTIR spectrum of (i) untreated geothite and goethite treated with 2.0 % mangrove tannins after (ii) 1 day, (iii) 1 week, (iv) 2 weeks and (v) 1 month immersion : FT-ferric-tannate, G-geothite.

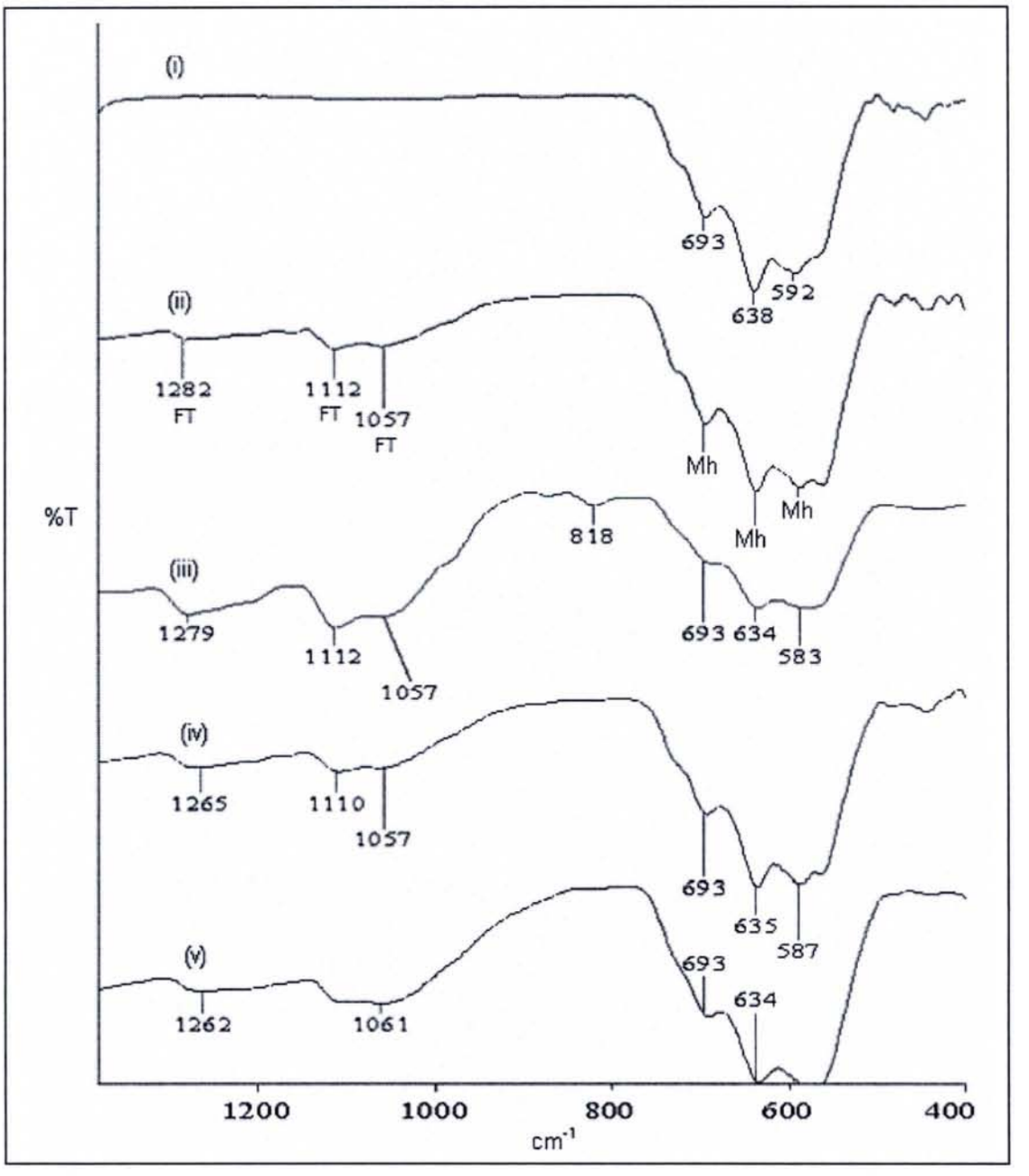

Fig. 3.63 FTIR spectrum of (i) untreated maghemite and maghemite treated with 0.5 % mangrove tannins after (ii) 1 day, (iii) 1 week, (iv) 2 weeks and (v) 1 month immersion : FT-ferric-tannate, Mh-maghemite.

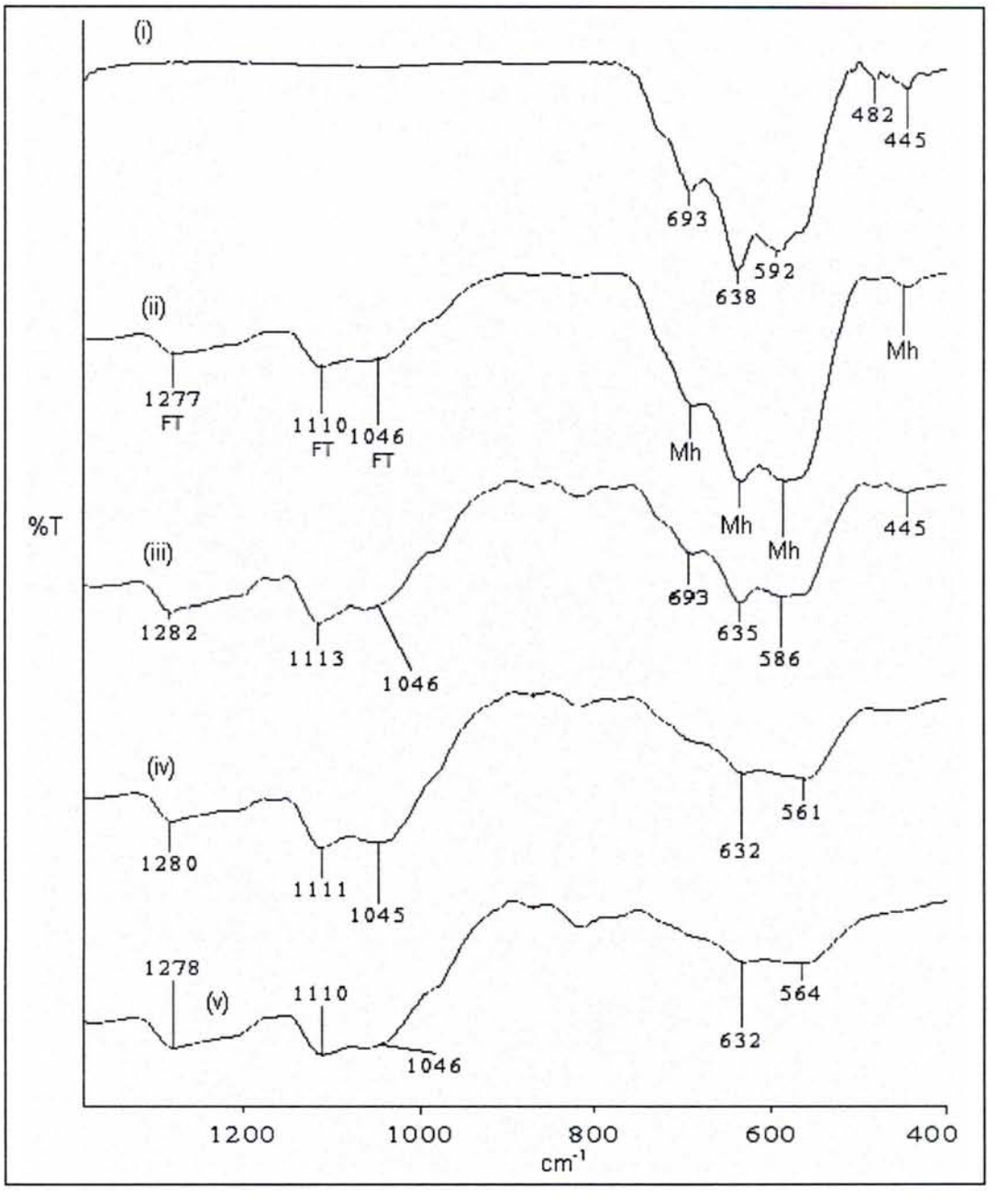

Fig. 3.64 FTIR spectrum of (i) untreated maghemite and maghemite treated with 2.0 % mangrove tannins after (ii) 1 day, (iii) 1 week, (iv) 2 weeks and (v) 1 month immersion : FT-ferric-tannate, Mh-maghemite.

3.5.3.2 Interactions of mangrove tannins with lepidocrocite, magnetite, goethite and maghemite via X-ray diffractions

The d values, characteristic of each rust component are tabulated in Table 3.18. The addition of 0.5 % tannin did not indicate any change in the lepidocrocite XRD patterns as shown in Fig. 3.65. On the other hand, treatment of lepidocrocite with 2.0 % tannin indicated the disappearance of several lepidocrocite peaks (d=1.5261, 1.7285, 6.3785) especially after 28 days of immersion. Loss of crystrallinity was also noticeable.

Table 3.18 The values of d-spacing for individual rust component.

Rust component	d-spacing
Lepidocrocite	6.3785, 3.2796, 2.4697, 1.92911, 1.7285, 1.5261
Magnetite	4.8699, 2.9768, 2.5325, 2.4303, 2.1025, 1.7158, 1.6174, 1.4854, 1.2810
Geothite	4.9376, 4.1524, 3.36263, 2.6827, 2.5731, 2.5154, 2.4811, 2.4406, 2.2464, 2.1823, 2.0069, 1.9168, 1.7954, 1.7731, 1.7163, 1.6876, 1.6560, 1.6010, 1.5613, 1.5087, 1.4530, 1.4196, 1.3909, 1.3446, 1.3157, 1.2910, 1.2628, 1.24305
Maghemite	2.9633, 2.5193, 2.0918, 1.7077, 1.6079, 1.4759, 1.3213, 1.2752

The XRD patterns of magnetite, goethite and maghemite in the presence of 0.5 % and 2.0 % tannin are shown in Fig. 3.66– Fig. 3.68.The XRD patterns of magnetite in the presence of 0.5 % and 2.0 % tannins did not show any changes to the untreated magnetite powder. This could be due to the fact that the ratio of the magnetite to tannate formation is too large and not sufficient to produce any changes to the magnetite XRD patterns.

The treated and untreated powder of goethite showed the same XRD pattern. The lower peak intensities is due to a small sample rather than a reduction in goethite content. Similarly to magnetite and goethite, the untreated and treated

maghemite did not show any change in XRD patterns with time of immersion except a loss in crystallinity with tannin treated powder.

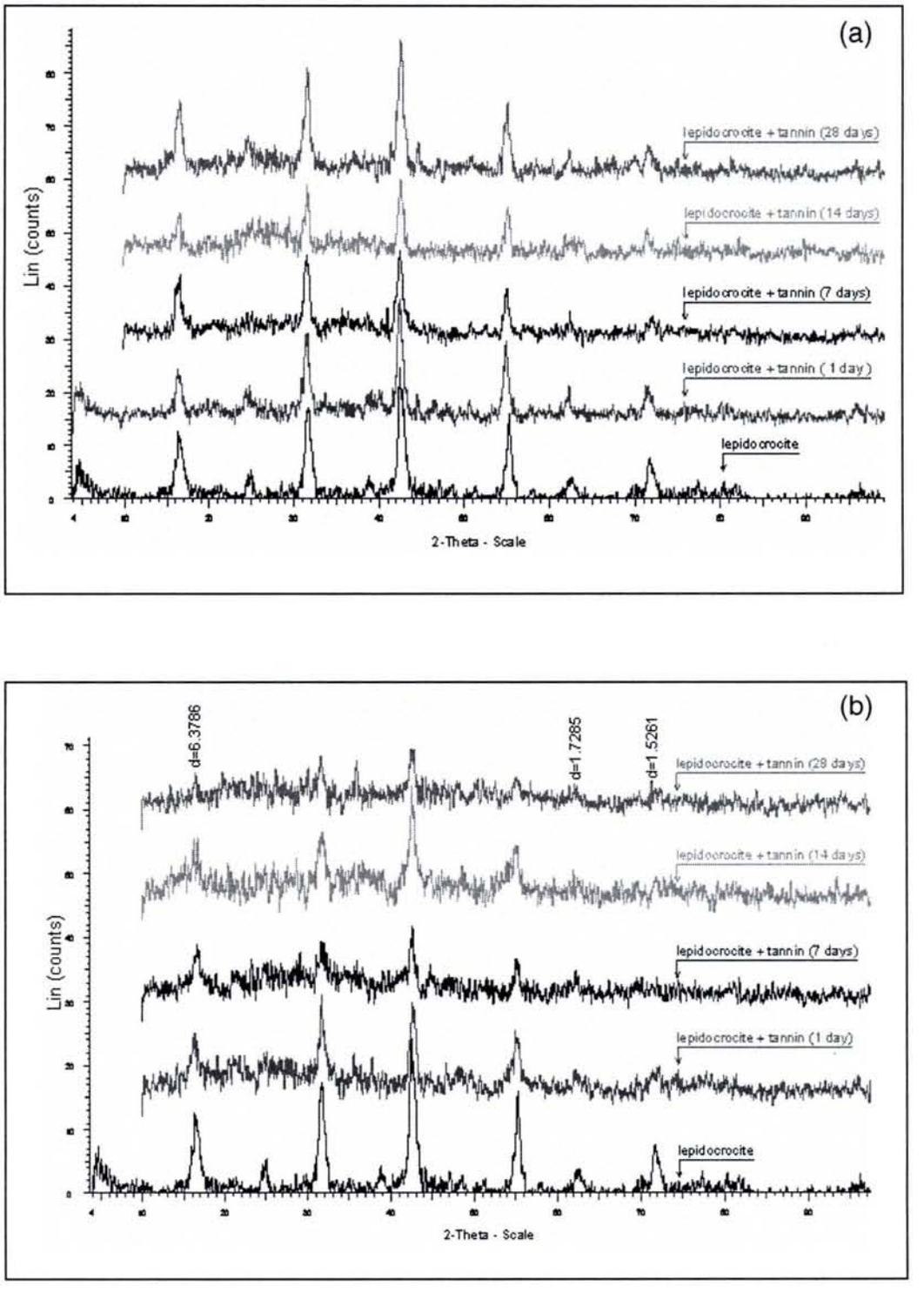

Fig. 3.65 XRD pattern of lepidocrocite treated with (a) 0.5 % and (b) 2.0 % mangrove tannins with respect to time of immersion.

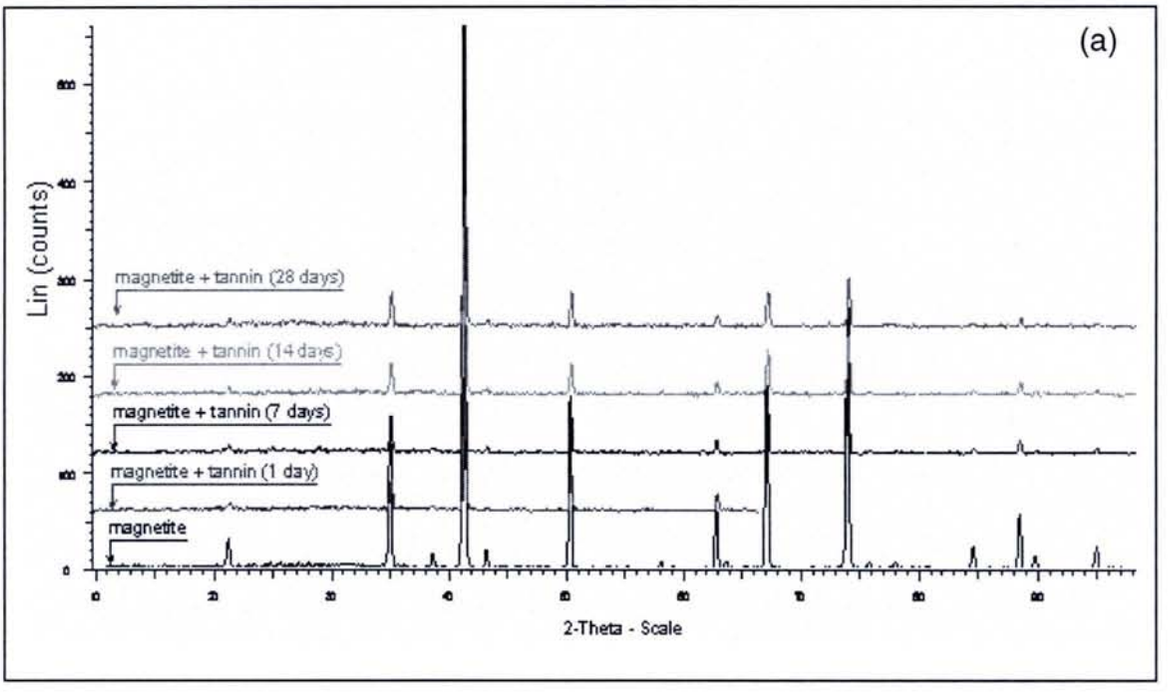

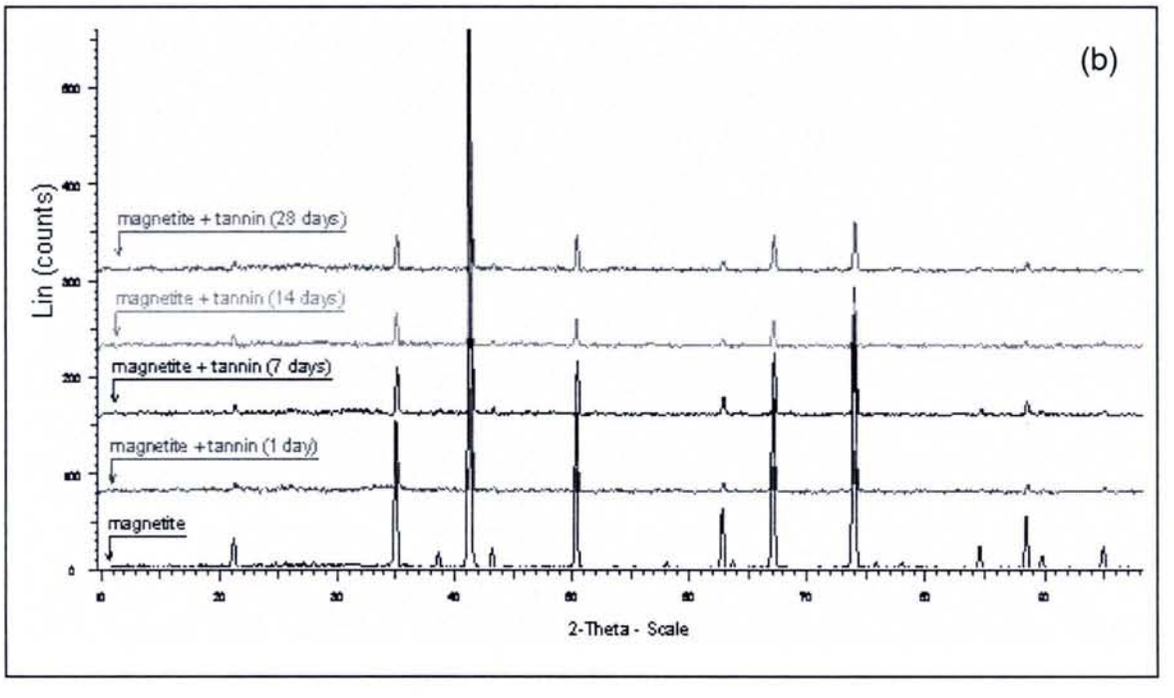

Fig. 3.66 XRD pattern of magnetite treated with (a) 0.5 % and (b) 2.0 % mangrove tannins with respect to time of immersion.

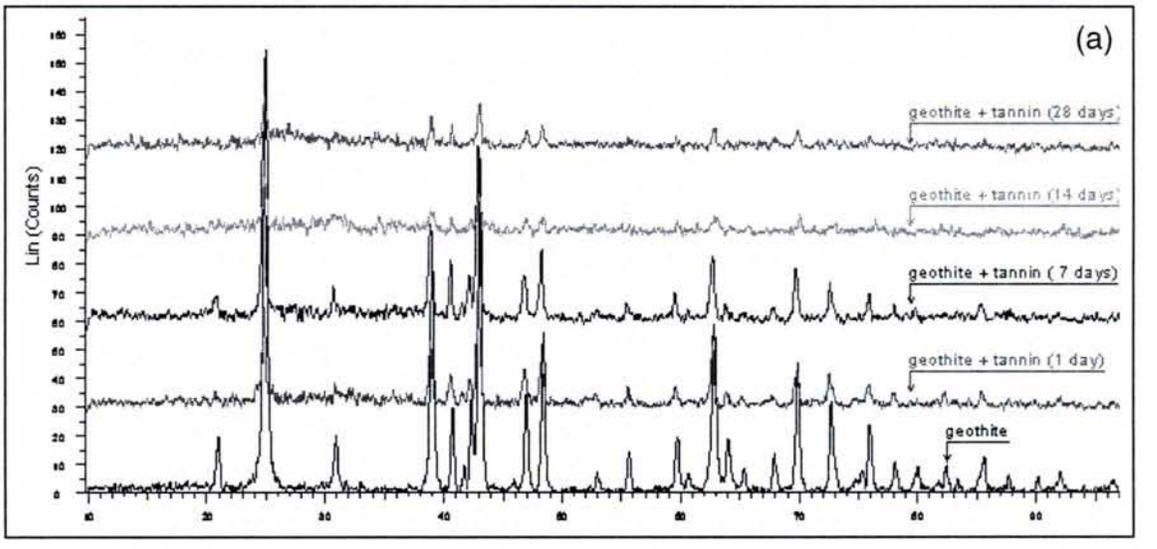

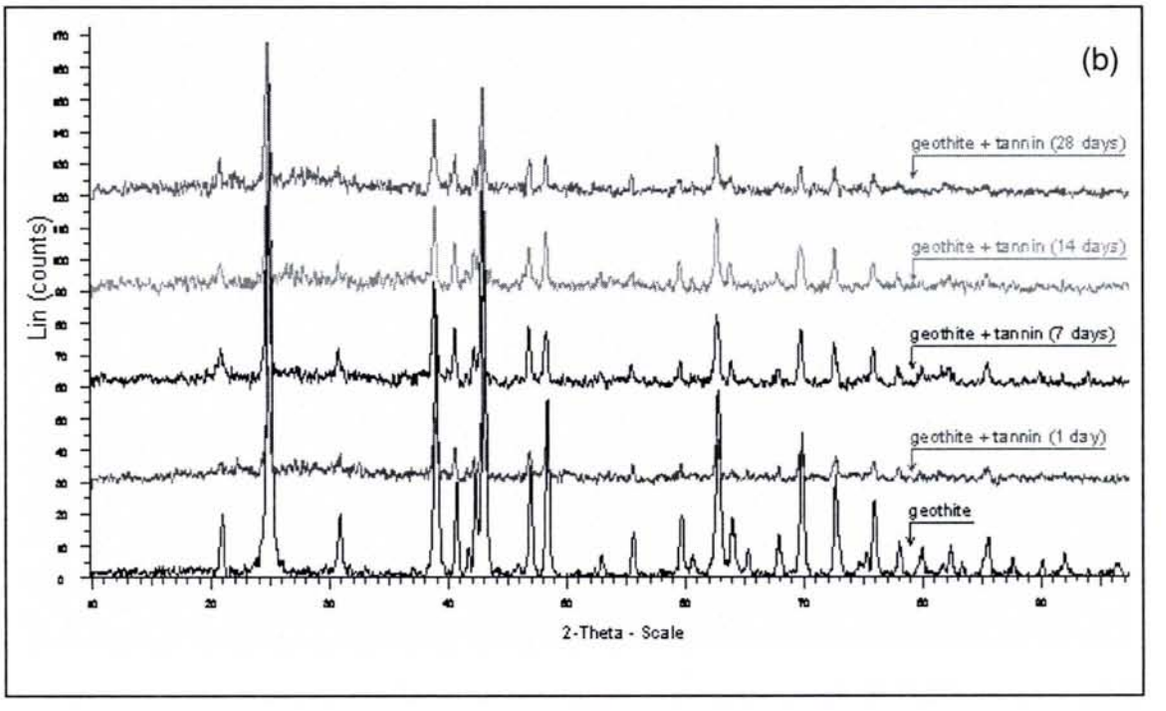

Fig. 3.67 XRD pattern of geothite treated with (a) 0.5 % and (b) 2.0 % mangrove tannins with respect to time of immersion.

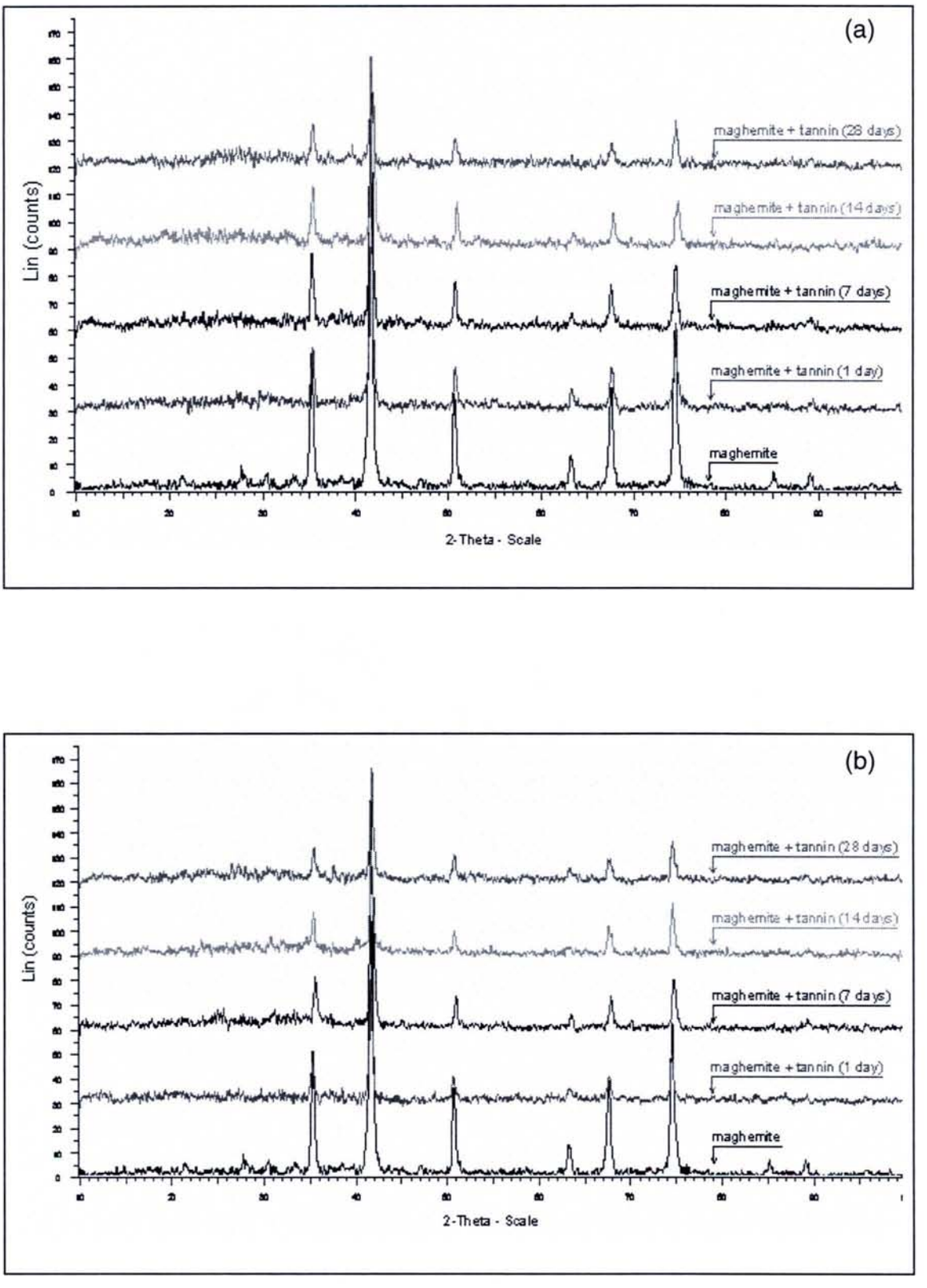

Fig. 3.68 XRD pattern of maghemite treated with (a) 0.5 % and (b) 2.0 % mangrove tannins with respect to time of immersion.

3.5.3.3 Interactions of mangrove tannins with lepidocrocite, magnetite, goethite and maghemite via scanning electron microscopy

The change in morphology of lepidocrocite, magnetite, goethite and maghemite powders after the addition of 2.0 % mangrove tannins were observed from Fig. 3.69, Fig. 3.70 and Fig. 3.71. Magnetite depicted aglomaretes of polygons and a lower magnification of magnetite revealed layers of sandwich-like structures stacked on top of another (Fig. 3.69). With the addition of mangrove tannins, these polygons seemed to break forming smaller aggregates of short finger-like structures after one day immersion. After 28 days these structures reduced in particle size [Fig. 3.70 (c)].

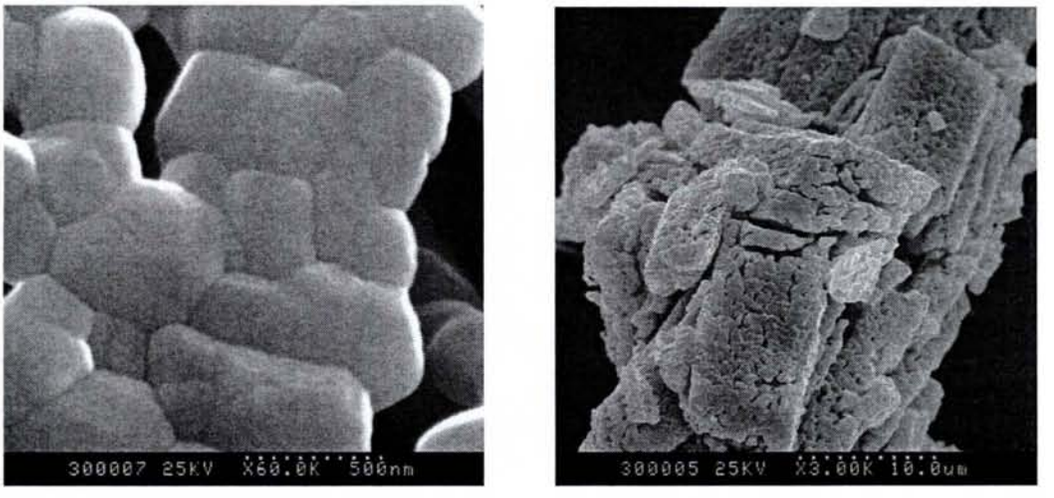

Fig. 3.69 SEM micrograpghs of magnetite with two different magnifications.

The untreated lepidocrocite powders showed finger-like structures clumped together to form cactus-like features [Fig. 3.70 (d)]. Once treated with mangrove tannins for one day, the morphology of lepidocrocite was partially transformed. And after 28 days of immersion, the cactus-like structures was completely transformed into irregular shaped sheets with tattered edges [Fig. 3.70 (f)]

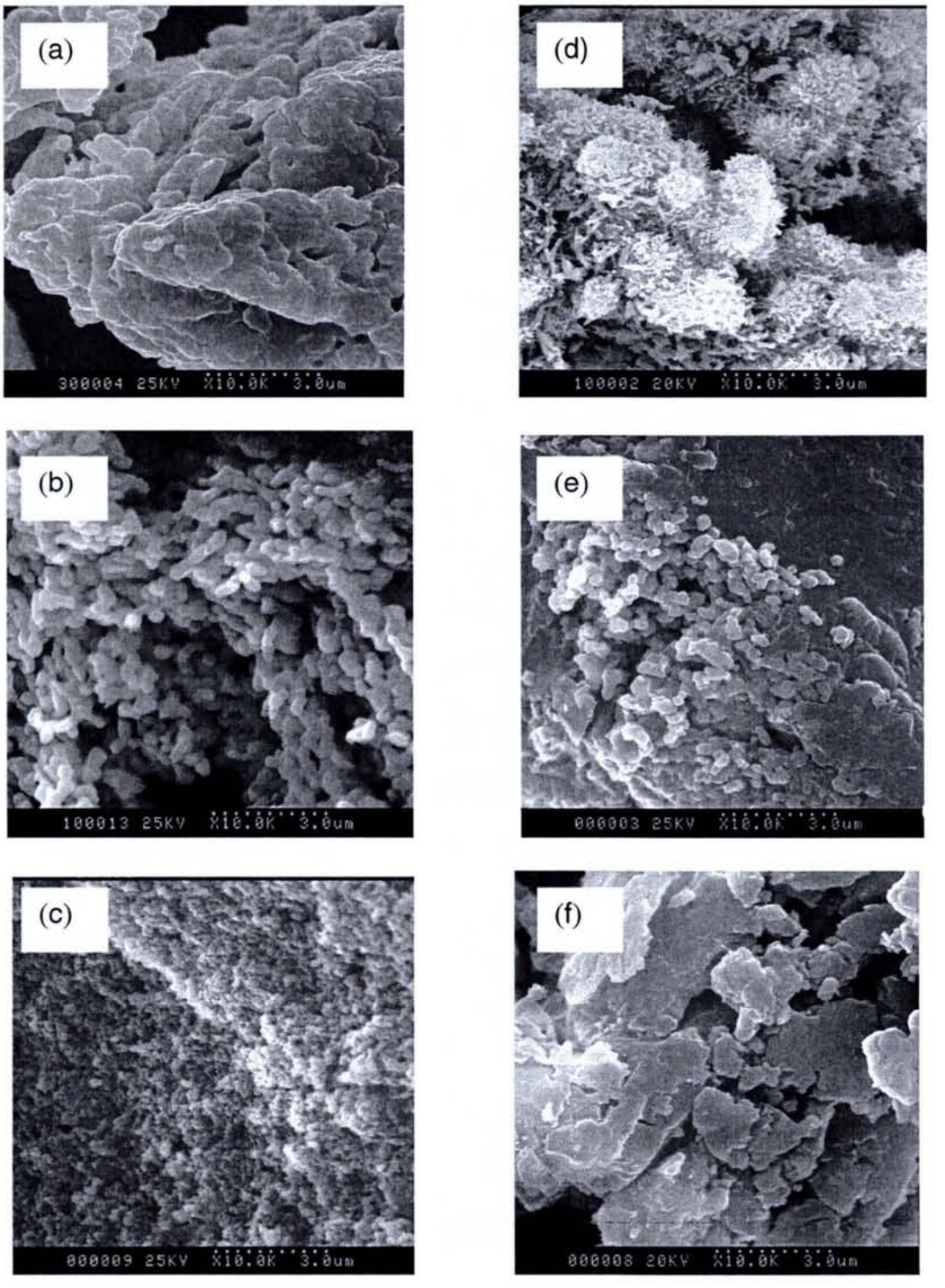

Fig. 3.70 SEM micrographs of (a) untreated magnetite and treated magnetite after (b) one day and (c) 28 days immersion; and (d) untreated lepidocrocite and treated lepidocrocite after (e) one day and (f) 28 days immersion.

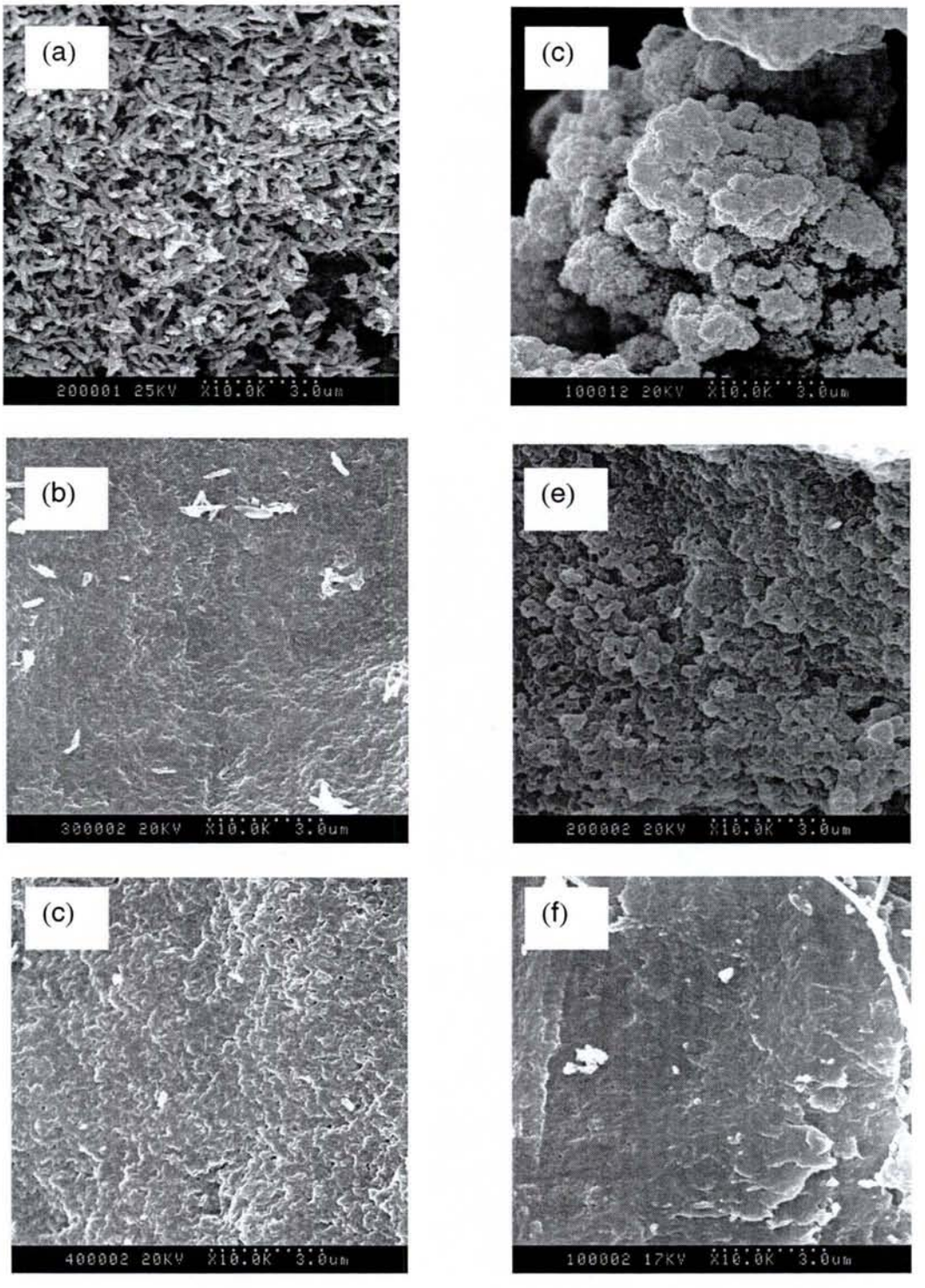

Fig. 3.71 SEM micrographs of (a) untreated goethite and treated goethite after one day and (c) 28 days immersion; and (d) untreated maghemite and treated maghemite after (e) one day and (f) 28 days immersion.

Geothite exhibited randomly scattered lath-shaped structures [Fig. 3.71 (a)]. Upon the addition of mangrove tannins, these structures were transformed into a coarse layer with tiny specks of untransformed goethite after one day immersion. A complete transformation was observed after 28 days of immersion [Fig. 3.71 (c)].

Maghemite presented structures similar to bunches of cauliflowers [Fig. 3.71 (d)]. The bunches of cauliflowers seems to have ruptured with the mangrove treated samples after one day immersion. These structures were similar to the transformed goethite powders but of larger sized particles. After 28 days of immersion, the structures were the same as the transformed goethite samples [Fig. 3.71 (f)].

3.5.4 Phase transformation of the individual rust component in the presence of phosphoric acid

The FTIR spectrum of lepidocrocite powder treated with phosphoric acid illustrated a broad phosphate peak (1000-1200 cm^{-1}) along with lepidocrocite peak at 1021 cm^{-1} (Fig. 3.72). The intensity of the lepidocrocite peak remained unchanged throughout the one month immersion. The treatment of phosphoric acid to magnetite produced a phosphate peak after one day onwards but this peak reduced with time until it was almost gone after one month. No effect was observed with the treatment of phosphoric acid to goethite. The magnetite and goethite peaks essentially remained unchanged throughout the one month immersion. Addition of phosphoric acid to maghemite gave rise to a weak

phosphate peak and unchanged maghemite peaks for all duration of immersion.

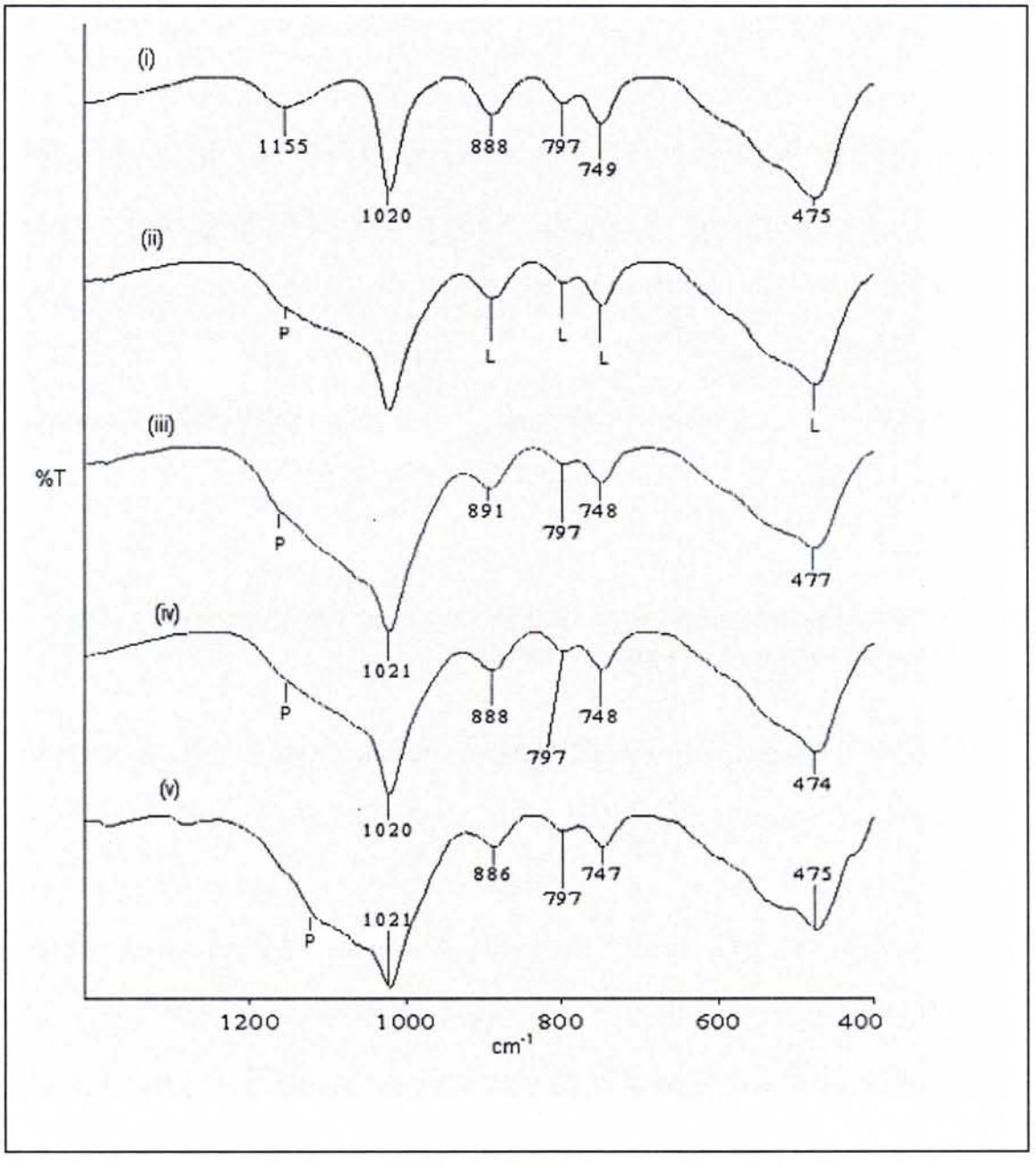

Fig. 3.72 FTIR spectrum of (i) untreated lepidocrocite and lepidocrocite treated with 15 % phosphoric acid after (ii) 1 day, (iii) 1 week, (iv) 2 weeks and (v) 1 month immersion : L-lepidocrocite, P-phosphates.

It has been shown that increment of tannin concentration from 0.5 % to 2.0 % resulted in an increased rust transformation. Nevertheless in this study the joint effect of 0.5 % mangrove tannins and 15 % phosphoric acid on the transformation of rust was investigated in order to illustrate the correlation between the degree of transformation of individual rust and the increased deposition of complex observed by the EDS analysis when treated with this same composition of mangrove tannins and phosphoric acid.

The FTIR spectrum of the treated lepidocrocite showed the appearance of tannate and phosphate peaks were observed as early as after one day immersion while not exerting any effect on the lepidocrocite peaks (Fig. 3.73). FTIR spectrums of the treated magnetite showed the appearance of initially a weak phosphate peak after one day to two weeks of immersion followed by both tannate and phosphate peaks only after one month immersion. Similarly to lepidocrocite, the magnetite peak remained undisturbed (Fig. 3.74). For goethite treated samples, weak phosphate and tannate peaks were formed after one and two weeks of immersion time and these peaks intensified with time. Nonetheless, the geothite peaks were not affected (Fig. 3.75). From Fig. 3.76 both tannate and phosphate peaks made their appearance after one day immersion, intensifying after two weeks immersion with the treatment of tannin and phosphoric acid to maghemite. Subsequently the peaks remained constant after one month. Like the rest of the rust components, the maghemite peaks was not affected.

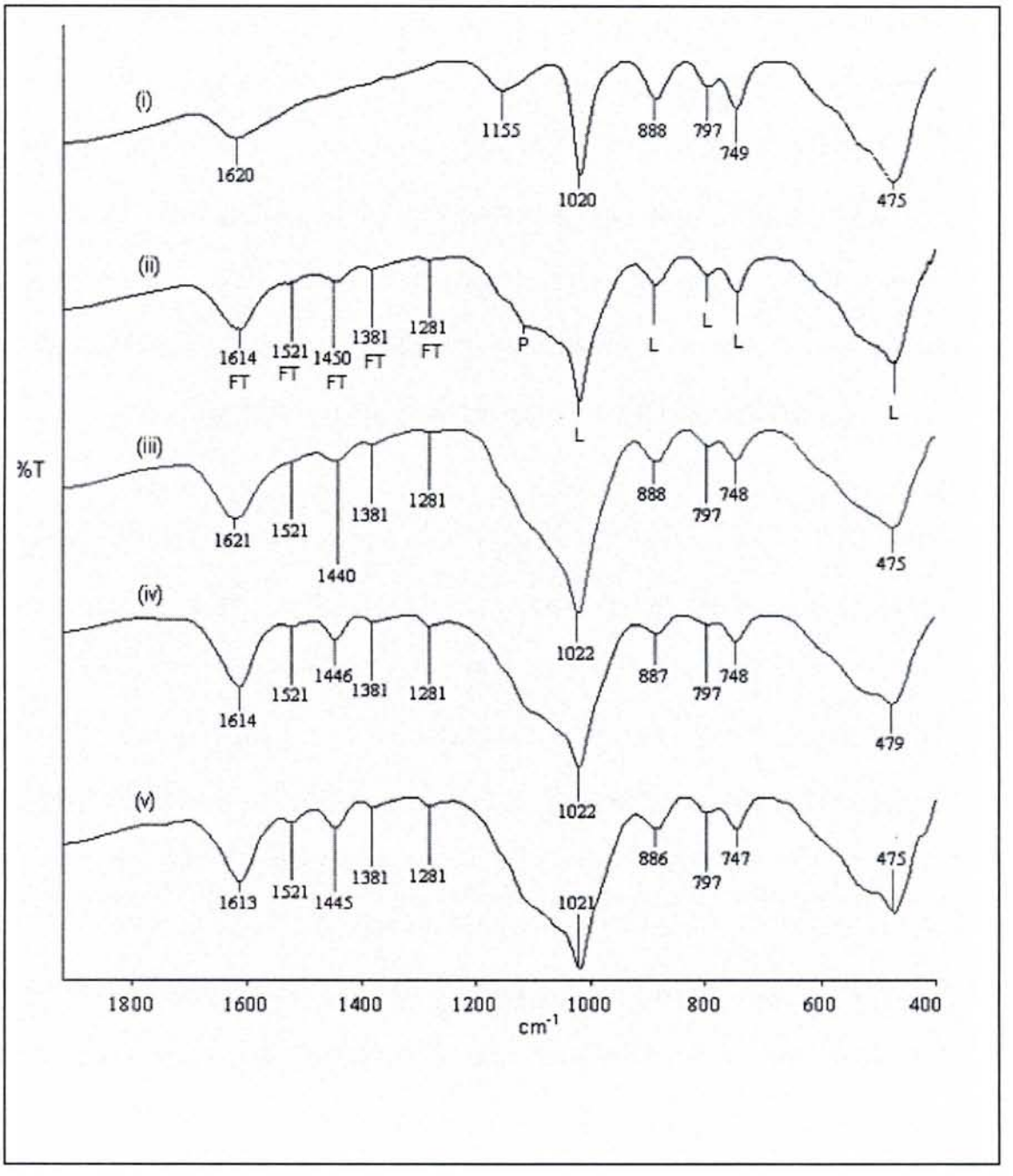

Fig. 3.73 FTIR spectrum of (i) untreated lepidocrocite and lepidocrocite treated with 0.5 % mangrove tannins and 15 % phosphoric acid after (ii) 1 day, (iii) 1 week, (iv) 2 weeks and (v) 1 month immersion : FT-ferric-tannate, L-lepidocrocite, P-phosphates.

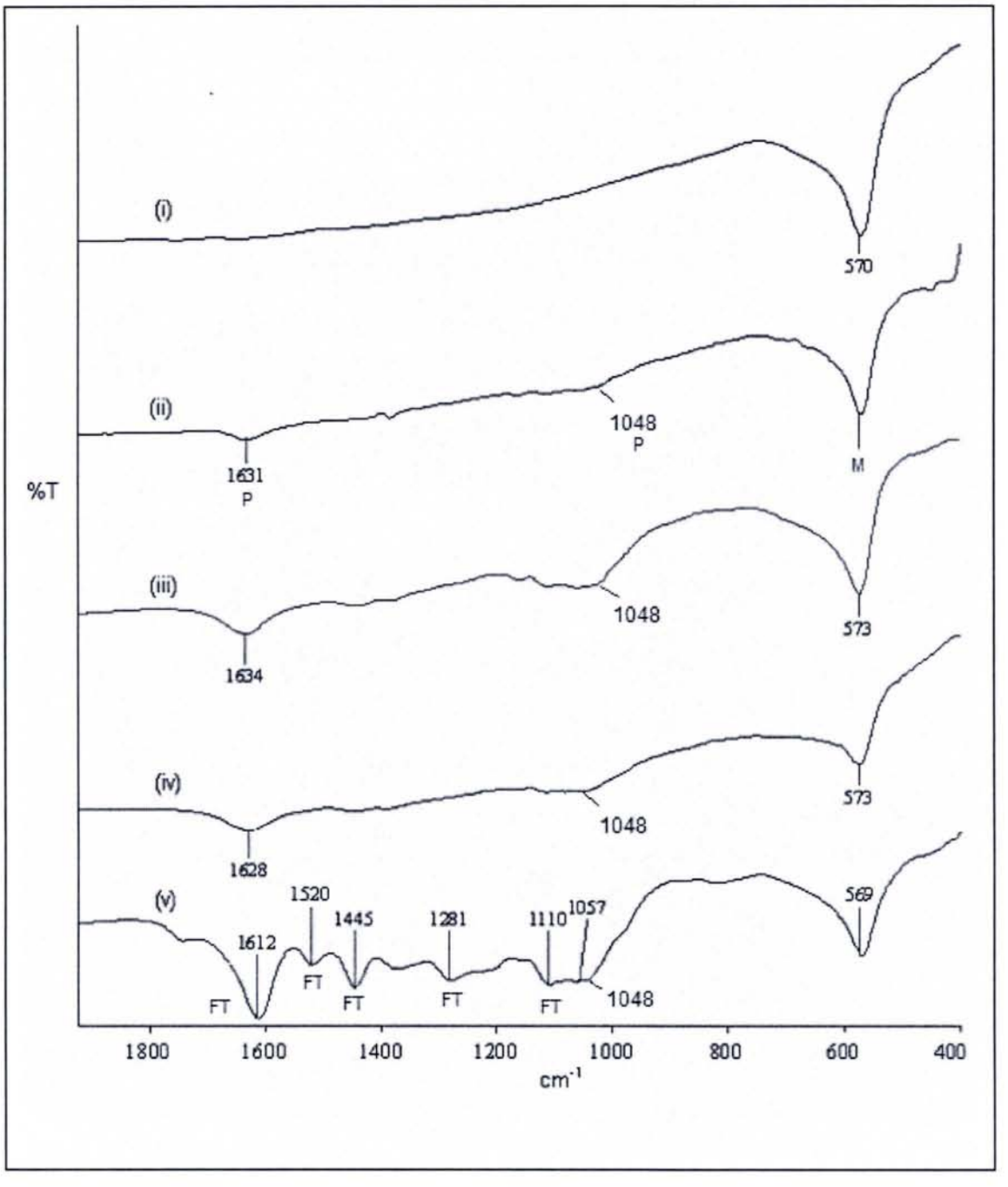

Fig. 3.74 FTIR spectrum of (i) untreated magnetite and magnetite treated with 0.5 % mangrove tannins and 15 % phosphoric acid after (ii) 1 day, (iii) 1 week, (iv) 2 weeks and (v) 1 month immersion : FT-ferric-tannate, M-magnetite, P-phosphates.

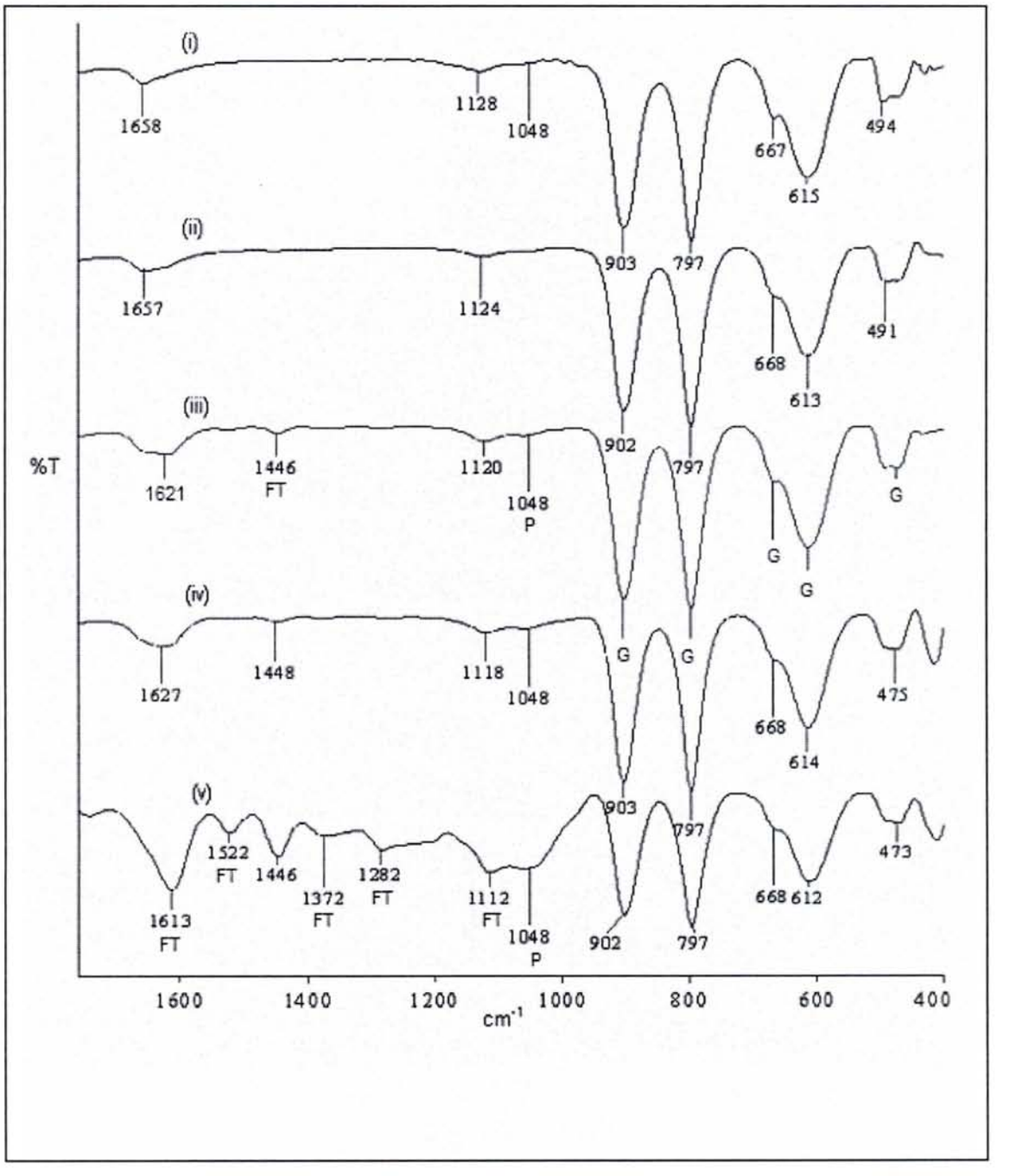

Fig. 3.75 FTIR spectrum of (i) untreated geothite and geothite treated with 0.5 % mangrove tannins and 15 % phosphoric acid after (ii) 1 day, (iii) 1 week, (iv) 2 weeks and (v) 1 month immersion : FT-ferric-tannate, G-geothite, P-phosphates.

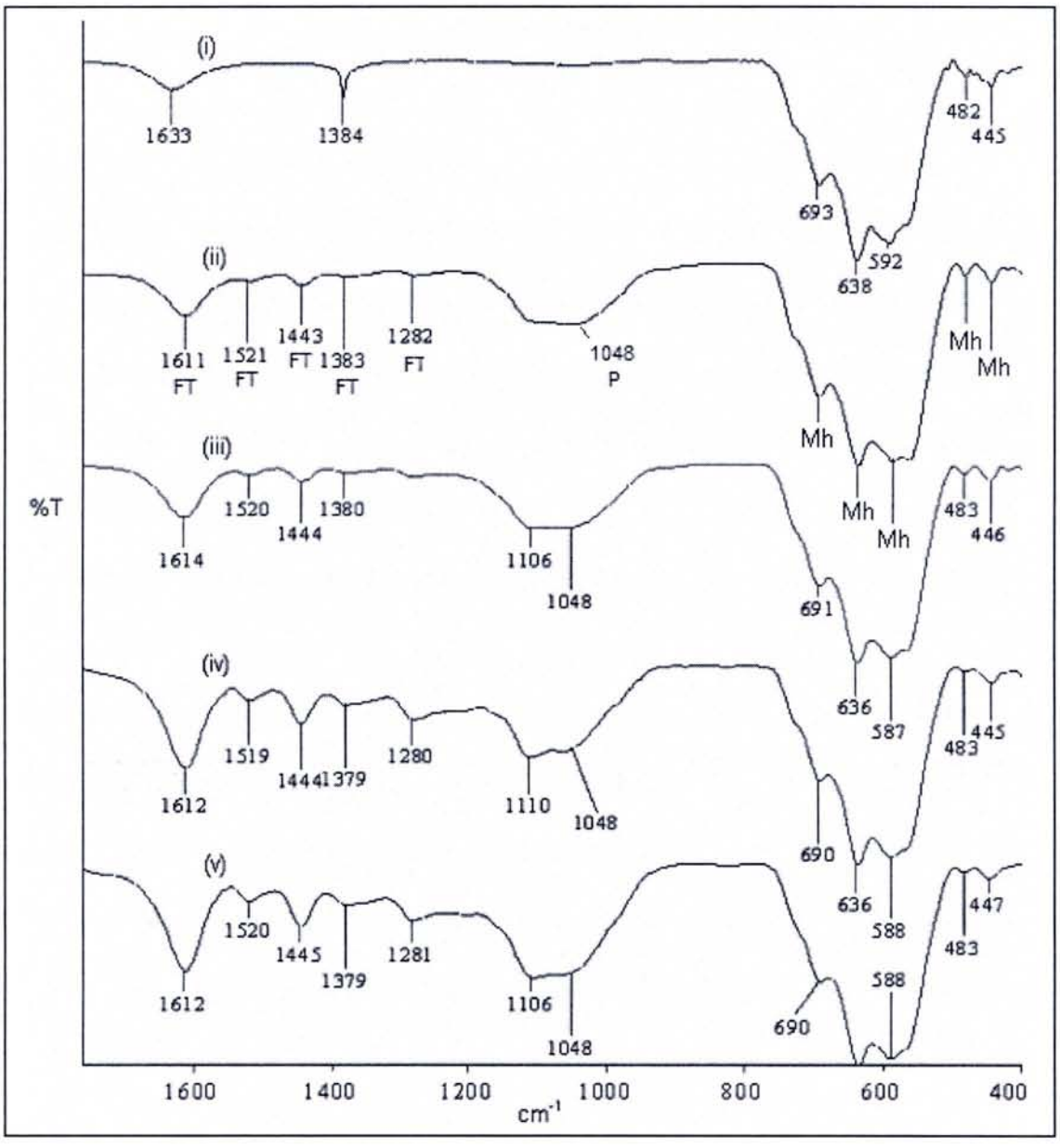

Fig. 3.76 FTIR spectrum of (i) untreated maghemite and maghemite treated with 0.5 % mangrove tannins and 15 % phosphoric acid after (ii) 1 day, (iii) 1 week, (iv) 2 weeks and (v) 1 month : FT-ferric-tannate, Mh-maghemite, P-phosphates.

3.5.5 Evaluation of protective efficiency

In order to evaluate the protective property imparted by mangrove tannins, pre-rusted plates immersed in 0.5 % mangrove tannins and 0.5 % mangrove tannins + 15 % phosphoric acid were exposed to the humidity chamber and salt spray chamber. The protective property was compared with that of mimosa tannins and phosphoric acid alone.

3.5.5.1 Evaluation of protective efficiency via the humidity chamber tests

The evolution of rust formation with time for the mangrove tannins treated plates are shown in Fig. 3.77. Rust formation was observed on the upper right hand of the plate after seven days. Although the rust intensified after 15 days, the extent of rust formation remained constant until 45 days. A large percentage of the plate was still covered with the blue-black ferric-tannate.

For mimosa tannins treated plates, an accumulation of rust occurred at the lower end of the plate and to a lesser extent at the upper part of the plate after one day of exposure (Fig. 3.78). The amount of rust increased slightly after seven days and remained constant from then on.

With the treatment of phosphoric acid alone, the bluish–white phosphate deposit was immediately transformed into rust after one day and the rust progressively increased especially at the lower end of the plate. When the plate

was finally removed from the chamber after 45 days, the plate was almost totally covered with rust (Fig. 3.79).

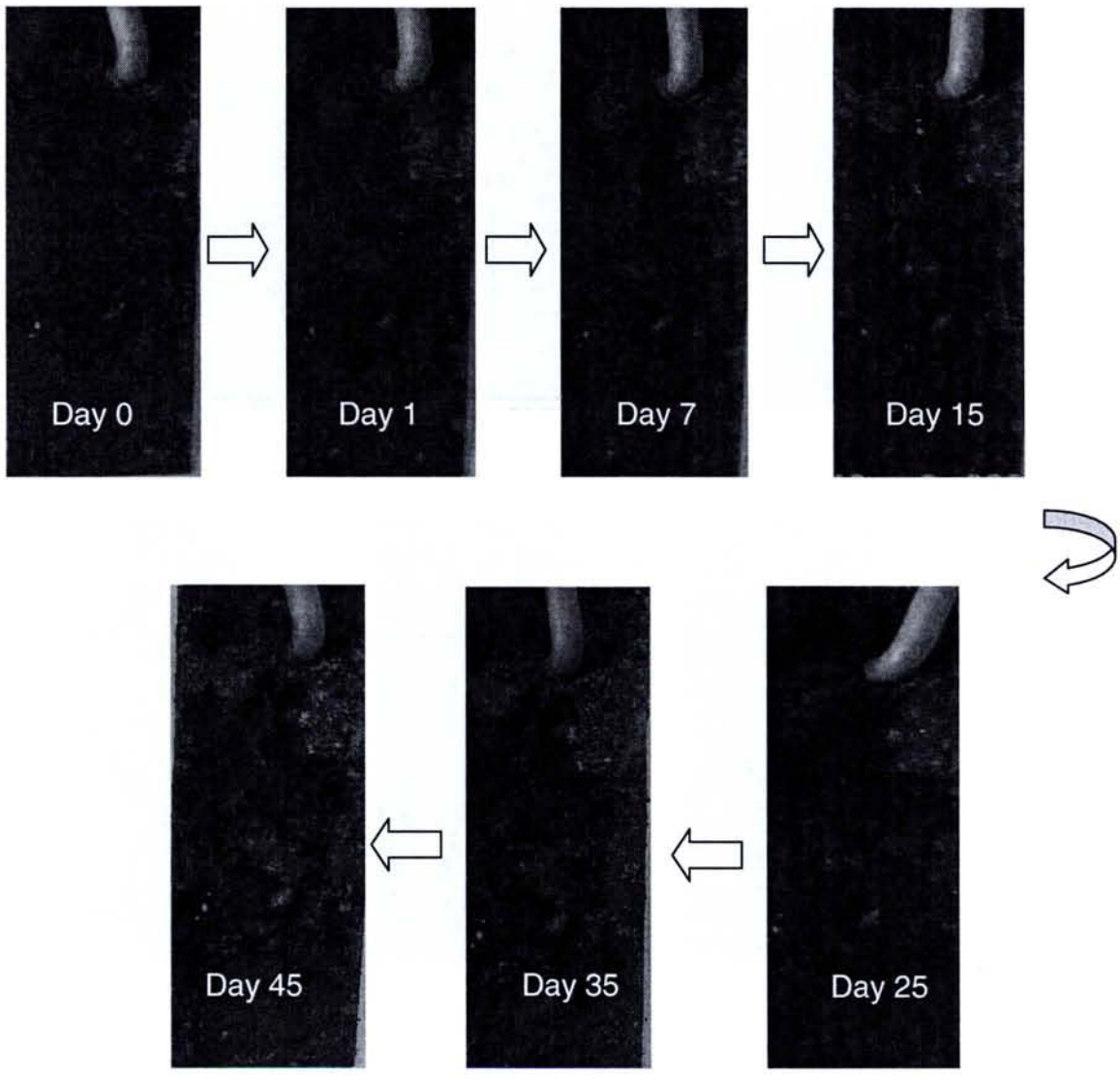

Fig. 3.77 Evolution of rust formation with time for pre-rusted samples treated with 0.5 % mangrove tannins.

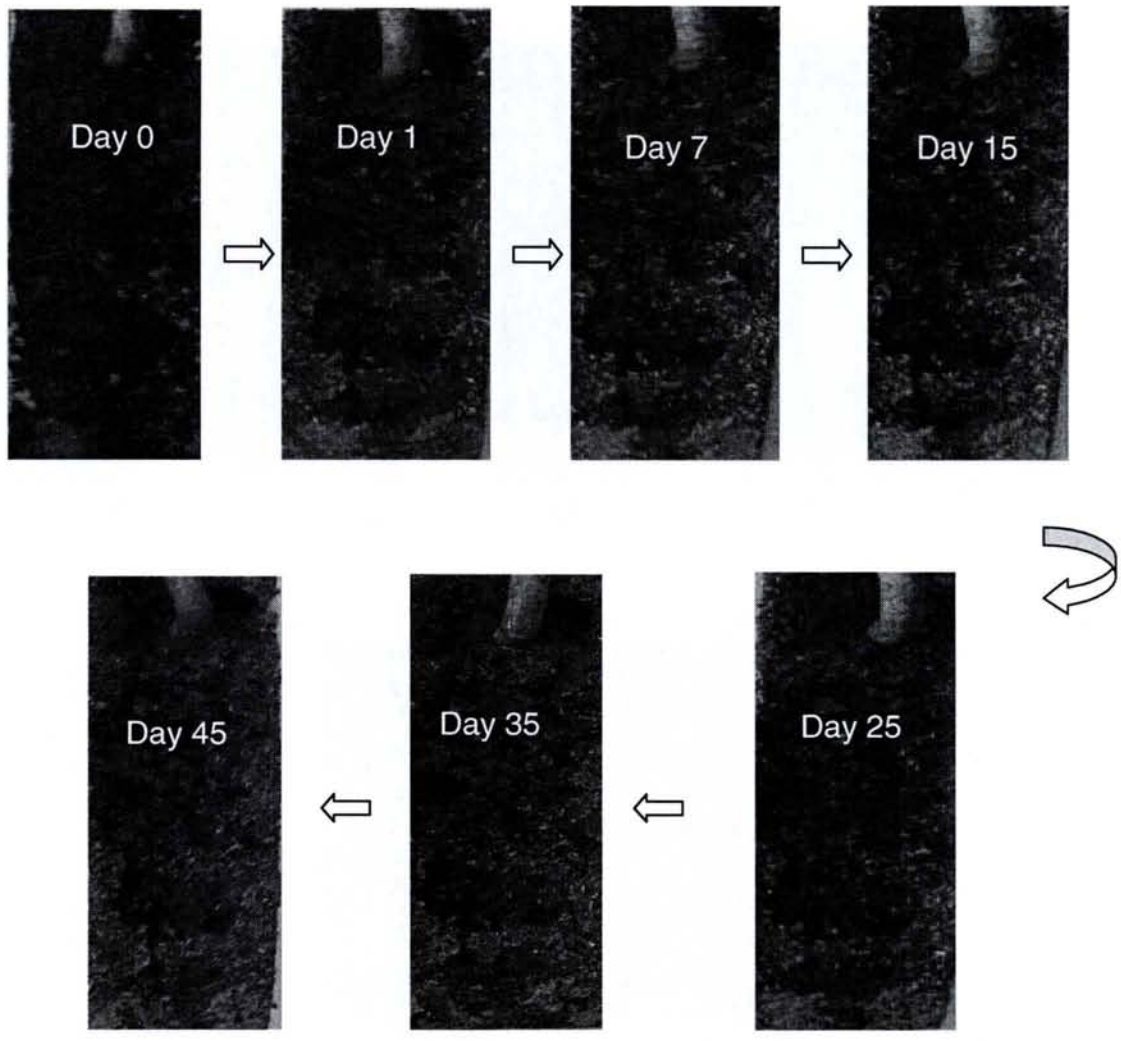

Fig. 3.78 Evolution of rust formation with time for pre-rusted samples treated with 0.5 % mimosa tannins.

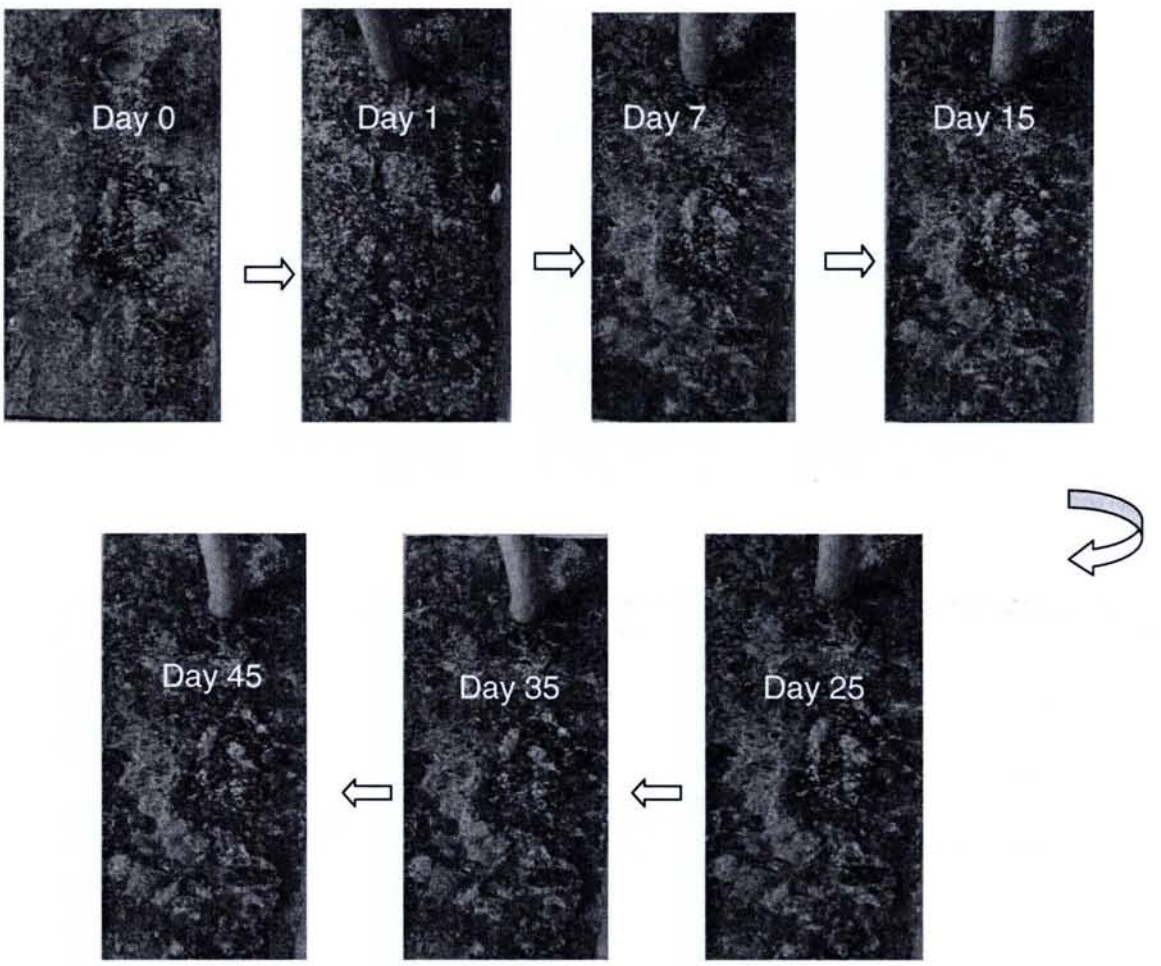

Fig. 3.79 Evolution of rust formation with time for pre-rusted samples treated with 15 % phosphoric acid.

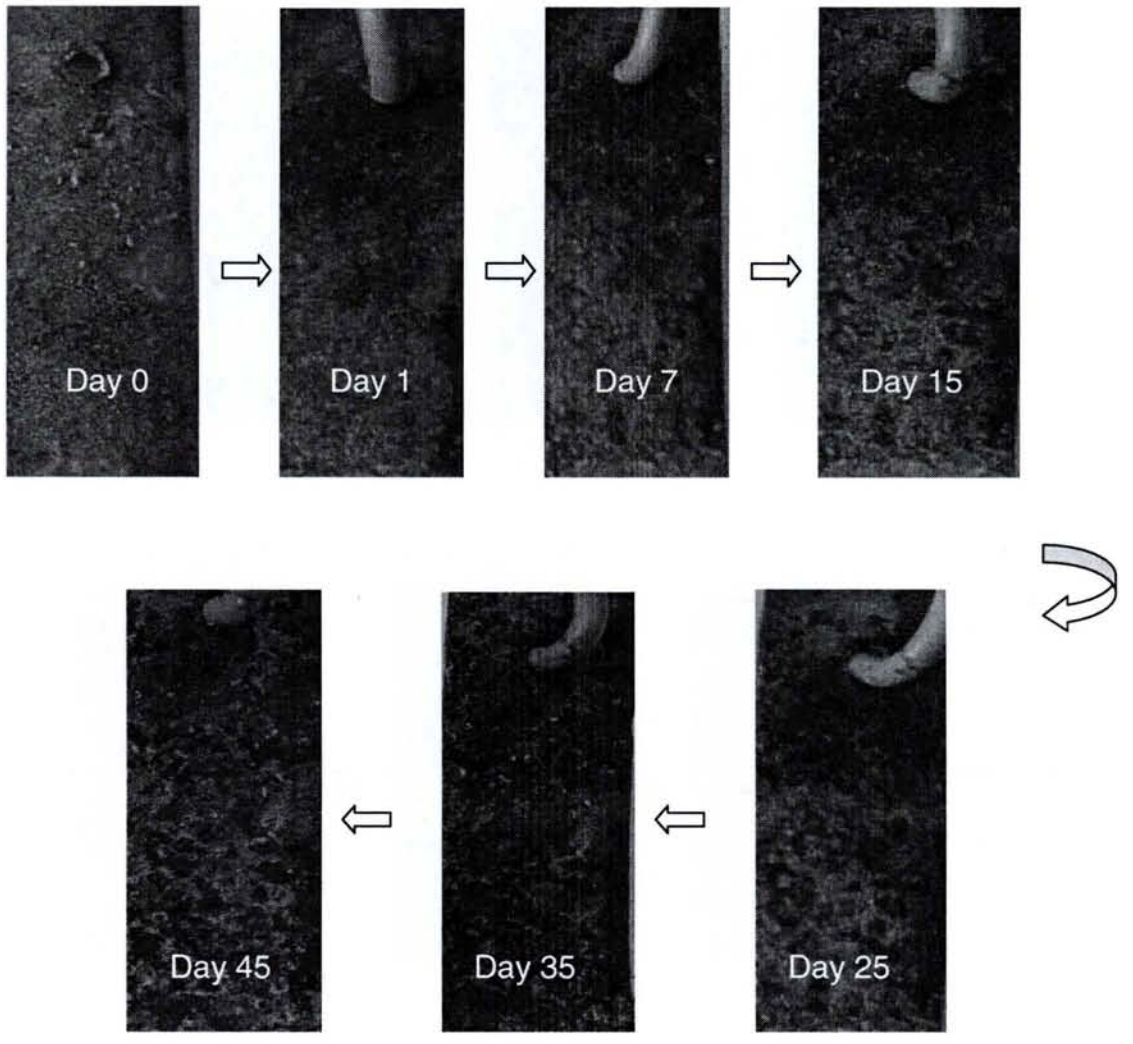

Fig. 3.80 Evolution of rust formation with time for pre-rusted samples treated with 0.5 % mangrove tannins and 15 % phosphoric acid.

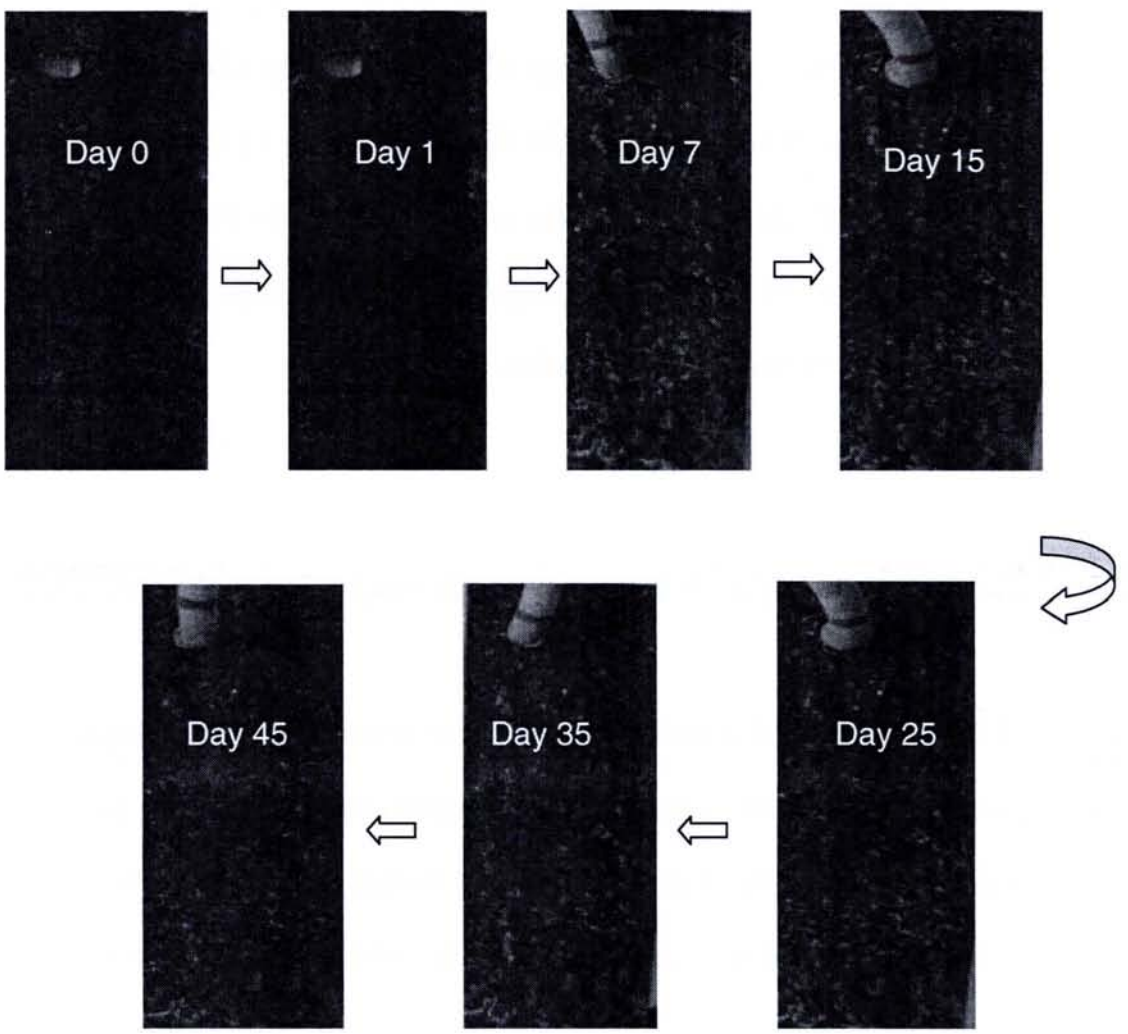

Fig. 3.81 Evolution of rust formation with time for pre-rusted samples treated with 0.5 % mimosa tannins and 15 % phosphoric acid.

The plates treated with mangrove tannins and phosphoric acid was initially covered with greyish deposits, presumably a blend of bluish-white phosphates and blue-black tannates (Fig. 3.80). The plate demonstrated a slow formation of rust after one day which increased slightly until 25 days. Then after 35 days, the plate revealed a high percentage of black deposits along with some red rust which increased in formation after 45 days. Treatment of samples with mimosa and phosphoric acid demonstrated an initial formation of rust at the lower end of the plate. The rusting increased slightly after seven days and remained constant until 45 days of exposure (Fig. 3.81).

3.5.5.1 Evaluation of protective efficiency using salt spray tests

All pre-rusted plates were prepared by exposing the mild steel plates in the salt spray chamber and the spraying process was carried out according to the ASTM B 117 standard procedure. Rust formation was observed after one hour. The steel surface was uniformly covered with rust as shown in Fig. 3.82 and was used as a standard.

Fig. 3.82 Rusted plate after six hours of exposure in the salt spray chamber.

The mangrove tannins treated samples showed the following changes when exposed in the salt spray chamber. Initially the surface was covered with blue-black deposits, typical of ferric-tannates and a sign of rust forming was observed after 4 hours of exposure. And after six hours, it was seen that the rust occupied regions where the plate was not covered with blue black deposits of tannates [Fig. 3.83 (a)]. For mimosa tannin covered samples, a slower rust process was observed after four hours but rust formation was enhanced after six hours [Fig. 3.83 (b)].

Treatment of the pre-rusted plate with phosphoric acid demonstrated a more rapid rusting process when the original bluish-white phosphate surface was covered with more rust than the phosphates after four hours. The rusting process continued to take place when more rust formation was observed after six hours [Fig. 3.83 (c)].

From Fig. 3.83 (d), it was observed that with the addition of both mangrove tannins and phosphoric acid, the surface was covered with more blue-black deposit of tannates than the whitish deposit of phosphates along with some untransformed rust. More rust was seen to form after four hours which subsequently thickened after six hours. Simiarly for mimosa tannins, the surface was coated with more ferric-tannates than phosphates. Formation of new rust was slow as witnessed from the plate showing hardly any changes to the original plate after six hours [Fig. 3.83 (e)].

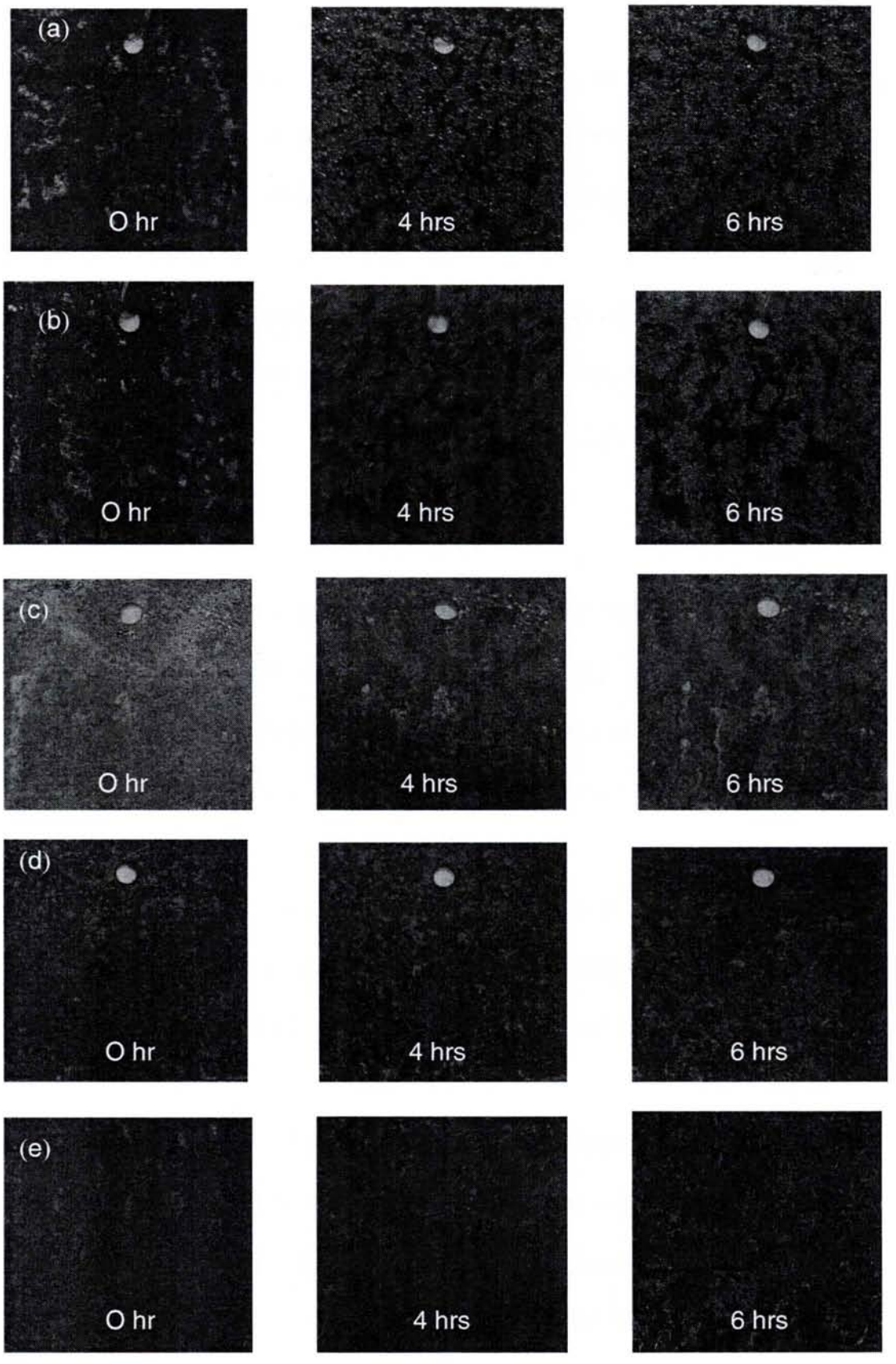

Fig. 3.83 Evolution of rust formation of pre-rusted plates immersed in (a) 0.5 % mangrove tannins, (b) 0.5 mimosa tannins, (c) 15 % phosphoric acid, (d) 0.5 % mangrove tannins and 15 % phosphoric acid and (e) 0.5 % mimosa tannins and 15 % phosphoric acid.

CHAPTER FOUR

DISCUSSION

4.1 Tannin extraction

The similarity of the IR spectrums of mangrove tannins to mimosa and quebracho tannins and especially the absence of the 1735 cm^{-1} band as depicted by chestnut tannins clearly show that mangrove tannins consisted of mainly condensed tannins.

A single extraction using sephadex LH-20 column chromatography was found to be sufficient in producing condensed tannins of high purity. The separation of tannins on sephadex LH-20 columns is induced by the difference in adsorptivity of each tannin on the gel. This gel however offers the disadvantage of strongly adsorbing several types of tannins especially condensed tannins of large molecules which are not recovered from the column (Okuda *et al.*, 1989). This could probably explain the fact that only 70 % (wt) tannin powders (acetone-water and methanol-water extracts) were retrieved when the tannins were subjected to this column.

4.1.1 Thermogravimetric analysis

Although the acetone-water extract produces similar IR spectrum to the methanol-water extract, different components are present in the two different extracts as witnessed by the different weight loss profiles of the TGA analysis of the extracts.

In a DTG analysis study of gallic acid by Garro Galvez *et al.,* (1996), three main peaks were detected. The first one at 260 °C is reported to correspond to carbon dioxide released upon heating (decarboxylation), the second peak at 308 °C is probably due to the further loss of water. The third peak at 503 °C corresponds to oxidation of high carbon residue. In this study, mangrove, mimosa and quebracho tannins exhibited two main peak temperatures as compared to three peak temperatures shown by chestnut tannins. Thus the thermal decomposition of chestnut tannins, a hydrolysable tannin is similar to gallic acid. These observations consequently further affirm the occurrence of mangrove tannins as mainly condensed tannin. Nevertheless, the different weight losses among mangrove, mimosa and quebracho tannins implied that each tannin constituted of different structural monomers. Whilst no reports on the structure of quebracho tannins have been encountered the following structure in Fig. 4.1 has been proposed by Martinez (2002) for mimosa tannins:

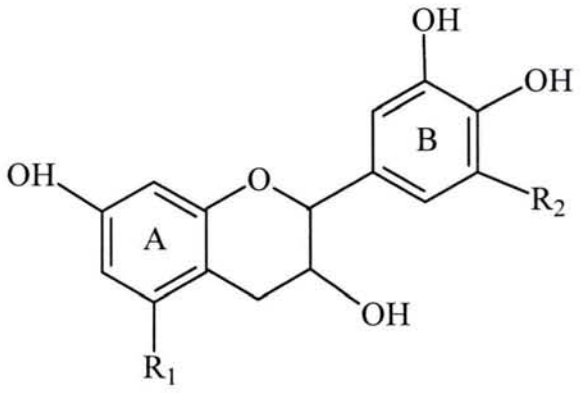

Fig. 4.1 Molecular structure of mimosa tannin: R_1 = H for resorcinol, R_1 = OH for phloroglucinol, R_2 = H for pyrocatechol and R_2 = OH for pyrogallol.

4.1.2 Prussian blue assay

In the Prussian blue assay, the summation of the phenolic content of the individual acetone-water and methanol-water extracts corresponded to the phenolic content of the mixed tannin, indicating that almost all phenolics are being extracted into the condensed tannin as well as the methanol-water components. Despite the laborious procedure associated with this determination, it provided a relevant method of quantifying total phenolics in mangrove tannins.

4.2 Identification of condensed tannins via HPLC analysis

Koupai-Abyazani *et al.* (1992) reported that the elution order of several flavan-3-ols is influenced by the substitution pattern of the B ring and the stereochemistry of the components. Thus the elution order is: (+)-gallocatechin, (-)-epigallocatechin, (+)-catechin, (-)-epicatechin. In this study the ascending elution order was as follows:

(-)-gallocatechin < (+)-catechin/(-)-catechin < (-)-epigallocatechin < (-)-epigallocatechin gallate < (-)-epicatechin < (-)-gallocatechin gallate < (-)-epicatechin gallate < (-)-catechin gallate. The same elution order was achieved by Pelilo *et al.* (2002) for green tea catechins. In contrary to the reports of Koupai-Abyazani *et al.* (1992) and Pelilo *et al.* (2002), this study showed the elution of (+)-catechin before (-)-epigallocatechin.

Indeed the stereochemical position of the OH group at C-3 of the C ring (see Fig. 3.8) was found to influence the elution order as witnessed from the shorter retention time of (+)-catechin to (-)-epicatechin. In the same way, (-)-gallocatechin was eluted before (-)-epigallocatechin. The introduction of a gallate group on the B ring however witnessed the elution of (-)-epicatechin gallate followed by (-)-catechin gallate. It was also noteworthy that the retention times of the trihydroxyl groups on the B ring were shorter than the dihydroxyl groups. The elution condition used could not separate peaks of optically different isomers as shown by overlapping peak for (+)-catechin and (-)-catechin.

The use of phloroglucinol in dioxane in the depolymerisation reaction produced unfavourable results. Besides producing a hump associated with the fraction resistant to the depolymerisation process (Matthews *et al.*, 1997) dioxane is toxic in nature. Hence, the use of phloroglucinol in ethanol was preferred. However, the outcome of the HPLC chromatogram was elution dependent.

The HPLC analysis following depolymerisation in phloroglucinol in ethanol of elution (ii) revealed mainly four terminal units and one extender unit. Spiking the samples with flavanoid standards ensured a correct identification of the individual monomer, avoiding the possibility of peak overlapping as shown in Fig. 3.7. In this study, the terminal units namely catechin, epicatechin, epigallocatechin and epicatechin gallate were identified for both mangrove samplings. The structures of these monomers are shown in Fig. 4.2.

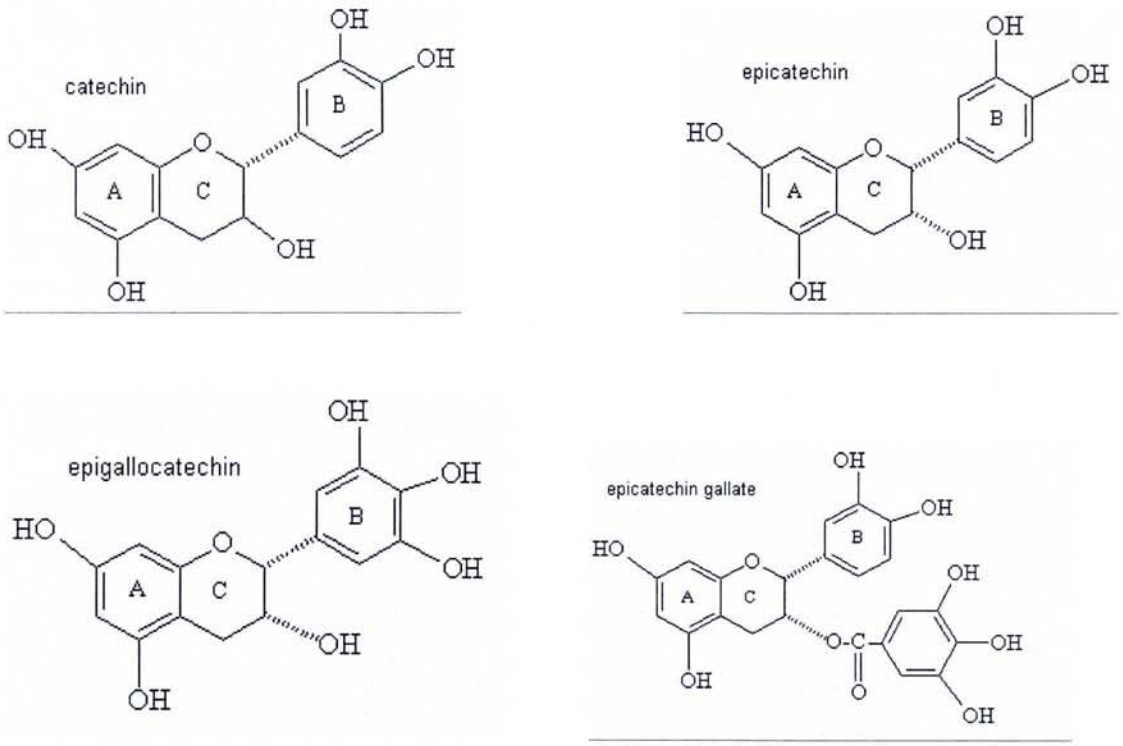

Fig. 4.2 Chemical structure of flavanoid monomers that constitute mangrove tannins.

The phloroglucinol adduct of condensed tannins was eluted faster than the flavan-3-ols (terminal units). This is also true for all the monomer adducts synthesised. This could be attributed to the higher polarity of the adduct due to the formation of stronger hydrogen bonds with the mobile phase as the phloroglucinol group at the C-4 position (see Fig. 3.8) was substituted. Spiking the samples with monomer adducts showed that none of the monomer standards were present as the extender unit. Considerable efforts were taken to further confirm and identify the terminal and extender units including preparative HPLC, column chromatography and NMR techniques. The phloroglucinol adduct was prepared according to the method proposed by Achmadi *et al.* (1994) as described in section 2.1.3.1 and purified by sephadex LH-20 chromatography and reversed-phase HPLC. However, due to the relatively low concentration of extracted adduct, recovery of pure samples was rendered

difficult. Although the elucidation of the extender unit was not successful, the identification of the terminal units was sufficient to confirm that mangrove tannins are mainly condensed tannins.

4.2.1 Quantification of condensed tannins

4.2.1.1 Vanillin assay

The 34-37 % (+)-catechin equivalent clearly illustrated the presence of condensed tannins in the first and second acetone-water extracts. On the other hand, a relatively low catechin equivalent content in the methanol-water extract indicated that a small amount of condensed tannins was present. Any attempt to further separate the condensed tannin from the methanol-water extract would prove to be a futile effort since the second methanol-water fraction again showed the presence of condensed tannin when subjected to the vanillin assay by producing the same catechin equivalent content. This observation is in agreement with the work reported by Achmadi *et al.* (1994). The presence of condensed tannins in the methanol-water extract was also shown by the HPLC chromatogram (Fig. 3.16).

4.2.1.2 Quantification of flavanoid monomers via HPLC analysis

Among the weaknesses associated with the vanillin assay is the lack of specificity for condensed tannins. Any appropriately substituted monomeric flavanol reacts in the assay. The major problem with the vanillin assay seems to derive from the variable reactivity of the subunits of the tannin polymer. The

structural variations in proanthocyanidins also affect the colour yield with vanillin (Schofield *et al.*, 2001). In view of these weaknesses the HPLC analysis offers an alternative method of quantification of condensed tannin. A rapid reversed-phase HPLC method was achieved in this study for the quantification of condensed tannins as opposed to the laborious vanillin assay.

Two samplings of mangrove barks were collected a year apart. For the first mangrove bark sampling, the ascending % (wt) of flavanoid monomers was found to be in the following order : epigallocatechin < epicatechin gallate < epicatechin < catechin and for the second sampling the % (wt) ascended in the order of catechin < epicatechin gallate < epicatechin < epigallocatechin. Despite having the same flavanoid constituents for both samplings these results demonstrated that the percentage composition of the individual flavanoid monomer varied with time. Supporting these results are the works of Pelilo *et al.* (2002). The variations in green tea catechin isomer contents were found to be dependent on the species, climate and conditions and technology used for the extraction and storage.

No correlation existed between the HPLC analysis and vanillin assay. The condensed tannins determined by vanillin assay were much higher than that was determined by HPLC. This could be explained by the fact that vanillin reacts with all units of the polymer, whereas only the flavanoid monomers constituting the terminal units were quantified through HPLC analysis. Similar observations have been demonstrated by Matthew *et al.* (1997) of low condensed tannins content and later supported by Ferreira *et al.* (2000) in a

study of the vanillin-condensed tannin reaction using flow injection spectrophotometry in comparison with the vanillin assay.

4.3 Anti-oxidant properties of mangrove tannins

According to Rice-Evans *et al.*, (1996), the chemical properties in terms of the availability of the phenolic hydrogens as hydrogen-donating radical scavengers predict their antioxidant activity. For a polyphenol to be defined as an antioxidant it must satisfy two basic conditions: first, when present in low concentration relative to the substrate to be oxidised it can delay or prevent the auto/self-oxidation or free radical-mediated oxidation; second, the resulting radical formed after scavenging must be stable through intramolecular hydrogen bonding on further oxidation. In view of these remarks, mangrove tannins are without doubt antioxidant species when it was found to show a considerable reducing power and DPPH as well as ABTS free radical scavenging abilities.

The reducing power of mangrove tannins was comparable to that of (+)-catechin standard. This is indeed not surprising since it has been confirmed from the HPLC analysis that catechin was present as one of the main components of mangrove tannins. The reducing power was also comparable with all other commercial tannins investigated especially at lower concentrations ($2.0x\ 0^{-2}$ mg mL^{-1} and $4.0x10^{-2}$ mg mL^{-1}).

The scavenging ability of tannins was essentially the same according to the DPPH and ABTS assays. Maximum scavenging abilities of tannins were recorded at 3.0x 10^{-2} mg mL^{-1} and 5.0x10^{-2} mg mL^{-1} for DPPH and ABTS assay respectively. Further increments in tannin concentrations did not improve the scavenging abilities. It is noteworthy that in the DPPH assay, mangrove tannin was shown to be more potent towards hydrogen donating than the BHT standard.

According to Noferi *et al.* (1997) the antioxidant capabilities of tannins are dependent on (1) the extent of its colloidal state, (2) the ease of interflavonoid bond cleavage or its stereochemical structure, (3) the ease of pyran ring (C ring) opening and (4) the relative numbers of –OH groups on A and B rings. The combination of these four factors will determine the behaviour of as an antioxidant under each set of particular application conditions. The view that the compounds with the trihydroxyl structure in the B ring exerted the greatest antioxidant activity are also shared by Salah *et al.* (1995) and Rice-Evans *et al.*, (1996).

4.4 Electrochemical tests

4.4.1 Inhibition studies of mangrove tannins on clean steel

The electrochemical studies have shown that the inhibitive efficiency of mangrove tannin on mild steel increased with increasing concentrations at pH 0.5. From the potentiodynamic curves (Fig. 3.21), it is clearly seen that the I_{corr} decreases as the concentration increases indicating that with the increase in concentration of tannin, more tannin molecules are being adsorbed on to the surface of the metal, enhancing more uniform surface coverage, which decreases the cathodic reaction rate of H^+ to H_2. This subsequently categorises the mangrove tannins as cathodic inhibitors.

Similar inhibition behaviour of tannins was observed at all pH. While at pH 0 and 0.5 all tannin have almost the same efficiency, the efficiency decreases in the order of mimosa tannin > mangrove tannin > quebracho tannin > chestnut tannin at pH 2.0. The inhibitive property of tannins at pH 0 and 0.5 could be due to the chemisorption of the tannin molecules onto the surface which was revealed by our surface observation and reported by Martinez and Stern (2001, 2002).

At higher pH, the cathodic action of tannins decreases, but they are able to complex with Fe^{2+} ions to form ferrous-tannates which can be easily oxidised into ferric-tannates, a blue-black deposit when in contact with oxygen. Thus tannins inhibit the oxidation of Fe^{2+} ions into ferric oxides/oxyhydroxides (Fe_3O_4, FeOOH) and the formation of red rust is avoided.

According to the TGA and XRD analyses, a bis-complex of ferric-tannate (Fig. 4.3) was formed from the reaction between ferric salts and mangrove tannins. Ferric-tannates were found to be present at pH 6.0 and pH 8.0, but other soluble complexes could have been formed which subsequently promotes the corrosion process based on the results of the UV-visible, FTIR, TGA/DTG and XRD experiments of synthesised ferric-tannates. Thus it was not surprising that no inhibition of steel corrosion was observed at pH 8.0 according to the electrochemical experiments on mangrove tannins.

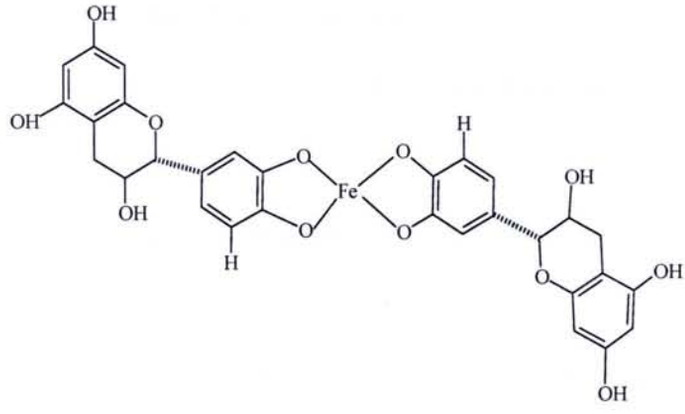

Fig. 4.3 Suggested structure for the ferric-tannate formed from mangrove tannins with catechin representing the monomer unit.

4.4.2 Inhibitory performance of catechin, epicatechin, epigallocatechin and epicatechin gallate

The electrochemical studies have shown that all flavanoid monomers investigated have an interesting behaviour of cathodic inhibiton in very acidic media. Comparison of the inhibition efficiency of the monomers at the same concentration, the inhibition efficiencies decrease in the order of epicatechin

gallate> catechin > epigallocatechin > epicatechin at $2.5x10^{-3}$ M, epicatechin > epigallocatechin > epicatechin gallate > catechin at $5.0x10^{-3}$ M and catechin > epicatechin gallate > epicatechin at $1.0x10^{-2}$ M. Thus, the dependency of inhibitory performance of the monomers on concentration is clearly evident.

The electrochemical experiments have shown that the inhibitive efficiency of mangrove tannins was largely contributed by the condensed tannins. Nevertheless it could be noted that when the flavanoid monomers were used individually a maximum of ~70 % inhibition was achieved. Hence a combination of these monomers are required to enhance individual's capacity, producing a synergistic effect in attaining more than 80 % inhibition produced by condensed tannins and entire mangrove tannins.

4.4.2.1 Molecular modelling of flavanoid monomers

At pH 0.5, the inhibitive property of flavanoid monomers is due to the chemisorption of the flavanoid molecules onto the surface. From the molecular modelling, it was found that adsorption of flavanoid molecules could take place on either A or B aromatic ring depending on the orientation of the flavanoid monomer and the number of phenolic groups attached to the molecule. Adsorption could therefore proceed via sharing of the donor group (-OH) electrons or aromatic π-electrons, between the flavanoid molecule and the partially filled d-orbitals of iron. According to Pearson's hard and soft acid and base (HSAB) principle, hard acids prefer to bind to hard bases and soft acids prefer to bind to soft bases. When the HOMO-LUMO energy gap is small, this

results in electron transfer from donor base atom to acceptor atom in the acid molecule and the resulting compound is covalent in nature. Thus soft-soft interactions are frontier-controlled (Sastri, 1998c). All the flavanoid molecules investigated gave rise to HOMO-LUMO energy gap of 8.92-9.12 eV, signifying soft acid-soft base interaction between iron metal and flavanoid molecule. This leads to the fact that since bulk metals are soft acids, flavanoid molecules as soft base inhibitors are most effective for metals corroding in acidic medium (Martinez, 2002). This is indeed consistent with the results obtained via the electrochemical studies which indicated various degree of inhibition by the flavanoid monomers in acidic solution. Although the molecular modelling shows two different sites of adsorption, these two sites have equal absorption efficiency according to the electrochemical measurements and the calculated fraction of electrons transferred from the flavanoid molecule to the iron atom, ΔN.

It was also noteworthy that the stereochemical position of the OH group at C-3 of the C ring was found to influence the total energy. For example, the heat of formation, binding energy and consequently the total energy of afzelchin (2R, 3S) were found to be larger than epiafzelchin (2R, 3R). Like wise, the total energy for catechin (2R, 3S) and gallocatechin (2S, 3S) were larger than epicatechin (2R, 3R) and gallocatechin (2R, 3R) respectively. The lower energy of the (2R, 3R) isomers implied a higher percentage occurrence and indeed our HPLC analysis have shown that mangrove tannins constituted of predominantly (2R, 3R) isomers namely epicatechin, epigallocatechin and epicatechin gallate and one (2R, 3S) isomer namely catechin.

The observed increase of the dipole moment with the increase in the number of –OH groups on the B ring is in accordance with the assumption that oxygen lone-pair electrons are major contributors to the overall dipole moment of the molecule of structure (a). However this assumption does not apply for structure (b). Thus the overall orientation of the flavanoid monomer as well as the number of phenolic groups attached to the molecule could be responsible for the overall dipole moment.

As observed for catechin, epicatechin and epicatechin gallate, the decrease of the inhibition efficiency with the increase of monomers concentration can be explained by the formation of soluble oligomers, causing a secondary desorption from the substrate (Ozcan *et al.*, 2004).

4.4.3 Cyclic voltammetry

From the redox potential measurements, it was revealed that the shape of the redox potential curves is greatly dependent on the scan rates and concentrations of catechin. Better redox signals were given by $1x10^{-3}$ M catechin. Catechin and epicatechin gave essentially the same redox potential patterns despite being different stereochemically. The actual redox reaction could not be ascertained but as an antioxidant, Kondo *et al.*, (1999) proposed the oxidation of catechin using 2, 2'Azobis (2-aminopropane) hydrochloride (AAPH) radical to be either a two electron reaction or a two step two electron reaction as shown in Fig. 4.4.

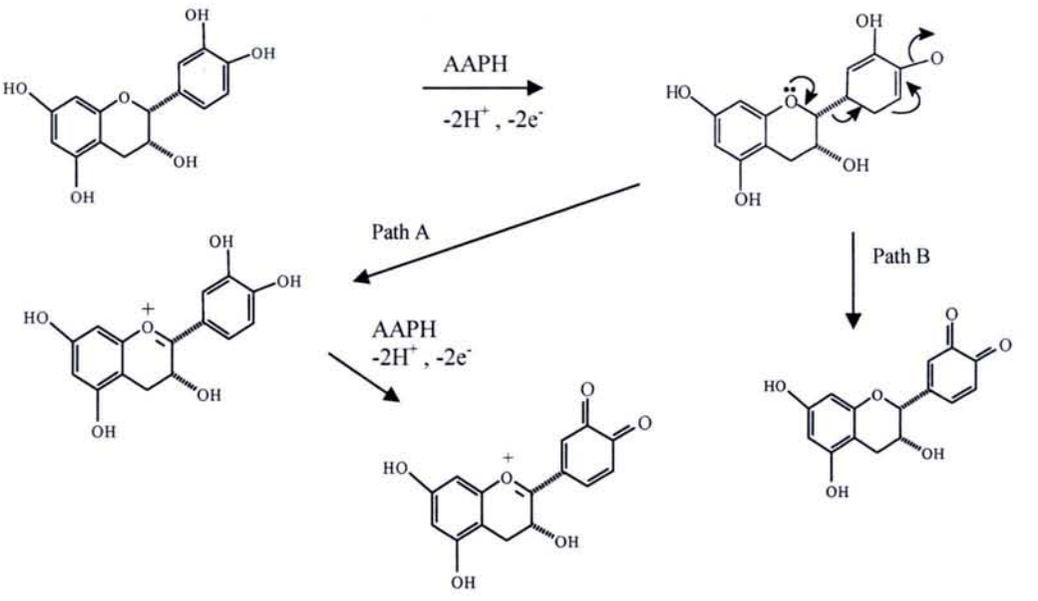

Fig. 4.4 Proposed mechanism of catechin in AAPH radical oxidation.

The shifts in redox peaks with respect to scan rates could be associated to the rate constant of the redox process. The kinetics of the reaction is 'slow' and thus the equilibrium is not rapidly established as a consequence of the current taking more time to respond to the applied voltage than the reversible reactions. The irreversibility behaviour of the flavanoid monomer and tannins were noted from the irregularities in the number of redox peaks at different scan rates. This behaviour can be explained by the fact that if some chemical reaction occurs, the return peak will be reduced and the return peak will be absent if the reaction half-life is much less than the scan duration (Evans *et al.*, 1983).

Comparison of the various tannins, the shapes of the redox curves again depended on the scan rates. Generally, all tannins gave similar curves to catechin and epicatechin regardless of whether they are hydrolysable or

condensed tannins. This similarity in behaviour thus explains the similarity in inhibitive behaviour of tannins and flavanoids as portrayed by the electrochemical experiments and the anti-oxidant capabilities of tannins previously discussed. The half wave potential, $E_{½}$ of the individual component investigated is tabulated in Table 4.1.

Table 4.1 Half wave potential, $E_{½}$ of catechin, epicatechin and tannins.

Type of solution	pH of solution	$E_{½}$ (half wave potential) (mV/SCE)
1.0 X 10^{-3} M catechin	5.80	355
1.0 X 10^{-3} M epicatechin	5.85	313
3.0 g L^{-1} mangrove tannin	3.60	375
3.0 g L^{-1} mimosa tannin	4.50	300
3.0 g L^{-1} quebracho tannin	3.90	200
3.0 g L^{-1} chestnut tannin	4.80	335

Based on the results obtained in Table 4.1, the Pourbaix diagram for iron (Sastri, 1998b) and the proposed oxidation mechanism of catechin in Fig. 4.3, the following inhibition mechanism of steel containing mangrove tannins is proposed for pH between 2.0 and 4.0 :

$$Fe \rightarrow Fe^{2+} + 2e^{-} \quad (4.1)$$

$$2H^{+} + 2e^{-} \rightarrow H_2 \quad (4.2)$$

$$Fe + 2H^{+} \rightarrow Fe^{2+} + H_2 \quad (4.3)$$

In the presence of oxygen,

$$Tannin_{red} \rightarrow Tannin_{ox} + 2e^{-} \quad (4.4)$$

The reduced and oxidised forms of tannins will then react with Fe^{2+} :

$$Tannin_{red} + Tannin_{ox} + Fe^{2+} \rightarrow (2Tannate_{ox/red}\text{-}Fe^{2+})_{soluble} \quad (4.5)$$

$$(Tannate_{ox/red}Fe^{2+})_{soluble} \xrightarrow{O_2} Fe^{3+}\text{-}Tannate_{ox/red}(\text{blue-black precipitate}) \quad (4.6)$$

4.4.4 Inhibitory performance of mangrove tannins, mimosa tannins and phosphoric acid on pre-rusted steel

From the electrochemical studies, inhibition efficiency of pre-rusted steel in 3.5 % NaCl solution containing 3 g L^{-1} tannins was found to be dependent on the concentration of phosphoric acid and pH of solution. At pH 0.5 and pH 2.0, inhibition was best achieved with mangrove and mimosa tannins alone. Enhancement of inhibition efficiency was negligible with the addition of 15 % phosphoric acid at pH 0.5 and pH 2.0. But reduction in efficiency appeared with 30 % and 50 % phosphoric acid additions. On the other hand, inhibition efficiency was enhanced with the addition of phosphoric acid at pH 5.5. Increasing in efficiency was in the order of 15 % < 50 % < 30 % phosphoric acid additions. An efficiency of 39 % was achieved with mangrove tannins alone as compared to 0 % shown by mimosa tannins implied the potential of mangrove tannins as corrosion inhibitor on pre-rusted steel over a wider pH range as compared to mimosa tannin.

In NaCl solution, ferrous chloride and sodium hydroxide are initially deposited at the anode and cathode respectively. The ferrous chloride formed is often transformed into ferrous hydroxide, which in turn combines with oxygen to form rust according to the following reactions (Shreir, 1978a) :

$$FeCl_2 + 2NaOH \rightarrow Fe(OH)_2 + 2NaCl \quad (4.7)$$

$$4Fe(OH)_2 + O_2 \rightarrow 4FeOOH + 2H_2O \quad (4.8)$$

While at pH 0.5 the inhibition mechanism is associated with chemisorption of tannin molecules onto the pre-rusted surface as shown from the molecular

modelling, at pH 2.0 and pH 5.5, the inhibition was achieved through the formation of ferric-tannates. Indeed, our results also show the ability of tannins to reduce Fe^{3+} ions into Fe^{2+} ions from the antioxidant experiments (section 3.3). Schematically, it is proposed:

$$n\ Fe^{3+} + ne^- \rightarrow nFe^{2+} \quad (4.9)$$

$$\text{tannins} \rightarrow \text{tannate} + ne^- + nH^+ \quad (4.10)$$

$$n\ Fe^{3+} + \text{tannins} \rightarrow (Fe^{2+})_n\ \text{tannate} + nH^+ \quad (4.11)$$

and

$$\text{Tannin}_{red} + \text{Tannin}_{ox} + Fe^{2+} \rightarrow (2\text{Tannate}_{ox/red}\text{-}Fe^{2+})_{soluble} \quad (4.5)$$

Consequently,

$$(Fe^{2+})_n\ \text{tannate} \rightarrow (Fe^{3+})_n\ \text{tannate} + ne^- + nH^+ \quad (4.12)$$

$$(\tfrac{1}{2}O_2 + 2H^+ + 2e^- \rightarrow H_2O) \times n/2 \quad (4.13)$$

$$(Fe^{2+})_n\ \text{tannate} + \tfrac{1}{4}\,n\,O_2 \rightarrow (Fe^{3+})_n\ \text{tannate} + \tfrac{1}{2}n\,H_2O \quad (4.14)$$

The reducing power of tannins allows the inhibition of Fe^{3+}- oxyhydroxides formation and the Fe^{3+}- oxyhydroxides are instead transformed into Fe^{3+}-tannates. Although several authors claim a protective effect of this deposit (Ross and Francis, 1978; Deslauriers, 1987; Ivanov and Kuznetsov, 1990,1991; Gust, 1991; Matamala *et al.*, 1994; Pardini *et al.*, 2001), our results indicated a low protective behaviour. However it has been shown (section 3.4.1.2) that at pH higher than 4.0, other soluble complexes may have formed, promoting corrosion and thus a low corrosion inhibition was achieved at pH 5.5.

The use of phosphoric acid alone was also dependent on the concentration of phosphoric acid and pH of solution. While the efficiency increased with increasing pH for 15 % phosphoric acid, inhibition was evident only at pH 5.5 for 30 % and 50 % phosphoric acid. Using 30 % phosphoric acid alone is certainly favoured at pH 5.5 when 90 % inhibition was achieved. According to Almeida *et al.* (1997), point of initiation of insoluble phosphates when the metal is iron occurs at pH 5-6. Thus in this study, phosphate formation was maximum with 30 % phosphoric acid as observed from the very thick deposit after the polarisation process. A passivation plateau which was induced by the reaction between phosphoric acid and rust forming phosphates subsequently retards the anodic dissolution reaction. Further increment to 50 % phosphoric acid may have resulted in formation of soluble complexes, leading to the reduction in inhibition efficiency. The joint effect of both tannins and phosphoric acid was unfavourable at this pH arising from the competing reactions between tannins and phosphoric acid on steel.

4.5 Phase transformation studies

Initial studies have shown that the rust composition on steel was found to be dependent on sample preparation. Samples prepared in total immersion in 3.5 % NaCl solution for 35 days (sample A) produced lepidocrocite and magnetite as its main components shown from surface observations, XRD patterns and FTIR analysis. Samples which were alternatively immersed in 3.5 % NaCl solution followed by drying (sample B) and samples prepared via salt spray (sample C) both exhibited the presence of lepidocrocite, magnetite and goethite

from surface observations, XRD patterns and FTIR analysis. These rust components have been described as the major constituents of rust systems on steel surfaces under normal ambient conditions (Gust, 1991; Almeida *et al.*, 1997; Nasrazani, 1997; Favre *et al.* 1998).

4.5.1 Phase transformation of rust by tannins

Transformation of rust when treated with mangrove tannins which was confirmed by XRD, FTIR and SEM experiments are summarised in Table 4.2. Transformations of rust into ferric-tannates were observed regardless of sample preparation.

Table 4.2 Transformation of rust components treated with mangrove tannins on samples A, B and C.

Surface reference	Components present	
	Before tannin immersion	After tannin immersion
Sample A	γ-FeOOH, Fe_3O_4 NaCl	Fe-tannate, γ-FeOOH, Fe_3O_4
Sample B	γ-FeOOH, Fe_3O_4, α-FeOOH	Fe-tannate, γ-FeOOH, Fe_3O_4, α-FeOOH
Sample C	γ-FeOOH, Fe_3O_4, α-FeOOH	Fe-tannate, γ-FeOOH, Fe_3O_4, α-FeOOH

Ross and Francis (1978) have claimed that tannins have the ability to transform lepidocrocite to magnetite. In this study, X-ray diffraction patterns of sample A (Fig. 3.50) showed the reduction of lepidocrocite peaks and a slight increment in the intensity of magnetite peaks. Therefore the initial assumption was that lepidocrocite could have transformed into magnetite. The results could also suggest that the corrosion products are accommodated in at least two layers :

one relatively compact inner layer close to the steel surface, dominated by magnetite and a second less compact outer layer dominated by lepidocrocite as shown in Fig. 4.5.

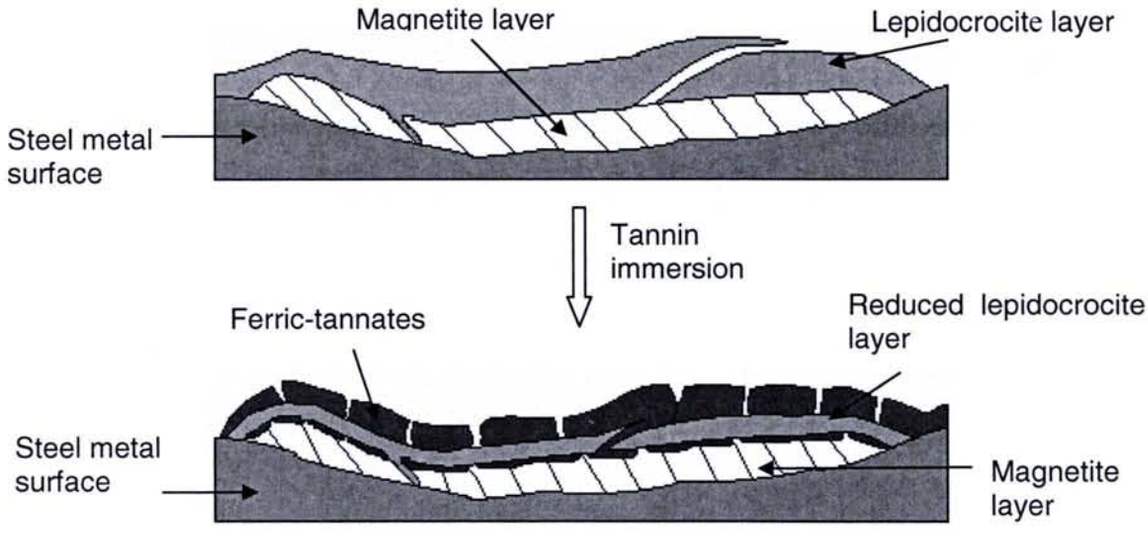

Fig. 4.5 Profile of the transformation of rust into ferric-tannates.

Upon treatment of tannins, penetration into the rust layers occurs and the tannins react with the iron phases to produce ferric-tannates. This reaction mainly takes place at the outer layer and to a lesser extent in the inner layer as shown from SEM analysis. Thus the magnetite layer is largely unaffected by the tannin addition. This is supported by the fact that a slower transformation of the magnetite component with the application of mangrove tannins was observed via FTIR spectroscopy.

Varying degree of rust transformation was observed from the FTIR analysis depending on the type of rust component employed. With the application of 0.5 % mangrove tannins, lepidocrocite and magnetite produced the highest degree of transformation after a day and a week of immersion respectively after which

re-rusting began to take effect. For maghemite, transformations were constant throughout the one month of immersion with the principal peaks remained unaffected. No effect was noted with goethite treated samples. This observation implied a slower transformation of maghemite and goethite as compared to lepidocrocite and magnetite. Similar rates of transformation have been reported by Gust (1991) and Naszarani (1997). The unchanged peaks of the individual rust component could be attributed to incomplete transformation of rust arising from re-rusting process occurring in parallel with the transformation to ferric-tannates. The XRD patterns of all rust components was not affected by the addition of 0.5 % mangrove tannins which is probably due to inappropriate tannin to rust component ratio.

The degree of rust transformation was enhanced with the addition of 2.0 % mangrove tannins as observed from the FTIR analysis and SEM micrographs. And again the FTIR analysis demonstrated that the transformation rate was in the following order :

lepidocrocite > magnetite > maghemite > goethite.

The morphology of converted rust was found to be dependent on the type of rust component and time of immersion as shown from the SEM micrographs. Generally, a more complete transformation was observed after 28 days of immersion. An increment in tannin percentage from 0.5 % to 2.0 % was not able to exert any effect on the XRD patterns of individual rust components except

lepidocrocite. This in turn further demonstrated the easier transformation of lepidocrocite as compared to the other rust components investigated.

It should be noted that the presence of tannins gave no other oxide or oxyhydroxides as reaction products. Thus it may be inferred that amorphous ferric-tannates were deposited. And indeed the deposition of ferric-tannates was confirmed by FTIR and EDS analyses as well as SEM micrographs. Similar observations have been demonstrated by Gust (1991) and Nasrazadani (1997) via FTIR spectroscopy and Jaen *et al.* (1999) and Barrero *et al.* (2001) via Mossbauer spectroscopy.

The absence of a chloride peak after the addition of mangrove tannins was observed from XRD and EDS analysis. The use of tannin thus poses as an advantage since chloride ions are known to be promoting atmospheric corrosion according to equations (4.7) and (4.8). This study indicated that instead of forming ferrous chloride, the ferrous ions reacted with tannins to form ferric-tannates according to equations (4.12) to (4.14).

4.5.2 Phase transformation of rust by phosphoric acid and a mixture mangrove tannins and phosphoric acid

The transformation of rust in the presence of phosphoric acid and a mixture of mangrove tannins and phosphoric acid are summarised in Table 4.3. Upon treatment of 15 % and 30 % phosphoric acid, the pre-rusted surfaces of samples A and C were found to be dominated by white-bluish vivianite, $Fe_3(PO_4)_2.8H_2O$ as confirmed by XRD and EDS analyses and reported by

Almeida *et al.* (1997). Nevertheless it was quite difficult to distinguish the extent of transformation between the addition of 15 % and 30 % phosphoric acid from the XRD patterns. Ferric phosphates are amorphous in nature (Nasrazadani, 1997) and thus could not be detected via XRD.

Table 4.3 Transformation of rust after immersion in phosphoric acid and a mixture of mangrove tannins and phosphoric acid on samples A and C.

Sample reference	Components present		
	Before tannin + phosphoric acid immersion	After phosphoric acid immersion	After tannin + phosphoric acid immersion
Sample A	γ-FeOOH, Fe_3O_4 NaCl	$FePO_4$, $Fe_3(PO_4)_2.8H_2O$ γ-FeOOH, Fe_3O_4	Fe-tannate, $FePO_4$, $Fe_3(PO_4)_2.8H_2O$ γ-FeOOH, Fe_3O_4
Sample C	γ-FeOOH, Fe_3O_4, α-FeOOH	$FePO_4$, $Fe_3(PO_4)_2.8H_2O$ γ-FeOOH, Fe_3O_4	Fe-tannate, $FePO_4$, $Fe_3(PO_4)_2.8H_2O$ γ-FeOOH, Fe_3O_4

The transformation of rust components with immersion time in the presence of 15 % phosphoric acid as viewed by FTIR spectroscopy showed that phosphate peak was present with lepidocrocite, magnetite and maghemite treated powders. However a slower transformation was displayed by maghemite and magnetite. Conversely, no reaction occurred between phosphoric acid and geothite. The transformation kinetics was slower to that of mangrove tannins.

The following phosphate precipitation reaction is thus proposed :

$$H_3PO_4 + FeOOH \rightarrow FePO_4 + 2H_2O \quad (4.15)$$

and

$$2H_3PO_4 + 3Fe_3O_4 + 5H_2O \rightarrow Fe_3(PO_4)_2.8H_2O + 3Fe_2O_3 \quad (4.16)$$

$$3Fe_2O_3 + 3H_2O \rightarrow 6FeOOH \quad (4.17)$$

$$2H_3PO_4 + 3Fe_3O_4 + 8H_2O \rightarrow Fe_3(PO_4)_2.8H_2O \text{ (vivianite)} + 6FeOOH \quad (4.18)$$

With the addition of 0.5 % mangrove tannins and 15 % and 30 % phosphoric acid, phosphates in the form of vivianite was again evident from the XRD experiments. Similarly the extent of transformation between the addition of 15 % and 30 % phosphoric acid to mangrove tannins could not be ascertained from the XRD experiments. The formation of ferric-tannates and phosphates was confirmed from the FTIR and EDS analyses as well as SEM micrographs.

The EDS analysis displayed a greater deposition with the application of mangrove tannins and phosphoric acid as compared to phosphoric alone for both sample preparations. This behaviour was similarly shown by mimosa tannin for sample C despite the difference in the morphology of mimosa tannins covered with phosphates to that of mangrove tannins. The advantage of mangrove tannins was also indicated by the presence of a chloride compound in the transformed mimosa deposit.

Gust (1991) reported that the reaction kinetics of tannins was slower to that of phosphoric acid while Nasrazadani (1997), Almeida *et al.* (1997) and Barrero *et al.* (2001) agreed that the rust transformation by phosphoric acid depended on the surface condition, solution concentrations and exposure time. In this study, the addition of 0.5 % mangrove tannin to 15 % phosphoric acid relatively improved the rate of rust transformation as compared to 15% phosphoric acid alone. Transformation of lepidocrocite treated samples was most rapid when both phosphate and tannate peaks were present after one day immersion. A competing reaction between mangrove tannins and phosphoric acid was

demonstrated by magnetite. The phosphates were initially formed after one day to two weeks immersion followed by tannates and phosphates after a month immersion. Transformation of maghemite to phosphates and tannates were evident after one day immersion, after which the rate of transformation increased gradually with time. The conversion was slowest with geothite, indicated by the appearance of both phosphates and tannates after a week of immersion which nonetheless intensified with time.

These observations could possibly suggest that the phosphoric acid initially dissolve the rust (Gust, 1991) and this is followed by the reducing ability of tannins to additionally reduce Fe^{3+} to Fe^{2+}, facilitating the precipitation of phosphates which would otherwise not formed with phosphoric acid alone, if for example when added to goethite. It could therefore be deduced that although 0.5 % mangrove may not be the optimum concentration to be used in conjunction with 15 % phosphoric acid, it was sufficient to exert an effect on the degree of transformation of rust. The observations also suggest that the more rapid transformation observed led to a better deposition as observed from the EDS analysis. In summary the transformation rate was in the following order :

lepidocrocite > magnetite > maghemite > goethite.

4.5.3 Evaluation of protective efficiency by tannins and phosphoric acid

In the previous study, the rate of rust transformation and deposition of tannates and phosphates was correlated. It was then necessary to evaluate the protective capacity of these deposits against corrosion and this was accomplished by the humidity chamber and salt spray tests. It was found that re-rusting of treated samples was the slowest with the application of mangrove tannins and the fastest with the application of phosphoric acid when exposed to the humidity chamber. This leads to the conclusion that corrosion protection was best provided by mangrove tannins with the present solution compositions employed. According to Almeida *et al.* (1997) maximum insoluble phosphates precipitation will occur at pH 5-6. Thus at pH 4.0, maximum precipitation of phosphates was not attained. This was also supported by the fact that phosphoric acid exhibited the slowest transformation kinetics from the FTIR experiments.

According to the humidity chamber tests, the application of mangrove tannins and phosphoric acid resulted in the formation of rust amidst black deposits after 35 days of exposure. This observation could infer that the region occupied by the less adhered phosphates was replaced by newly formed rust, leaving the tannates intact. Since it has been shown that phosphoric acid has comparatively low protection efficiency, the application of phosphoric acid to mangrove tannins resulted in reduced corrosion protection as compared to the application of mangrove tannins alone. Although the EDS analysis (Table 3.16)

portrayed a greater deposition with the addition of both mangrove tannins and phosphoric acid, this study indicated that the protective efficiency is dependent on the adherence of phosphates and tannates deposited. In comparison, no difference could be noted between the protective efficiency of mimosa tannins alone and the addition of phosphoric acid to mimosa tannins. This could be explained from the fact that the original blue-black treated sample was covered with more tannates than phosphates and hence exhibited more or less equal protective efficiency to mimosa tannins alone.

For samples exposed to the salt spray chamber, all treated samples exhibited some degree of resistance to corrosion as compared to the standard sample (Fig. 3.82) for the same exposure time. The slowest rust conversion was again shown by mangrove tannins and the fastest by phosphoric acid alone. A lower corrosion protection was also shown by the addition of both mangrove tannins and phosphoric acid as compared to the addition of mangrove tannins alone. On the other hand, the protective efficiency was slightly improved when both mimosa tannins and phosphoric acid were added. A synergistic effect between the tannates and phosphates must have occurred which resulted in better adherence and consequently an enhancement in protective efficiency. It has been shown that solution composition and exposure conditions are contributing factors to the contradictory reported results by Gust and Bobrowicz (1993), Matamala *et al.* (1994), Barrero *et al.* (2001) and Pardini *et al.* (2001) pertaining to the protective capacity of tannins and phosphoric acid.

Temporary corrosion protection was shown by all treated samples regardless of the type of evaluation employed. The outer layer, predominantly lepidocrocite was easily transformed and the inner more impermeable layer remained unchanged as shown from the XRD experiments and SEM micrographs. The initial transformation of lepidocrocite increased the outer layer impermeability, adding a new barrier, hence protection against corrosion. However, the varying degree of rust transformation by tannins and phosphoric acid as shown from the FTIR analysis led to the various degrees of tannates and phosphates deposited. In addition, the lack of adhesion of tannates and phosphates as shown from SEM micrographs inferred a physical absorption of deposits of which is in agreement with the report by Martinez and Stern (2001). On top of that, the cracked morphology of deposits provided easy penetration of moisture into the cracks leading to the formation of new rust. All of these factors contributed to the observed protective efficiency.

CHAPTER FIVE

CONCLUSION

Tannins from mangrove barks have been successfully extracted with 70 % aqueous acetone, yielding 27-29 % (wt) dark brown powder. Purification by LH-20 column chromatography afforded condensed tannins of high purity as confirmed from FTIR spectroscopy, TGA/DTG analysis and reversed-phase HPLC.

The elution of flavanoid standards using reversed-phase HPLC was found to be influenced by the substitution pattern of the B ring and the stereochemistry of the components. The ascending elution order was as follows:
(-)-gallocatechin < (+)-catechin/(-)-catechin < (-)-epigallocatechin < (-)-epigallocatechin gallate < (-)-epicatechin < (-)-gallocatechin gallate < (-)-epicatechin gallate < (-)-catechin gallate.

The HPLC analysis of condensed tannins following depolymerisation in phloroglucinol and acidic ethanol revealed mainly four terminal units and one extender unit. In this study, the terminal units namely catechin, epicatechin, epigallocatechin and epicatechin gallate were identified for both mangrove samplings. Attempts to identify the extender unit proved unsuccessful. A rapid reversed-phase HPLC method was achieved in this study for the quantification of condensed tannins as opposed to the laborious vanillin assay. Substantial reducing power, DPPH as well as ABTS free radical scavenging abilities have

been shown by mangrove tannins of which were comparable to the synthetic standards used.

The electrochemical studies have shown that the inhibitive efficiency of mangrove tannin on mild steel increased with increasing concentrations at very low pH. The electrochemical experiments have also shown that the inhibitive efficiency of mangrove tannins was largely contributed by the condensed tannins. All tannins investigated are cathodic inhibitors in acidic media and the inhibition efficiency of all tannins was found to decrease with increasing pH. The inhibitive performance of mangrove tannin was comparable with that of commercial mimosa, quebracho and chestnut tannins at pH 0, 0.5 and 2.0 and exhibited superiority over the rest of the tannins at pH 4.0. At pH 0 and 0.5 the adsorption mechanism was attributed to chemisorption of tannin molecules onto the iron surface and the adsorptive behaviour of the molecules on the steel surface was explained by a semi empirical approach involving quantum chemical calculations of flavanoids. At higher pH, the formation of ferric-tannates resulted in a low protective effect. Tannins, being anti-oxidant species are able to reduce ferric ions into ferrous ions, which in turn react to form ferrous-tannates and in the presence of oxygen, the ferrous-tannates are readily converted into insoluble blue-black ferric-tannates. At pH higher than 4.0, other soluble complexes may form apart from ferric-tannates which promote corrosion.

The electrochemical studies have shown that the flavanoid monomers that constitute mangrove tannins are potential inhibitors for steel in acidic medium. All monomers act mainly as cathodic inhibitors of the steel corrosion and its inhibitive performance dependent on concentration in acidic conditions. The inhibition efficiencies decrease in the order of epicatechin gallate> catechin > epigallocatechin > epicatechin at $2.5x10^{-3}$ M, epicatechin > epigallocatechin > epicatechin gallate > catechin at $5.0x10^{-3}$ M and catechin > epicatechin gallate > epicatechin at $1.0x10^{-2}$ M for pH 0.5. The inhibitive performances of the monomers at this pH were comparable with that of 2-napthalene sulfonic acid, a cathodic inhibitor.

Molecular modelling studies have shown that adsorption of flavanoids occurs within the vicinity of the phenolic groups on either A or B aromatic ring of the flavanoid molecule. These two sites have equal absorption efficiency according to the calculated fraction of electrons transferred from the flavanoid molecule to the iron atom, ΔN. The stereochemical position of the OH group at C-3 of the C ring was found to influence the total energy of the flavanoid molecule with the 2R, 3R isomers having lower total energy than the 2R, 3S isomers. The study also shows that the monomers are effective inhibitors for corroding metals in acidic medium in accordance with the results of the electrochemical studies.

From the redox potential measurements, it was revealed that the shape of the redox potential curves is greatly dependent on the scan rates. Generally, all tannins gave similar curves to catechin and epicatechin. This similarity in behaviour thus explains the similarity in inhibitive behaviour of tannins and

flavanoids as portrayed by the electrochemical experiments and the anti-oxidant capabilities of tannins.

From the electrochemical studies, inhibition efficiency of pre-rusted steel in 3.5 % NaCl solution containing 3.0 g L^{-1} tannins was found to be dependent on the concentration of phosphoric acid added and pH of solution. At pH 0.5 and pH 2.0, inhibition was best achieved with mangrove and mimosa tannins alone while at pH 5.5 using phosphoric acid alone especially 30 % phosphoric acid was favoured. It was noteworthy that regardless of pH, higher inhibition efficiencies were always shown by mangrove tannins in comparison to mimosa tannins.

The role of mangrove tannins and phosphoric acid as rust converters was accomplished by phase transformation studies. Initial studies have shown that the rust composition on steel was found to be dependent on sample preparation as shown by XRD and FTIR spectroscopy. Mainly lepidocrocite, magnetite and goethite were formed. Partial transformations of rust into ferric-tannates and phosphates without other oxide or oxyhydroxides as reaction products were confirmed by XRD, FTIR and SEM experiments regardless of sample preparation. This partial transformation was explained by the varying degree of rust transformation observed from the FTIR analysis which was found to be dependent on the type of rust component employed. Generally the kinetics of rust transformation was the same for all the solution compositions. Transformation of lepidocrocite was always the fastest, consistent with the reduced lepidocrocite component of treated samples observed from the XRD

and FTIR experiments. This was followed by magnetite and maghemite and the slowest with goethite. Although the rate of rust transformation was enhanced with the addition of 2.0 % mangrove tannins the kinetics of rust transformation was the same as when treated with 0.5 % mangrove tannins. The rate of transformation was the least with phosphoric acid addition and was enhanced with the application of both 0.5 % mangrove tannins and 15 % phosphoric acid, leading to greater depositions as shown by EDS analysis.

Evaluation of protective efficiency of tannins and phosphoric acid via humidity chamber tests and salt spray chamber tests showed temporary corrosion protection regardless of the type of evaluation employed. Corrosion protection was best provided by mangrove tannins and the least by phosphoric acid. However the lack of adhesion of tannates as shown from SEM micrographs inferred a physical adsorption of deposits and the cracked morphology of deposits provided easy penetration of moisture into the cracks leading to the formation of new rust. This resulted in a low protective behaviour. Hence the correlation between ferric-tannate formation and the low inhibition efficiency observed at high pH from the electrochemical studies was established.

As regards to the use of phosphoric acid and the joint effect of tannins and phosphoric acid as rust converters, the pH of complexes deposited, the ratio of tannates and phosphates deposited and evaluation conditions are contributing factors to the contradictory results obtained via electrochemical studies and humidity chamber as well as salt spray chamber tests. Similar arguments have been put forward by Barrero *et al.* (2001) and Ocampo *et al.* (2004). To date no

universal agreement has been found and it is evident that further research on this complex matter is required.

CHAPTER SIX

FUTURE RESEARCH RECOMMENDATIONS

1. Isolation and characterisation of condensed tannins of mangrove barks is still at the preliminary stage. More refined separation techniques should be carried out in order to further confirm the constituents of mangrove tannins.

2. Flow injection techniques have been successfully applied to the determination of several organic components (Saad, 2001 and Rahman, 2005) including condensed tannins (Ferreira, 2000). This technique presented reproducibility, high sampling frequency providing speed and low costs. Thus the determination of condensed tannins of mangrove barks using this technique should be explored and determination conditions optimised so as the laborious preparations in the manual biological procedures could be avoided.

3. Molecular modelling studies have shown that adsorption of flavanoids occurs within the vicinity of the phenolic groups on either A or B aromatic ring of the flavanoid molecule. It has also been shown that the lowest energy conformation corresponded to the binding of Fe^{3+} to the B ring for catechin molecule (Musa, 2004). In order to have a better insight and understanding of the adsorption phenomena of flavanoids and the stability of the Fe-tannates formed, further studies could be expended to include the interaction of other flavanoids monomers as well as combination of monomers and Fe ions.

4. In view of the findings in this study it is suggested that continued studies on the joint effects of several formulations of mangrove tannins and phosphoric acid on the different corrosion degrees and on the nature of the rust to be converted (e.g. age of formation, exact composition, thickness) should lead to a universal novel corrosion inhibitor and rust converter.

APPENDIX 1

Title : Standard curve of gallic acid for the Prussian blue assay.

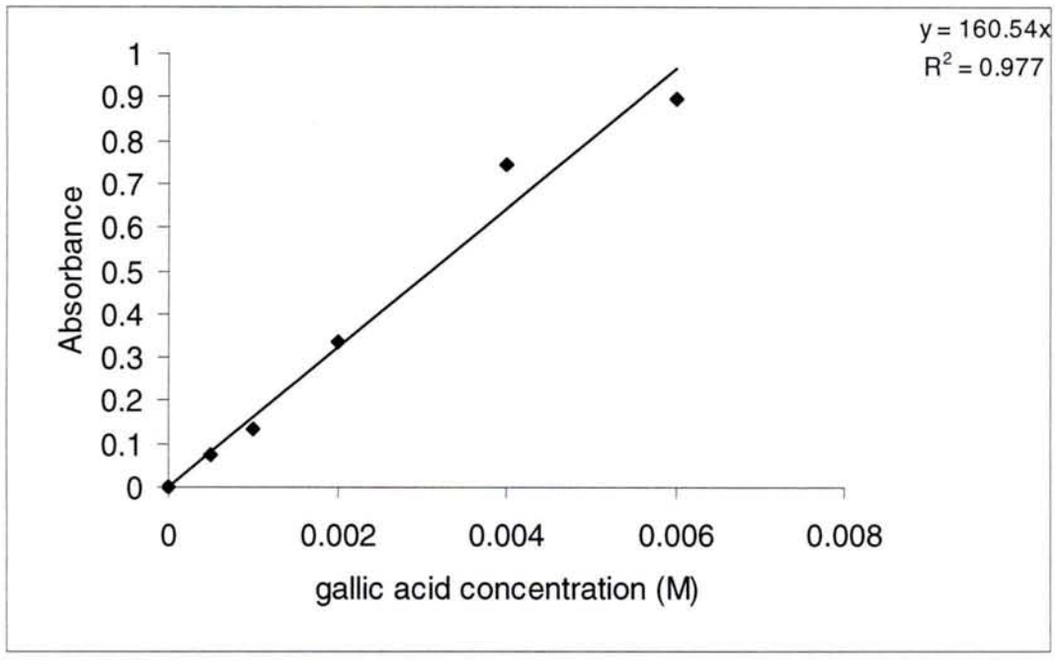

APPENDIX 2

Title : Standard curve of (+)-catechin for the vanillin assay.

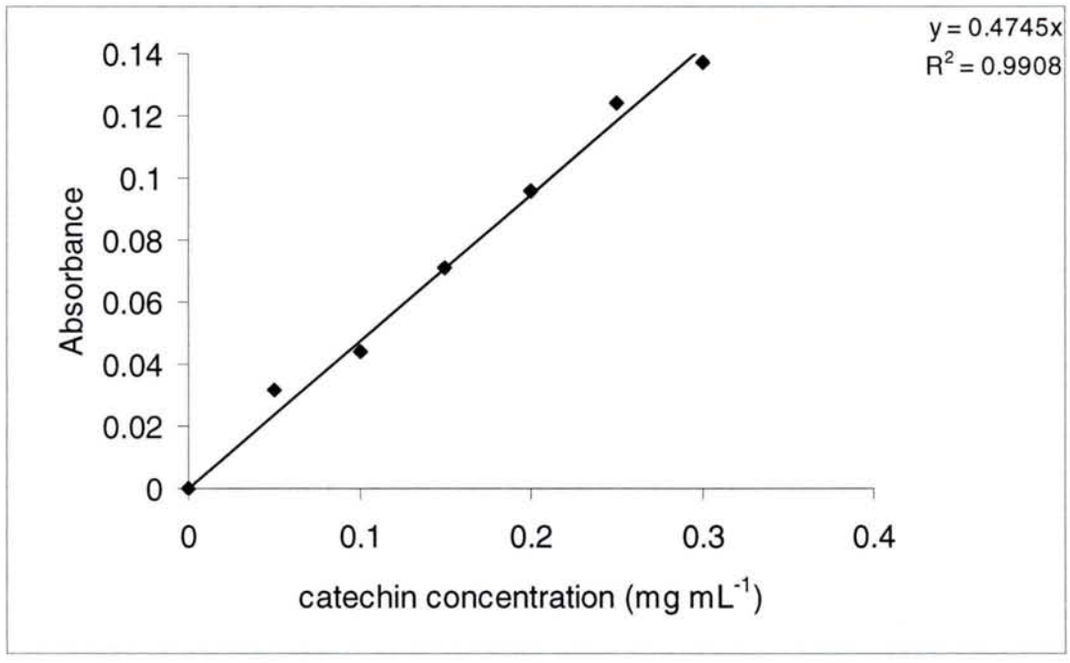

APPENDIX 3

Title : Standard curve of (+)-catechin for quantification of flavanoid monomers.

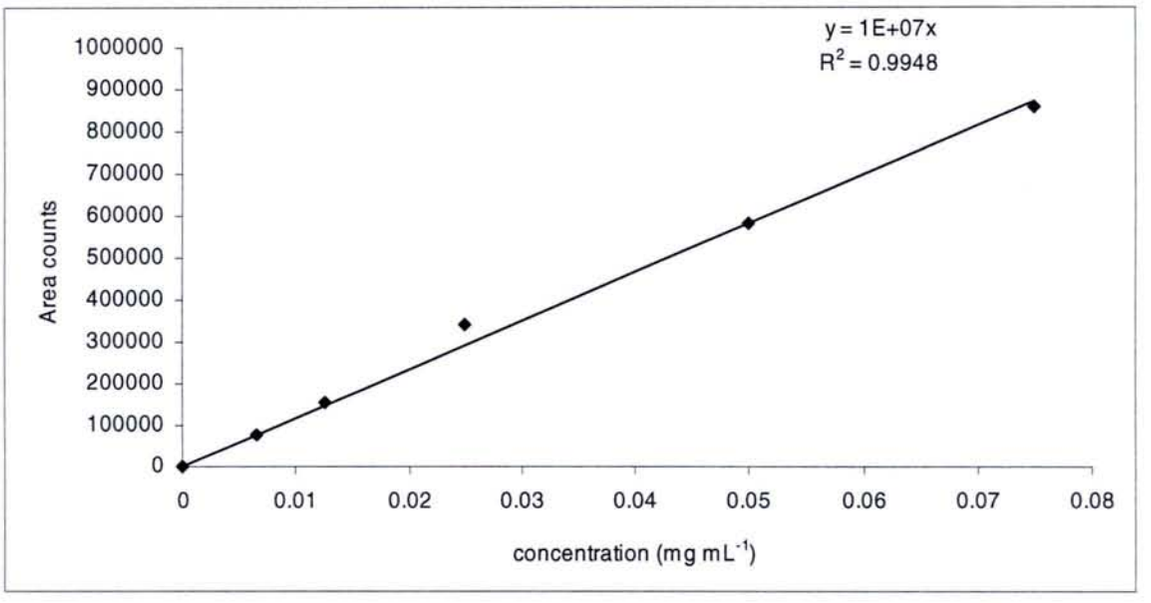

APPENDIX 4

Title : Standard curve of (-)-epicatechin for quantification of flavanoid monomers.

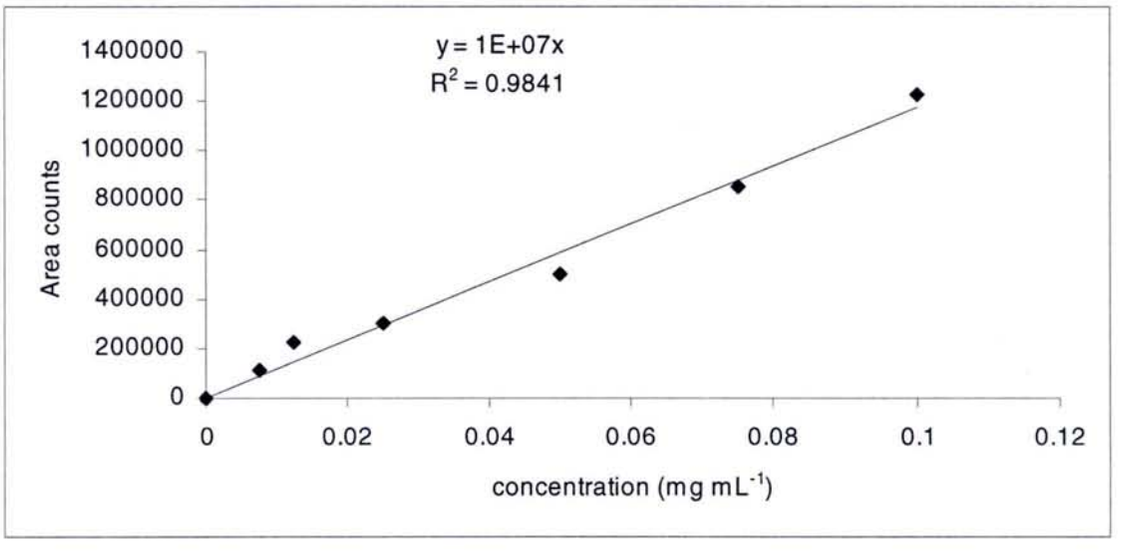

APPENDIX 5

Title : Standard curve of (-)-epigallocatechin for quantification of flavanoid monomers.

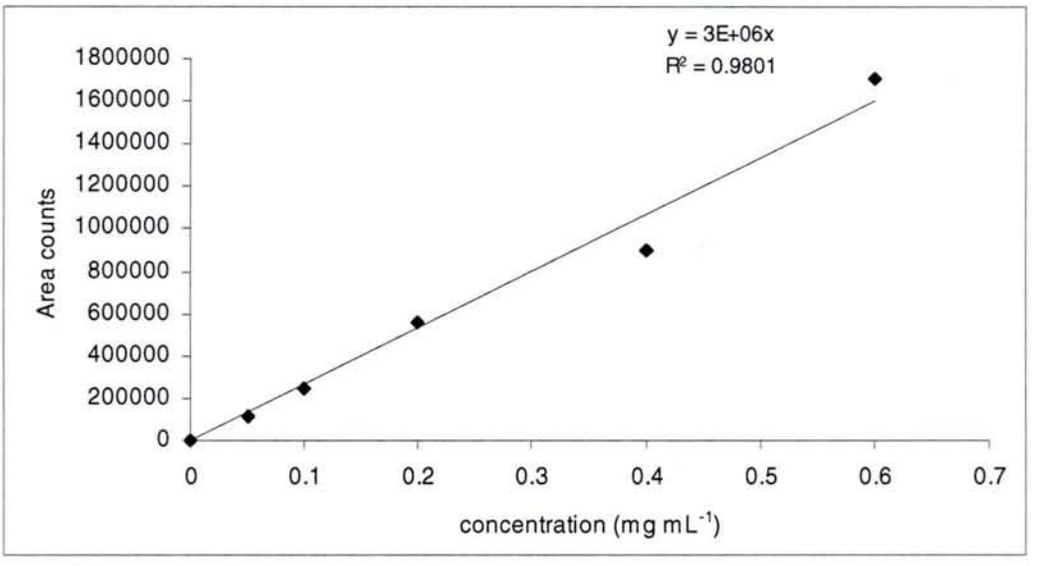

APPENDIX 6

Title : Standard curve of (-)-epicatechin gallate for quantification of flavanoid monomers.

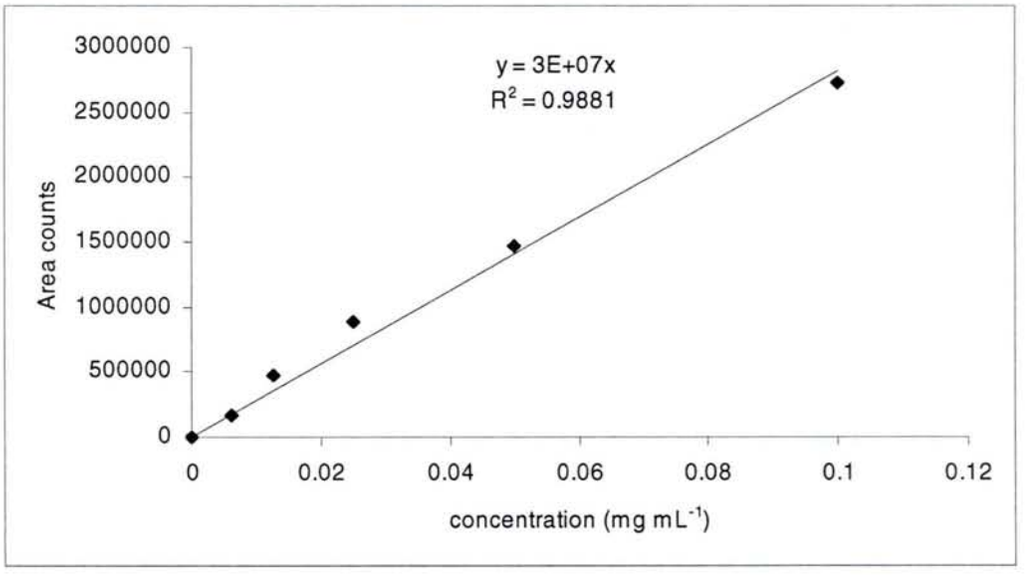

APPENDIX 7

Title : Stoichiometric determination of ferric tannate.

$$\frac{\text{mole Fe-tannate}}{\text{mole } Fe_2O_3\ H_2O} = \frac{2}{1}$$

REFERENCES

Abd El Rehim, S. S., Hassan, H. H. & Mohamed, N. F. (2004). Anodic behaviour of tin in maleic acid solution and the effect of some inorganic inhibitors. *Corrosion Science.* **46**, 1071-1082.

Abd El-Maksoud, S.A. (2002). Studies on the effect of pyranocoumarin derivatives on the corrosion of iron in 0.5 M HCl. *Corrosion Science*, **44**, 803-813.

Abdel Rehim, S. S., Hassan, H.H. & Amin, M. A. (2004). Chronoamperometric studies of pitting corrosion of Al and (Al-Si) alloys by halide ions in neutral sulphate solutions. *Corrosion Science.* **46**, 1921-1938.

Achmadi, S., Shahbirin, G., Choong, E.T. & Hemingway, R.W., (1994), Catechin-3-*O*-rhamnoside chain extender units in polymeric procyanidins from mangrove bark. *Phytochemistry,* **36**(1), 217-219.

Al-Mayouf, A.M. (1997). Corrosion of iron in aqueous solutions containing a chemical cleaning agent. *Desalination.* **114**, 29-36.

Almeida, E., Pereira, D, Figueiredo, M.O., Lobo, V.M.M. & Morcillo, M. (1997). The influence of the interfacial conditions on rust conversion by phosphoric acid. *Corrosion Science.* **39** (9), 1561-1570.

Alonso, A.M., Guillen, D.A. & Barroso, C.G. (2003). Development of an electrochemical method for the determination of antioxidant activity. Application to grape-derived products. *European Food Res. Technology.* **216**, 445-448.

Amin, M.A. (2005). Passivity and passivity breakdown of a zinc electrode in aerated neutral sodium nitrate solutions. *Electrochimica Acta.* **50**, 1265-1274.

ASTM B 117. (1973). *Salt spray resistance test.* Philadelphia : American Society for testing and materials.

Barrero, C. A., Ocampo, L.M. & Arroyave, C.E. (2001). Possible improvements in the action of some rust converters. *Corrosion Science.* **43**, 1003-1018.

Bates-Smith, E.C. and Swain, T., *Flavonoid compounds*, in Mason, H.S. and Florkin, A.M. (eds). Comparative Biochemistry, Vol. 3. New York : Academic Press (1962) p. 755-809.

Batis, G., Kouloumbi, N., & Kotsakou, K. (1997). Corrosion and protection of carbon steel in low enthalpy geothermal fluids. The case of sousaki in Greece. *Geothermics.* **26** (1), 65-82.

Brandon, M.J., Foo, L.Y., Porter, L.J. & Meredith, P. (1989). Proanthocyanidins of barley and sorghum; composition as a function of maturity of barley ears. *Phytochemistry.* **21** (12), 2953-2957.

Branzoi, V., Golgovici, F. & Branzoi, F. (2002). Aluminium corrosion in hydrochloric acid solutions and the effect of some organic inhibitors. *Materials Chemistry and Physics.* **78**, 122-131.

Bulatovic, S. & Salter, R.S. (1989). Separation of polymetallic sulphides by froth flotation. US Patent application 192567. 4880529.

Cai, Y., Evans, F.J., Roberts, M.F., Phillipson, J. D., Zenk, M.H & Gleba, Y.Y. (1991). Polyphenolic compounds from *Croton lechleri. Phytochemistry.* **30** (6), 2033-2040.

Cakir, A., Mavi, A., Yildirim, A., Duru, M.E., Harmandar M. & Kazaz, C. (2003). Isolation and characterization of antioxidant phenolic compound from the aerial parts of *Hypericum hyssopifolium* L. by activity-guided fractionation. *Journal of Ethnopharmacology.* **87**, 73-83.

Clough, B. F. (1993). Technical report of the project : *The economic and environmental values of mangrove forests and their present state of conservation in the south-east Asia/Pacific region, Australia : International Society for Mangrove Ecosystems.*

Clough, T.J. (1997). Corrosion inhibiting compositions containing plant derived catechol complexes. US Patent application 466479. 5656070.

Da Silva, R.J.M., Rigaud, J., Cheynier, V., Cheminat, A. & Moutounet, M. (1991). Procyanidin dimers and trimers from grape seeds. *Phytochemistry.* **30** (4), 1259-1264.

Danne, A., Peteriet F. & Nahrstedt, A.(1993). Proanthocyanidins from *Cistus incanus. Phytochemistry.* **34** (4),1129-1133.

De Bruyne, T., Pieters, L., Deelstra, H. & Vlietinck, A. (1999). Condensed vegetable tannins: biodiversity in structure and biological activities. *Biochemical Systematics and Ecology.* **27**, 445-459.

Deslauriers, P.J. (1987). Rust conversion coatings. *Material performance.* **26**, 35 – 39.

Do-Chul, S. & Won-Hwa, K. (2004). Waterproof admixture composition for concrete having excellent anti-corrosive performance. US patent application 20040103814. 723466.

El Azhar, M., Traisnel, M., Mernari, B., Gengembre, L., Bentiss, F. & Langrenee, M. (2002). Electrochemical and XPS studies of 2,5-bis(n-pyridyl)-1,3,4-thiadiazoles adsorption on mild steel in perchloric acid solution. *Applied Surface Science.* **185**, 197-205.

El Sherbini, F.E. E. & Abd El Rehim, S. S. (2000). Pitting corrosion of zinc in Na_2SO_4 solutions and the effect of some inorganic inhibitors. *Corrosion Science.* **42**, 785-798.

Evans, D.H., O'Connell, Petersen, R.A. & Kelly, M.J. (1983). Cyclic voltammetry. *Journal of Chemical Education.* **60** (4), 290-293.

Farreira, D., Neel, R.J.J. & Becker, R. (1999). Condensed Tannins. In *: Comprehensive Natural Products Chemistry.* [Barton, D., Nakanishi, K., Meth-Cohn, O., Mario Pinto, B. (eds.)] Vol. 3 : Carbohydrates and their derivatives including tannins, cellulose and related lignins. United Kingdom : Elsevier Science Ltd. Chap 3, p. 748-797.

Favre, M. & Landolt, D. (1993). The influence of gallic acid on the reduction of rust on painted steel surfaces. C*orrosion Science.* **34** (9), 1481 – 1494.

Fedeli, D., Berrettini, M., Gabryelak, T. & Falcioni, G. (2004). The effect of some tannins on trout erythrocytes exposed to oxidative stress. *Mutation Research.* **563**, 89-96.

Ferreira, C.E. & Nogueira, A.R.A. (2000). Vanillin-condensed tannin study using flow injection spectrophotometry. *Talanta.* **51**, 1-6.

Ferreira, E.S., Giacomelli, C., Giacomelli, F.C. & Spinelli, A. (2004). Evaluation of the inhibitor effect of L-ascorbic acid on the corrosion of mild steel. *Materials Chemistry and Physics.* **83,** 129-134.

Foo, L.Y & Karchesy, J. J. (1991). Procyanidin tetramers and pentamers from douglas fir bark. *Phytochemistry.* **30** (2), 667-670.

Foster, T., Blenkinsop, G.N., Blattler, P. and Szandorowski, M. (1991). Search for a chromate-free wash Primer. *Journal of Coating Technology.* **63**, (801), 91-99.

Gan, B.K. (1995). *A working plan for the Matang Mangrove Forest Reserve, Perak (4th Revision).* State Forestry Department of Perak Darul Ridzuan, Peninsular Malaysia.

Garnier, S. & Pizzi, A. (2001). CHT and TTT curing diagrams of polyflavonoid tannin resins. *Journal of Applied Polymer Science*, **81**, 3220-3230.

Garnier, S., Pizzi, A., Vorster, O.C. & Halasz, L. (2002b). Rheology of polyflavanoid tannin-formaldehyde reactions before and after gelling. II. Hardener influence and comparison of different tannins. *Journal of Applied Polymer Science.* **86**, 864-871.

Garnier, S.,Pizzi, A., Vorster, O.C. & Halasz, L. (2001). Comparative rheological characteristics of industrial polyflavonoid tannin extracts. *Journal of Applied Polymer Science.* **81**, 1634-1642.

Garnier, S.,Pizzi, A., Vorster, O.C. & Halasz, L. (2002a). Rheology of polyflavanoid tannin-formaldehyde reactions before and after gelling. I. Methods. *Journal of Applied Polymer Science.* **86**, 852-863.

Garro Galvez, J. M., Fechtal, M & Riel, B. (1996). Gallic acid as a model of tannins in condensation with formaldehyde. *Thermochimica Acta.* **274**, 149-163.

Goh, L.M., Barlow, P.J. & Yong, C.S. (2003). Examination of antioxidant activity of *Ginkgo biloba* leaf infusions. *Food Chemistry.* **82**, 275-282.

Gulcin, I., Oktay M., Kirecci E. & Kufrevioglu, O.I. (2003). Screening of antioxidant and antimicrobial activities of anise (*Pimpinella anisum L.*) seed extracts. *Food Chemistry,* **83**, 371-382.

Gust, J. & Bobrowicz, J. (1993). Sealing and anti-corrosive action of tannin rust converters. *Corrosion NACE.* **49** (1), 24 -30.

Gust, J. & Suwalski, J. (1994). Use of Mossbauer Spectroscopy to study reaction products of polyphenols and iron compounds. *Corrosion Science.* **50** (5), 355-365.

Gust, J. (1991). Application of infrared spectroscopy for investigation of rust phase componenet conversion by agents containing oak tannin and phosphoric acid. *Corrosion NACE.* **47** (6), 453 – 457.

Guyot, S., Doco, T., Jean-Marc, S., Moutounet, M. & Jean-Francois, D. (1997). Characterisation of highly polymerised procyanidins in cider apple (*malus sylvestris* var. *Kermerrien*) skin and pulp. *Phytochemistry.* **44** (2), 351-357.

Hagerman, A.E. & Butler, L.G. (1989). Choosing appropriate methods and standards for assaying tannin. *Journal of Chemical Ecology.* **15**, 1795-1810.

Hammerstone, J.F., Lazarus S.A., Mitchell A.E., Rucker, R & Schmitz, H.H. (1999). Identification of procyanidins in cocoa (*Theoroma cocoa*) and chocolate using high performance liquid chromatography. *Journal of Agricultural and Food Chemistry.* **47**, 490-496.

Harrop D. (1991). Chemical inhibitors for corrosion control. In : *Chemical Inhibitors For Corrosion Control.* B.G. Clubley, (ed). Cambridge : Royal Society of Chemistry. Ch. 1, p.1-20.

Hayashi, T., Nishihara, H. & Aramaki, K. (1996). The inhibition effect of bismuth(III) compounds on the corrosion of iron in 1N HCl at elevated temperature. *Corrosion Science.* **38,** 867-879.

Hernes, P.J., Benner, R., Cowie, G.L., Goni, M.A., Bergamashi, B.A. & Hedges, J.I. (2001), Tannin diagenesis in mangrove leaves from a tropical estuary: A novel molecular approach. *Geochimica et Cosmochimica Acta*. **65** (18), 3109-3122.

Hosseini, M., Mertens, S.F.L., Ghorbani, M. & Arshadi, M.R. (2003). Asymmetrical Schiff bases as inhibitors of mild steel corrosion in sulphuric acid media. *Materials Chemistry and Physics*. **78**, 800-808.

Hui-Long, W., Rui-Bin, L. & Jian, X. (2004). Inhibiting effects of some mercapto-triazole derivatives on the corrosion of mild steel in 1.0 M HCl medium. *Corrosion Science*. **46**, 2455-2466.

Ishimatsu, M., Tanaka, T., Gen-Ichiro, N. & Nishioka, I. (1989). Alnusnins A and B from the leaves of *Alnus sieboldiana*. *Phytochemistry*. **28** (11), 3179-3184.

Ivanov, E. & Kuznetsov, Y.I. (1990). Corrosion behaviour of iron in tannin solution. *Zashchita Metallov*. **26** (1), 48-53.

Ivanov, E. & Kuznetsov, Y.I. (1991). Inhibiting the corrosion of iron in tannin compositions. *Zashchita Metallov*. **27** (3), 379-387.

Jaen, J.A., Garcia de Saldana, E. & Hernandez., C.(1999). Characterization of reaction products of iron and aqueous plant extracts. *Hyperfine Interactions*. **122**, 139-145.

Jean-Marc, S., Cheynier, V., Brossaud, F. & Moutounet, M. (1996). Polymeric proanthocyanidins from grape skins. *Phytochemistry*. **43** (2), 509-512.

Karchesy, J.J. & Hemingway, R.W. (1980). Loblolly pine bark polyflavanoids. *Journal of Agricultural and Food Chemistry*. **28**, 222-228.

Kashiwada, Y., Gen-Ichiro, N. & Nishioka, I. (1986).Tannins and related compounds. XLV. Rhubarb. (5). Isolation and characterization of Flavan-3-ol and procyanidin glucosides. *Chemical and Pharmaceutical Bulletin*. **34** (8), 3208-3222.

Kelly, D.W., Paul, S.N. & Waller, J.E.(1988). Method for flocculating and removing solids suspended in water. US Patent application 106474. 4781839.

Khaled, K. F. (2004). An electrochemical study for corrosion inhibition of iron by some organic phosphonium chloride derivatives in acid media. *Applied Surface Science*. **230**, 307-318.

Khanbabaee, K. & Van Ree, T. (2001). Tannins: Classification and definition. *Natural Products Reports*. **18**, 641-649.

Kolodziej, H., Sakar, M.K., Burger, J.F.W., Engelshowe, R. & Ferreira, D. (1991). A-type proanthocyanidins from *Prunus spinosa*. *Phytochemistry.* **30** (6), 2041-2047.

Kondo, K, Kurihara, M, Miyata, N, Suzuki, T & Toyoda,M. (1999). Mechanistic studies of catechins as antioxidants against radical oxidation. *Archives of Biochemistry and Biophysics.* **362** (1), 79-86.

Koupai-Abrayani, M., McCallum,R. and Bohm, B.A. (1992). Identification of the constituent flavanoid units in sainfoin proanthocyanidins by reversed-phased high performance liquid chromatography. *Journal of Chromatography.* **594**, 117-123.

Lagrenee, M., Mernari, B., Bouanis, M., Traisnel, M. & Bentiss, F. (2002). Study of the mechanism and inhibiting efficiency of 3,5-bis(4-methylthiophenyl)-4H-1,2,4-triazole on mild steel corrosion in acidic media. *Corrosion Science.* **44**, 573-588.

Lahodny-Sarc, O. & Kapor, F. (2002). Corrosion inhibition of carbon steel in the near neutral media by blends of tannin and calcium gluconate. *Materials and Corrosion.* **53**, 264-268.

Lamb, L.H. & Decusati, O.G. (2002). Manufacturing process for quartenary ammonium tannate, a vegetable coagulating/flocculating agent. US Patent application 09/640861. 6,478,986B1.

Lampart-Szczapa, E., Korczak, J., Nogala-Kalucka, M. & Zawirska-Wojtasiak, R. (2003) Antioxidant properties of lupin seed products. *Food Chemistry.* **83**, 279-285.

Latté, K.P. & Kolodziej, H. (2004). Antioxidannt properties of phenolic compounds from *pelargonium reniform. Journal of Agricultural and Food Chemistry.* **52**, 4899-4902.

Lgamri, A., Abou El Makarim, H., Guenbour, A., Ben Bachir, A., Aries, L. & El Hajjaji, S. (2003). Electrochemical study of the corrosion behaviour of iron in presence of new inhibitor in 1 M HCl. *Progress in Organic Coatings.* **48**, 63-70.

Lgamri, A., Abou El Makarim, H., Guenbour, A., Ben Bachir, A., Aries, L., El
Li, K., Geng, X., Simonsen, J. & Karchesy, J. (2004). Novel wood adhesives from condensed tannins and polyethylenimine. *International Journal of Adhesion & Adhesives.* **24**, 327-333.

M. L. Price, & L. G. Butler. (1977). Rapid visual estimation of tannin content and spectrophotometric determination of sorghum grain. *Journal of Agricultural and Food Chemistry*, **25**, 1268-1273.

Maayta, A.K. & Al-Rawashdeh, N.A.F. (2004). Inhibition of acidic corrosion of pure aluminium by some organic compounds. *Corrosion Science.* **46**, 1129-1140.

Makkar, H.P.S. & Becker, K. (1994). Isolation of tannins from leaves of some trees and shrubs and their properties. *Journal of Agricultural and Food Chemistry.* **42**, 731-734.

Makkar, H.P.S. (1989). Protein precipitation methods for quantitation of tannins: A review. *Journal of Agricultural and Food Chemistry.* **37**, 1197-1202.

Makkar, H.P.S., Gamble, G. & Becker, K. (1999). Limitation of the butanol-hydrochloric acid-iron assay for bound condensed tannins. *Food Chemistry.* **66**, 129-133.

Mansfield, F. (1987a). *Corrosion mechanisms.* New York : Marcel Dekker Inc. p.119-164.

Mansfield, F. (1987b). *Corrosion Mechanisms.* New York : Marcel Dekker Inc. p. 202-204.

Martinez, S & Stalgar, I. (2003). Correlation between the molecular structure and the corrosion efficiency of chestnut tannin in acidic solutions. *Journal of Molecular Structure (Theochem).* **640**, 167-174.

Martinez, S. & Stern, I. (2001). Inhibitory mechamism of low-carbon steel corrosion by mimosa tannin in sulfuric acid solutions. *Journal of Applied Electrochemistry.* **31**, 973-978.

Martinez, S. & Stern, I. (2002). Thermodynamic characterization of metal dissolution and inhibitor adsorption processes in the low carbon steel/mimosa tannin/sulfuric acid system. *Applied Surface Science.* **9149**, 1 -7.

Martinez, S. (2002). Inhibitory mechanism of mimosa tannin using molecular modelling and substitutional adsorption isotherms. *Materials Chemistry and Physics.* **77**, 97-102.

Matamala, G., Smeltzer, W. & Droguett, G. (1994). Use of tannin anticorrosive reaction primer to improve traditional coating systems.*Corrosion NACE.* **50** (4), 270-275.

Matamala, G., Smeltzer, W., & Droguett, G. (2000). Comparison of steel anticorrosive protection formulated with natural tannins extracted from acacia and from pine bark. *Corrosion Science.* **42**, 1351 – 1362.

Matthews, S., Mila, I., Scalbert, A., Pollet, B., Lapierre, C., Herve du Penhoat, C.L.M, Rolando, C. & Donnelly, D.M.X. (1997). Method for estimation of proanthocyanidins based on their acid depolymerization in the presence

of nucleophiles. *Journal of Agricultural and Food Chemistry.* **45**, 1195-1201.

Mercer, A. D. (1985). Test methods for corrosion inhibitors. *British Corrosion Journal.* **20,** (2), 61-70.

Meyer, E.M. & Woods, M.R. (1993). Methods of removing oil and metal ions from oily wastewater. US Patent application 893483. 5256304.

Minussi, R.C.,Rossi, M.,Bologna, L., Cordi, L., Rotilio D., Pastore, G.M. & Duran, N. (2003). Phenolic compounds and total antioxidant potential of commercial wines. *Food Chemistry.* **82**, 409-416.

Mi-Yea, S., Tae-Hun, K. & Nak-ju, S. (2003). Antioxidants and free radical scavenging activity of *Phellinus baumii (Phallinus of Hymenochaetaceae). Food Chemistry.* **82**, 593-597.

Morales-Gil, P., Negron-Silva, G., Romero-Romo, M., Angeles-Chavez, C. & Palomar-Pardave, M. (2004). Corrosion inhibition of pipeline steel grade API 5L X52 immersed in a 1 M H2SO4 aqueous solution using heterocyclic organic molecules. *Electrochimica Acta.* **49**, 4733-4741.

Morimoto, S., Gen-Ichiro N. & Nishioka, I. (1986). Tannins and related compounds. XXXVIII. Isolation and characterization of flavan-3-ol glucosides and procyanidin oligomers cassia bark of (*Cinnamomum cassia* BLUME). *Chemical and Pharmaceutical Bulletin.* **34** (2), 633-643.

Musa, N.H. (2004). *Kajian teoritikal mekanisme penukar karat* Fe^{3+}*-katechin.* BSc. Thesis. Universiti Sains Malaysia.

Naczk, M, Nichols, T, Pink, D. & Solulski, F. (1994). Condensed tannins in canola Hulls. *Journal of Agricultural and Food Chemistry.* **42**, 2196-2200.

Nam-In, B., Kennelly, E.J., Kardono, L.B.S., Tsauri, S., Padmawinata, K., Soejarto, D.D. & Kinghorn, A.D. (1994). Flavonoids and proanthocyanidin from rhizomes of *Selliguea feei. Phytochemistry.* **36** (2), 513-518.

Nasrazadani, S. (1997). The application of infrared spectroscopy to a study of phosphoric and tannic acids interactions with magnetite (Fe_3O_4), goethite (α-FeOOH) and lepidocrocite (γ-FeOOH). *Corrosion Science.* **39** (10-11), 1845-1859.

Nessa, F., Ismail, Z., Mohamed, N. and Mas Haris, M. R. H. (2004). Free radical-scavenging activity of organic extracts and of pure flavonoids of *Blumea balsamifera. Food Chemistry*, **88**, 243-252.

Ng, P.K.L. & Sivasothi, N. (2001). *Guide to the mangrove of Singapore* [Online]. [Accessed 19th August 2004]. Available from World Wide Website: http://mangrove.nus.edu.sg/guidebooks/text/1069.htm

Noferi, M., Masso, E., Merlin, A., Pizzi, A. & Deglise, X. (1997). Antioxidant characteristics of hydrolysable and polyflavonoid tannins: An ESR kinetics study. *Journal of Applied Polymer Science*. **63**, 475-482.

Ocampo, L.M., Margarit, I.C.P., Mattos, O.R., Cordoba-de-Torresi, S.I. & Fragata, F.L. (2004). Performance of rust converter based in phosphoric and tannic acids. *Corrosion Science*. **46**, 1515-1525.

Ohara, S. & Ohmura, W. (1998). Utilisation of condensed tannins from the barks of acacia mearnsii. *Proceeding of Acacia species-wood properties and utilization, Acacia 98,* 16-18 March, Penang, Malaysia, 36-42.

Ohtani, I.I., Gotoh, N.,Tanaka, J., Higa, T., Gyamfi, M.A. & Aniya, Y. (2000) Thonningianins A and B, New Antioxidants from the African Medicinal Herb *Thonningia sanguinea. Journal of Natural Products*. **63**, 676-679.

Okuda, T., Yoshida, T. & Hatano, T. (1989). New methods of analyzing tannins. *Journal of Natural Products*, **52** (1), 1-31.

Osman, M.M., El-Ghazawy, R.A. & Al-Sabagh, A.M. (2003). Corrosion inhibitor of some surfactants derived from maleic-oleic acid adduct on mild steel in 1 M H_2SO_4. *Materials Chemistry and Physics*. **80**, 55-62.

Ozcan, M., Dehri, I. & Erbil, M. (2004). Organic siphur-containing compound as corrosion inhibitors for mild steel in acidic media: correlation between inhibition afficiency and chemical structure. *Applied Surface Science*. **236**, 155-164.

Pardini, O.R., Amalvy, J.I.,.Di Sarli, A.R., Romagnoli R. & Vetere. V.F. (2001). Formulation and testing of a waterborne primer containing chestnut tannin. *Journal of Coating Technology*. **73** (913), 99-111.

Pelillo, M, Biguzzi, B., Bendini, A., Toschi, G., Vanzini, M. & Lercker, G. (2002). Preliminary investigation into the development of HPLC with UV and MS-electrospray detection for the analysis of tea catechins. *Food Chemistry*. **78**, 369-374.

Peng, A. & Allemand. (1999). Use of antioxidants in extraction of tannins from walnut plants. *Journal of Chemical Ecology*. **17** (5), 887-896.

Peultier, J., Rocca, E. & Steinmetz, J. (2003). Zinc carboxylating: a new conversion treatment of zinc. *Corrosion Science*. **45**, 1703-1716.

Pizzi, A & Stephanou, A. (1993). A comparative C^{13} NMR study of polyflavanoid tannin extracts for phenolic polycondensates. *Journal of Apllied Polymer Science*. **50**, 2105-2113.

Pizzi, A. Simon,C., George, B., Perrin, D. & Triboulot, M.C. (2004). Tannin antioxidant characteristics in leather versus light stability: Model. *Journal of Applied Polymer Science*. **91**, 1030-1040.

Popova, A., Sokolova, E., Raicheva, S. & Christov, M. (2003). Mild steel corrosion in acidic media in the presence of benzimidazole derivatives. *Corrosion Science*. **45**, 33-58.

Porter, L.J., Foo, L.Y. & Furneaux, R.H. (1985). Isolation of three naturally occurring O-β-glucopyranosides of procyanidin polymers. *Phytochemistry*. **24** (3), 567-569.

Porter, L.J., Newman, R.H., Foo, L.Y. & Wong, H. (1982). Polymeric proanthocyanidins. ^{13}C N.M.R. studies of procyanidins. *Journal of Chemical Society Perkin Transaction 1*. 1217-1221.

Pourbaix, M. (1973). *Lectures on Electrochemical Corrosion*. New York : Platinum Press. p. 201-203.

Price, M.L., Scoyoc, S.V. & Butler, L.G. (1978). A critical evaluation of the vanillin reaction as an assay for tannin in sorghum grain. *Journal of Agricultural and Food Chemistry*. **26** (5), 1214-1218.

Prieur, C., Rigaud, J., Cheynier, V. & Moutounet, M. (1994). Oligomeric and polymeric procyanidins from grape seeds. *Phytochemistry*. **36** (3), 781-784.

Quraishi, M.A., Jamal, D. (2003). Dianils as new and effective corrosion inhibitors for mild steel in acidic solutions. *Materials Chemistry and Physics*. **78**, 608-613.

Quraishi, M.A., Sardar, R. & Jamal, D. (2001). Corrosion inhibition of mild steel in hydrochloric acid by some aromatic hydrazides. *Material Chemistry and Physics*. **71**, 309-313.

Rahman, I.A., Sing, Y.Y., Bari M.F. & Saad, B. (2005). Adsorption of paraquat by rice husks studied using flow injection-spectrophotometry. *Research Journal of Chemistry and Environment*. **9**, 17-22.

Ravichandran, R., Nanjundan, S. & Rajendran, N. (2004). Effect of benzotriazole derivatives on the corrosion of brass in NaCl solutions. *Applied Surface Science*. **236**, 241-250.

Refaey S. A. M. & Abd El. Rehim, S. S. (1996). Inhibition of chloride pitting corrosion of tin in alkaline and near neutral medium by some inorganic anions. *Electrochimica Acta*. **42**(4), 667-674.

Refaey, S. A. M. (2005) Inhibition of steel pitting corrosion in HCl by some inorganic anions. *Applied Surface Science*. **240**, 396-404.

Rice-Evans, C.A., Miller, N.J., Paganga, G. (1996). Structure-antioxidant activity relationships of flavanoids and phenolic acids. *Free Radical Biology & Medicine*. **20** (7), 933-956.

Rigaud, J., Escribano-Bailon, M. T., Prieur, C., Souquet J. M. & Cheynier, V. (1993). Normal-phase high-performance liquid chromatographic separation of procyanidins from cacao beans and grape seeds. *Journal of Chromatography A.* **654**, 255-260.

Rocca, E. & Steinmetz, J. (2001). Inhibition of lead corrosion with saturated linear aliphatic chain monocarboxylates of sodium. *Corrosion Science.* **43**, 891-902.

Rocca, E., Bertrand, G., Rapin, C., Labrune, J.C. (2001). Inhibition of copper aqueous corrosion by non-toxic linear sodium heptanoate: mechanism and ECAFM study. *Journal of Electroanalytical Chemistry.* **503**, 133-140.

Rocca, E., Rapin, C. & Mirambet, F. (2004). Inhibition treatment of the corrosion of lead artefacts in atmospheric conditions and by acetic acid vapour: use of sodium decanoate. *Corrosion Science.* **46**, 653-665.

Ross, T.K. & Francis, R.A. (1978). The treatment of rusted steel with mimosa tannin. *Corrosion Science.* **18,** 351- 361.

Saad, B., Cheng, W.L., Jab, M.S. & Boey, P.L. Flow injection non-aqueous titrimetric method for the determination of free fatty acids in palm oil samples. Submitted to *Food Chemistry.*

Saad, B., Leng, Y.B., Saleh, M.I., Rahman, I.A. & Mahsufi, S.M. (2001). Polyvinyl chloride-based membranes for the flow injection analysis of quinine in beverages. *Journal of AOAC International.* **84**, 1151.

Salah, N., Miller, N.J., Panganga, G., Tijburg, L., Bolwell, G.P. & Rice-Evans, C. (1995). *Achives of Biochemistry and Biophysics*, **322** (2), 339-346.

Sastri, V. S. (1998a). Chemical aspects of corrosion inhibition. In : *Corrosion Inhibitors. Principles and Applications.* England : John Wiley & Sons. Ch. 4, p. 64-74.

Sastri, V. S. (1998b). Chemical aspects of corrosion inhibition. In : *Corrosion Inhibitors. Principles and Applications.* England : John Wiley & Sons. Ch. 4, p. 110.

Sastri, V. S. (1998c). Chemical aspects of corrosion inhibition. In : *Corrosion Inhibitors. Principles and Applications.* England : John Wiley & Sons. Ch. 5, p. 219-240.

Sastri, V.S. & Perumareddi, J.R. (1994). Selection of corrosion inhibitors for use in sour media. *Corrosion.* **50** (6) 432-437.

Sastri, V.S. & Perumareddi, J.R. (1997). Molecular orbital theoretical studies of some organic corrosion inhibitors. *Corrosion.* **53** (8), 617-622.

Sato, T., Ueda, T., Kobayashi, K. (1990). Corrosion inhibitors for boiler systems. US patent application 893483, 5256304.

Schofield, P., Mbugua, D.M. & Pell, A.N. (2001). Analysis of condensed tannins: a review. *Animal Feed Science and Technology.* **91**, 21-40.

Seavell, A.J. (1992). The preparation of an iron tannate anticorrosive pigment of commercial potential. *Journal of Oil Colour Chemistry Association.* **8**, 293-306.

Shreir L.L. (ed). (1978a). Conditioning the environment. In *: Corrosion. Vol. 2. Corrosion Control.* 2nd edition. London : Newnes-Butterworth. Ch. 15, p. 25.

Shreir L.L. (ed). (1978b). Conditioning the environment. In *: Corrosion. Vol. 2. Corrosion Control.* 2nd edition. London : Newnes-Butterworth. Ch. 18, p. 34-56.

Silvius, M.J., Chan, H. T. & Shamsudin, I. (1986). *Evaluation of Wetlands of the West Coast of Peninsular Malaysia and Their Importance for Natural Resource Conservation.* WWF Malaysia, Kuala Lumpur.

Simon, C. & Pizzi, A. (2003). Tannins/melamine-urea-formaldehyde (MUF) resins substitution of chrome in leather and its characterization by thermomechanical analysis. *Journal of Applied Polymer Science.* **88**, 1889-1903.

Stern, M. & Geary, J. (1957). *Journal of Electrochemical Society.* **104**, 390.

Stratmann, M. (1990). The atmospheric corrosion of iron – A discussion of the physico-chemical fundamentals of this omnipresent corrosion process. Invited review. *Ber. Bunsengers. Physical Chemistry.* **94**, 626-639.

Tan, R. (2001). *Bakau Rhizophora spp.* [Online]. [Accessed 19th August 2004]. Available from World Wide Website: http://www.naturia.per.sg/buloh/plants/rhizophora.htm

Tannins : chemical structure (2001) [Online]. [Accessed on 7th July 2003]. Available from the World Wide Website: http://www.ansci.cornell.edu/plants/toxicagents/tannin/chemical.html

Toki, K., Terahara, N., Saito, N., Honda, T. & Shioji, T. (1991). Acetylated anthocyanins in *Verbena* flowers. *Phytochemistry.* **30** (2), 671-673.

Tommesani, L., Brunoro, G., Frignani, A., Monticelli, C. & Colle, M.D. (1997). On the protective action of 1,2,3-benzotriazole derivative films against copper corrosion. *Corrosion Science.* **39** (7), 1221-1237.

Vazquez, G., Gonzalez-Alvarez, J., Lopez-Suevos, F. & Antorrena, G. (2003). Effect of veneer side wettability on bonding quality of Eucalyptus globulus

plywoods prepared using a tannin-phenol-formaldehyde adhesive. *Bioresource Technology*. **87**, 349-353.

Vracar, Lj. M., Drazic, D. M. (2002). Adsorption and corrosion inhibitive properties of some organic molecules on iron electrode in sulfuric acid. *Corrosion Science*. **44**, 1669-1680.

Wang, D., Tang, X., Qiu, Y., Gan, F. & Chen, G. Z. (2004). A study of the film formation kinetics on zinc in different acidic corrosion inhibitor solutions by quartz crystal microbalance. *Corrosion Science*, in press.

Ximenes F. (1998) *Tannins* [Online]. [Accessed on 7th July 2003]. Available from the World Wide Website: http://sres.anu.edu.au/associated/fpt/nwfp/tannins/tannins.html

Yadaf, A.P., Nishikata, A., Tsuru, T. (2004). Electrochemical impedance study on galvanized steel corrosion under cyclic wet-dry conditions-influence of time of wetness. *Corrosion Science.* **46**, 169-181.

Yazaki, Y. (1985). Extraction of polyphenols from *Pinus radiata* bark. *Holzforschung.* **39**, 267-271.

Yen, G.H. & Duh, P.D. (1994). Scavenging effect of methanolic extracts of peanut hulls on free radical and active oxygen species. *Journal of Agriculture and Food Chemistry*. **42**, 629-632.

Yoshiaki, S. & Toshinobu, I. (1994). Treatment of boiler water. Japan patent application 04-267887. 06-108274.

Young-Soo, B., Burger, J.F.W., Steynberg, J.P, Ferreira, D. and Hemingway, R.W. (1994). Flavan and procyanidin glycosides from the bark of blackjack oak. *Phytochemistry*. **35** (2), 473-478.

Madame **AFIDAH BINTI ABDUL RAHIM**

DOCTORAT DE L'UNIVERSITE HENRI POINCARE, NANCY 1

en CHIMIE DES MATERIAUX

VU, APPROUVÉ ET PERMIS D'IMPRIMER N°1160

Nancy, le 23 mai 2006

Le Président de l'Université

LE PRÉSIDENT

J.P. FINANCE

Université Henri Poincaré, Nancy I
24-30 rue Lionnois - B.P. 3069 - 54013 NANCY Cédex
Tél. : 03 83 68 20 00 - Fax : 03 83 68 21 00